The Dissertation Committee for Jeffrey Lik Yeung Lee Certifies that this is the approved version of the following dissertation:

Improved Rolling Dynamic Deflectometer Testing and Analysis Procedures

Committee:

Kenneth H. Stokoe,II , Supervisor

James A. Bay

David W. Fowler

Jorge A. Prozzi

Clark R. Wilson

Improved Rolling Dynamic Deflectometer Testing and Analysis Procedures

by

Jeffrey Lik Yeung Lee, B.E. ; M.S.

Dissertation

Presented to the Faculty of the Graduate School of

The University of Texas at Austin

in Partial Fulfillment

of the Requirements

for the Degree of

Doctor of Philosophy

The University of Texas at Austin

August 2006

Dedicated

To

My Parents,

My Wife and My Son.

Acknowledgements

I would like to thank my supervising professor Dr. Kenneth H. Stokoe, II for his guidance, support, and encouragement through the course of this study. His passion and enthusiasm in the area of Nondestructive Testing and Evaluation of Dynamic Material Properties has always inspired me.

Thanks are also extended to the remaining members of my dissertation committee, Dr. James A. Bay, Dr. David W. Fowler, Dr. Jorge A. Prozzi, and Dr. Clark R. Wilson for reviewing this dissertation and for their valuable contributions to this work. I also would like to extend my gratitude to the rest of the current geotechnical engineering faculty.

The support from the Texas Department of Transportation for the cost of developing the second-generation rolling sensor is gratefully acknowledged.

I would like to thank the former graduate students Dr. Farn-Yuh Menq, Dr. Brent L. Rosenblad, Dr. Celestino Valle for their help and guidance. Thanks are also extended to other graduate students of whom I had the pleasure of making acquaintance; Yin-Cheng Lin, Wonkyoung Choi, Boo Hyun Nam and many others that I unfortunately omitted.

I would also like to thank Teresa Tice-Boggs, Alicia Zapata, and Chris Trevino for their administrative support, and Frank Wise and Andrew Valentine for their technical assistance over the years. The assistance from Mr. Paul Walters in operating the RDD on highway project-level studies is especially appreciated.

Improved Rolling Dynamic Deflectometer Testing and Analysis Procedures

Publication No._____

Jeffrey Lik Yeung Lee, Ph.D.

The University of Texas at Austin, 2006

Supervisor: Kenneth H. Stokoe, II

A three-part study was undertaken to further improve the Rolling Dynamic Deflectometer (RDD). The first part involved the development of second-generation rolling sensors. Key benefits of this new rolling sensor are: (1) increased testing speed from 1 to 3 mph (1.6 to 4.8 km/hr), and (2) reduced the level of rolling noise during RDD measurements. With this rolling sensor, the RDD can collect more deflection measurements at a speed of 3 mph (4.8 km/hr). Field trials using the first- and second-generation rolling sensors on both flexible and rigid pavements were performed to evaluate the performance of the second-generation rolling sensor.

The second part of this study involved improving the understanding of rolling noise collected on highway and airport pavements. This effort was accomplished by analyzing RDD data that were collected over the last seven years. A total of 46 different highway and airport test sites were evaluated to systematically investigate the effects of deflection levels, pavement surface roughnesses, and testing speeds on the rolling noise

characteristics. These findings allow the development of a rolling noise envelope to estimate the rolling noise components.

The third part of this study involved improving the data analysis method for RDD testing. An alternative data analysis method was developed. This new analysis method produces results that are comparable to the existing analysis method. Key benefits of this analysis method that were not previously available are: (1) analysis of the rolling noise characteristics, (2) design of individual digital filters for a particular set of RDD measurements, and (3) filtering of the RDD data at the operating frequency without performing the amplitude demodulation procedure. Finally, a Windows-based computer software, called WinRDD, was developed to automate the data analysis method presented in this dissertation.

Table of Contents

List of Tables

List of Figures

Chapter 1 Introduction to the Rolling Dynamic Deflectometer

1.1 BACKGROUND

Considerable amount of funds are spent annually to maintain the nation's transportation infrastructure. In the context of highway and airport pavements, different methods are used to ensure proper management of these valuable structures. In-situ nondestructive testing of pavement materials is one of the many methods used to determine the material properties of in-service pavements. Nondestructive testing devices which measure pavement material properties at discrete locations are commonly used in engineering practice and research projects. However, there is an increasing need to measure in-situ pavement material properties continuously and at a faster rate. A number of devices were developed by different researchers to fulfill this purpose, and the Rolling Dynamic Deflectometer is one of such devices.

The Rolling Dynamic Deflectometer (RDD) is a nondestructive deflection testing device developed by researchers at the University of Texas at Austin in the 1990s (Bay, 1997). During the last decade, use of the RDD in highway and airport pavement projects has increased significantly. When comparing the RDD with other nondestructive deflection testing devices, the RDD has the advantage of measuring deflections continuously as it rolls along the pavement surface. The deflection measurements are typically presented as a continuous deflection profile, which consists of numerous, closely spaced deflection measurement points. In the present configuration, each measurement point represents an average deflection over a distance of 3 ft. This "continuous" profile allows easy identification of critical sections along a pavement

system. Furthermore, the confidence of the measurements improves significantly as the number of samples collected per linear distance increases.

1.2 OBJECTIVES OF RESEARCH

The objectives of this research are: (1) to improve the quality of the RDD deflection measurements, and (2) to investigate ways to improve the operational efficiency of this testing device.

Research efforts were focused in three major areas to accomplish these objectives. First, the second-generation rolling sensor was developed to improve the RDD operating speed and the quality of the measured deflections. Second, our understanding of rolling noise, which is inherent in the RDD testing technique, was improved. Rolling noise will always exists when making "in-motion" deflection measurements. Based on the study of rolling noise collected during the past seven years of highway measurements, the characteristics of rolling noise can better be understood and methodologies can be devised to both minimize and quantify the effect of the rolling noise. Last, RDD test data collected at 46 different project-level studies were integrated throughout the work presented in this dissertation.

1.3 ORGANIZATION OF THE DISSERTATION

This chapter (Chapter 1) serves as an introduction to the RDD as a nondestructive deflection testing device for evaluating the conditions of highway and airport pavements. It also summarizes the research objectives and outlines the remaining chapters of this dissertation.

Chapter 2 is a literature review. First, a summary is provided about the different pavement applications which use deflection measurements collected with nondestructive

testing devices. Then, different nondestructive deflection testing devices that are commonly available are presented.

In Chapter 3, the study of the effects of rolling noise on RDD measurement is presented. Based on the data collected in project-level studies over the past seven years, the rolling noise characteristics measured in the field were analyzed and are used to develop different rolling noise envelopes. Knowledge from this study can be used in two aspects. First, this knowledge can be incorporated into the design of the second-generation rolling sensor. Second, the current signal filtering scheme can be improved by incorporating the extensive knowledge of the understanding of the rolling noise component within our deflection measurements.

In Chapter 4, a summary of the development of the second-generation rolling sensor is provided. The second-generation rolling sensor has been developed to increase the RDD testing speed from 1 to 3 mph. Furthermore, the rolling noise is less (i.e. this sensor improves the quality of the RDD measurements) than the first-generation rolling sensor when both sensors were tested at the same speed along the pavement.

In Chapter 5, field trials results using the second-generation rolling sensors are presented. These results are compared with the first-generation rolling sensors to demonstrate the improvements in both the testing speed and the quality of the collected deflection measurements. Two aspects were considered in the study: (1) decoupling of the rolling sensor, and (2) reduction of the rolling noise level in the RDD measurements.

In Chapter 6, discussion of the improvements to the current digital filtering scheme used to analyze the raw RDD signal is presented. This chapter has two parts. First, limitations and tradeoffs of the current digital filtering scheme are discussed. Second, an alternative digital filtering scheme is presented. This scheme allows the user

to adjust the filter specifications according to the characteristics of the collected RDD signals.

In Chapter 7, a software program called WinRDD was written to improve the existing analysis procedure for the collected RDD data. In this chapter, a detailed discussion of this program is presented.

In Chapter 8, the conclusions of this research are presented. A summary of the improvements made to the current RDD configuration is provided. These improvements represent the efforts provided by the University of Texas at Austin to continue developing and broadening the understanding of and measurements made with the RDD.

Chapter 2 Overview of Nondestructive Testing of Pavements

2.1 INTRODUCTION

The use of different nondestructive deflection testing techniques to evaluate the condition of a pavement is very common in many parts of the world. In particular, some state transportation agencies in the United States incorporate this type of measurement in their daily pavement management (asset management) systems. The primary purpose of nondestructive deflection testing devices is to evaluate the in-situ material properties of pavement systems. When deflection data are collected regularly from a section of highway, pavement engineers can monitor the condition of the highway, and correlate its deterioration (or lost of serviceability) with time and levels of accumulated traffic. Nondestructive testing methods have gained in popularity over other destructive testing methods because these measurements can be collected at a relatively fast rate, and the disruption (due to material sampling) to the general public can often be minimized.

2.2 PROJECT-AND NETWORK-LEVEL PAVEMENT STUDIES

Different discrete-type testing devices are commonly used by different transportation agencies to perform nondestructive deflection testing. The complexity and the required sampling intervals depend on the type of pavement studies. Pavement evaluation studies can be categorized into two major types. The first type is the project-level pavement study, and the second group is the network-level pavement study. A rigid guideline does not exist to classify a pavement study as either a network- or project-level study. However, a brief explanation is provided in the AASHTO standard T256-8. A network-level, deflection testing study provides a general overview of a pavement's bearing capacity. Deflection testing is often performed at 200-m to 500-m intervals. In a

general project-level study, the purpose is to provide a more detailed analysis of the pavement. Typically, deflection testing is performed at 50-m to 200-m intervals. If testing was performed for a Jointed Concrete Pavement (JCP), a minimum joint coverage rate of 25% is recommended. For a detailed project-level study, testing is performed at 10-m to 50-m intervals. All joints are usually evaluated at this level of analysis as indicated in AASHTO T256-01. Deflection data are often collected in both project-level and network-level pavement evaluation studies. Over the last decade, the RDD has been used primarily in project-level studies.

2.3 STRUCTURAL CAPACITY EVALUATION: USING DEFLECTION DATA

Structural capacity evaluation is used to: (1) determine the remaining life of a pavement and (2) devise an appropriate rehabilitation scheme. In the United States, the AASHTO methodology is the most commonly used method for evaluating the structural capacity of flexible pavements (AASHTO, 1996). This method was based on regression analysis of measurements collected during the AASHTO Road Test conducted in 1960 (McKendrick, 1962). The structural capacity is defined as the number of standard 18-kips Equivalent Single Axle Load (ESALs) for a pavement with a particular Structural Number (SN). The SN is a questionable number which characterize the pavement's structural capacity. The SN can be calculated if the material, thickness and condition of a flexible pavement are known (Liddle et al., 1962; Duzan et al., 1962). Shortcomings of using the SN are that two pavement systems with different layer configurations can result in the same SN, and SN itself cannot be correlated directly with engineering material properties.

Other than using the AASHTO methodologies, there are other methods for quantifying the structural capacity of a pavement. These include different kinds of deflection basin characterization methods, and different mechanistic analysis methods

that predict different modes of pavement failure based on calculated stress, strain and other response variables (Murphy, 1998). Nevertheless, it is a common practice to calculate these response variables from nondestructive deflection testing data using backcalculation procedures.

ASTM indicates that nondestructive pavement deflections can be used as an input for structural analysis of pavement systems. Other than using the pavement deflection to delineate a test site into homogenous sections with similar deflection values, deflection data collected from the field can be analyzed in a variety of ways. The type of analysis chosen depends on two major factors. The first factor is the required level of complexity, and the second factor is the aspect of pavement condition that is of interest to the decision markers. For example, in a JCP rehabilitation project, the primary objective of the deflection testing is likely to be evaluating the load-transfer characteristic across each concrete joint. This effort often involves analysis which compares the ratio between deflections measured across a concrete joint (Harvey et al., 2003). On the other hand, determining the load carrying capacity of a low traffic volume road requires a fairly simple approach. In this case, the measured surface deflection can be correlated to a commonly used pavement structural capacity indicator, a questionable parameter known as SN that was developed by the AASHTO design guide (Romanoschi et al., 2000). If more detailed analysis is required, such as identifying a problematic layer within a pavement system, backcalculation analysis are often used to compute the variation of elastic modulus for each layer along a pavement project (Meshkani, 2003).

Even though it is common to evaluate structural capacity of a pavement system using nondestructive deflection testing device, it is important for engineers to be caution when interpreting deflection measurements. This caution is needed because there are many factors that can influence the measured deflections. Some of the factors which can

affect the measured deflection were summarized by Weaver (Weaver, 2000). These factors include: (1) pavement structure, (2) load magnitude, (3) types of loading, (4) load distribution, (5) pavement temperature during testing, and (6) testing season.

At this time, the linear elastic theory is one of the most widely used in practice. Limitations on utilizing the linear elastic theory for backcalculating pavement layer modulus were widely discussed in the technical literature (Ullidtz et al., 1995). However, the simplicity of this theory often justifies for its limitations when used for backcalculation purposes (i.e. only two elastic material parameters were needed: (1) Poisson's ratio and (2) Youngs' modulus).

2.4 ELASTIC-MODULUS BACKCALCULATION

Backcalculation of layer moduli is an inverse problem where the pavement response is measured and then used to calculate the moduli value of the pavement layers. In the backcalculation analysis, theoretical deflection basins are generated from a set of layer moduli. Then, multi-layer elastic theory is used to perform forward calculations using layer moduli results obtained from different backcalculation programs. It is common to perform backcalculation on in-situ deflection measurements. Nowadays, there are many different backcalculation programs that are available. Some researchers provided a concise summary of the different backcalculation programs that are available (Ullidtz et al.,1995; Hossain, 1990). Some of the backcalculation programs for flexible pavements are summarized in Table 2.1. Backcalculation programs are also used to determine design parameters for rigid pavements. Uzan et al. presented a backcalculation procedure to determine the layer properties of rigid pavements using field deflection measurements (Uzan et al., 1992).

One of the shortcomings of the backcalculation procedure is that the calculated set of moduli is not a unique solution from the measured deflection basins. Nevertheless,

engineering judgment and some general guidelines can help eliminate solutions that do not make much sense. It is well known that the backcalculation procedure is very sensitive to the thickness input of the different pavement layers. This viewpoint is supported by a number of research studies on the effect of backcalculated moduli when layer thickness varies along a pavement test section (Zaniewski et al., 1992; Irwin et al., 1989; Nazarian et al., 1997).

Table 2.1 Available Backcalculation Programs (after Hossain, 1990)

Title	Source	Pavement Model	Response Program	NDT
SEARCH	Lytton & Mitchalak, 1979	3-layer	MET	RR2008
CHEVDEF	Bush, 1980	4-layer	CHEVRON	RR2008
ISSEM4	Sharma & Stubstad, 1980	4-layer	FEM	FWD
ILLI-CALC	Hoffman & Thompson, 1982	3-layer	Charts & Nomographs	RR2008, FWD
FPEDDI	Uddin et al., 1984	4-layer	ELSYM5	Dynaflect FWD
ELSDEF	Lytton et al., 1985	4-layer	ELSYM5	Dynaflect FWD
MODCOMP2	Irwin, 1985	8-layer	CHEVRON	RR2008, Dynaflect, FWD
IMD	Husain & George, 1985	4-layer	CHEVRON	Dynaflect FWD
ELMOD	Dynatest, 1987	4-layer	MET	FWD
DYNAMIC1	Sebaaly, 1987	4-layer	Dynamic Analysis	Dynaflect
DYNAMIC2	Sebaaly, 1987	4-layer	Dynamic Analysis	FWD
EVERCALAC	Lee et al., 1988	3-layer	CHEVRON	FWD
BKCHEVM	Mamlonk et al., 1988	4-layer	CHEVRON	FWD
MODULUS	Uzan et al., 1988	4-layer	BISAR	FWD
ADAM	Hossain, 1990	6-layer	CHEVRON	FWD

2.4.1 Backcalculation for Flexible Pavements

In short, the backcalculation procedure calculates the theoretical deflection basin using assigned layer moduli and layer thicknesses. An iterative or a database searching approach is used to obtain a set of layer moduli which corresponds to the theoretical deflection basin that best matches with the measured deflection basin. The theoretical deflection basins are typically calculated using forward calculation methods, which compute stress and strain at any location using the assigned elastic moduli, Poisson's ratios, and assumed layer thicknesses. As mentioned earlier, multi-layer elastic theory is often used to compute the pavement response. Murphy provided a summary of research findings on the validity of the multi-layer, linear-elastic theory for evaluating flexible pavements (Murphy, 1998).

This inverse problem is opposite to the forward problem where the layer moduli properties are given and used to calculate the pavement response parameters. Unfortunately, the inverse problem is considerably more difficult to solve then the forward problem. This difficulty can be partly explained by the inaccurate material models and non-uniqueness of the backcalculated solutions. The non-uniqueness of the backcalculated solution was further discussed by (Stolle et al., 1989). Backcalculation programs often use different optimization techniques to search for a set of moduli value based on a different objective function (Johnson, 1992). The aim for most of these objective functions is to minimize the differences between the measured and theoretical deflection basins, and the optimization techniques are used to seek the set of modulus values which minimize the objective function using the least number of iterations (Hossain, 1990).

There are two different approaches that are commonly used to backcalculate layer material properties using deflection measurements. First, backcalculation is performed

using a multi-layer linear elastic assumption. This approach is used for both flexible and rigid pavements. Second, backcalculation is performed using the assumptions in the slab on an elastic solid (ES) or a dense liquid (DL) foundation. Both the ES and DL assumptions are based on plate theory, and are typically used only for rigid pavements.

2.4.2 Backcalculation for Rigid Pavement

There are two methods for backcalculating layer material properties in rigid pavements. First, the best-fit method, which solves for a combination of the radius of relative stiffness (l) and coefficient of subgrade reaction (k) to minimize the error between the theoretical and measured deflection basins. Second, the AREA method which utilizes the unique relationship between the AREA parameter and the radius of relative stiffness (Ioannides et al., 2001) to match the theoretical and measured deflection basins. To quantify the degree of agreement between the theoretical and measured deflection basins, a relative error term is often used as shown in Figure 2.1. When compared with backcalculation performed on flexible pavements, backcalculation performed on rigid pavements can be tricky. Some of the factors that can influence the backcalculated results include: (1) layer thickness, (2) effect of base layer, (3) effect of modular ratio, (4) effect of sensor configuration, and (5) effect of slab size (FHWA, 2001).

$$\varepsilon_i = \frac{w_{i,c} - w_{i,m}}{w_{i,m}} * 100\% \quad (45)$$

where ε_i = relative error for sensor i
$w_{i,c}$ = computed deflection for sensor i
$w_{i,m}$ = measured deflection for sensor i

The mean absolute relative error for a deflection basin is defined using the following equation:

$$\varepsilon_m = \frac{|\varepsilon_1| + |\varepsilon_3| + |\varepsilon_5| + |\varepsilon_6|}{4} \quad (46)$$

where ε_1, ε_3, ε_5, and ε_6 are relative errors of the sensors located 0, 305, 610, and 914 mm from the center of the FWD plate.

Figure 2.1 Relative Error between the Theoretical and Measured Deflection Basins (from FHWA, 2001)

2.5 NONDESTRUCTIVE DEFLECTION TESTING DEVICES

There are many different types of nondestructive deflection testing devices that are available. ASTM D 4695-96 provides a broad categorization of the different types of nondestructive deflection testing devices (ASTM, 1996). Many of these devices only measure in-situ material properties at discrete locations. Consequently, localized changes in material properties often cannot be captured, even in detailed project-level studies. The most common of these test devices are presented in the remaining part of this chapter.

2.5.1 Benkelman Beam

The first nondestructive deflection device in modern pavement engineering was the Benkelman Beam, which was developed by A. C. Benkelman. A diagram of the Benkelman Beam is shown in Figure 2.2. The device was developed during the WASHO Road Test in the mid-1950's (Forsyth et al., 1966), and was later used to measure deflection in the AASHO Road Test. The Benkelman beam measures the rebound pavement deflection at the probe point as a standard 18-kips axle drives away from the probe point.

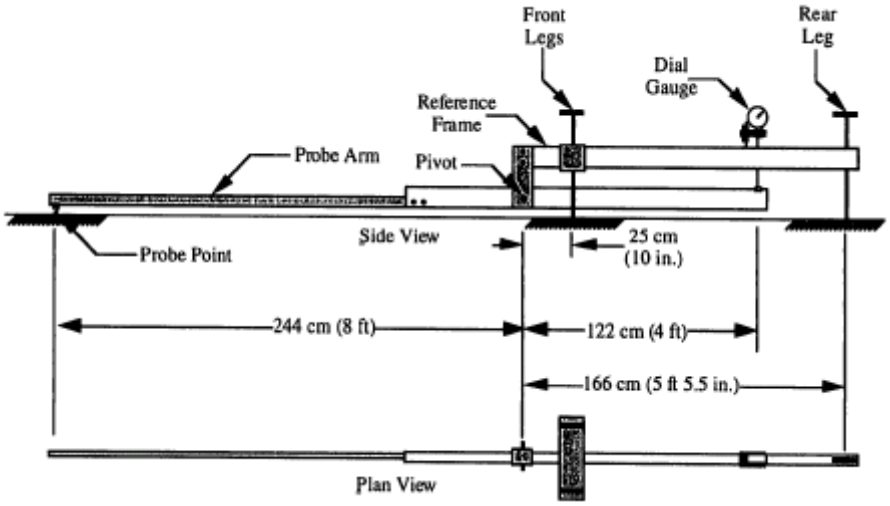

Figure 2.2 Simplified Drawing of Benkelman Beam (after Carneiro, 1966)

2.5.2 Falling Weight Deflectometer

The Falling Weight Deflectometer (FWD) is a standard nondestructive deflection testing device used by many state transportation agencies. It was first developed in France (Bretonniere, 1963). The FWD is properly the most commonly used nondestructive deflection testing device today. It is a trailer mounted device that applies a dynamic impulsive force to the pavement surface. Surface deflection basin is measured using a number of geophones that are arranged in an array. The device generates a dynamic impulsive force to the pavement surface by releasing weights from different heights. The loading system and the array of geophones are mounted on a trailer so that it can be quickly moved from one location to the next. Over the years, different models of FWD devices have become available. Each model has slightly different loading configurations and geophones arrangements. However, they all share the same basic principle.

A schematic diagram of a Dynatest FWD trailer owned by TxDOT is shown in Figure 2.3. This model of FWD is typically equipped with seven geophones (Murphy, 1998). Typical TxDOT FWD load and deflection time histories are shown in Figure 2.4. The typical load duration is around 30 ms, and the pulse travels from the center of the loading pad to each geophone. The peak deflection of each geophone is typically the only deflection data recorded. This configuration is slightly different from the sensor array configuration recommended by the Long Term Pavement Performance (LTPP) program sponsored by the Federal Highway Administration (FHWA), which has a total of nine geophones along the sensor array.

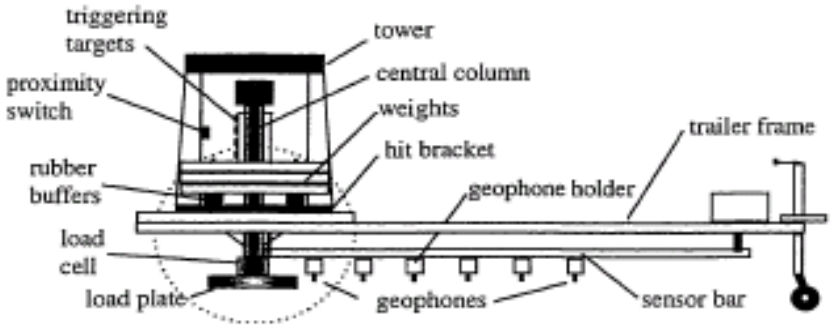

Figure 2.3 Schematic of a Dynatest FWD trailer (from Murphy, 1998)

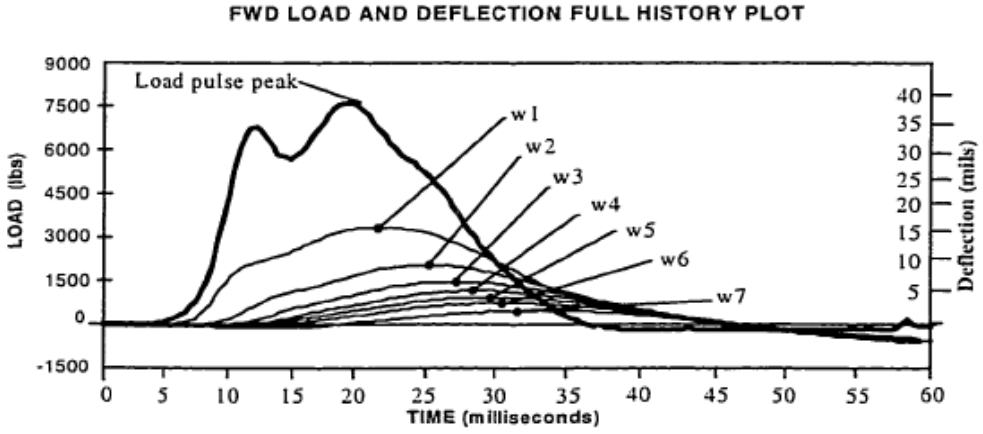

Figure 2.4 FWD load and deflection time history plot (from Murphy, 1998)

The LTPP program was initiated in 1987. Different sections of highways throughout the United States and Canada were established and subsequently monitored to observe the long-term performance of these pavements. In an effort to compare and analyze FWD deflection data from different test sections collected at different times, the FHWA provides guidelines and configuration of the FWD device for use in collecting FWD deflection data under the LTPP program (FHWA, 2000). The LTPP program uses a Dynatest Model 8000 FWD for collecting in-situ deflection data. This model has nine geophones and the geophones are arranged as shown in Figure 2.5. The LTPP also provides guidelines pertaining to the FWD testing operation. Also, a concise summary of factors that can affect the FWD deflections are also provided. For example, variations of the pavement cross-section (i.e. layer thickness, layer material property, and subgrade support) certainly affect the measured deflections. However, there are other factors that can significantly affect the pavement deflection. These factors are: (1) environmental factors, (2) pavement discontinuities, and (3) variability in the pavement structure (FHWA, 2000).

Different comparison studies between the FWD and other nondestructive deflection testing devices can be found in the literatures (Bentson, 1989; Hudson, 1987; Smith, 1985). As noted above, there are many factors that can influence the deflection measurements collected in the field. Other than factors that are specific to the test site, equipment-related factors can also have a significant role. Murphy (1998) summarizes equipment-related factors that can influence the deflection measurements collected using a FWD. Some of these factors include sensor misalignment, geophone and load cell calibration and other equipment-variability factors (Murphy, 1998).

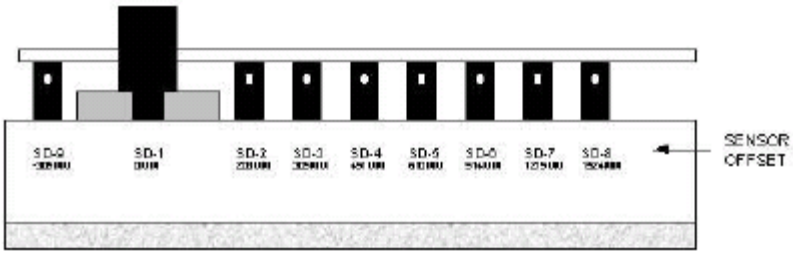

(a) Fixed Sensor Configurations for All Testing

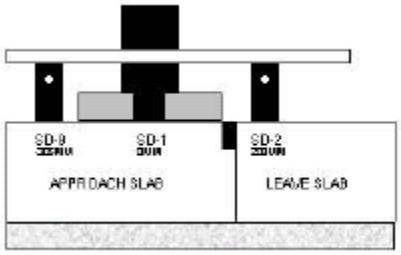

(b) Approach Slab Load Transfer

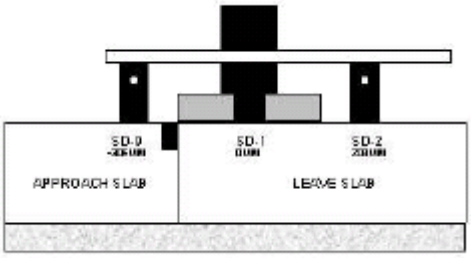

(c) Leave Slab Load Transfer

Figure 2.5 Geophone Configuration of the FWD Model used in the LTPP Program (after FHWA, 2000)

2.5.3 Dynaflect and Road Rater

The Dynaflect is an NDT device that is mounted on a small two-wheeled trailer. The Dynaflect has a static load of approximately 2-kips (9 kN) and a steady-state sinusoidal dynamic load ranging from 1.5 to 2.5 kips (6.8 to 11.2 kN) at a frequency of 8 Hz can be applied (Huang, 1993). The force is applied to the pavement using two rubber

coated steel wheels. A photograph of a Dynaflect is shown in Figure 2.6, and the typical sensor configuration is shown in Figure 2.7.

Figure 2.6 Photograph of a Dynaflect (Geo-Log, Inc)

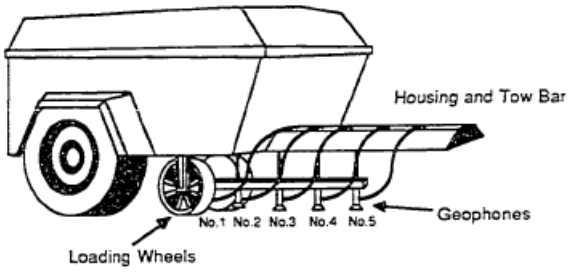

(a) The Dynaflect with Load Wheels in the Test Position

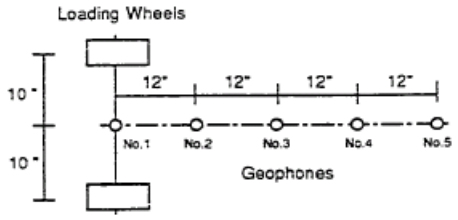

(b) Configuration of Dynaflect Load Wheels and Geophones

Figure 2.7 Configuration of Dynaflect Loading Wheels and Geophones Locations (After Haas et al., 1994)

Another NDT device which is functionally very similar to a Dynaflect is known as the Kentucky Road Rater. The Kentucky Road Rater has a 160-lb vibrating mass and applies loads to the pavement through two feet. The surface deflections are measured at 1-ft spacing from the center of the load (Kallas, 1985). This particular device has not gained use in other states.

2.5.4 LaCroix Deflectograph

There are a variety of automated deflection beam devices which have been used. They all function on the same principle as the Benkleman Beam device. Hudson et al., 1987 compared some of these devices, which include the Benkelman Beam, California Traveling Deflectometer, and the LaCroix Deflectograph. The Lacroix Deflectograph is a continuous deflection measuring device that was developed in the mid-1960s by the Laboratoire Central des Ponts et Chaussees in France. The deflection measurements are made under a 28.6-kips (13-metric tonne) load. Two sets of deflection measurements are made along the inner and outer wheel paths. Deflection measurements are made between each dual tire assembly (Murphy, 1998). A photograph of the beam assembly of a LaCroix Deflectograph is shown in Figure 2.8, and an illustration of the operating principles of this device is shown in Figure 2.9. Basically, it is an automatic version of a Benkleman Beam. The testing vehicle travels at about 1.2 mph and takes deflection measurement at every 11.5 ft (Hunter et al., 2000). This assembly is pulled at twice the testing vehicle speed, and then come to a stop as the rear wheels of the Deflectograph approach the deflection measurement location (Croney et al., 1997).

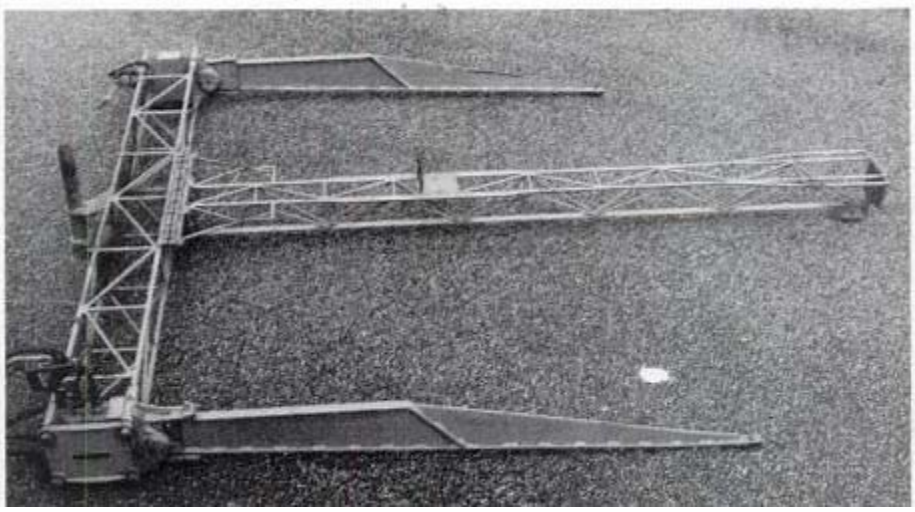

Figure 2.8 Beam Assembly of a LaCroix Deflectograph (from Croney et al., 1997)

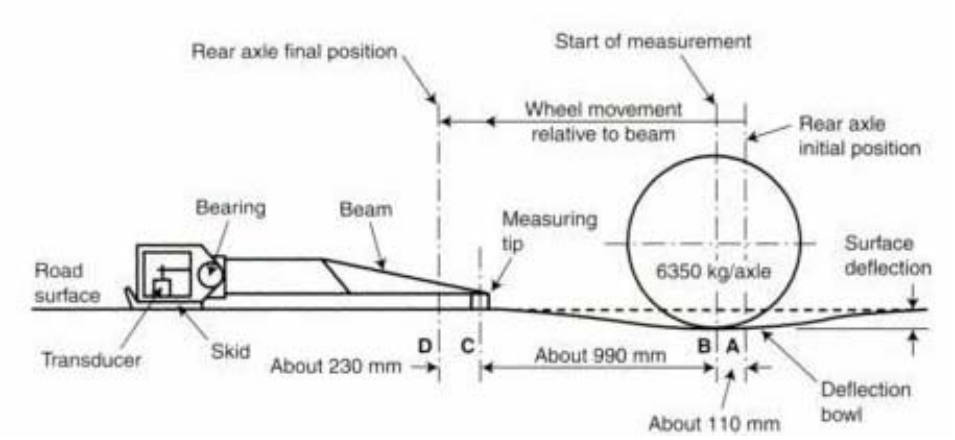

Figure 2.9 Principles of a LaCroix Deflectograph (from Hunter, 2000)

2.5.5 Rolling Weight Deflectometer

The Rolling Weight Deflectometer (RWD) is a trailer-mounted prototype device. It typically has a set of four non-contact optical sensors which measure the distance between the optical sensor and the pavement surface using the principle of optical triangulation. Based on a two-step process developed by Harr at Purdue University, the pavement deflection due to the dead weight of the back wheel can be determined. This

two-step process is illustrated in Figure 2.10. In the first step, sensors A, B and C collect deflections over a region that is away from the deflection basin. In the second step, sensors B, C and D measure the deflections at the previous three locations. A simple algorithm is then used to calculate the pavement deflection due to the load wheel.

Unlike other nondestructive deflection testing devices, the RWD does not measure the entire deflection basin. Furthermore, the approach proposed by Harr requires the supporting beam, where the optical laser sensors are mounted, to remain perfectly straight at all times during testing. This issue was solved in the 1990s by running a laser beam along the long axis of the supporting beam to provide a reference datum for correcting any vibration and thermal beam bending during the RWD operation.

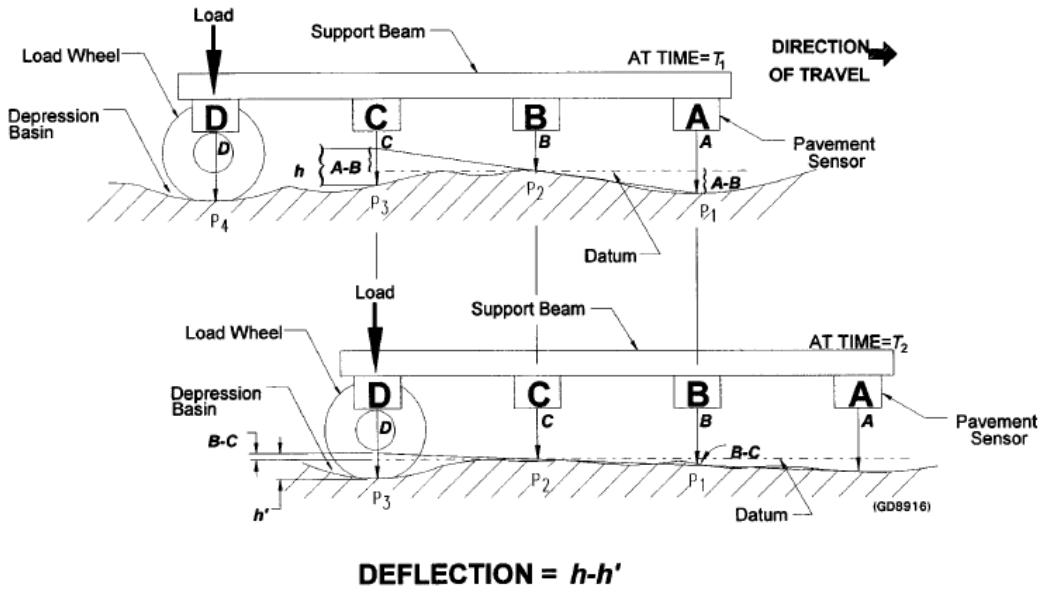

Figure 2.10 Illustration of principle used for deflection measurement in a Rolling Wheel Deflectometer (from Johnson et al., 1998)

In July 2003, a comprehensive field test was carried out in College Station, Texas. During this field test, the RWD, FWD and RDD were used to measure the deflections of 38 individual sections of highway (ERES Consultants, 2004). The 53-ft (16.2-m) trailer was custom designed which minimizes the laser sensor range needed to accommodate the bouncing motion of the truck during testing. A photograph of the RWD is shown in Figure 2.11. Furthermore, the trailer has a natural frequency between 1.45 and 1.8 Hz, which is sufficiently low compared to the high-frequency vibration of the 25.5 ft (7.8 m) aluminum supporting beam (Bandara and Briggs, 2004)

Figure 2.11 Photograph of the RWD Trailer and Laser Displacement Sensors

2.5.6 Ground Penetrating Radar (GPR)

Even though the ground penetrating radar (GPR) does not measure pavement surface deflection, it has been used extensively in recent years to measure thickness of different pavement layers. Therefore, it is briefly discussed below.

As noted earlier, backcalculation of deflection data often require accurate estimation of the layer thicknesses, and GPR units are often used to collect layer thickness measurements. The GPR transmits short pulses of electromagnetic (EM) energy into the pavement from an antenna. Depending on the required depth of penetration, two types of antennas can be installed on a GPR unit. The first type is a horn antenna which has an EM-pulse wavelength that can resolve asphalt layers down to around 2.5 in (63.5 mm). The second type of antenna is known as the ground coupled dipole antenna, which allow greater depth penetration (i.e. penetrate two to three times greater depth than the horn antenna). However, the poor thickness resolution of the ground coupled dipole antenna limited its use to the evaluation of thicker subbase or subgrade material.

The GPR share a lot of similarity with the shallow seismic reflection methods which are used in sub-surface geophysical exploration. Both methods utilize wave theory, and GPR signals are usually characterized by changes in reflection amplitudes and changes in the arrival times of reflected waves (Kim, 2003). The GPR measures the reflected electromagnetic (EM) waves that occur at the interface boundary between two materials which have different dielectric constants.

A diagram which illustrates a typical GPR signal is shown in Figure 2.12. The EM-pulse is reflected back to the GPR receiver at each interface. The magnitude of the reflection is governed by the ratio of the dielectric constants of the two materials which forms the reflection boundary. The difference in arrival time between subsequent reflections allows the computation of the layer thicknesses using wave theory (Bandara and Briggs, 2004). A software program is often used to post-process the GPR raw signal, and the GPR data are usually presented as a continuous pavement profile in a graphical form as shown in Figure 2.13.

Limitations of the GPR include: (1) resolving thin layers, (2) resolving the layer boundary with two very similar dielectric constants, and (3) assumptions of homogenous and nonconductive layers.

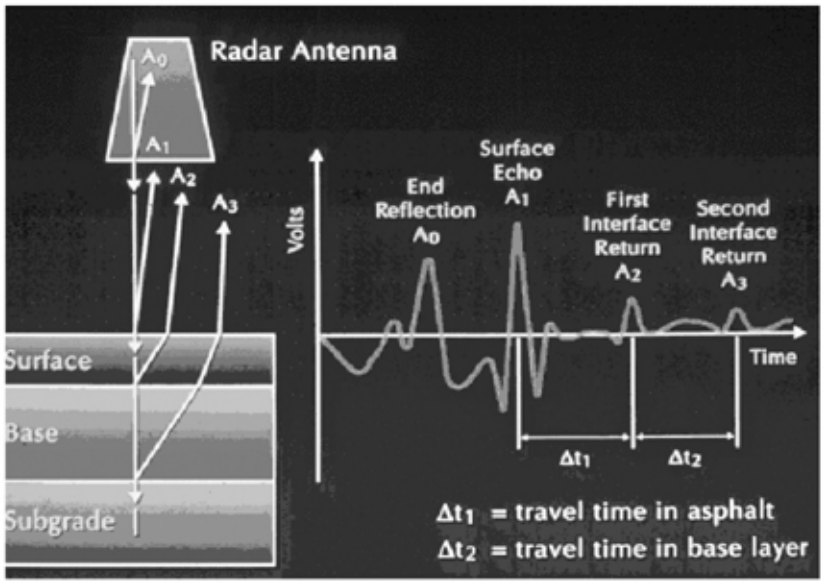

Figure 2.12 Typical GPR Reflection Signal (from Bandara et. al, 2004)

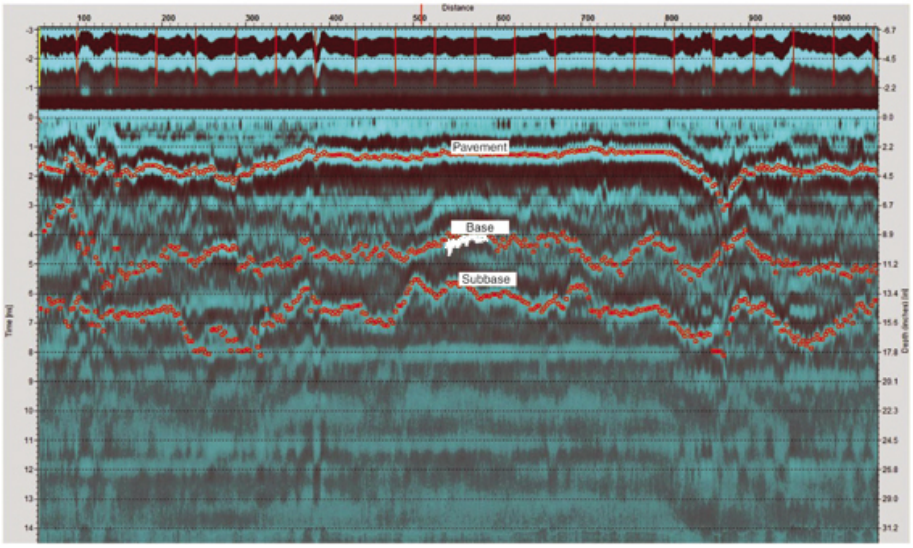

Figure 2.13 Typical GPR layer thickness profile (from Bandara et. al, 2004)

2.6 SUMMARY

In United States, state transportation agencies had utilized nondestructive deflection testing techniques to evaluate the structural condition of a pavement for many years. This chapter contains a brief summary of the common applications of deflection data. The limitations of these applications are also presented. Then, several commonly used nondestructive testing devices and their properties are also summarized in this chapter.

Chapter 3 Rolling Noise Characteristics in RDD Measurements

3.1 INTRODUCTION

Researchers at the University of Texas at Austin first developed the RDD in the late 1990's. A comprehensive description of this device is given by Bay in 1997 (Bay, 1997). The RDD is a truck-mounted system that dynamically loads the pavement and simultaneously monitors the pavement response while continuously moving at about 1.6 km/hr (1 mph). The RDD is a research prototype device that was converted from a Vibroseis, a geophysical exploration tool. A schematic diagram of the device is shown in Figure 3.1(a). The major components include: (1) an electro-hydraulic dynamic loading system, (2) a force measurement system, (3) an array of rolling sensors that are located underneath the RDD, and (4) a distance measurement system. A typical rolling sensor configuration is shown in Figure 3.1(b). This device was developed in cooperation with the Texas Department of Transportation and the Federal Highway Administration. The main objective of this developmental project was to design a prototype, heavy-load, deflection profiler for nondestructive testing of pavements.

The RDD has a gross weight of about 50 kips (222 kN). The hydraulic system can generate dynamic sinusoidal forces ranging from about 2 to 70 kips peak-to-peak (9 to 310 kN peak-to-peak) over a frequency range of about 20 to 100 Hz. Furthermore, the hydraulic system generates a constant hold-down force ranging from 3 to 40 kips (13 to 180 kN). During testing, the RDD applies both static and dynamic loads on the pavement surface. A typical RDD loading function is shown in Figure 3.2(a). The loading function is composed of a constant component that is the static hold-down force and a steady-state sinusoidal component that is the dynamic force. The static and dynamic forces are

transferred to the pavement through two polyurethane loading rollers. The applied forces are measured by four load cells located between the loading rollers and the upper loading platform. Rolling sensors, that are located at multiple points under the RDD as shown in Figure 3.1(b), continuously measure the dynamic deflections due to the sinusoidal loading. As a result, continuous deflection profiles are obtained. An example set of measurements that was made on a flexible pavement with three rolling sensors is shown in Figure 3.2(b). Each line in Figure 3.2(b) represents a continuum of deflection readings from one rolling sensor along the test section, with the deflection values representing an averaged deflection measured over every 2 to 3 ft (0.6 to 0.9 m). In general, the deflection level decreases as the sensor is located further away from the loading rollers. Deflection basins can also be constructed from the continuous profiles at selected locations as shown in Figure 3.2(c). The deflection basins shown in Figure 3.2(c) were measured at three highlighted locations in Figure 3.2(b). The shape and the absolute value of each deflection basin represent the structural stiffness at different points along this flexible pavement.

A rotary optical encoder is used to measure the distance traveled along the pavement during testing. Individual analog signals from the load cells, rolling sensors and the distance encoder are continuously recorded by a PC-based data acquisition system during testing. These measurements are then post-processed after field testing to obtain the continuous deflection profile as shown in Figure 3.2(b).

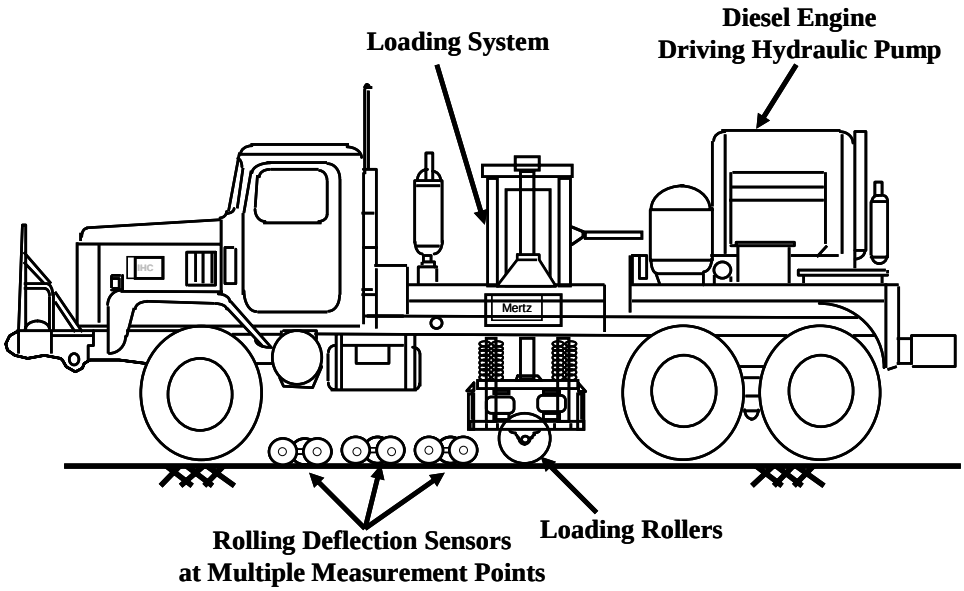

(a) Rolling Dynamic Deflectometer

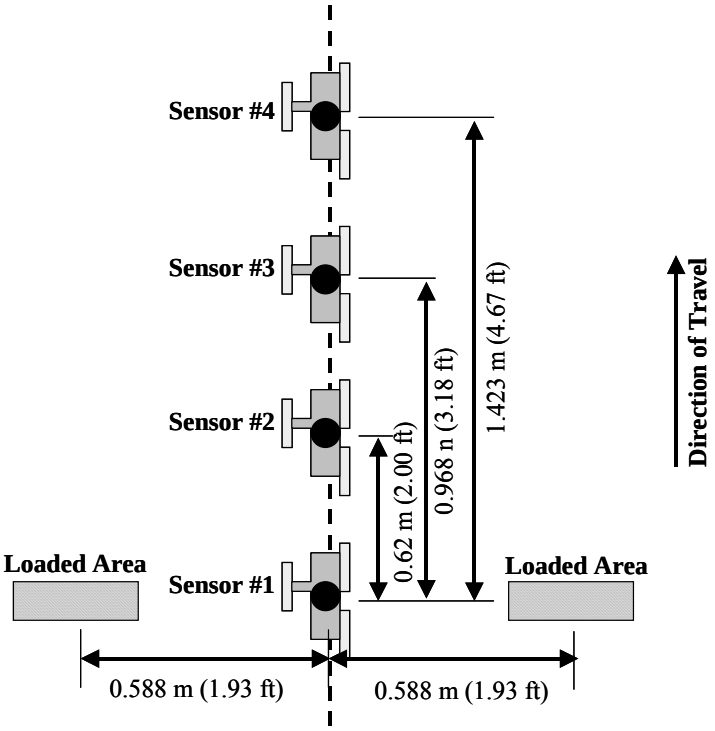

(b) Typical Rolling Sensor Configuration for RDD Testing

Figure 3.1 General RDD arrangement with rolling sensor array (from Lee et al., 2005).

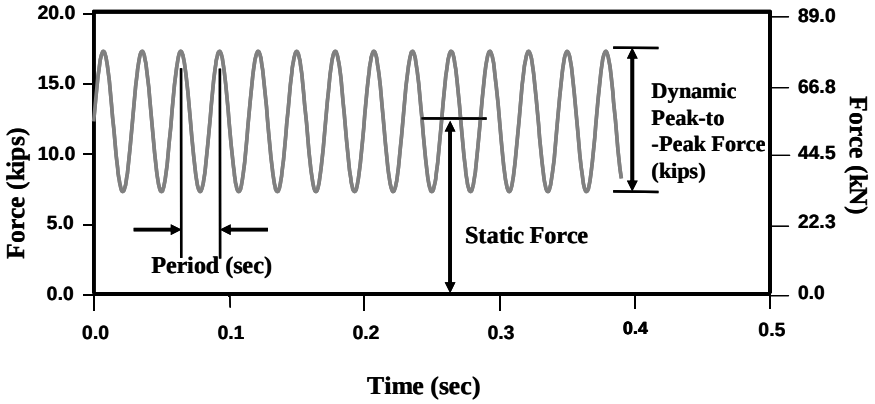

(a) Static and Dynamic Components of the RDD Loading Function

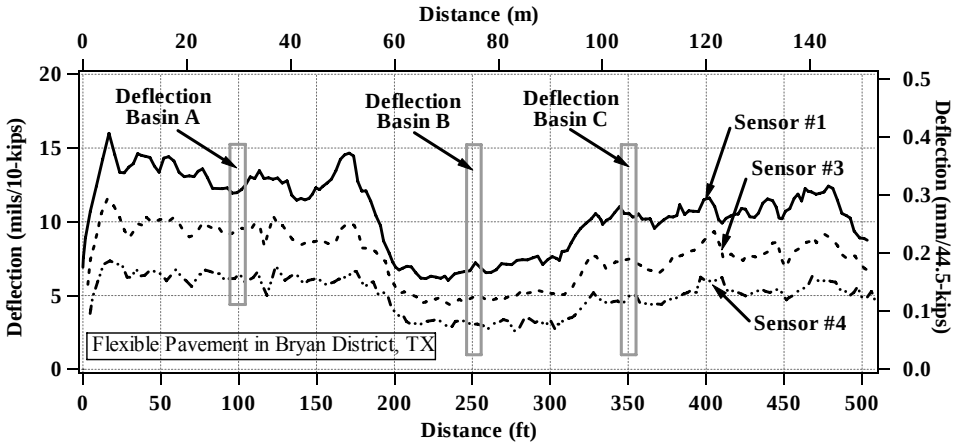

(b) Continuous Deflection Profiles at Three Different Sensor Locations Adjusted to a 10-kips (44.5-kN) Peak-to-Peak Force Level

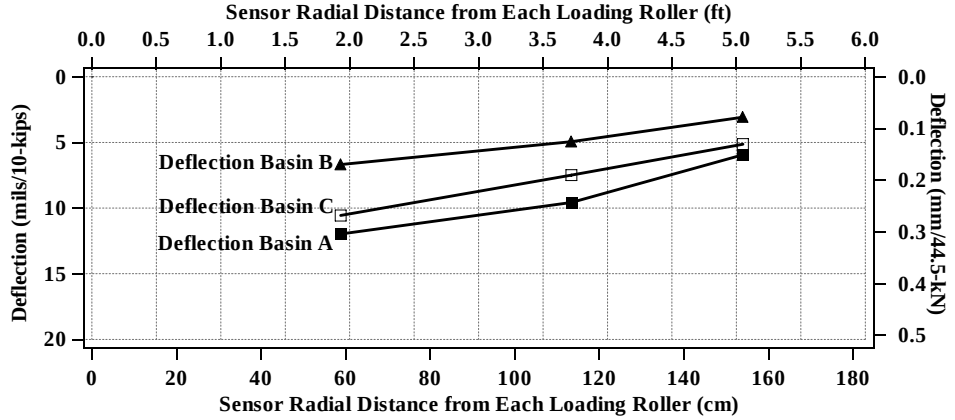

(c) Deflection Basins at Three Points Along the Profile

Figure 3.2 Typical RDD loading function and continuous deflection profile (from Lee et al., 2005).

The major benefit of the RDD is the ability to collect continuous deflection profiles along a test path, providing virtually 100% coverage of the entire project length. By using carefully designed rolling sensors to measure pavement surface dynamic deflections, the RDD is able to collect deflection measurements as the RDD rolls along the test path. The RDD rolling sensors are contact-type sensors. Each sensor is a geophone mounted on a 3-wheel cart. Unlike other non-contacting type sensors where a known position datum is required to obtain accurate measurement, the RDD rolling sensor measures the surface deflections accurately using an inertial reference. During the development of the second-generation rolling sensors, there were two issues being considered. First, due to the contacting nature of the RDD rolling sensors, the testing speeds are limited by the ability of the rolling sensor to stay in-contact with the pavement surface. As long as the rolling sensor stays in-contact with the pavement, the sensor measures the pavement surface motion correctly.

Second, rolling sensor design needs to minimize rolling noise measured. It is important to note that rolling noise is present whenever "in-motion" deflection measurements are made. Rolling noise does exist whether deflection measurements are made using contact or non-contact type sensors. Rolling noise is the result of "in-motion" deflection testing devices collecting deflection measurements along a surface that is not perfectly smooth (i.e. all pavements have roughness and different elevation profiles). The rolling noise is a function of the roughness of the pavement, sensor configuration (e.g. diameter of rolling wheels) and testing speed. In general, the rolling noise is reduced when large diameter rolling wheels were used to make the deflection measurements. This is because large diameter rolling wheels will ride over less high points along the pavement surface, which the rolling sensor in effect "sees" the pavement as a smoother pavement than it actually is. On the other hand, if a non-contact type sensor such as a

laser displacement sensor is used, the rolling noise in the measurement will be very high because the small diameter laser target tracks the entire roughness of the pavement (i.e. the small laser target can be seen as a rolling wheel with diameter that approaches zero).

These two issues are addressed during the development of the second-generation rolling sensor. This development forms one part of the dissertation research. The design of the second-generation rolling sensor is presented in Chapter 4, and field trials using the second-generation rolling sensor are presented in Chapter 5. Based on the results collected during field trials along different pavements, it was found that the second-generation rolling sensor can achieve a test speed of 3 mph. At a testing speed of 1 mph, the level of rolling noise measured with the second-generation rolling sensor is less than the rolling noise level measured with the first-generation rolling sensor.

At present, the RDD uses digital filters to isolate the RDD signal at the operating frequency from the surrounding noise in the frequency domain. Even though it has been demonstrated in field trials using the second-generation rolling sensor that the measured rolling noise level has been reduced, a study of the rolling noise characteristics is conducted to help design digital filters with improved performance in both the time and frequency domains. In this chapter, a study of the rolling noise characteristics is presented. The findings from this chapter are to be used in the digital filter design methodology presented in Chapter 6.

3.2 RDD ROLLING NOISE

The RDD applies both static and dynamic forces on the pavement as illustrated in Figure 3.1. The dynamic force is a single-frequency (f_o) sinusoidal load with a period $T_o=1/f_o$. Typically, the frequency of the dynamic force ranges between 20 and 40 Hz. In contrast, the Falling Weight Deflectometer (FWD) applies a dynamic impulsive force on the pavement by dropping different weights from pre-defined heights. The typical

duration of the impulsive load is around 30 ms (i.e. predominant frequency around 33 Hz) for FWD load drops. Since the RDD applies a single-frequency load, it is a very robust dynamic deflection measurement technique. This robustness comes from the fact that any frequencies outside the RDD loading frequency can be regarded as measurement noise, and therefore can be effectively filtered using different digital filters. This characteristic allows the RDD to distinguish pavement surface deflections induced by the actual dynamic forcing function from other sources of noise (primarily rolling noise).

In most engineering applications, it is desirable to measure signals with high signal-to-noise ratios (SNR). However, this is often impossible due to different sources of noise that are present in the signal measurements. Some of the noise sources measured during RDD testing are listed as follows:

1. rolling noise caused by the rolling sensor moving along a rough pavement surface (can be smooth or rough),
2. harmonic distortion from the RDD hydraulic loading system,
3. noise from motion of surrounding traffic,
4. noise from the RDD truck engines,
5. noise from the RDD truck moving along the pavement,
6. noise from construction activities,
7. electro-magnetic interference (EMI) from electrical power sources (i.e. 60-Hz power line noise in the United States), and
8. electro-static radio frequency interference (RFI)

In fact, the signal collected by each rolling sensor during RDD testing contains a lot of noise in the time domain. Also, the noise level can be of the same magnitude as the deflection signal itself. Typical rolling sensor time records when the RDD is in the stationary and in the rolling modes are shown in Figure 3.3.

After the raw RDD measurements were collected, data analysis is performed on the collected data to obtain the RDD deflection profile for the pavement. The deflection profile is usually presented in terms of mils per 10 kips (mm/44.5 kN). The current data analysis procedure uses a notch-pass digital filter to attenuate noise signals at frequencies outside the RDD operating frequency. As a result, only deflections at the RDD operating frequency are identified and used to calculate the RDD continuous deflection profile. This data analysis procedure requires knowledge of the precise RDD operating frequency. This knowledge is available because a function generator is used to drive the RDD at a precise loading frequency.

Even though the current analysis procedure can attenuate noise effectively, it is always a good practice to reduce the level of noise as much as possible in the measurements. Since the typical RDD operating frequency ranges from 20 to 40 Hz, the 60-Hz power line noise is easily filtered out and does not affect the measurements in any significant way. However, both traffic noise and rolling noise contain wide-band frequencies, and the characteristics of their spectra may affect the RDD measurements if much energy is concentrated near the selected RDD operating frequency. In this case, digital filters cannot separate noises at the operating frequency from the actual RDD deflection signal.

To illustrate this point, Figure 3.4(a) shows a three-second time record of a typical RDD rolling sensor measurement, and Figure 3.4(b) shows the same signal represented in the frequency domain. It is difficult to judge the quality of the measurement just by looking at the RDD rolling sensor signal in the time domain. But the RDD signal at 35 Hz is clearly shown in the frequency domain. All the other frequency components shown in Figure 3.4(b) are regarded as noise. As can be seen in Figure 3.4(b), there is obviously some noise present at the RDD operating frequency, but it is very small percentage

(typically less than a few percent) of the RDD deflection signal and, hence, is neglected in the present data analysis procedure.

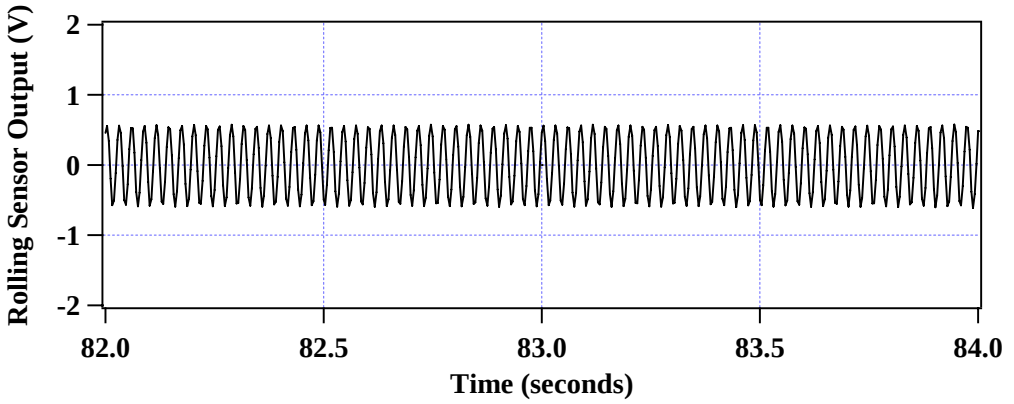

(a) When Stationary

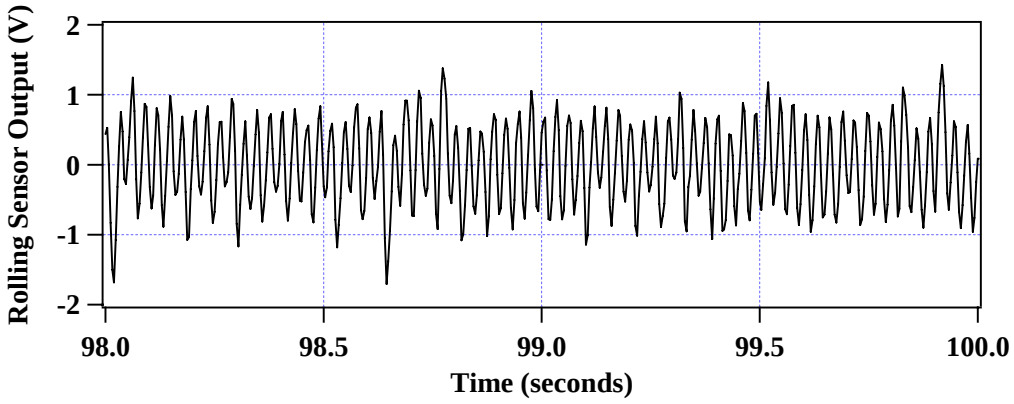

(b) When Rolling

Figure 3.3 Two-Seconds of the Time Record of a Rolling Sensor on a Highway Rigid Pavement: (a) When Stationary and (b) When Rolling.

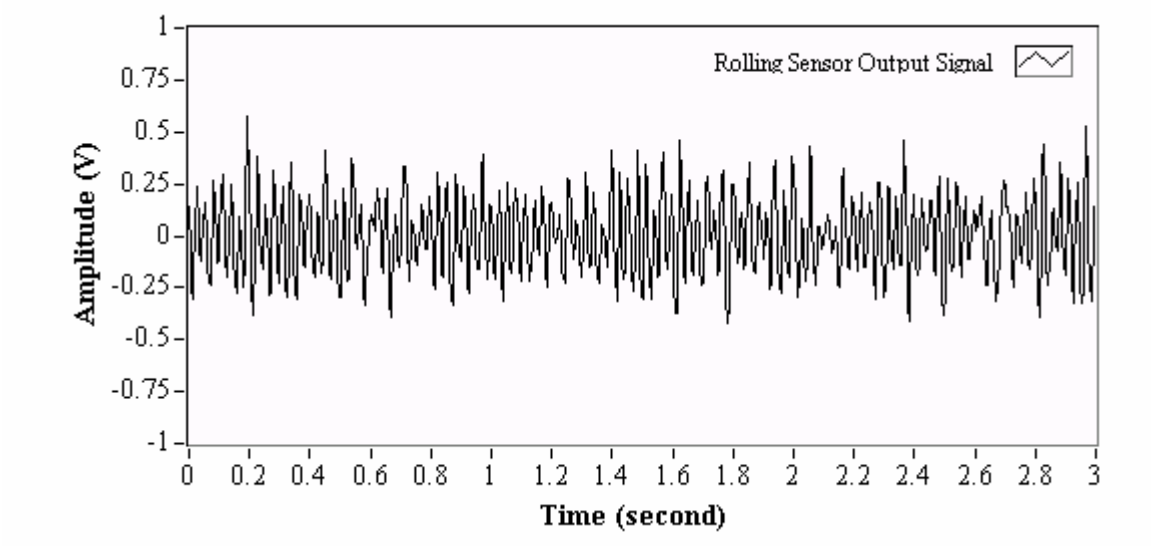

(a) Time Domain

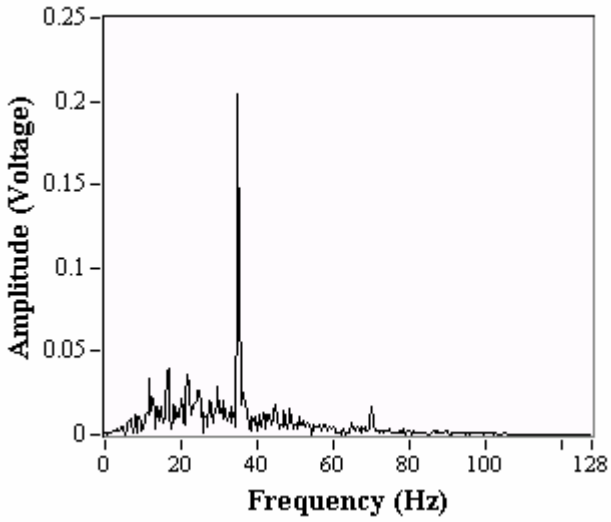

(b) Frequency Domain

Figure 3.4 Typical RDD Rolling Sensor Output Signal in the Time and Frequency Domains.

Rolling noise spectra calculated using a 6-inch (152 mm) diameter wheel rolling on a synthetic pavement surface are shown in Figure 3.5. As shown by Bay (1997), different diameters of rolling wheels will theoretically generate different noise spectra

when rolled at a speed of 1 fps (0.68 mph). As the rolling wheel diameter increases, the level of rolling noise tends to decrease as shown in Figure 3.5. Two parts of this research are to build a new rolling sensor (with larger wheels) and to study the rolling noise characteristics of this sensor.

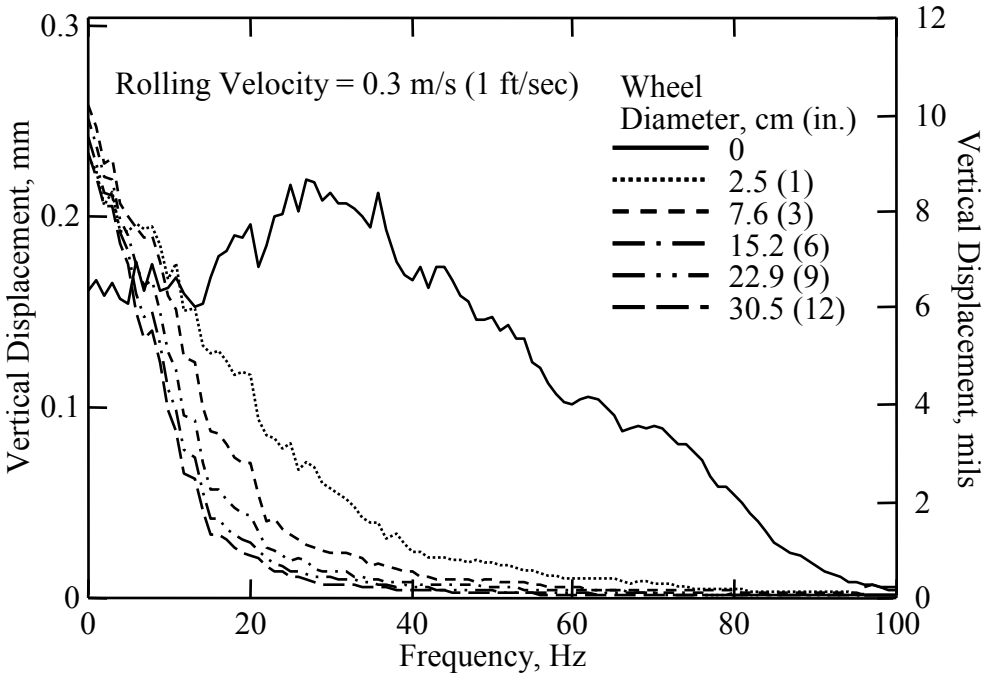

Figure 3.5 Vertical Displacement Spectra for Wheels with Various Diameters Rolling Over a Synthesized Pavement Surface (from Bay et al., 1998).

3.3 DESIRABLE CHARACTERISTICS OF ROLLING NOISE

Rolling noise can be regarded as a random process which is controlled primarily by the testing speed and the diameter of the wheels mounted on each rolling sensor. In general, rolling noise increases with increasing testing speed. Also, a rolling sensor with larger diameter wheels generates lower noise level than a rolling sensor with smaller diameter wheels when rolled over the same pavement at the same speed. The two main improvements in the second-generation rolling sensor are larger diameter wheels and the addition of a hold-down force to keep the sensor in contact with the pavement at higher

testing speeds. These improvements allow RDD deflection profiles to be collected at speeds up to 4.5 fps (3 mph), and to generate less rolling noise than if the same measurements were made using the first-generation rolling sensors. The desired rolling noise characteristics are as follows.

1. It is desirable to have a low level of rolling noise when compared with the RDD signal. This noise level yields a higher signal-to-noise ratio (SNR).
2. It is desirable to have rolling noise that is evenly distributed across the frequency domain rather than concentrated rolling noise near the RDD operating frequency.
3. It is desirable to have rolling noise located far away from the RDD operating frequency in the frequency domain. This relationship requires a digital filter with moderate frequency response in the transition band (often resulting in better time resolution). This noise distribution improves the time (or spatial) resolution of the digital filter.

3.4 FREQUENCY CONTENT OF ROLLING NOISE

One factor that impacts the beneficial filtering performance of a digital filter is the frequency content of the rolling noise. Since the RDD outputs a dynamic sinusoidal force at a single frequency, the precise input frequency is known. This fact allows the design of an effective digital filter to remove rolling noise at frequencies other than the RDD operating frequency. In general, a more demanding filter is required if a sharp transition band is needed to distinguish between pass-band and stop-band frequencies. The primary reason for using a notch-pass filter with a sharp transition band is to ensure that little to no rolling noise that is located close to the operating frequency is allowed to pass through the digital filter. By the same token, the distribution of the rolling noise in the frequency

domain governs a particular digital filter design if an optimal digital filter design is pursued. Therefore, the characteristics of rolling noise are discussed next.

The RDD signal and different types of synthetic rolling noises are illustrated in Figure 3.6. In each case, the synthetic rolling noise has a different distribution in the frequency domain. In Figure 3.6(a), the RDD signal is superimposed with a low level of uniformly distributed rolling noise. In Figure 3.6(b), the RDD signal is superimposed with a moderate level of uniformly distributed rolling noise. In Figure 3.6(c), the RDD signal is superimposed with a "1/f-type" of rolling noise. The amplitude of this type of noise decreases with increasing frequency. If an optimal digital filter design is pursued, a digital filter should be chosen according to the distribution of the rolling noise measurement.

3.5 THEORETICAL ROLLING NOISE MODEL

During the design of the rolling sensor, Bay (1997) used a simplified theoretical model to study the effects that different parameters have on the measured rolling noise. Some of the parameters that were studied include:

1. diameter of rolling wheels,
2. number of rolling wheels, and
3. RDD test speed.

In his study, Bay modeled a rigid wheel rolling over a synthetic pavement surface which had vertical obstacles that are much smaller than the diameter of the rigid wheel. Furthermore, the model assumed that the rigid wheel traveled in a circular arc path as it moved over different vertical obstacles. This is the only study which has been carried out to understand the rolling noise characteristics of the rolling sensor. However, due to the limited number of test sites that were available at that time, a complete field database

could not be established to investigate the field rolling noise characteristics of the rolling sensor.

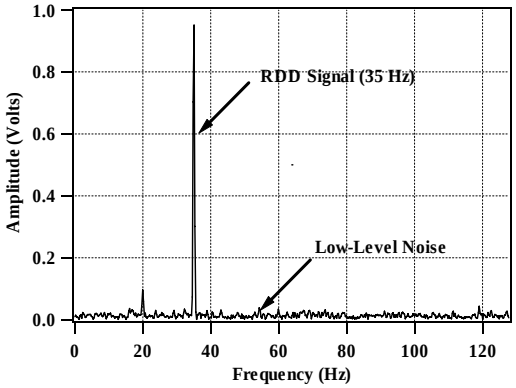

(a) RDD signal and low level of uniformly distributed rolling noise.

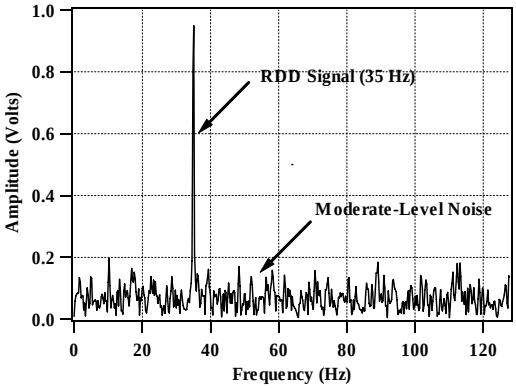

(b) RDD signal and moderate level of uniformly distributed rolling noise.

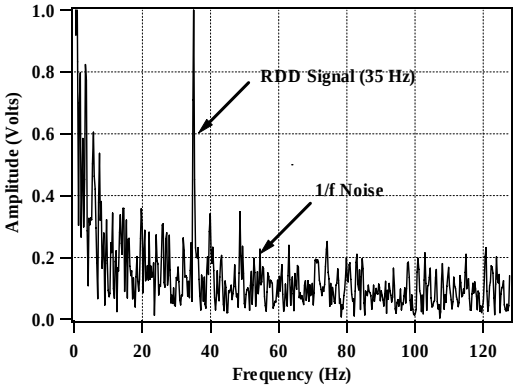

(c) RDD signal and non-evenly distributed rolling noise.

Figure 3.6 RDD Signal and Different Types of Synthetic Rolling Noise.

3.6 FIELD RDD NOISE MEASUREMENTS

Over the last seven years, the RDD has been used in many different project-level studies. These studies include test sites that range from local farm-to-market roads to runways at major international airports. The types of pavements include different types of concrete pavements, flexible pavements and composite pavements. A list of the RDD test sites are given in Table 3.1.

Table 3.1 List of RDD Test Sites Between Year 1999 and 2005.

	Surface Pavement Type	Airport / Highway	State	Year	Location	Highway / Airport
1	Concrete	Airport	Texas			Fort Worth Alliance Airport
2	Concrete	Airport	Georgia			Atlanta Hartsfield Airport
3	Concrete	Airport	Texas			George Bush Airport
4	Concrete	Airport	Texas			Fort Worth Meacham Airport
5	Concrete	Highway	Pennsylvania		Mercer County	IH-80
6	Concrete	Highway	Texas		Fort Worth	Business 287
7	Concrete	Highway	Texas		Dallas	US-175
8	Concrete	Highway	Texas		Hillsboro	IH-35
9	Concrete	Highway	Texas		Beaumont	IH-10
10	Concrete	Highway	Texas		Orange	IH-10
11	Concrete	Highway	Texas		Dallas	IH-20
12	Concrete	Highway	Texas	1999 / 2000	Fort Worth	IH-30
13	Concrete	Highway	Texas		Sulphur Spring	IH-30
14	Concrete	Highway	Texas		West	IH-35
15	Concrete	Highway	Texas		Texas City	IH-45
16	Concrete	Highway	Texas	2005	Fort Worth	IH-30
17	Concrete	Highway	Texas		Bryan / College Station	SH-6
18	Concrete	Highway	Texas		Port Arthur	SH-73
19	Concrete	Highway	Texas		Houston	SH-225
20	Concrete	Highway	Texas		Navasota	US-6
21	Concrete	Highway	Texas	2005 / 2006	Queen City	US-59
22	Concrete	Highway	Texas		Beaumont	US-69
23	Concrete	Highway	Texas		Beaumont	US-69
24	Concrete	Highway	Texas		Bells	US-69
25	Concrete	Highway	Texas		Whitewright	US-69
26	Concrete	Highway	Texas		Lufkin	US-69
27	Concrete	Highway	Texas	2003 / 2005	Gainsville	US-82
28	Concrete	Highway	Texas		Silsbee	US-96
29	Concrete	Highway	Texas		Seagoville	US-175
30	Concrete	Highway	Texas		Wichita Falls	US-281
31	Concrete	Highway	Texas		Wichita Falls	US-287
32	Concrete	Highway	Texas		Vernon	US-287
1	Asphalt Concrete (AC)	Airport	Texas			Grayson County Airport
2	Asphalt Concrete (AC)	Highway	Texas		Artesia Wells	IH-35
3	Asphalt Concrete (AC)	Highway	Texas		College Station	SH-21
4	Asphalt Concrete (AC)	Highway	Texas		Navasota	FM-2
5	Asphalt Concrete (AC)	Highway	Texas		Greenville	IH-30
6	Asphalt Concrete (AC)	Highway	Texas	2001 - 2004	Marshall	IH-20
7	Asphalt Concrete (AC)	Highway	Texas		Austin	IH-35
8	Asphalt Concrete (AC)	Highway	Texas		Austin	MLS Pad
9	Asphalt Concrete (AC)	Highway	Texas		Navasota	SH-6
10	Asphalt Concrete (AC)	Highway	Texas		Bryan / College Station	SH-47, FM,, IH-45
11	Asphalt Concrete (AC)	Highway	Texas		Bryan	SH-21
12	Asphalt Concrete (AC)	Highway	Texas		Crowell	US-70
13	Asphalt Concrete (AC)	Highway	Texas		Puducah	US-83
14	Asphalt Concrete (AC)	Highway	Texas		Childress	US-93

There are a number of benefits in studying the characteristics of noise in RDD measurements. First and most important of all, one can better define the specifications for digital filters. Since the rolling sensor will inevitably contains noise, a better digital filter is one which can effectively attenuate noise and yet maintain a satisfactory time (or spatial) resolution. The alternative RDD analysis procedure is discussed in Chapter 6 and the digital filters proposed in this study are based on knowledge gained in the rolling noise characteristics that is discussed in the remainder of this chapter.

3.7 ROLLING NOISE CHARACTERISTICS

It has been observed in this work that the noise characteristics depend on the following three factors during testing:

1. Pavement surface roughness,
2. Testing speed, and
3. Level of deflection (depends on the type of pavement).

The types of pavements where RDD deflection profiles were collected often controls the expected level of deflections and surface roughness. Diagrams illustrating the properties of different pavement types and the effect that these properties has on the average rolling noise level is shown in Figure 3.7. Three observations were made:

(1) the average rolling noise increases with increasing testing speed,

(2) the average rolling noise increases with increasing pavement surface roughness,

(3) the average rolling noise increases (SNR decreases) in the decibel scale with decreasing level of deflection being measured, and

(4) lastly, the testing speed, level of deflection and pavement surface roughness affects the average rolling noise and their noise characteristics in the frequency domain.

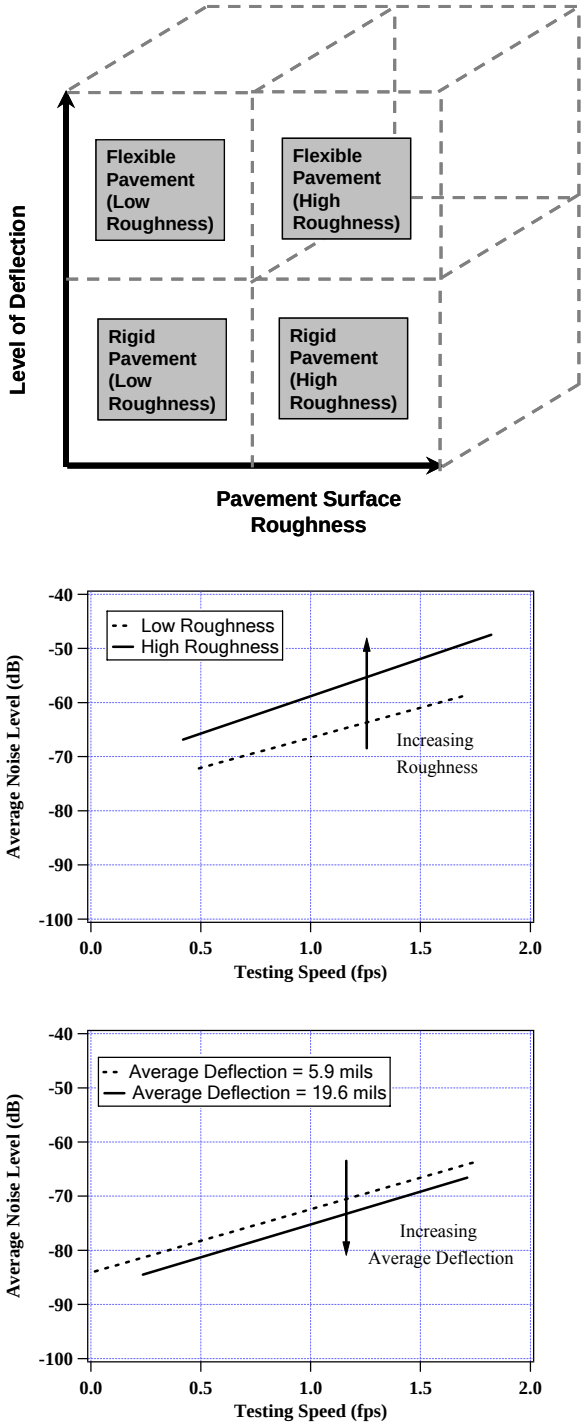

Figure 3.7 Properties of Different Pavement Types and Influence on the Measured RDD Rolling Noise.

An FFT spectrum for rolling sensor measurements collected along the runway of Grayson County Airport is shown in Figure 3.8. The FFT spectrum can be separated into three parts: (1) RDD signal (at the fundamental operating frequency), (2) higher-order harmonics of the RDD signal, and (3) background rolling noise. The first spike at 35 Hz represents the fundamental energy at the RDD operating frequency. There are two more spikes located inside the Nyquist frequency band. These are first and second harmonics of the RDD signal and are located at multiples of the RDD operating frequency. These higher order harmonics are mainly caused by the servo hydraulic loading system. It is also affected by the nonlinearity of a pavement site to a minor degree in comparison to the characteristic of the servo hydraulic system. Typical harmonic distortion observed in different field-operated hydraulic loading system is about 20%. It was found that the harmonic distortion not only changes between different pavement sites, but it also changes throughout the day during operation. One way to characterize the higher order harmonics is to use the total harmonic distortion (THD) calculation. The THD can be calculated using Eq. 3.1:

$$THD = \frac{\sqrt{H_1^2 + H_2^2 + ... + H_N^2}}{F} \tag{3.1}$$

where H_j = amplitude in the j^{th} harmonic

F = amplitude of the fundamental

The background rolling noise forms the remaining part of the FFT spectrum. The vertical axis can be presented in either arithmetic or decibel (dB) scales. The relationship between these two scales is given in Equation 3.2:

$$dB = 20\log_{10}\left(\frac{V_1}{V_{reference}}\right) \qquad (3.2)$$

where V_1 = voltage of the signal measured, and

$V_{ref.}$ = voltage of the reference signal (in this dissertation, the signal at RDD operating frequency is used as the reference signal)

In general, it was observed that the background rolling noise is fairly constant at frequencies near but below the RDD operating frequency. At frequencies above the RDD operating frequency, the noise amplitude decreases linearly with increasing frequency. With this knowledge in mind, the background rolling noise can be approximated with a rolling noise envelope as shown in Figures 3.8 and 3.9. Such a rolling noise envelope can help define the required digital filter specification (i.e. the required filter attenuation over a frequency range). The noise envelope has a constant part up to 40 Hz, which is the highest RDD operating frequency that would typically be used. Then, the envelope decreases linearly with increasing frequency above 40 Hz.

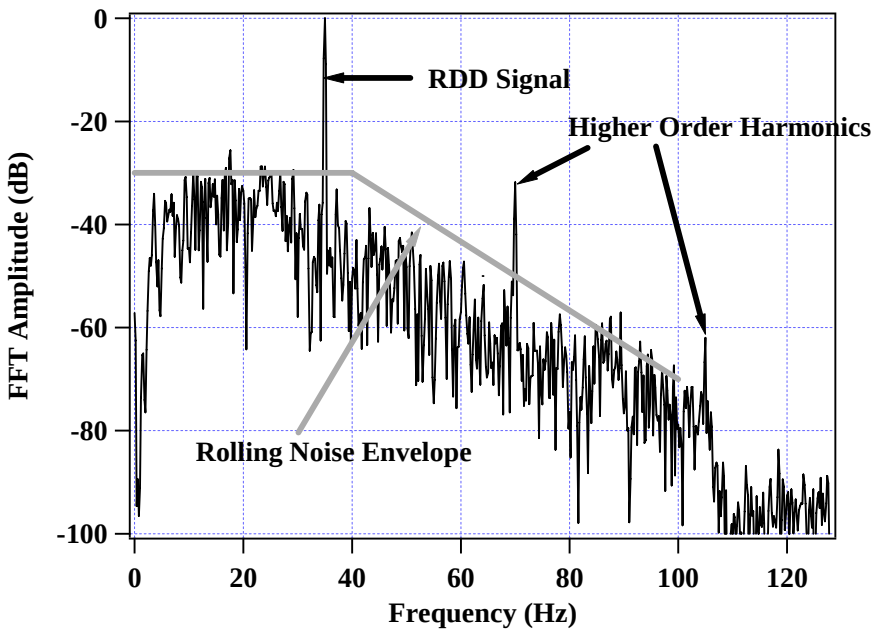

Figure 3.8 FFT Spectrum of a Rolling Sensor Measurement Collected Along a Flexible Runway Pavement at Grayson County Airport.

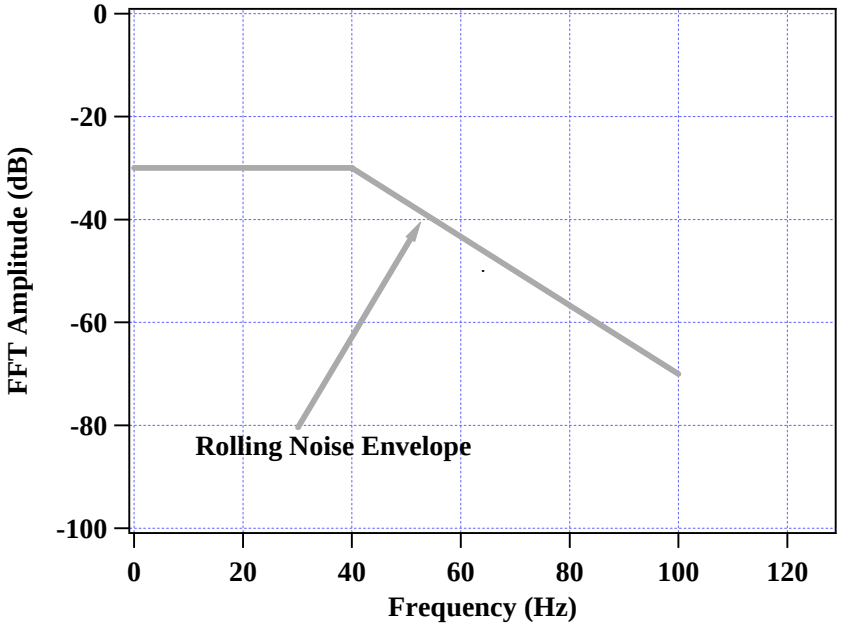

Figure 3.9 An Approximate Rolling Noise Envelope.

In this rolling noise study, it was found that the testing speed is a dominant factor which controls the measured rolling noise characteristics. The average noise floor has an approximate linear relationship with the mean speed, as shown in Figure 3.10. Furthermore, the gradient for the sloping part of the noise envelope (i.e. 40 Hz to 100 Hz) is also controlled by the testing speed. A least-squared, best-fit line, using a linear model of Y = a X + b, is drawn for the part of the noise envelope above 40 Hz. The relationship between the best-fit slope coefficient (a) and intercept (b) with mean RDD speed is shown in Figures 3.11 and 3.12, respectively. The "a" coefficient decreases with increasing speed, and the "b" coefficient increases with increasing speed. This relationship helps to identify the trend for the assumed noise envelope model.

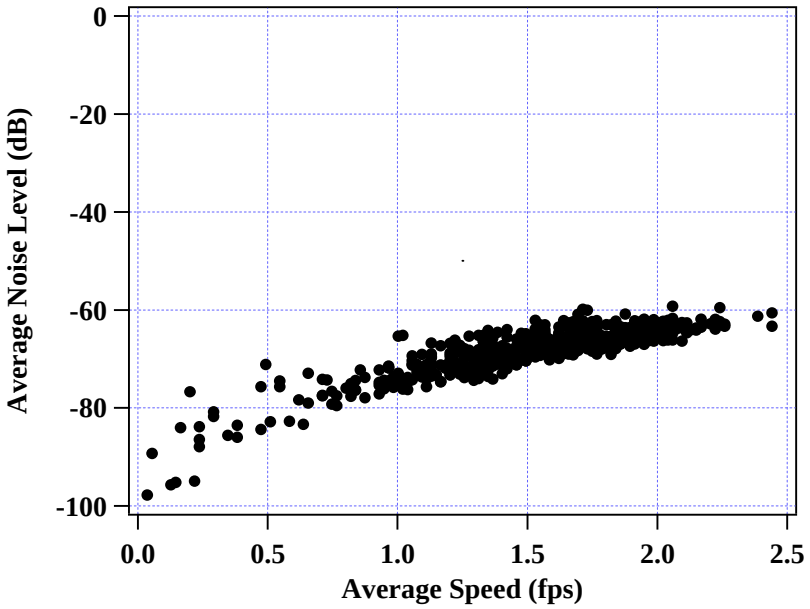

Figure 3.10 Relationship between Average Noise Level and Mean RDD Test Speed Collected Along a Flexible Runway Pavement.

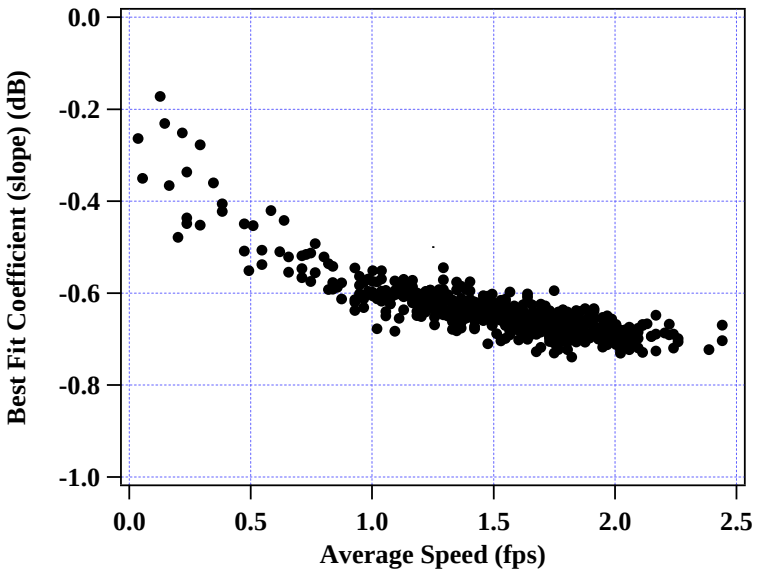

Figure 3.11 Relationship between Best-Fit Slope Coefficient and Mean RDD Test Speed Collected Along a Flexible Runway Pavement.

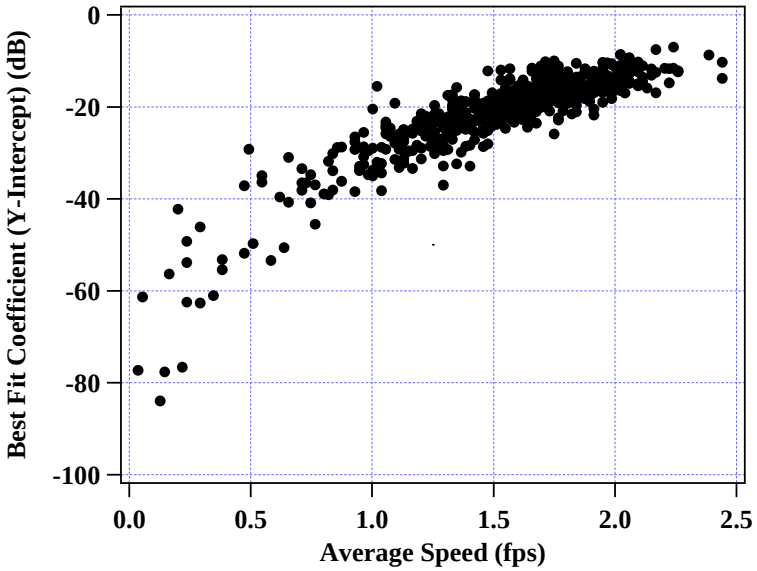

Figure 3.12 Relationship between Best-Fit Intercept Coefficient and Mean RDD Test Speed Collected Along a Flexible Runway Pavement.

A similar analysis was carried out on an RDD record collected along a JCP near Queen City, Texas. An FFT spectrum at a particular instant is shown in Figure 3.13. In this record, the spectrum is also characterized by spikes which represent the RDD signal and other higher harmonics. At this particular site, the second harmonic is not as distinctive as the one shown in Figure 3.8. This can be partially explained by the operating status of the hydraulic system and the difference in site response when the RDD interacts with a flexible and a rigid pavement. The shape of the background rolling noise envelope appears to have a similar shape as the one collected along a flexible runway pavement (shown in Figure 3.8).

The average noise level is plotted against the mean RDD test speed in Figure 3.14. It appears that the average noise floor collected along a concrete pavement increases linearly at a faster rate as the test speed increases. This can be explained by the fact that the roughness of a concrete pavement (more ups and downs when compared with a flexible pavement) increases the level of rolling noise. A linear best fit model is also used to model the background rolling noise at frequency above 40 Hz. The relationship between the best fit slope coefficient (a) and intercept (b) with mean RDD speed are shown in Figures 3.15 and 3.16, respectively.

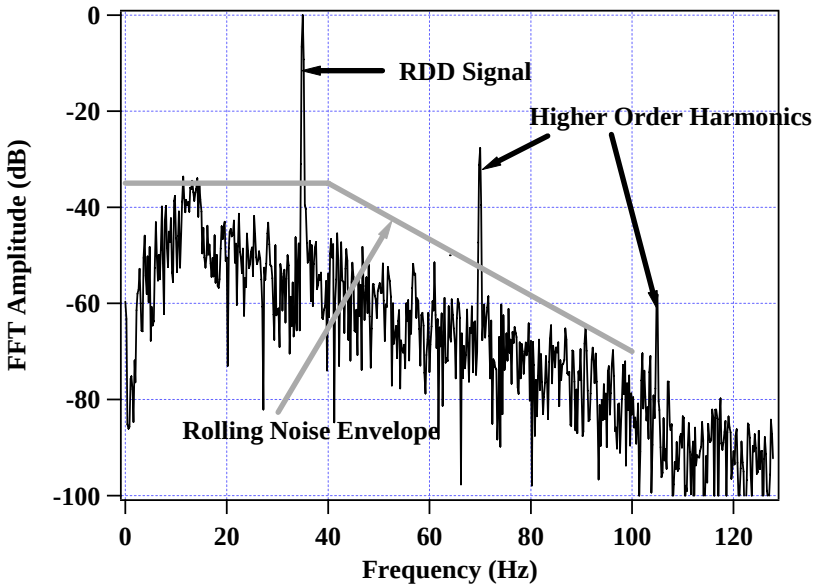

Figure 3.13 FFT Spectrum of a Rolling Sensor Measurement Collected Along a Jointed Concrete Pavement near Queen City, Texas.

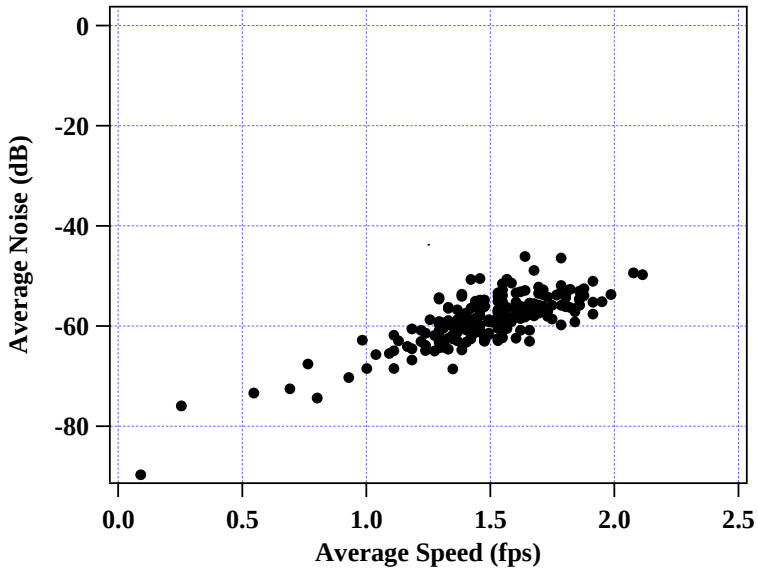

Figure 3.14 Relationship between Average Noise Level and the Mean RDD Test Speed Collected Along a Jointed Concrete Pavement.

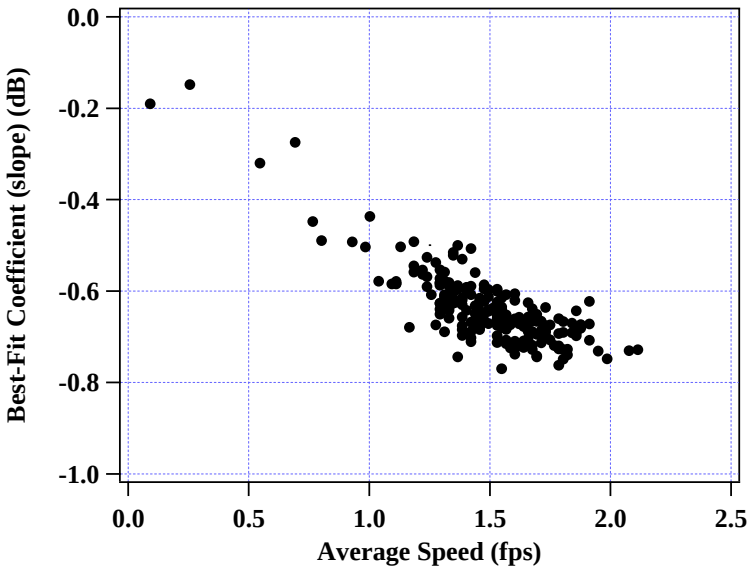

Figure 3.15 Relationship between Best-Fit Slope Coefficient and Mean RDD Test Speed Collected Along a Jointed Concrete Pavement.

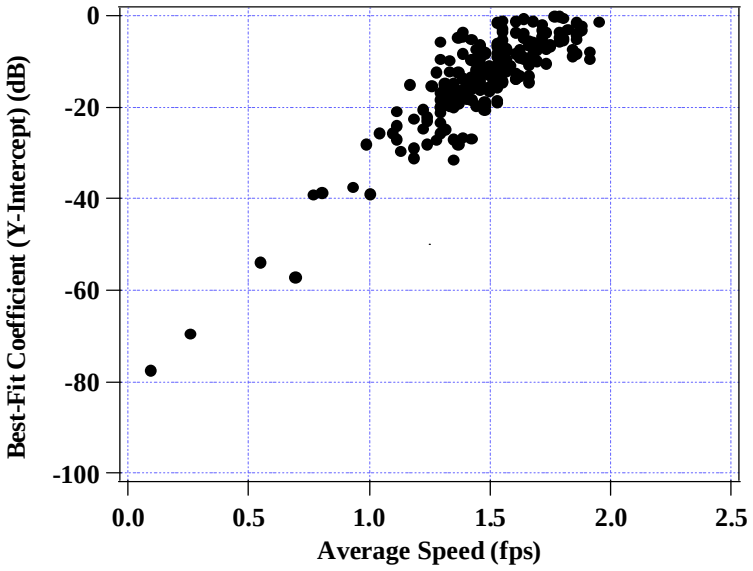

Figure 3.16 Relationship between Best-Fit Intercept Coefficient and Mean RDD Test Speed Collected Along a Jointed Concrete Pavement.

3.8 CURVE FITTING OF ROLLING NOISE AND AVERAGE SPEED

From the earlier discussion, it was concluded that as a general trend, the level of background rolling noise increases as the RDD test speed increases. Based on the RDD data collected in the past, it was observed that the trend between the average noise level and the mean RDD test speed can be approximated with a linear or an exponential equation. The following curve fitting equations were used:

$$Y = K0 + K1 \exp(-K2 * X) \quad (3.3)$$

$$Y = a + b * X \quad (3.4)$$

where a, b, K0, K1 and K2 are curve fitting coefficients,

X = average RDD test speed (fps), and

Y = average rolling noise in decibels (dB) (excluding fundamental and higher-order harmonics of the RDD operating frequency).

The exponential curve fitting model shown in Equation 3.3 appears to be a better fit for concrete pavements. An exponential curve is fitted to a dataset collected along the runway in Fort Worth Meacham Airport as shown in Figure 3.17. This test site consists of Jointed Concrete Pavement. Instead of using an exponential curve to fit this dataset, a bi-linear curve can also be used to approximate this relationship. The same data were approximated using a bi-linear curve as shown in Figure 3.18. This simpler method is justified because the RDD rarely operates in the low test speeds range (i.e. < 0.5 fps). This justification is supported by observing the sparse amount of data points when compared to the normal test speed range of between 0.5 and 1.7 fps.

The linear curve fitting model shown in Equation 3.4 appears to have a better fit on flexible pavements or concrete pavements with asphalt overlay surfaces. A linear curve is also fitted to a dataset collected along Interstate Highway 20 near Marshall,

Texas. This fit is shown in Figure 3.19. This test site consists of an asphalt concrete overlay on top of a Continuously Reinforced Concrete Pavement (CRCP).

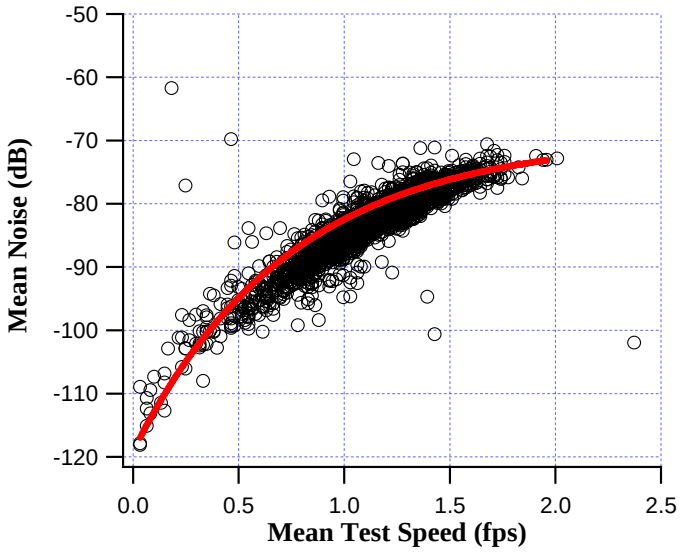

Figure 3.17 Exponential Curve Fit of Data Collected at Fort Worth Meacham International Airport Runway (2002 data).

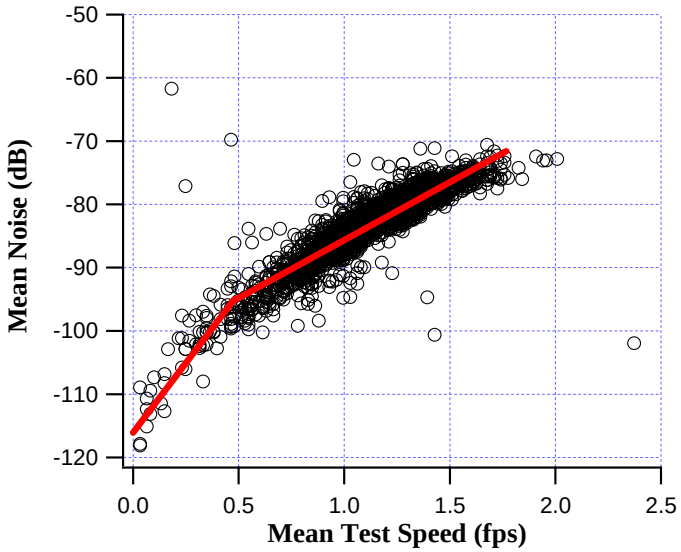

Figure 3.18 Bi-Linear Curve Fit of Data Collected at Fort Worth Meacham International Airport Runway (2002 data).

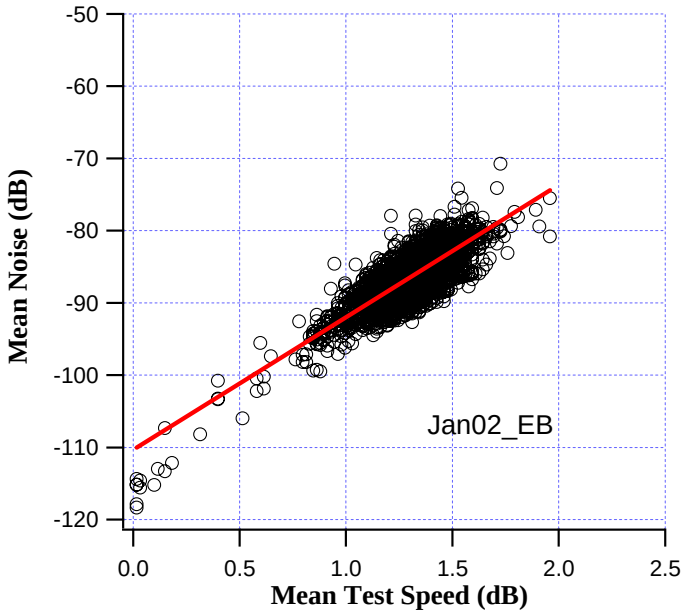

Figure 3.19 Relationship between Mean Rolling Noise and Mean RDD Test Speed Collected Along Interstate Highway 20 near Marshall, Texas.

The general trend of the rolling noise collected by the RDD rolling sensor is shown in Figure 3.20. By studying the measurements made from the rolling sensor #1 (in the frequency domain) at different test sites, the following observations were made:

1. The average rolling noise level increases with increasing test speeds,
2. The rate of change of rolling noise increases more rapidly along a rigid pavement than along a flexible pavement, with respect to increasing test speeds,
3. An approximate rolling noise envelope (as shown in Figure 3.9) can be used to describe the rolling noise components with respect to RDD testing speeds,
4. This approximate rolling noise envelope can be described using two straight segments,

5. Higher order harmonics do exist in the rolling sensor measurements and the THD is controlled by the RDD servo-hydraulic electronics and site material properties, and
6. Increases in high frequency noise with increasing testing speed is the same phenomenon as playing a LP record at higher speed.

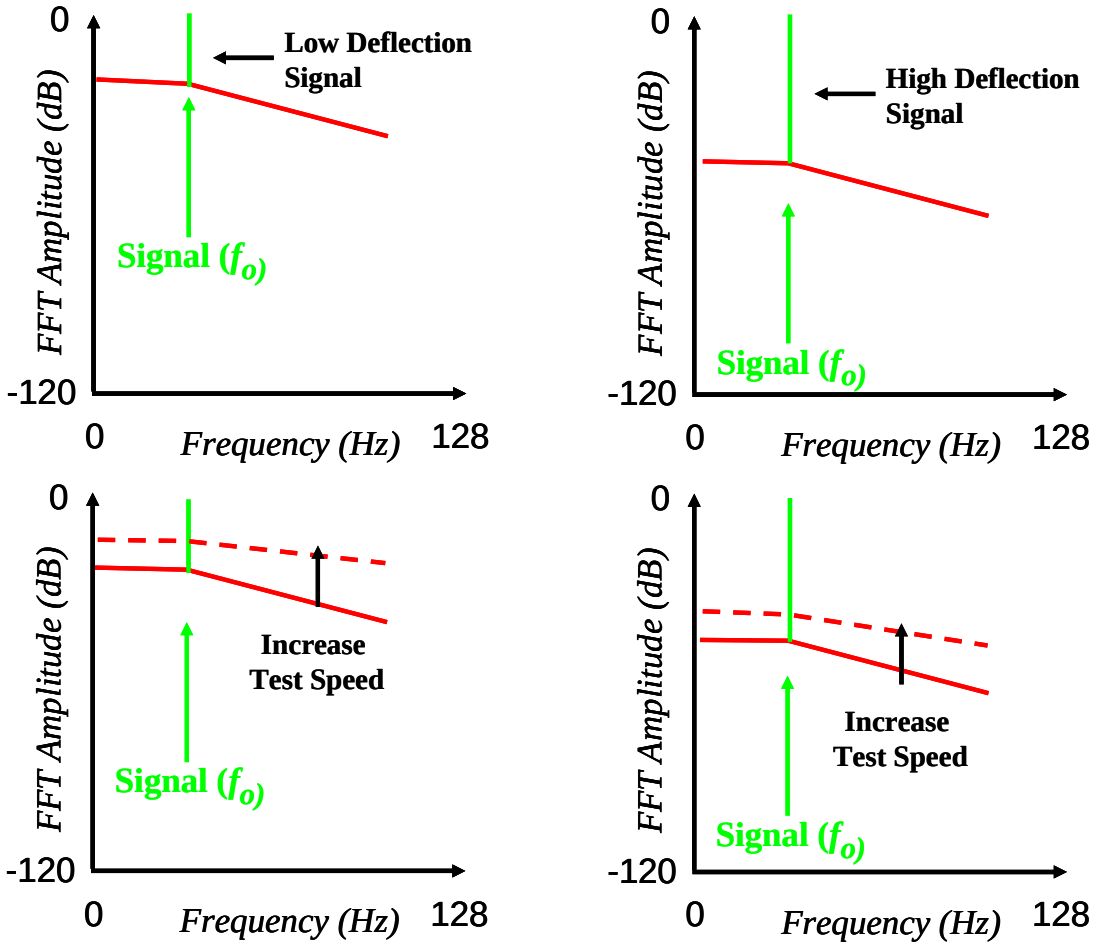

Figure 3.20 General Trends for the Rolling Noise Envelope Collected Along Rigid and Flexible Pavement Test Sites Using the First-Generation Rolling Sensors.

3.9 PROGRESSION OF ROLLING NOISE WITH PAVEMENT SERVICEABILITY

A common term that has been used to describe the performance of a pavement section is the present serviceability index (PSI). It is an objective quantitative measure of the performance of a pavement. Some of the factors which influence the PSI values are:

1. slope variance (SV) = mean of the slope variance in the two wheel paths
2. crack (C) = measures of cracking in the pavement surface
3. patch (P) = measures of patching in the pavement surface
4. rut depth (RD) = depth of rutting along wheel path

An ideal pavement will have a PSI value of 5.0. This PSI value represents the perfect condition of a pavement. In reality, this PSI value can not be achieve in practice, and the typical value being around 4.6 for a pavement with new AC overlay. Over time, the accumulated traffic load reduces the serviceability of a pavement and results in a decline of the PSI value. The rate of declination, as shown in Figure 3.21, is expected to increase with time (i.e. the pavement will start to deteriorate more rapidly after water infiltrates into the first few cracks). As the pavement approaches the end of its design life, the PSI value should approach the terminal PSI value. Pavement rehabilitation should be performed before the pavement approach this terminal PSI value (Huang, 2003). The general trend of the PSI value as a function of time is shown in Figure 3.21. Another parameter which is commonly used to describe the serviceability of a pavement is the International Roughness Index (IRI). The IRI is often computed based on measurements made from different profilers.

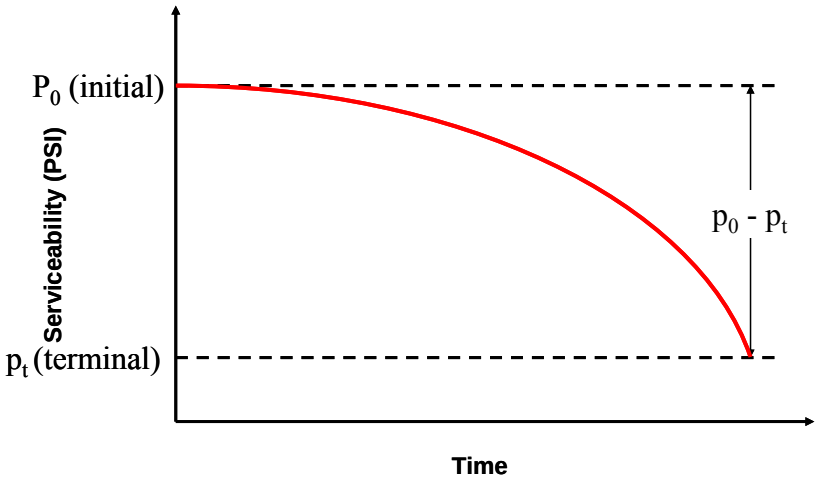

Figure 3.21 Present Serviceability Index (PSI) as a Function of Time.

It was found that the condition (or serviceability) of a pavement also affects the measured rolling noise from the RDD rolling sensors. The rolling noise is expected to be small along a smooth flexible pavement (high PSI value). On the same token, the rolling noise is expected to be large if rolling sensors were rolled along a distressed concrete pavement with lots of severe cracks and patching.

An example is used to illustrate this point further. RDD deflection profiles were used to monitor an overlay rehabilitation project along Interstate Highway 20 near Marshall, Texas between the period of April 2001 and November 2004. The objective of this project-level study was to monitor the condition of this overlay rehabilitation project over time. Table 3.2 summarizes the different stages during which RDD deflection profiles were collected. Then, the rolling sensor records were analyzed in similar manor as discussed in the previous section.

Average noise was computed using the time record collected from rolling sensor #1, which is located mid-way between the two loading rollers. The average noise is plotted against the average test speed for different stages as shown in Figures 3.22

through 3.27. A linear regression line was used to fit the data and the 95% confidence bounds, A, for the regression line were also determined. The average noise at a nominal RDD testing speed of 1.5 fps (1 mph), $Y_{1\ mph}$, was also computed. The A and $Y_{1\ mph}$ values for the six different stages of the Interstate Highway 20 project are summarized in Table 3.3. Plots of the A and $Y_{1\ mph}$ values are as shown in Figure 3.28.

The data shown in Figure 3.22 were collected before the old AC overlay was milled. The PSI value of the pavement has decreased to a point where rehabilitation is needed, and there are a lot of severe distress conditions found on the surface. The localized distress such as cracks and patching resulted in a lot of scattering in the linear regression line. The next stage is shown in Figure 3.23 with data collected along the CRCP surface just after milling the old AC overlay. There is still scattering in the linear regression fit, but the extent of scattering is not as much as the one shown in Figure 3.22. Changes in the average rolling noise are illustrated for the new overlaid pavement in Figures 3.24 through 3.27. These data were collected soon after the overlay was placed and then 11, 23 and 35 months after the AC overlay was placed. During the course of the 35 months, the RDD was used to monitor the condition of this pavement. There were increasing numbers of cracks, full-depth repairs, and patching work that were needed along this section. Some of the cracks were formed shortly after the overlay was initially placed. In all cases, the average noise increases with speed. But, it was found that there are noticeably more scatter in this linear regression function (as shown by the width between the lower and upper 95% confidence intervals) as the pavement roughness and condition worsen with time.

Table 3.2 Schedule of the RDD Testing Along Interstate Highway 20

	Westbound Lane	Eastbound Lane
Stage 1 (before milling)	March 02, 2001	April 05, 2001
Stage 2 (after milling)	August 30, 2001	September 28, 2001
Stage 3 (after overlay)	January 08, 2002	January 09, 2002
Stage 4 (11 months after overlay)	November 13, 2002	November 14, 2002
Stage 5 (23 months after overlay)	November 18, 2003	November 19, 2003
Stage 6 (35 months after overlay)	November 9, 2004	November 10, 2004

Table 3.3 Summary of Confidence Intervals (A) and Average Noise Values (Y_{1mph})

Stage	**95% confidence interval, A (dB)**	**Noise at 1mph, $Y_{1\ mph}$ (dB)**
1	23.4	-53.9
2	12.4	-52.7
3	9.5	-54
4	9.4	-59.5
5	8.19	-62.2
6	10.24	-58.8

*note: These values are shown between Figures 3.22 and 3.27

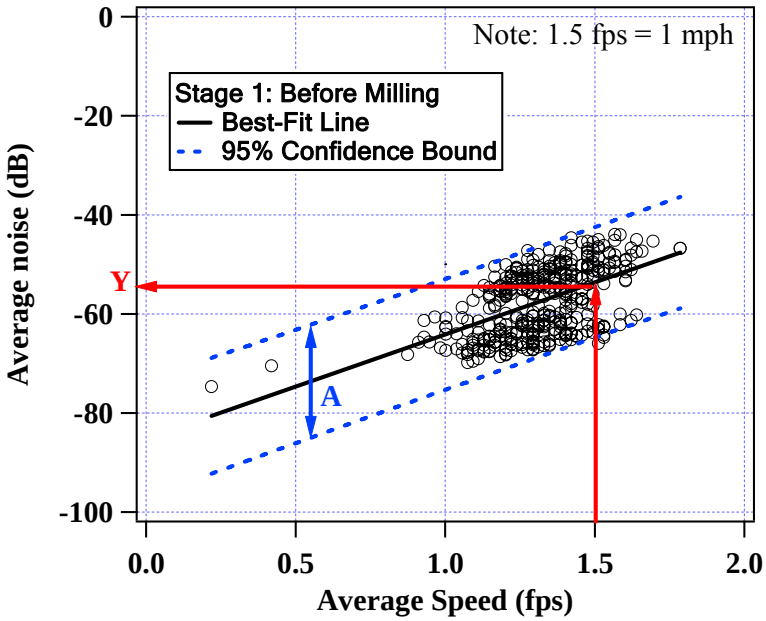

Figure 3.22 Average Noise vs Average Speed along IH-20 near Marshall, Texas (Before Milling)

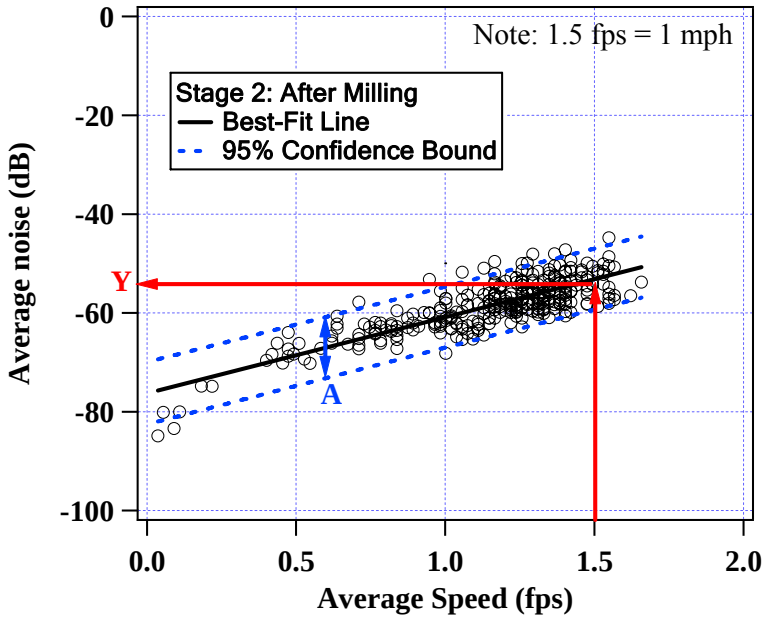

Figure 3.23 Average Noise vs Average Speed along IH-20 near Marshall, Texas (After Milling)

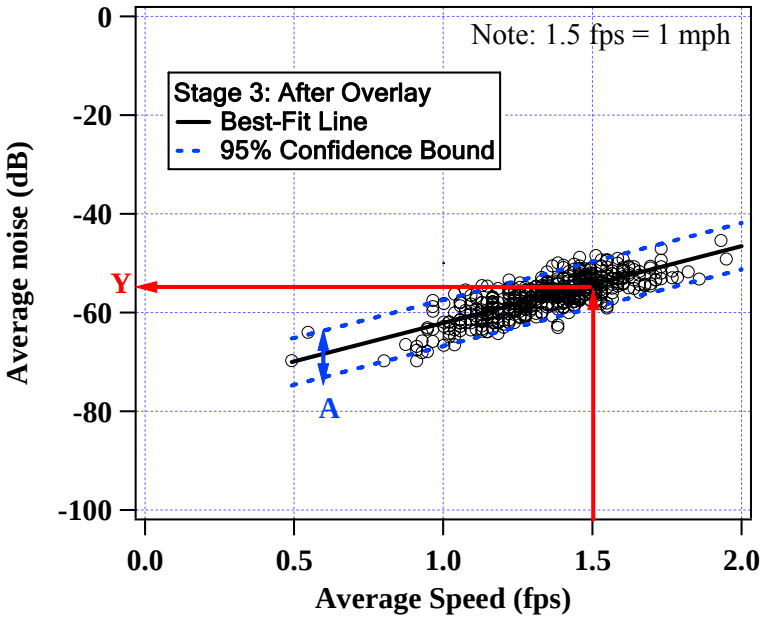

Figure 3.24 Average Noise vs Average Speed along IH-20 near Marshall, Texas (After Overlay)

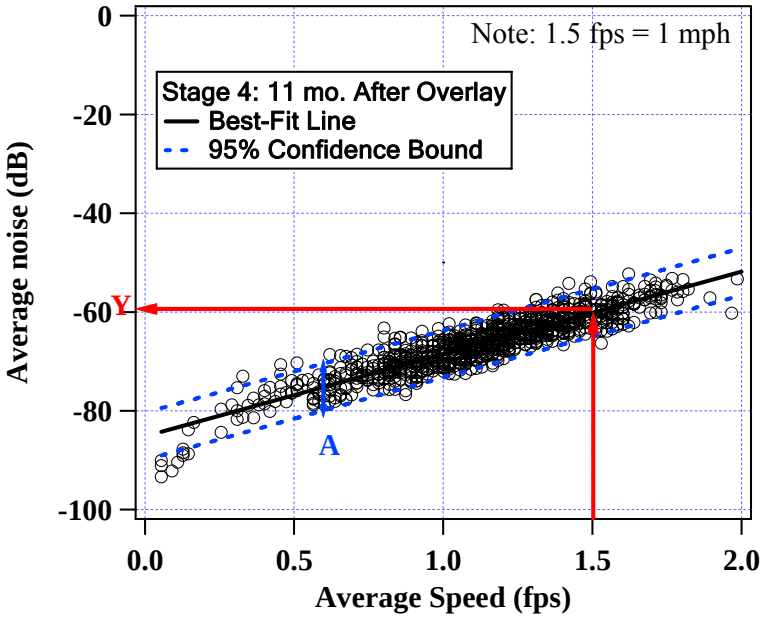

Figure 3.25 Average Noise vs Average Speed along IH-20 near Marshall, Texas (11 Months After Overlay)

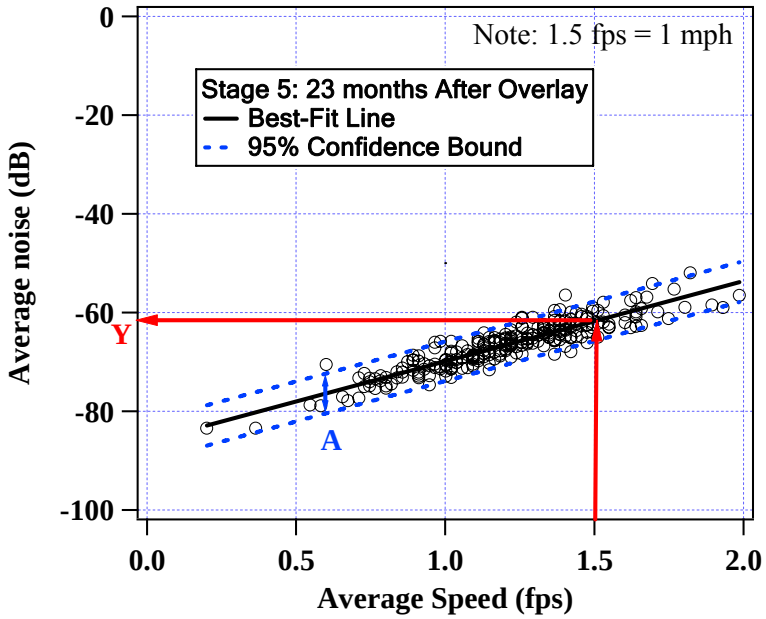

Figure 3.26 Average Noise vs Average Speed along IH-20 near Marshall, Texas (23 Months After Overlay)

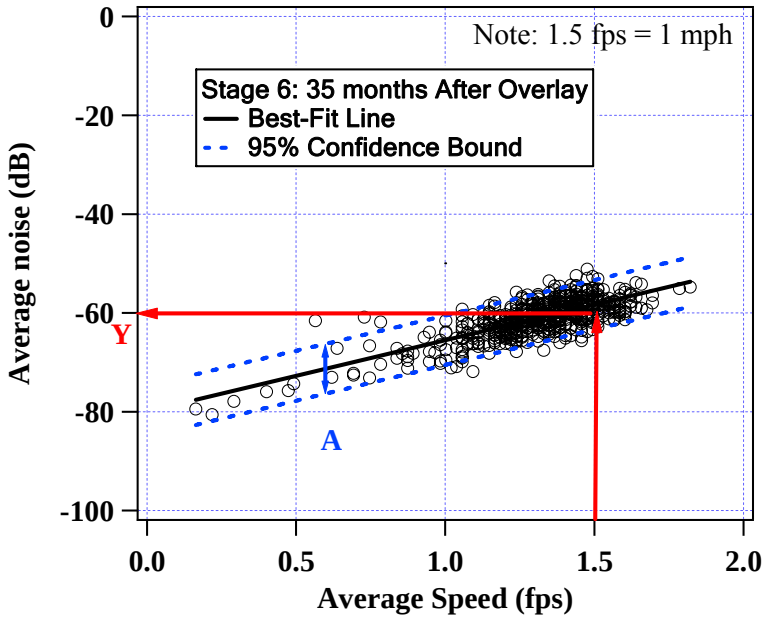

Figure 3.27 Average Noise vs Average Speed along IH-20 near Marshall, Texas (35 Months After Overlay)

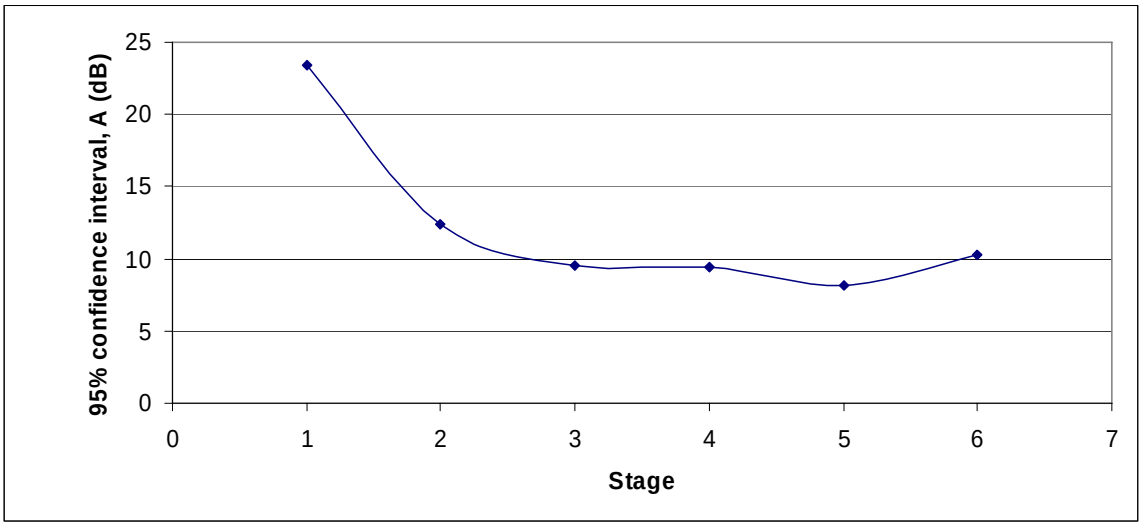

(a) 95% Confidence Intervals Value (A)

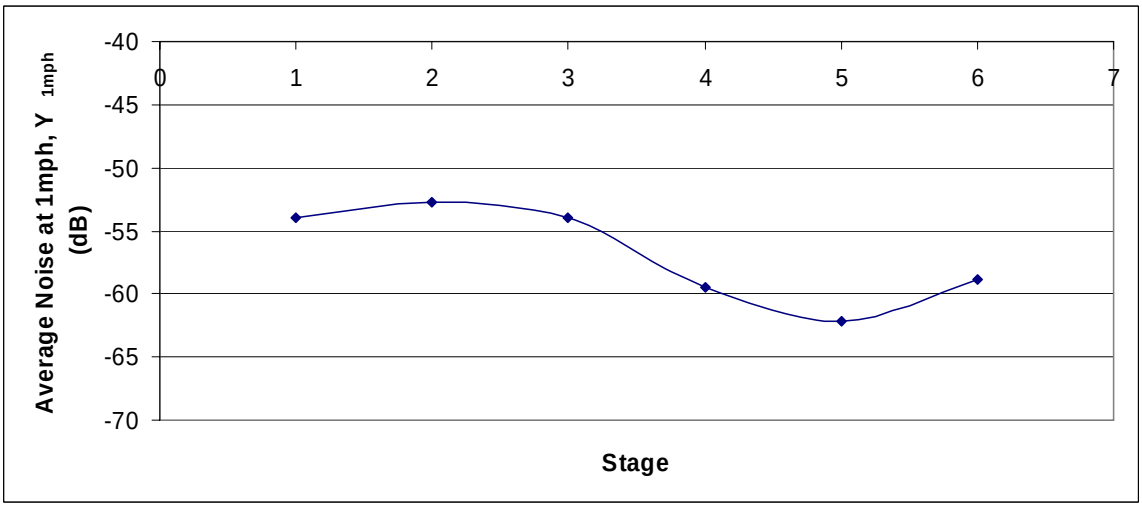

(b) Average Noise at Testing Speed of 1 mph

Figure 3.28 Plots of 95% Confidence Interval (A) and Average Noise at Testing Speed of 1 mph (Y_{1mph}) for Different Stages of the IH-20, Marshall Rehabilitation Project.

The following observations were made on the confidence interval values (A):

1. **Stage 1:** The confidence interval, A, is the widest when data was collected before milling the AC overlay. This data corresponds to a pavement with poor serviceability (low PSI value), which is characterized by rutting along wheel paths and reflected cracking on the old AC overlay surface,
2. **Stage 2:** The second widest A value corresponds to data collected after milling the old AC overlay. The rolling sensor rolls along the exposed concrete surface underneath the old AC overlay. There should be no rutting on the concrete pavement, but occasional loose aggregate is expected along the RDD test path,
3. **Stages 3 through 6:** The A values are less than the A values measured in the previous two stages. Small fluctuations of the A values in subsequent stages after the initial placement of the new AC overlay (i.e. Stage 3). The A values started to show an increasing trend which can be explained by the increasing number of distress (supported by observations made during visual condition survey).

The serviceability of a pavement can be estimated based on: (1) results from visual condition survey, and (2) PSI values computed from TxDOT raw profile data (collected using ultrasonic profiler vehicle). Surprisingly, there appears to be a strong correlation between the A values and the pavement serviceability. However, the correlation between the Y_{1mph} values and the pavement serviceability was not strong. The high A value during Stage 1 corresponds to a pavement structure with poor serviceability (i.e. PSI value is sufficiently low to commence a rehabilitation project). Then, the A values decrease after milling and decrease even more after the subsequent placement of new overlay. This is as expected because the serviceability on a concrete pavement after milling the top AC overlay exposes cracks and other distress features, and these features

are then covered up by the new AC overlay which is also accompanied by a smooth surface finishing. This is followed by small fluctuations in the A values during the next two years after placement of new AC overlay (supported by PSI measurements collected during Dec. 2001 and Nov. 2002; indicating insignificant changes in PSI values between the years) (Yetkin et al., 2003). Even though the A values show a decreasing trend (i.e. less scattering after more accumulated traffic load applied to the pavement), this can be explained by the initial settling of the pavement system and other measurement errors involved during NDT testing. An example would be caused by the rolling sensor array not testing along the outside wheel path at all times. Lastly, both A and Y value shows an increasing trend 2 years later. This can be explained by the increasing number of distress and increasing variation in the surface profile.

3.10 IMPROVED DATA ANALYSIS METHODOLOGY

As discussed earlier, the digital filter is one of the most critical components for analyzing RDD deflection data. The characteristics of the digital filter control the reported RDD deflection profile. Yet, the digital filter should be designed according to the signal and noise in which it needs to process. Therefore, it is crucial to understand the characteristics of the noise and incorporate this knowledge into the selection of digital filter. The flow diagram of the improved data analysis methodology is shown in Figure 3.29. Each step in the flow diagram is discussed below.

In step one, the pavement type in which the deflection data are collected needs to be known. More importantly, the type of top surface course controls the rolling noise measured. In another words, a rolling sensor should have a lower noise level if the deflection profiles are collected along a CRCP with a thin AC overlay layer than directly on a gravelly pavement surface.

In step two, the average deflection over the entire analysis pavement section needs to be estimated. This factor has a direct influence on the selection of the required attenuation in the stop band.

The first two steps can be elaborated further using RDD data collected in the field. Data from the following two test sites are presented:

1. FM-2 near Navasota, Texas (Gravelly Pavement Surface on a Thin Flexible Pavement), and
2. IH-35 near Hillsboro, Texas (New 14-in. thick CRCP).

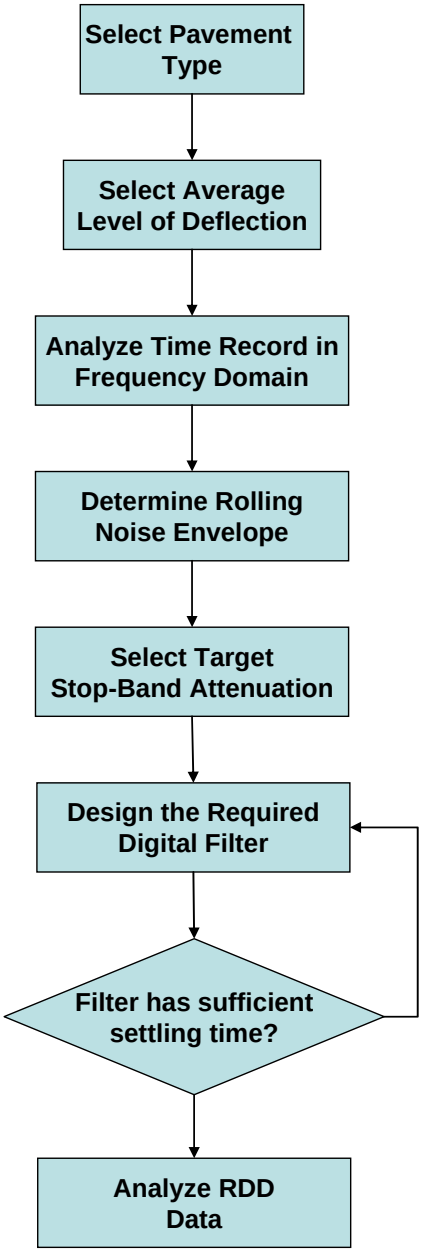

Figure 3.29 Improved Procedure for Post-Processing RDD Data.

Photographs showing the surface characteristics of these two pavement test sites are shown in Figures 3.30 and 3.31, respectively. The expected level of deflections and the pavement surface characteristics are very different in these two sites. Typical sensor

#1 deflections for an interstate highway are around 3 to 5 mils, while typical sensor #1 deflections for a farm-to-market road can be around 20 to 40 mils. In terms of the pavement surface characteristics, the surface along FM-2 consists of loose gravel-sized aggregate, while the surface along IH-35 consists of a smooth concrete surface.

Figure 3.30 Photograph of the Gravelly Pavement Surface of Farm-to-Market Road 2 (FM-2) near Navasota, Texas.

Figure 3.31 Photograph of the Continuously Reinforced Concrete Pavement (CRCP) Along IH-35 near Hillsboro, Texas (Before Opened to Traffic).

The rolling sensor measurements in both the time and frequency domains for FM-2 are shown in Figure 3.32. The time record of the rolling sensor appears to be noisy due to the rolling action of the rolling sensor along this rough gravelly surface. This characteristic is reflected in the time record by the large spikes in the record. The record was also analyzed in the frequency domain, and these results are shown in Figure 3.32; in this case, the RDD signal at 35 Hz is clearly distinguishable from the surrounding rolling noise, and a filter with moderate attenuation in the stop-band is required to resolve the RDD signal at the operating frequency.

For comparison purposes, the measurements from rolling sensor #1 along IH-35 are also presented in both the time and frequency domains as shown in Figure 3.33. The time record is less noisy than the one collected along FM-2 due to the smoother concrete surface along IH-35. However, since the typical deflection levels along an interstate highway system are small (in the range of 3 to 5 mils), the signal and rolling noise in the frequency domain appears to be similar to the one shown in FM-2. In this case, the same digital filter can be used to retrieve the RDD signal from the rolling sensor time record. Based on the data shown in Figures 3.32 and 3.33, the following observations were made:

1. the rolling noise is higher in Figure 3.32(c) than in Figure 3.33(c),
2. the SNR is higher in Figure 3.33(c) than in Figure 3.32(c), even though the motion of the concrete is less, and
3. the higher order harmonics are present as shown in Figure 3.33(c). However, the higher order harmonics were masked out by the rolling noise as shown in Figure 3.32(c).

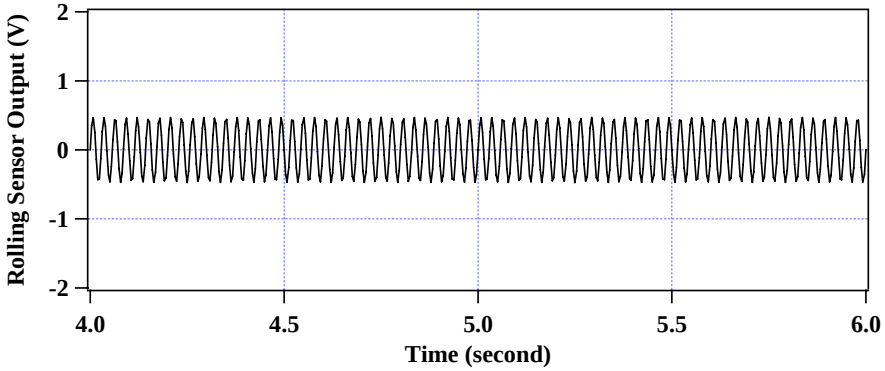

(a) Time Record of Pure RDD Signal

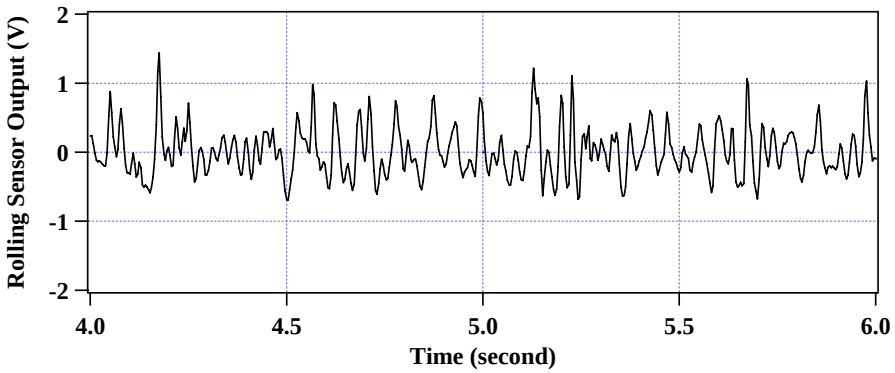

(b) Time Record of RDD Signal and Noise

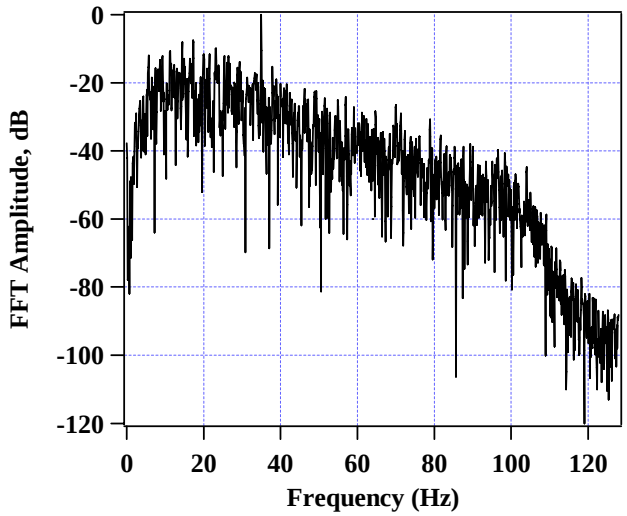

(c) Frequency Spectrum of RDD Signal and Noise

Figure 3.32 Rolling Sensor Records Collected Along FM-2

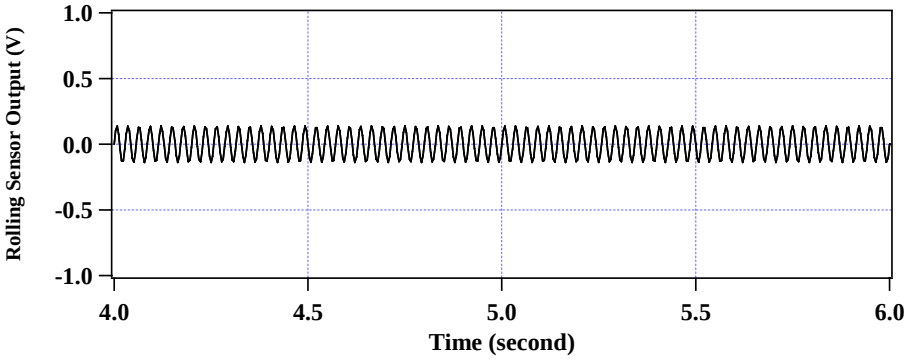

(a) Time Record of Pure RDD Signal

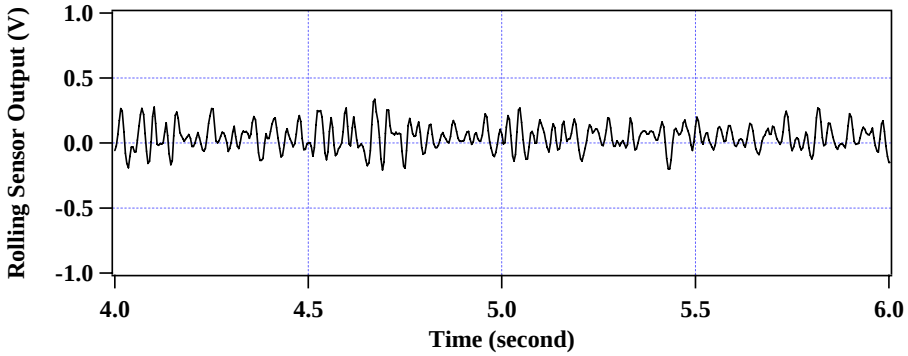

(b) Time Record of RDD Signal and Noise

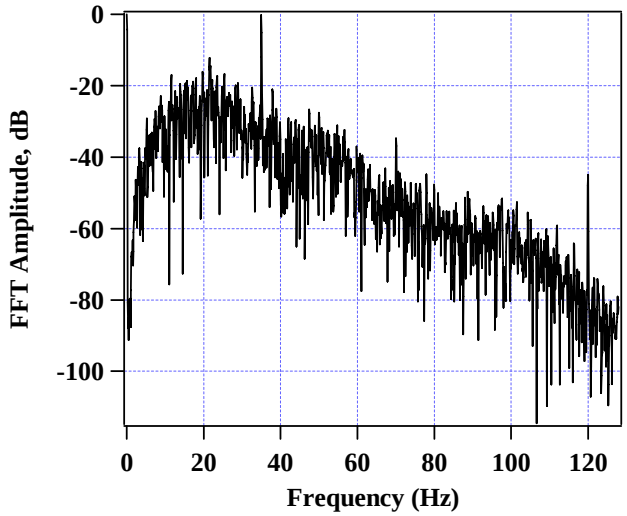

(c) Frequency Spectrum of RDD Signal and Noise

Figure 3.33 Rolling Sensor Records Collected Along IH-35.

In summary, the key point to obtaining good quality RDD data is to maintain a good SNR. In saying so, an underlying assumption is that the rolling sensor stays in contact with the pavement and there is sufficient time to measure the dynamic deflection of the pavement. A data record collected along a very rough pavement surface can be resolved accurately with the same digital filter specification if the signal is high enough to maintain a good SNR (as in the case of FM-2). On the other hand, a pavement with small dynamic deflections may require stricter control on the level of acceptable noise to maintain a good SNR (in the case of IH-35). The dilemma for choosing the correct RDD operating parameters (such as test speed, load levels) and the required resolution in the reported RDD deflection profiles are illustrated in Figure 3.34. In the worst case scenario, there maybe times when RDD profiles are needed along a rough pavement with very small dynamic deflections. Then, one of the following parameters may need to be adjusted:

1. reduce speed (i.e. typically reduce the noise level),
2. increase dynamic load level (i.e. typically increase the measured dynamic deflection), and
3. use a notch-pass digital filter with very high attenuation in the stop band (i.e. this would result in a filter with very poor time resolution, which can be acceptable in the case of flexible pavement where the pavement deflections are not expected to be change as rapidly as on a rigid pavement).

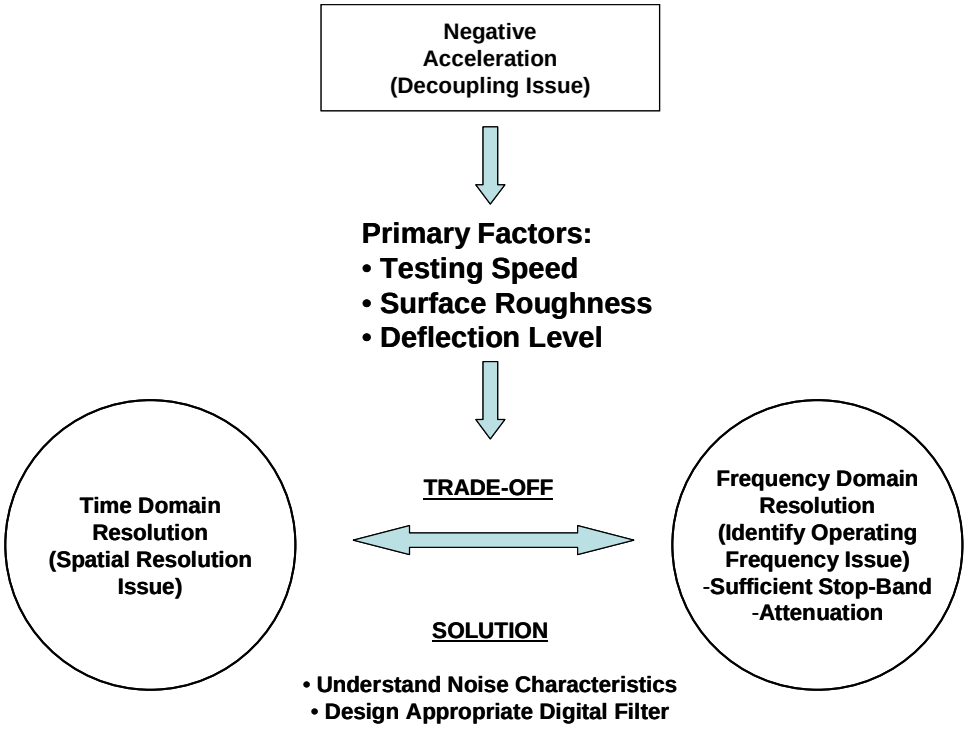

Figure 3.34 Factors Affecting the Analysis of RDD Measurements.

The first two parts of the improved procedure can provide a general guideline as to the quality of the measurements that can be measured on different category of pavement sites as shown in Figure 3.7. However, to optimize the output (i.e. RDD deflection profiles), the uniqueness of each set of collected RDD time records should be interpreted separately and choose the most appropriate filter which will give the best balance in terms of the required frequency and time resolution. An optimized RDD deflection profile is not likely to be obtained if only one digital filtering scheme is applied to all different pavement conditions. It follows that each RDD dataset should be analyzed and characterized separately. In particular, the rolling noise envelope should be characterized for the unique case of one set of averaged testing speed, pavement

roughness and level of dynamic deflection on the pavement surface. This procedure is presented in step three of the improved procedure.

It is important to note here that this type of processing can be done during testing or after the testing is completed.

In step three in this analysis process, each RDD raw data file is analyzed in both the time and frequency domains. The raw data are usually analyzed over a set time interval, where the average speed can also be determined. Important information such as the RDD operating frequency, average rolling noise, deflection signal level at the operating frequency are obtained in the analysis. These parameters are plotted against the testing speed to understand how these factors change with respect to varying test speeds on a particular pavement.

In step four, the rolling noise envelope is determined. A rolling noise envelope is needed to generalize the rolling noise characteristics for each RDD raw data file because, as discussed earlier, the rolling noise is fairly random in nature and it is neither practical nor necessary to design a new digital filter for every instant of the time record. Therefore, the approach taken is to choose a rolling noise envelope where only a certain probability of time along the entire record will the rolling noise exceed this chosen rolling noise envelope. A typical acceptable probability can be an alpha (α) value of 5 %.

Once the rolling noise envelope is chosen, the rest of the procedure involves trial-an-error to find a digital filter that satisfies both the target stop-band attenuation, frequency resolution and the time resolution of the RDD record. These remaining parts of the procedure is discussed in more detail in Chapter 6.

3.11 IMPROVING RDD MEASUREMENT ACCURACY

As discussed earlier in this chapter, the RDD measurement will inevitably contain rolling noises. There are two approaches that can be taken to improve the RDD deflection measurements, both in terms of frequency and time resolutions. These two areas are:

1. reduce the rolling noise by improving the design of the rolling sensor, and
2. reduce the effects of rolling noise using improved digital filtering schemes.

In the first area, the second-generation rolling sensor was designed as discussed in detail in Chapters 4 and 5. The improved design allows the testing speed to increase to 3 mph. In the second area, a better digital filtering scheme can be designed to more accurately measure the dynamic deflections (and with more frequently reported deflection points) by studying the characteristics of the RDD signal and associated rolling noise under different pavement conditions. It is important to note that advances in both areas are needed to improve the quality of the RDD measurements. This point is best illustrated using the example below.

In the new design of the rolling sensor, better coupling between the rolling sensor and the pavement surface is accomplished. The rolling sensor measurement can theoretically sense the amplitude which corresponds to the pavement deflection at the RDD operating frequency. Design features such as an air-spring to add a hold-down force, number of rolling wheels, tread coating on the wheels, width of each rolling wheel, and frequency response of the rolling sensor can reduce the rolling noise. As shown earlier in this chapter, the physical law of rigid-body motion rolling along a rough surface cannot be denied (i.e. the rolling noise will increase with increasing test speed, refer Figure 3.7). The current digital filtering scheme presented by Bay (1997) appears to be sufficient for filtering rolling noise even at a testing speed of 3 mph. This means that the

digital filter can resolve the RDD signal at the operating frequency accurately and also has a sufficient time (or spatial) resolution for pavement engineering applications. However, as the new generations of rolling sensor becomes available which can travel at a much higher testing speed, the rolling noise may become overwhelming for the current digital filtering scheme to resolve. This problem is true even though the rolling sensor senses the correct motion at the RDD operating frequency, because the situation can exist where we do not have any technique to retrieve the signal from the overwhelming noise floor (i.e. low SNR). Therefore, a study of the rolling noise needs to be carried out to compliment advances in the rolling sensor design.

At this stage, the only piece of information that is available to retrieve the RDD signal is the knowledge of the precise RDD operating frequency (i.e. knowing exactly where to look for the dynamic deflection signal). Yet, information such as the distribution of the rolling noise and the associated amplitude in the frequency domain has not been taken into consideration when choosing a digital filtering scheme. By utilizing this extra information about the rolling noise and the signal, a better digital filtering scheme can be used to resolve more closely spaced pavement features (e.g. cracks which have less than 3-ft spacing along a CRCP). As more field data and correlations with other information concerning the pavement sections (e.g. roughness characteristics) become available, our knowledge about the rolling noise can improve. Ultimately, an accurate model can be derived to predict the rolling noise measured in the field. This model is needed to continue making advances in the signal analysis method for RDD testing.

3.12 ESTIMATION OF THE ROLLING NOISE ENVELOPE

The first step in understanding the rolling noise is to define a rolling noise envelope, which is basically an upper bound representation of the rolling noise. This envelope is necessary to describe the rolling noise because of the random nature of the

rolling noise characteristics at any instance in time. Based on the many years of RDD deflection profiles collected at different highways and airport runways, some general trends can be observed which are discussed with the following objectives in mind:

1. to develop an understanding of the trends of the rolling noise envelope with different speeds, roughness, and level of deflections, and
2. to develop the ability to detect when the rolling noise envelope is very different from the envelope noise characteristics expected from pavements with similar attributes.

A simplified model to develop the rolling noise envelope is shown in Figure 3.35. This model is made up of two linear parts: (1) a flat envelope between 0 to 40 Hz, and (2) a sloping envelope between 40 to 100 Hz.

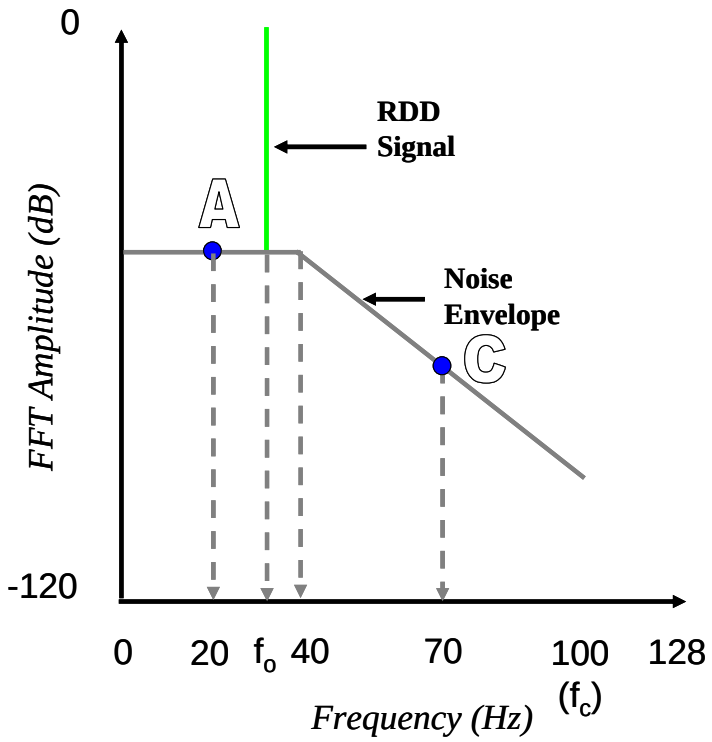

Figure 3.35 Model for the Rolling Noise Envelope

This simplified model assumes that the rolling noise does not vary between 0 to 40 Hz (where 40 Hz is the highest RDD operating frequency that is typically used), and the rolling noise decreases linearly between 40 to 100 Hz, where 128 Hz is the Nyquist Frequency (f_{nq} = fs / 2) and 100 Hz is the cut-off frequency (f_c) for the analog low-pass filter with attenuation of -100dB beyond f_c . These assumptions are necessary because it is impractical to model precisely the ever changing rolling noise envelope. Furthermore, due to the simplicity of this model, only the computation of the average FFT amplitude between 0 to 40 Hz (Point A), and 40 to 100 Hz (Point C) are required to define the entire rolling noise envelope. The objective of this study justifies the limitations that such model has for estimating the rolling noise envelope. For more complex cases, a site-specific rolling noise estimation procedure can be used as presented in Chapter 7 of this dissertation.

3.13 CALIBRATION OF THE ROLLING NOISE ENVELOPE MODEL

The noise envelope model (shown in Figure 3.35) was calibrated using data collected from rolling sensor #1 at different types of pavement sites as follows:

Flexible Pavements

1. Grayson County Municipal Airport Runway, and
2. IH-20 near Marshall, Texas (with overlay on top of CRCP).

Rigid Pavements

1. Fort Worth Alliance Airport,
2. SH-225 near Houston, Texas,
3. US-59 near Queen City, Texas, and
4. IH-20 near Marshall, Texas (along exposed CRCP surface).

Information needs to be extracted from the previous RDD rolling sensor time records so that the rolling noise envelope model can be calibrated accordingly. The procedure to calibrate the model is discussed below. First, the FFT spectrum for the rolling sensor records was computed in 5-second intervals. Then, the average rolling noise level for each frequency range was computed and plotted against the average test speed in every 5-second intervals. It is important to note that this 5-second interval was chosen arbitrarily in the analysis. The time window that is used to calculate the FFT spectra will inevitably affect the results of the spectra (i.e. affects both the shape and magnitude of the spectra). However, it was found that 5-second time window produce reasonably good result in the FFT analysis without having to average over too long of a time record where pavement deflections are likely to change significantly over this time (or distance) interval. As long as a consistent time window is used when calibrating the rolling noise model and any subsequent analysis, then meaningful results can be obtained. A typical relationship is shown in Figure 3.36. A simple linear regression model ($Y = b X + c$) is used for each frequency range and the best-fit line is also shown in Figure 3.36. This procedure is repeated for each raw data file on the selected sites. The regression analysis equations for selected rigid and flexible pavement sites are presented in Tables 3.4 and 3.5, respectively.

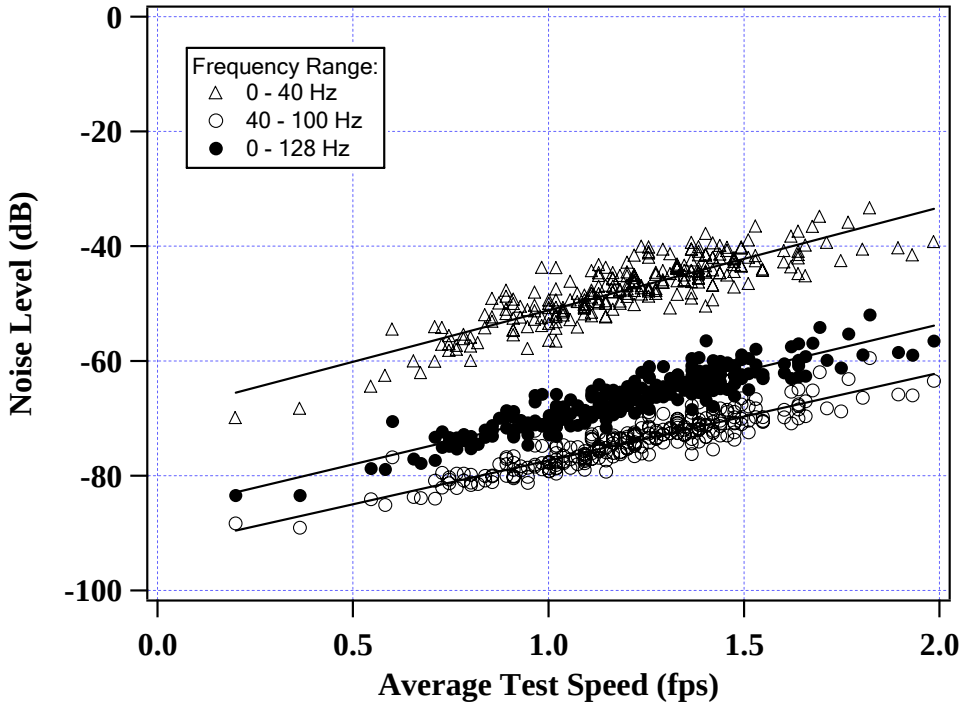

Figure 3.36 Measured Noise Levels as a Function of Average Test Speed for Different Frequency Ranges (Test Site: IH-20, Marshall, TX)

As shown in Tables 3.4 and 3.5, there is only small variability in the regression equation coefficients between sections of different test locations. However, there is clearly a difference between the flexible and rigid pavement sites. Since the target testing speed for all these data was around 1.5 fps (1 mph), the noise level for each frequency band were computed and their mean values for each test location were used to define the rolling noise envelope for a particular test location. These approximated rolling noise envelopes are shown in Figure 3.36.

Table 3.4 Rolling Noise Regression Analysis for Selected Rigid Pavement Sites

Fort Worth Alliance Airport (AFW)								
	bx	c		bx	c		bx	c
y=	13.405	-53.131	y=	16.739	-71.704	y=	18.024	-79.065
	21.686	-66.145		24.469	-84.812		25.465	-92.136
	22.994	-63.2		24.238	-80.472		12.523	-87.166
	20.428	-61.432		17.475	-73.443		15.947	-77.853
	12.345	-48.187		14.076	-66.262		14.711	-73.468
	15.382	-56.614		16.673	-73.959		17.078	-80.768
	14.592	-55.624		17.399	-75.454		18.467	-83.341
	18.289	-58.365		19.271	-76.34		19.493	-83.375
	12.014	-54.234		14.506	-73.286		15.457	-80.854
	18.947	-59.271		14.137	-69.184		11.757	-72.629
	22.781	-62.288		18.07	-72.384		15.7	-75.882
	20.402	-6.747		21.581	-84.268		21.884	-91.09
	25.493	-65.938		20.208	-76.654		17.58	-80.425
	21.85	-66.133		18.005	-78.189		15.946	-82.486
	19.499	-60.917		20.103	-77.222		20.172	-83.568
	21.979	-68.933		20.41	-83.631		19.479	-89.18
	20.907	-68.242		19.38	-32.773		18.465	-88.231
	16.274	-64.094		15.353	-78.893		14.713	-84.421
	16.58	-66.154		15.05	-80.391		14.18	-85.722
	12.044	-59.324		12.086	-76.254		11.95	-82.827
	11.88	-56.249		13.417	-75.327		13.945	-82.874
	13.837	-56.199		13.985	-73.405		13.892	-80.136
	9.5437	-48.905		13.635	-67.75		15.307	-75.313
	12.877	-53.207		15.876	-70.293		17.068	-77.088
	9.808	-53.65		15.319	-75.545		17.623	-84.43
	15.029	-63.238		18.033	-81.76		19.193	-89.093
	13.338	-57.766		14.014	-74.75		14.165	-81.436

SH-225, Houston, TX								
	bx	c		bx	c		bx	c
y=	28.255	-66.722	y=	24.442	-80.97	y=	22.498	-86.326
	14.473	-57.541		15.125	-75.401		15.296	-82.46

US-59 Queen City (befoe repair)								
	bx	c		bx	c		bx	c
y=	12.881	-63.468	y=	13.922	-78.682	y=	14.279	-84.536
	12.588	-59.678		15.604	-79.785		16.823	-87.802
	8.4304	-55.074		12.091	-76.538		13.581	-85.12
	13.531	-62.442		15.07	-81.144		15.621	-88.488
	10.543	-58.934		14.189	-81.439		15.686	-90.489
	8.6646	-56.108		11.195	-76.596		12.239	-84.811

US-59 Queen City (Jan 2006)								
	bx	c		bx	c		bx	c
y=	13.089	-61.147	y=	13.268	-77.542	y=	13.22	-83.919
	13.065	-61.939		15.144	-80.221		15.935	-87.432
	11.905	-61.637		15.117	-82.469		16.405	-90.788
	12.223	-63.238		13.012	-80.469		13.229	-87.194
	11.007	-56.417		13.245	-76.984		14.139	-85.252
	10.996	-57.631		12.981	-78.42		13.753	-86.757
	14.536	-61.771		14.977	-81.1		15.034	-88.743

IH-20 Marshall (Aug 2001)								
	bx	c		bx	c		bx	c
y=	17.478	-61.566	y=	15.518	-76.371	y=	14.448	-81.974
	21.233	-65.595		17.439	-80.309		15.498	-85.786
	18.223	-62.615		15.528	-78.09		14.134	-83.97
	28.952	-67.774		19.214	-78.529		14.521	-82.165
	23.075	-56.784		15.87	-71.069		12.357	-76.36
	17.824	-58.551		14.025	-74.571		12.121	-80.706
	17.328	-59.762		15.395	-76.251		14.298	-82.572
	13.708	-55.622		12.392	-71.563		11.63	-77.713
	3.5997	-38.106		5.9574	-62.14		6.97	-72.067
	13.426	-52.562		13.795	-72.636		13.821	-80.669
	17.076	-61.972		14.544	-76.115		13.19	-81.393
	18.139	-64.122		14.583	-77.458		12.753	-82.324

Table 3.5 Rolling Noise Regression Analysis for Selected Flexible Pavement Sites

Grayson County Airport

	(0 - 40 Hz)			(0 - 128 Hz)			(40 - 100 Hz)	
	bx	c		bx	c		bx	c
y=	12.362	-73.759	y=	9.1824	-83.378	y=	7.5654	-86.446
	17.51	-79.914		12.837	-88.822		10.512	-91.549
	16.209	-76.966		11.916	-85.904		9.7976	-88.688
	13.586	-73.389		10.118	-83.791		8.373	-87.249
	13.501	-74.114		10.69	-84.595		9.2581	-88.093
	5.3276	-59.414		5.4351	-76.01		5.398	-82.429
	8.7013	-66.802		8.439	-2.039		8.1982	-87.779
	12.479	-70.188		10.453	-84.2		9.3955	-89.387
	13.635	-69.868		11.224	-93.853		10.018	-87.94
	14.954	-70.04		12.922	-87.788		11.873	-94.257
	12.417	-65.939		11.158	-84.46		10.477	-91.694
	13.028	-69.976		10.886	-85.817		9.81	-91.849
	16.231	-67.417		12.998	-82.058		11.425	-87.608
	12.412	-63.154		9.9939	-78.815		8.8113	-84.85
	11.446	-71.91		10.8888	-88.056		10.508	-94.171
	12.451	-70.816		11.469	-87.552		10.897	-93.945
	11.607	-70.84		10.752	-87.309		10.237	-93.571
	10.801	-66.916		9.4661	-82.325		8.7556	-88.216
	10.731	-68.66		9.242	-93.306		8.4673	-88.82
	9.5886	-68.923		9.217	-85.481		8.9468	-91.814
	11.657	-74.069		9.4972	-86.483		8.4034	-90.904
	12.593	-71.724		11.064	-87.284		10.267	-93.12
	10.192	-64.181		9.5878	-82.505		9.2403	-89.718
	12.107	-65.555		11.536	-84.908		11.185	-92.541
	10.72	-61.653		10.492	-81.812		10.291	-89.804
	7.3764	-62.119		8.0969	-81.508		8.3274	-89.157

IH-20 Marshall (Apr 2001)

	bx	c		bx	c		bx	c
y=	23.414	-75.589	y=	18.212	-85.189	y=	15.538	-88.222
	16.38	-64.839		14.405	-80.425		13.317	-86.317
	21.481	-67.12		21.02	-85.152		20.588	-92.133
	13.922	-58.945		14.18	-78.14		14.116	-85.68
	11.693	-57.886		12.468	-77.73		12.688	-85.625
	12.45	-60.188		12.493	-78.506		12.384	-85.715
	13.535	-60.094		12.739	-77.856		12.263	-84.828
	15.799	-61.955		12.667	-77.616		11.089	-83.573

IH-20 Marshall (Jan 2002)

	bx	c		bx	c		bx	c
y=	13.313	-62.844	y=	17.983	-81.39	y=	19.765	-88.508
	12.96	-63.305		18.649	-84.066		20.855	-92.045
	8.716	-54.891		15.389	-77.406		18.126	-86.35
	14.982	-81.517		9.597	-60.525		17.156	-89.739
	12.076	-63.72		15.466	-83.225		16.676	-90.673
	9.4055	-62.785		15.223	-85.078		17.549	-93.785
	8.5614	-61.021		14.875	-84.74		17.458	-94.157

IH-20 Marshall (Nov 2003)

	bx	c		bx	c		bx	c
y=	23.597	-72.619	y=	19.204	-86.663	y=	16.997	-91.817
	17.885	-66.785		15.56	-83.043		14.312	-90.077
	17.951	-69.139		16.258	-86.14		15.301	-92.642
	17.779	-68.686		15.882	-85.033		14.833	-91.244
	15.922	-61.486		18.212	-82.913		19.038	-91.431
	20.907	-70.638		19.65	-87.41		18.891	-93.827
	15.388	-65.759		13.162	-81.843		11.994	-87.959
	17.437	-68.289		14.838	-83.177		13.501	-88.761

IH-20 Marshall (Nov 2004)

	bx	c		bx	c		bx	c
y=	18.468	-69.567	y=	15.324	-82.044	y=	13.736	-86.56
	17.193	-65.09		14.887	-80.564		13.706	-86.466
	21.423	-72.225		15.353	-83.267		12.477	-87.16
	12.155	-61.035		10.181	-77.135		9.2316	-83.408
	14.692	-64.625		12.542	-80.132		11.5	-86.121
	17.574	-66.39		16.199	-83.397		15.427	-89.962
	13.802	-60.991		12.104	-78.843		11.234	-85.846
	12.524	-60.755		11.718	-80.361		11.285	-88.181

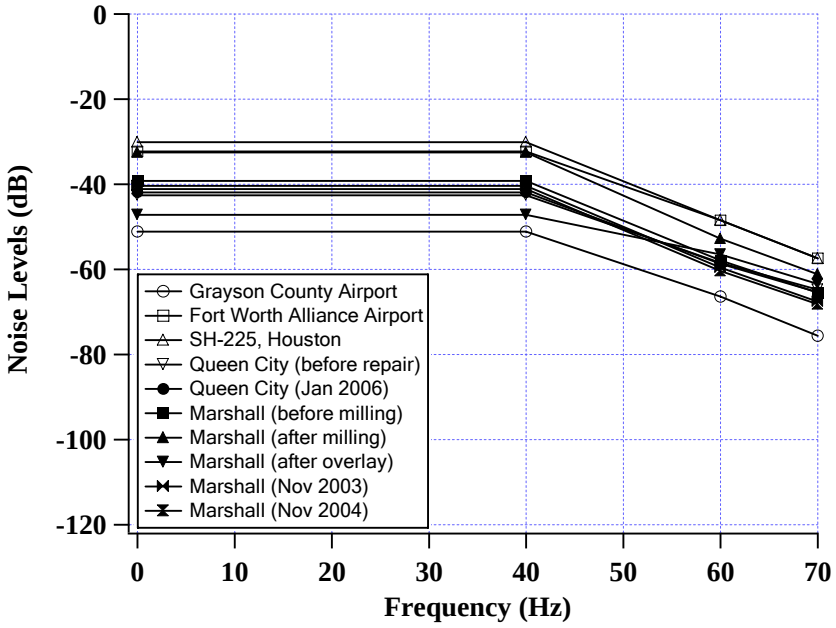

Figure 3.37 Approximate Rolling Noise Envelopes for Different Test Sites

The rolling noise envelopes shown in Figure 3.37 were obtained from a range of different test sites. These test sites include flexible and rigid highway pavements, and also flexible and rigid airport pavements. The level of deflections and roughness characteristics can be very different among these sites. Therefore, these envelopes are grouped into different categories as presented in Figures 3.38 through 3.40.

The rolling noise envelopes obtained from IH-20 near Marshall are shown in Figure 3.38. It was found that the rolling noise envelope collected after milling the old AC overlay is the highest among the five envelopes. The high rolling noise envelope is caused by the rough CRCP surface on which the rolling sensor has to roll. On the other hand, the data collected shortly after the overlay was placed has the lowest rolling noise envelope because of the smooth AC overlay surface. The other three rolling noise envelope lies between these two bounds, and represents the change in pavement conditions over the 3 years after the AC overlay was initially placed.

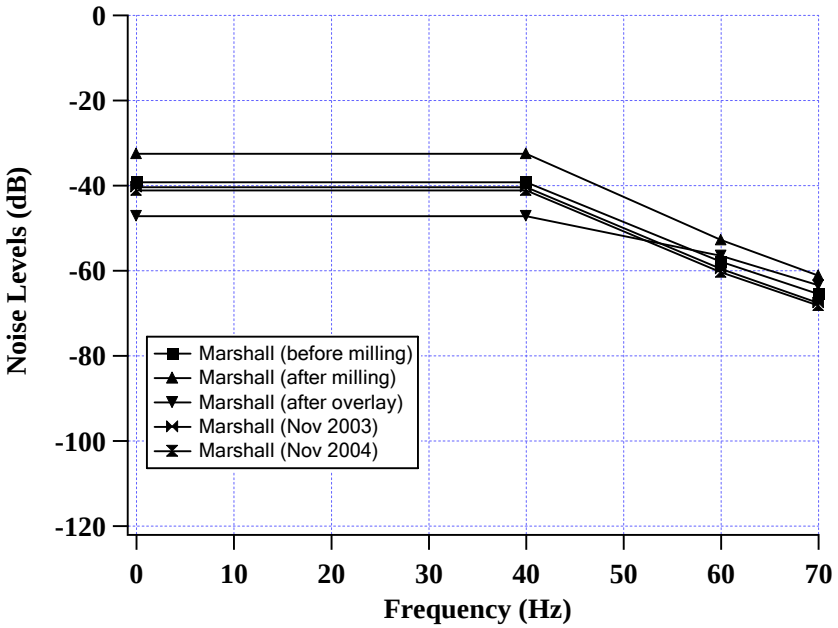

Figure 3.38 Approximate Rolling Noise Envelopes for IH-20 near Marshall, TX.

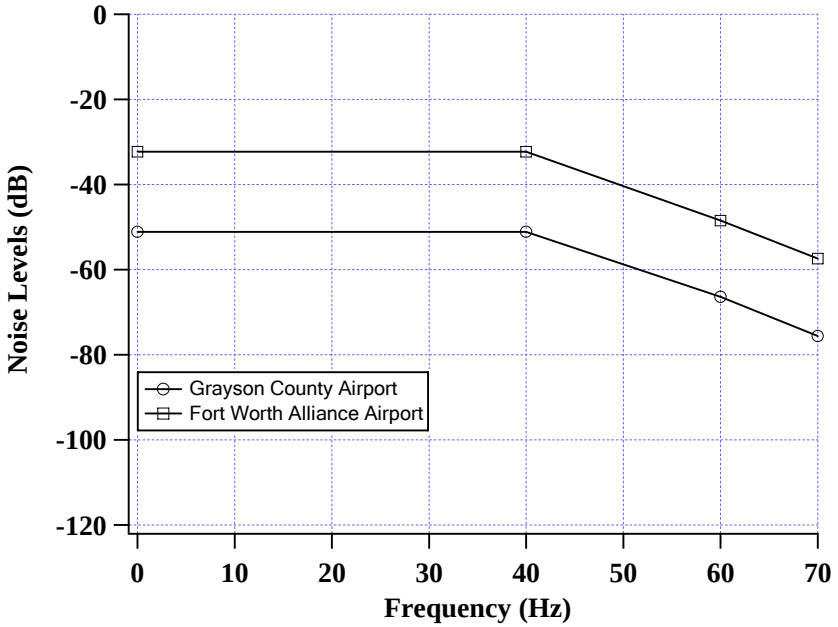

Figure 3.39 Approximate Rolling Noise Envelopes for Grayson County (flexible) and Fort Worth Alliance (rigid) Airports.

Two rolling noise envelopes collected from the Grayson County Airport and the Fort Worth Alliance Airport are shown in Figure 3.39. As expected, the Grayson County Airport, which is a runway with the majority of the runway being flexible pavement, and higher deflection level were observed. On the other hand, the Fort Worth Alliance Airport consists of concrete pavements (JCP), which have lower deflections and higher roughnesses than the Grayson County Airport.

Last, two rolling noise envelopes collected from US-59 near Queen City, TX are shown in Figure 3.40. These two profiles were collected before and after repair work had been performed on a JCP. The particular problem with this test site is that there is significant faulting at the joints before rehabilitation. Rehabilitation work includes diamond grinding, dowel retrofitting, and cross-stitching. Based on these results, it was found that the rolling noise envelopes are similar on the same section before and after the rehabilitation. This can be explained by the fact that the repair works were carried out at localized areas at the concrete joints, and therefore should not affect the roughness and deflection characteristics for the majority of the pavement.

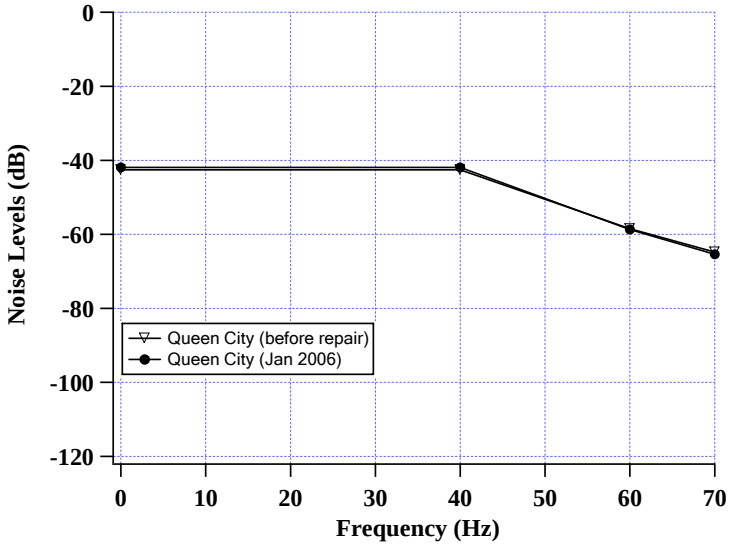

Figure 3.40 Approximate Rolling Noise Envelopes for US-59 near Queen City, TX.

3.14 SIGNAL-TO-NOISE RATIO (SNR)

Detailed discussion on the development of the rolling noise envelope was presented in the earlier sections of this chapter. When analyzing RDD deflection data, the relative amplitudes of the RDD deflection signal and the surrounding noises are important (i.e. in general, a higher ratio allows deflections to be resolved at closer spacing). A quantitative parameter known as the signal-to-noise ratio (SNR) are often used to describe the relative amplitudes between a signal and the noise. There are different definitions for SNR, but the following equation is used to define SNR in the context of this study:

$$SNR(dB) = 20\log_{10}\left(\frac{V_{RDD\_fo}}{V_{20-40Hz}}\right) \qquad (3.5)$$

where

V_{RDD_fo} = Voltage measured at RDD operating frequency

$V_{20\text{-}40\ Hz}$ = Averaged voltage measured in the frequency band between 20 – 40 Hz (excluding the amplitude at RDD operating frequency)

When comparing Eq. 3.5 with Eq. 3.2, it was found that the two equations are very similar except that the voltage ratio is the reciprocal of the other. This means that the SNR can be readily calculated from the rolling noise envelope in Eq. 3.6. Also, Eq. 3.6 is illustrated in Figure 3.41.

SNR = - (Average Noise Envelope between 20 – 40 Hz) (3.6)

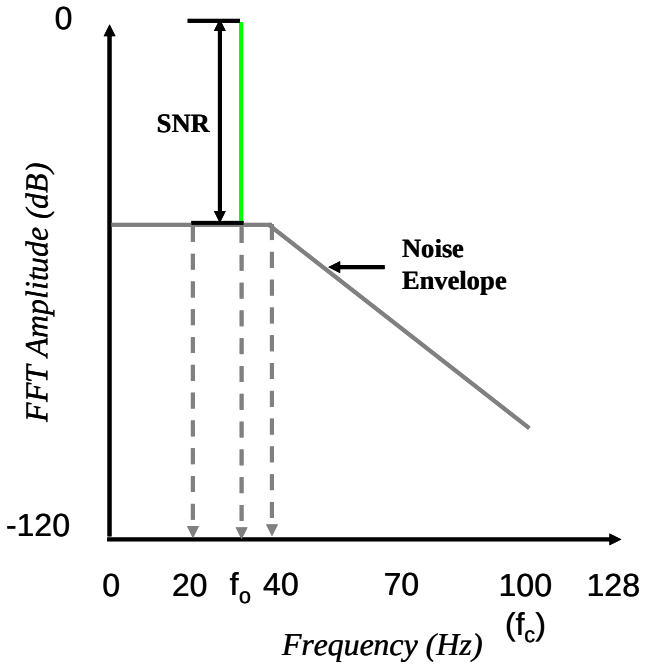

Figure 3.41 Definition of Signal-to-Noise Ratio (SNR) Using the Proposed Noise Envelope.

3.15 SUMMARY

Rolling noise is inherent in the current RDD measurement, and this statement will remain true as long as "in-motion" deflection measurements are made. A study of the rolling noise characteristics was carried out using rolling sensor measurements from 46 different highway and airport test sites collected over the years. These measurements were all performed with the first-generation rolling sensors developed by Bay (1997). The primary goal of this study was to better understand the rolling noise characteristics in RDD measurements. Two areas in which such information can be used are: (1) design of the second-generation rolling sensor, and (2) improvement to the current data analysis method.

Three factors which control the rolling noise characteristics were identified in this study. These factors are: (1) deflection levels, (2) pavement surface roughnesses, and (3)

testing speeds. Due to the complex and random nature of rolling noise measurements, a simplified rolling noise envelope was proposed to describe the rolling noise in the frequency domain. Site-specific rolling noise envelope can be also calibrated using rolling sensor measurements collected in the field as shown in this chapter.

Chapter 4 Development of the Second-Generation Rolling Sensor

4.1 INTRODUCTION

The primary objective of this research project is to increase the RDD testing speed from 1 to 3 mph (1.6 to 4.8 km/hr). The major technical hurdle in accomplishing this objective is developing rolling sensors which perform properly at 3 mph (4.8 km/hr). The two key factors that limit the existing testing speed are: (1) the negative acceleration of the rolling sensor as it moves along a rough surface, and (2) the level of rolling noise measured during testing. To accomplish the objective of increasing the RDD testing speed, new rolling sensors were designed. These new sensors are designed so that the RDD testing speed can be increased by a factor of three. The new rolling-sensor design is called the second-generation rolling sensors hereafter.

During the duration of the project, two rolling sensor designs evolved. Two design approaches were considered. The first design provided an additional hold-down force by adding a mass suspended on a soft spring, and the second design provided an additional hold-down force by pressurizing an air-spring which is located at the top of each rolling sensor. In the end, the second-generation rolling sensors were built using the second design, which uses the air-spring for an additional hold-down force. This design was preferred because it allows a larger hold-down force to be applied and the geophone is located lower in the rolling sensor assembly. Four rolling sensors were constructed using the second design. In this chapter, the design, fabrication, and laboratory calibration procedures associated with the second-generation rolling sensors are discussed.

4.1.1 Negative Vertical Acceleration - Maintaining Coupling with Pavement

A critical factor for successful RDD measurements is to maintain good coupling between the pavement surface and the rolling sensors. This coupling is necessary because the rolling sensors need to be able to sense the dynamic motion of the pavement that is induced by the RDD loading system. By limiting the negative vertical acceleration of the rolling sensors to less than –1.0g, it can be assured that the rolling sensor stays coupled with the pavement surface during RDD testing. Two major factors that control the negative vertical acceleration were identified in the previous TxDOT research project No. 0-1422. These factors were: (1) the rolling speed and (2) the diameter of the rolling wheels.

Two improvements to the existing rolling sensor design were made to increase rolling speed. First, an additional hold-down force was provided to each rolling sensor. The allowable negative vertical acceleration was increased by the addition of a hold-down force on each sensor. Second, the diameter of the rolling wheels was also increased. Larger-diameter rolling wheels result in a smaller negative vertical acceleration than smaller-diameter rolling wheels at the same rolling speed over the same rough pavement.

4.1.2 Rolling Noise

At the current stage in the RDD development, contact-type sensors are used to measure dynamic pavement deflections. The dynamic pavement deflections induced by the RDD dynamic force are measured by the geophone mounted on each rolling sensor. Rolling noise refers to the noise when “in-motion” deflection measurements are made. The rolling noise will be present whether contact or non-contact type sensors are being used. Since the rolling noise has a detrimental effect on the deflection measurements, this factor has always been a major consideration in the rolling sensor design. Hence, the

second-generation rolling sensors have larger diameter rolling wheels to reduce the level of rolling noise.

Signals collected with the rolling sensors may have noise that is of the same magnitude in the time domain as the signal that represents the dynamic pavement response. This fact has been discussed in Chapter 3 and was illustrated in Figure 3.3. Appropriate signal processing techniques are used to attenuate noise. The noise can usually be filtered out because the loading system of the RDD loads the pavement at a single operating frequency, f_o. However, digital filters can only be used to attenuate rolling noise at frequencies other than the chosen operating frequency. They cannot distinguish the rolling noise component that is at the operating frequency (f_o) from the RDD signal. Therefore, it is very beneficial to minimize rolling noise in the RDD operating frequency range.

Even though the RDD data processing techniques can effectively attenuate most of the noise that is away from the chosen operating frequency, it is still important to minimize the rolling noise for two reasons. First, reduction of rolling noise will increase the SNR of the measurements. This is important because digital filters cannot distinguish between noise and signal if both of them occur at the same frequency which is operating frequency in the case of the RDD. Second, most digital filters have increasing difficulty in resolving the frequency components that are closely located. In this case, the signal needs to be resolved at the operating frequency. The second point is related to the relationship between bandwidth in the pass-band of the filter and the attenuation level at the stop-band of digital filters.

4.2 DESIGN CONSIDERATIONS FOR ROLLING SENSORS

4.2.1 Overview

The design of the rolling sensor affects the: (1) testing speed, (2) accuracy of the deflection measurements, and (3) the measured rolling noise spectra. Therefore, the rolling sensor design is essential to the overall performance of the RDD. Three major factors that govern the design of the second-generation rolling sensors are: (1) the frequency response of the rolling sensors, (2) the hold-down force required to maintain good coupling of the rolling sensors at the target testing speed, and (3) the acceptable level of rolling noise. It is important to note that all three factors are closely related.

4.2.2 Frequency Response of a Rolling Sensor

The frequency response of a rolling sensor can be measured by taking the ratio between the rolling sensor motions and the pavement motions at different frequencies. The frequency response illustrates the dynamic characteristics of the system. The rolling sensor can be modeled as a single-degree-of-freedom (SDOF) system with a lumped mass (m) supported by a spring that has a spring constant (k) and a viscous dashpot coefficient (c). Such a SDOF system is shown in Figure 4.1.

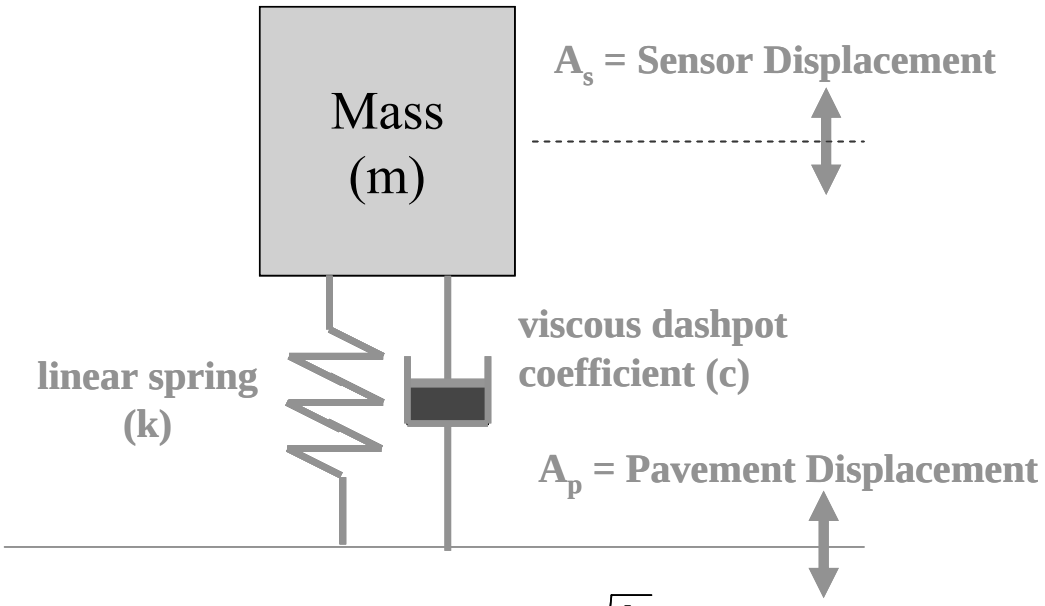

$$\omega_n = \text{natural circular frequency} = \sqrt{\frac{k}{m}}$$

$$\omega_D = \text{damped natural circular frequency} = \omega_n \sqrt{1 - D^2}$$

$$c_{cr} = \text{critical viscous damping coefficient} = 2m\omega_n$$

$$D = \text{damping ratio} = c/2m\omega_n = c/c_{cr}$$

Figure 4.1 Single-Degree-of-Freedom (SDOF) System Used to Model a Rolling Sensor

The RDD loading system can operate between frequencies of 5 and 100 Hz. However, RDD testing is typically performed between frequencies of 30 and 40 Hz. For all practical purposes, it is desirable to have a constant frequency response over the range of frequencies used in RDD testing. Furthermore, the natural frequency (ω_n) of a rolling sensor should be far away from the RDD operating frequency range. In fact, the natural frequency (ω_n) should be well above the operating frequency so that lower frequencies (often below 20 Hz) associated with traffic-generated noise do not resonate the rolling sensor. There are three main ways to achieve a high-natural-frequency SDOF system.

Two of the ways are: (1) a lighter rolling sensor (i.e., decrease the mass of the SDOF system) which increases the ω_n and / or, (2) increase the stiffness of the rolling sensor (i.e., increase the spring constant (k) of the SDOF system) which also increases the ω_n. Since the polyurethane thread on the rolling wheels controls the stiffness of the rolling sensor, the stiffness of this polyurethane coating is important. The third way to achieve a high-natural-frequency SDOF system is to increase the hold-down force, which increases the stiffness of the overall system and consequently also increase ω_n.

4.2.3 Second-Generation Rolling Sensor—First Design

During this project, two rolling sensor designs were considered. Both designs involved some type of system to provide an additional hold-down force. The main difference between the two designs is the way the hold-down force is provided to the rolling sensor. The first design involved a heavy mass supported on a soft spring as shown in Figures 4.2 and 4.3. This hold-down system is enclosed inside a cylindrical acrylic tube, and the acrylic tube forms part of the rolling cart.

Three, 12-in. (305-mm) diameter aluminum wheels support this rolling sensor. In addition, this rolling sensor design has hinge connections at both ends of the cart where the positioning mechanisms are located. The hinge connection minimizes noise transmission from the RDD truck through the towing frame to the rolling sensor as well as minimizing noise transmission by the towing frame itself.

There are major limitations to this rolling sensor design. First, the amount of hold-down force is controlled by the size of the steel mass. The size of the steel mass is in turn limited by the size of each rolling sensor. It is important that the rolling sensor does not have a large footprint, which would cause the measurement to be averaged over a large area. Second, there must be sufficient headroom provided for the steel mass to move as the rolling sensor rolls along the pavement. It is detrimental if the steel mass ever reaches

the top, because this would affect the reading of the geophone and might even uplift the rolling sensor in the worst case. Due to the limited hold-down force and the head-room restrictions, this first rolling sensor design was abandoned.

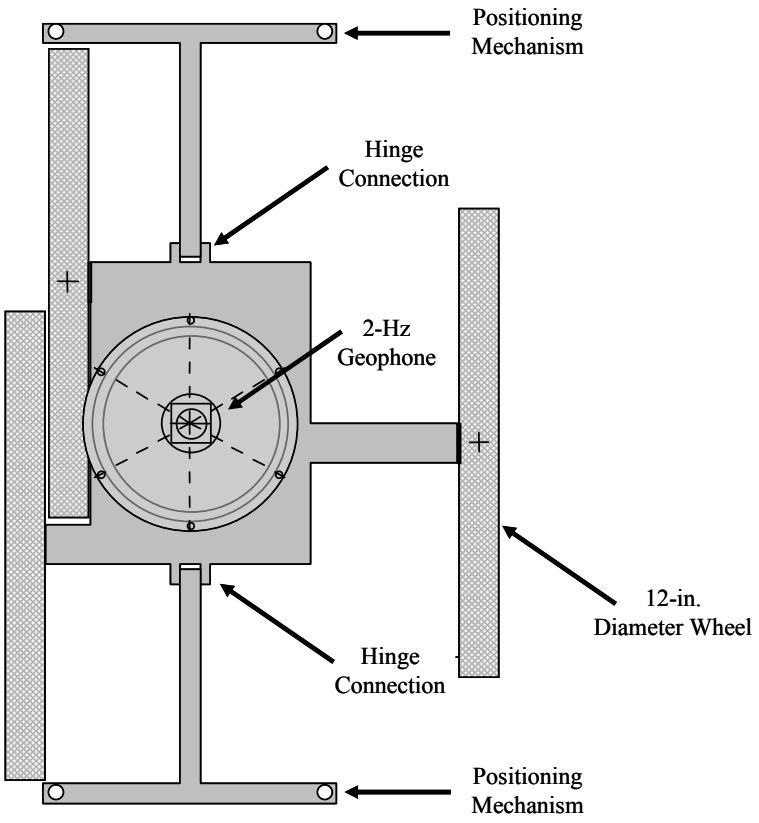

Figure 4.2 Top View of the First Design Considered for the Second-Generation Rolling Sensor

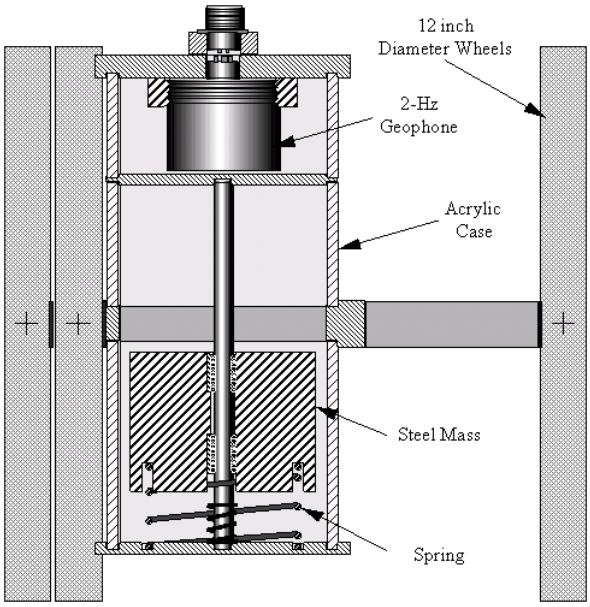

Figure 4.3 Side View of the First Design Considered for the Second-Generation Rolling Sensor

4.2.4 Second-Generation Rolling Sensor—Second Design

The second-generation rolling sensors were built using the second design. The rolling carriages and rolling wheels are made at the machine shop of the Physical Plant Department, The University of Texas at Austin. The entire rolling carriage is built from an aluminum alloy. When compared with the first-generation rolling sensor, the size of the carriage is substantially increased to accommodate the externally applied hold-down force and the larger rolling wheels. Each sensor is equipped with either 9-in. (229-mm) or 12-in. (305-mm) diameter rolling wheels for rolling-noise reduction. Furthermore, this wheel arrangement minimizes the footprint of the rolling sensor.

The second rolling sensor design uses a pressurized air spring to provide the required hold-down force. A custom-made polyurethane air spring is attached to the top of each rolling sensor, and a significant hold-down force can be achieved even when the air spring is pressurized at a small pressure level. For example, the air springs can each be

pressurized individually from 1 to 5 psi (6.9 to 34.5 kPa), resulting in around 7 to 35 lbs (31 to 156 N) of hold-down force, respectively. The second rolling sensor design is shown in Figures 4.4 through 4.7.

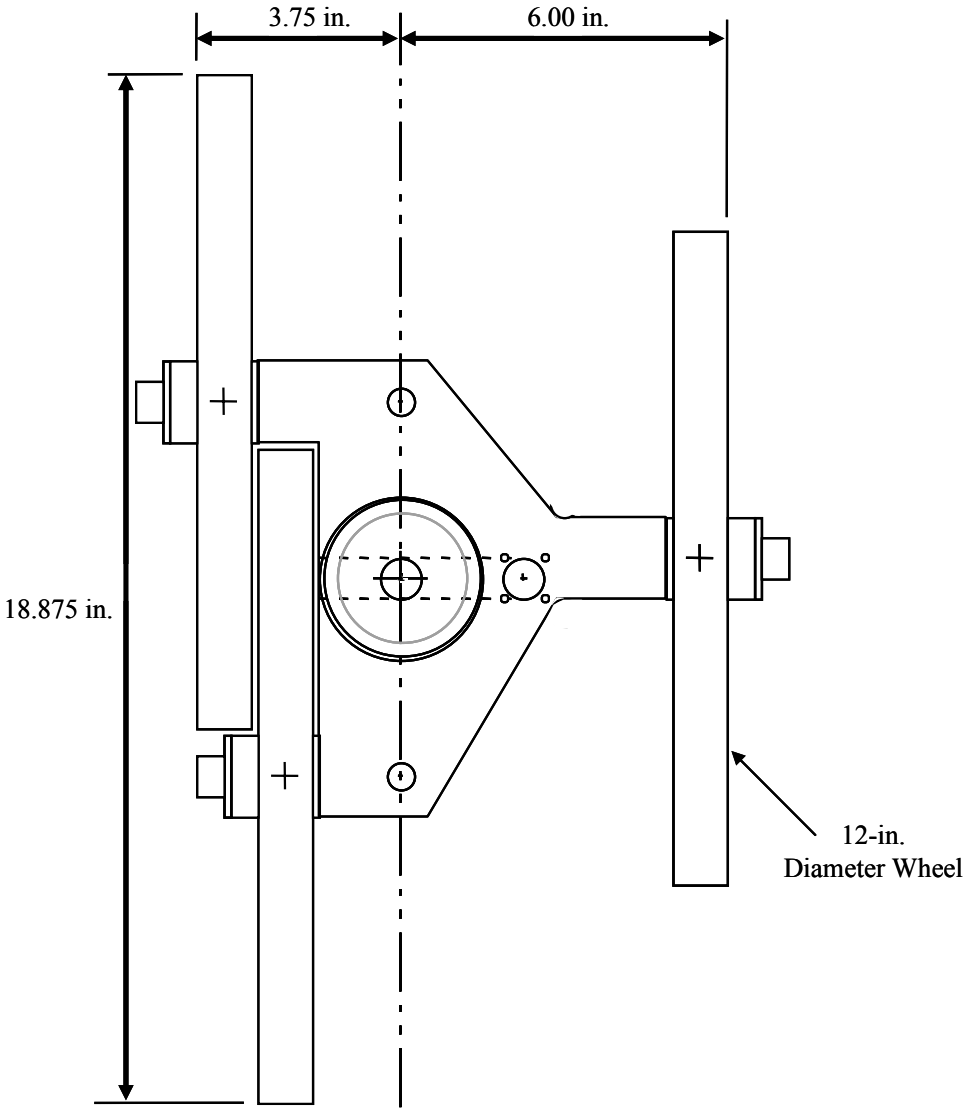

Figure 4.4 Plan View of the Second Design Considered for the Second-Generation Rolling Sensor

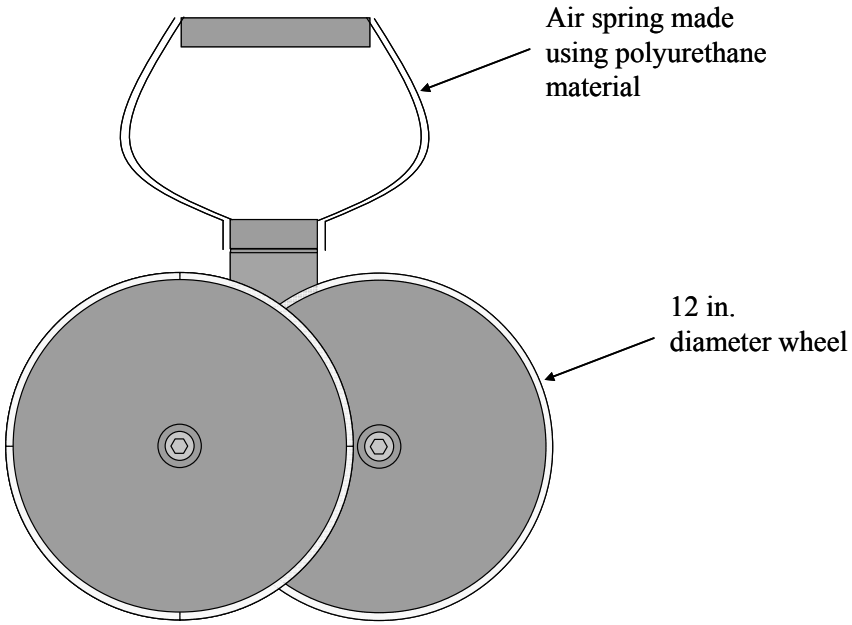

Figure 4.5 Side View of the Second Design Considered for the Second-Generation Rolling Sensor

This second-generation rolling sensor design has two components that are made of polyurethane material. These components include the air spring and the coating on the rolling wheels. The polyurethane components are custom molded by PSI Urethanes, Inc. located in Austin, Texas. There are many reasons for choosing polyurethane. Some of the reasons are as follows:

1. high abrasion and impact resistances,
2. good bonding properties with metals,
3. high chemical resistance,
4. a wide range of hardnesses, and
5. more durability than most conventional elastomers and plastics.

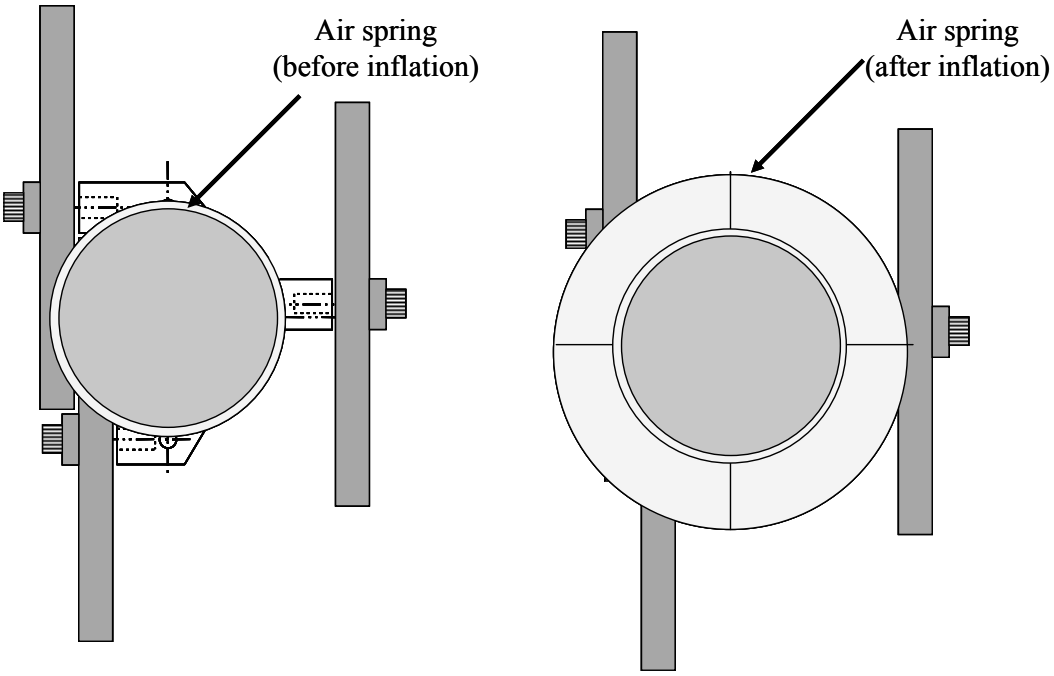

Figure 4.6 Top View of the Air Spring Used in the Second-Generation Rolling Sensor

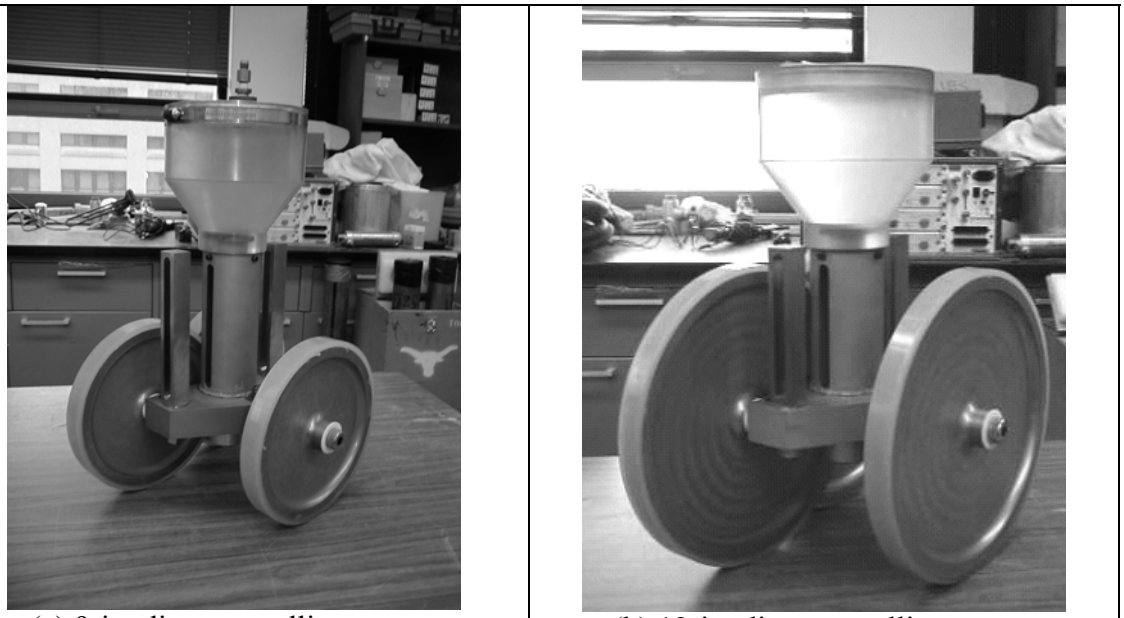

(a) 9-in. diameter rolling sensor (b) 12-in. diameter rolling sensor

Figure 4.7 Photographs of the Second-Generation Rolling Sensors

Typical hardness levels and applications are shown in Figure 4.8. Each air spring is made from polyurethane with a 40 durometer on the A scale as shown in Figure 4.8. An aluminum mold was used to cast the air spring. This aluminum mold was made at the machine shop in the UT Austin Department of Civil Engineering and then used by PSI Urethane, Inc. to cast the polyurethane air spring. This soft polyurethane was chosen because it can minimize vibrations between the towing frame and the rolling sensor. As shown in Figure 4.8, the 40 durometer on the A scale is approximately equivalent to the hardness of rubber bands. The shape of the air spring was specially designed so that it would approach a sphere when pressurized. This inflated shape is important because the geometry of a sphere should minimize the chance of over-turning the rolling sensors. Each air spring has a bottom cross-sectional area of 7 in^2, and if pressurized at 5 psi (34.5 kPa), an equivalent hold-down force of 35 lbs (156 N) is provided to each rolling sensor. A photograph of the configuration used to connect the second-generation rolling sensors to the towing frame is shown in Figure 4.9.

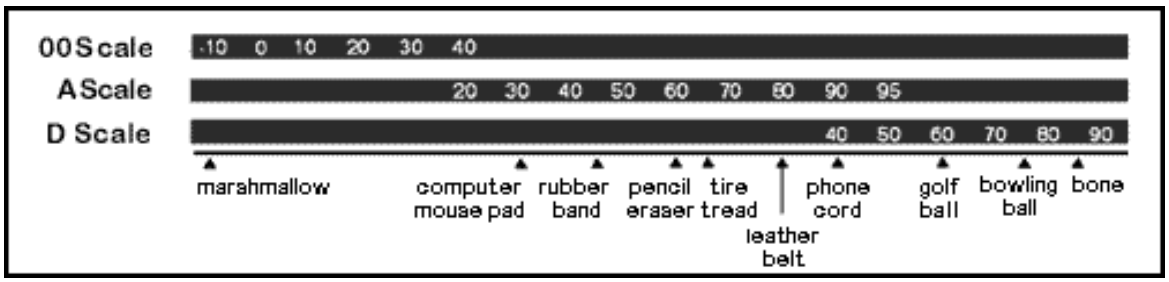

Figure 4.8 Typical Hardness Range for Polyurethane and Their Applications (from PSI Urethanes, Inc.)

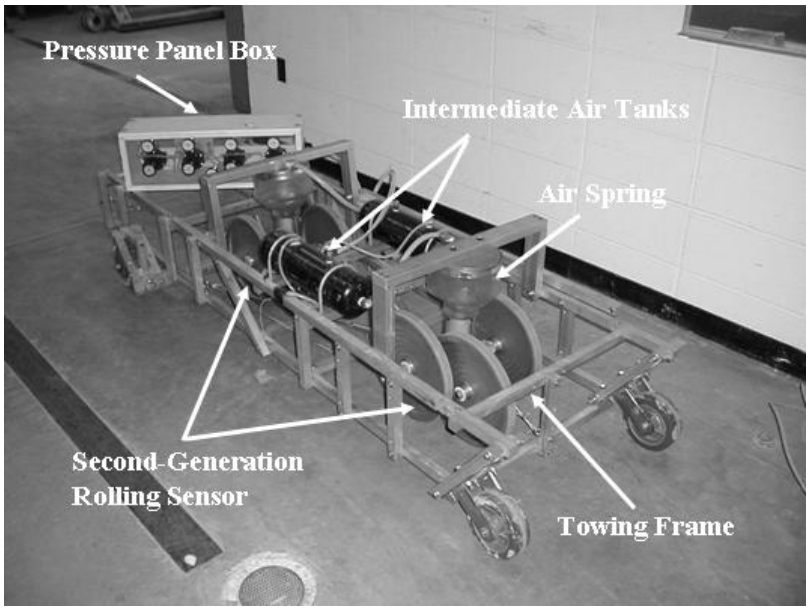

Figure 4.9 Photograph of Towing Frame and Second-Generation Rolling Sensors

In this rolling sensor design, special considerations have been made to minimize the level of rolling noise. First, the diameter of rolling wheels was increased. The diameter of the rolling wheels was increased from 6 in. (152 mm) to 9 in. (229 mm) in some sensors and to 12 in. (305 mm) in other sensors. Sensor #1 was constructed with 9-in. (229-mm) diameter rolling wheels, and Sensor #2, #3 and #4 were constructed with 12-in. (305-mm) diameter rolling wheels. The use of 9-in. (229-mm) diameter rolling wheels was necessary for Sensor #1 because of the limited space underneath the RDD truck in the location of Sensor #1. These smaller diameter wheels were positioned at locations that were closer to the loading rollers because the Signal-to-Noise Ratio (SNR) at these locations tends to be higher. The 12-in. (305-mm) diameter rolling wheels are used to improve the SNR at locations that are farther away from the loading rollers.

Second, each rolling wheel is coated with a stiff polyurethanes coating of 0.25 in. (6.4 mm) in thickness. This coating serves to protect the aluminum hub and to reduce the noise level during rolling. There is a trade-off between the natural frequency and the level

of rolling noise. Intuitively, a softer polyurethane thread should reduce the level of rolling noise. However, a softer polyurethane thread has a lower spring constant (k) that results in a lower natural frequency for the rolling sensors. Therefore, a tradeoff is needed between the level of rolling noise and the overall frequency response of the rolling sensor system. A polyurethane material with a hardness of 50 durometer on the D scale was chosen. This material is roughly equivalent to the hardness between a phone cord and a golf ball as seen in Figure 4.8.

Aluminum molds for the rolling wheel coatings were made at the machine shop in the Physical Plant Department at The University of Texas at Austin. The dimensions of the aluminum mold have to be very precise so that each rolling wheel has a uniform polyurethane coating. This is crucial because a non-uniform polyurethane coating would change the stiffness of the rolling sensor during testing and would also introduce unnecessary noise due to uneven rotation of the rolling wheels.

The polyurethane coating was molded by PSI Urethane, Inc. There are two main reasons for using hard polyurethane material as a coating for the rolling wheels. First, since the stiffness of each rolling sensor is controlled by properties of the rolling-wheel coating, a SDOF system with a higher stiffness (k) has a higher natural frequency. A high natural frequency is desirable in the rolling sensor design as discussed earlier. Second, a stronger bonding between the polyurethane coating and the aluminum hub can avoid damaging the rolling wheels during testing. However, the use of a stronger polyurethane coating is expected to have a small negative effect on the level of rolling noise.

4.2.5 Rolling Sensor Modeled as a Single-Degree-Of-Freedom (SDOF) System

During RDD testing, the rolling sensor is used to measure the dynamic part of the pavement deflection induced by the two RDD loading rollers. A rolling sensor is basically a geophone mounted on a specially designed rolling cart. For the rolling sensor

to accurately measure the pavement deflection, the rolling sensor has to stay coupled with the pavement surface at all times. The motion of the rolling sensor can be simply modeled as a single-degree-of-freedom (SDOF) system, which consists of a lumped mass, m, attached to a linear spring with a spring constant, k, and a viscous damper with a viscous damping coefficient, c. The spring constant can be divided into two parts: (1) spring constant (k_S) which represents the elastic property of the rolling sensor (i.e. the stiffness of the polyurethane coating on each rolling wheel controls this parameter, and (2) spring constant (ka) which represents the elastic property of the air spring (i.e. higher volume of air results in a softer spring with a lower ka constant). The relationship between these spring constants is:

$$k = k_S + ka \tag{4.1}$$

On one hand, we would like to have a low k_S value so that the natural frequency of the entire rolling sensor is high relative to the typical RDD operating frequency. This explains why a stiff polyurethane coating was chosen for the rolling wheel tread. On the other hand, we would like to have a high ka value for the air-spring so that the rolling sensor is isolated from any vibrations that might be transmitted to the rolling sensor through the top of the air-spring.

A SDOF model and associated parameters are illustrated in Figure 4.1. When the rolling sensors move along a pavement surface, the deflection of the pavement, A_p, is transmitted through the rolling sensor. Then the geophone measures the displacement of the rolling sensor, A_S. The mathematical solutions which describe motion of the rolling sensor when it is subjected to a pavement excitation can be represented by Equations 4.2 and 4.3 (Richart et al., 1970). The graphical representation of Equations 4.2 and 4.3 is shown in Figure 4.10.

$$\frac{A_S}{A_P} = \frac{\sqrt{1+\left(2D\frac{\omega}{\omega_r}\right)^2}}{\sqrt{\left[1-\left(\frac{\omega}{\omega_r}\right)^2\right]^2+\left[2D\frac{\omega}{\omega_r}\right]^2}} \tag{4.2}$$

$$\tan\phi_1 = \frac{2D\left(\frac{\omega}{\omega_r}\right)}{1-\left(\frac{\omega}{\omega_r}\right)^2\left(1-4D^2\right)} \tag{4.3}$$

where

A_s = peak amplitude of rolling sensor displacement,

A_P = peak amplitude of dynamic pavement deflection,

ϕ_1 = phase angle between the rolling sensor motion relative to the motion of the pavement surface,

c = viscous damping coefficient,

c_{cr} = critical viscous damping coefficient,

D = damping ratio = c / c_{cr} ,

ω = angular frequency, and

ω_r = angular resonant frequency.

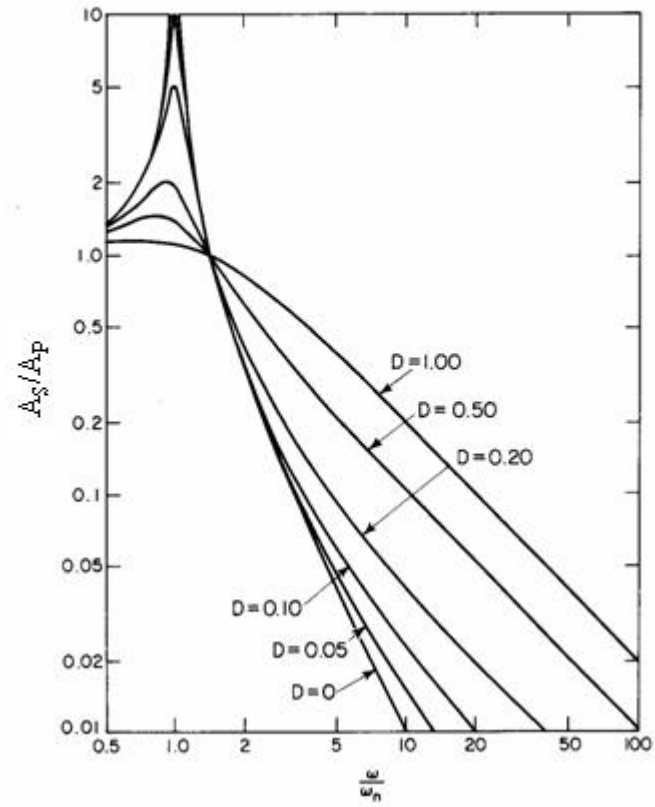

(a) Frequency Response

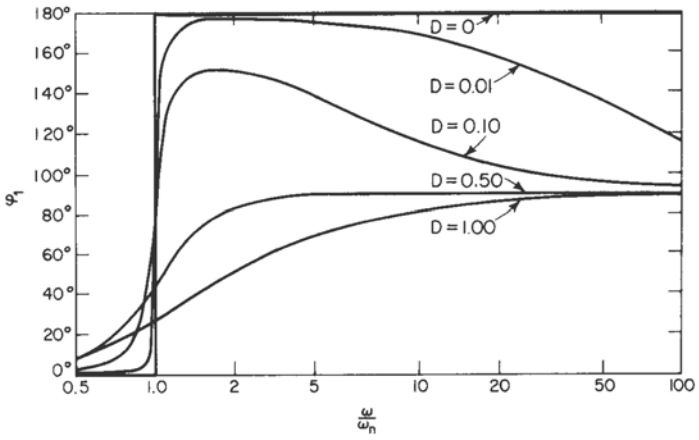

(b) Phase Response

Figure 4.10 Graphical Representation of the Dynamic Motion of a Rolling Sensor from Movement of the Pavement (after Richart et al., 1970)

4.3 LABORATORY CALIBRATION OF THE ROLLING SENSORS

Each rolling sensor needs to be calibrated individually in the laboratory before it can be used to make deflection measurements in the field. The layout of the equipment used for laboratory calibration of the second-generation rolling sensors is shown in Figure 4.11. Photographs of the laboratory calibration setup are shown in Figures 4.12 and 4.13. Each rolling sensor was calibrated with the air-spring pressurized to 5 psi. Furthermore, the reaction frame which provides the reaction force against the pressurized air-spring, was rigidly bolted to the shaker. A heavy reaction frame was not needed because the connecting rods were in tension when the air-spring was pressurized, providing the required hold-down force for the sensor.

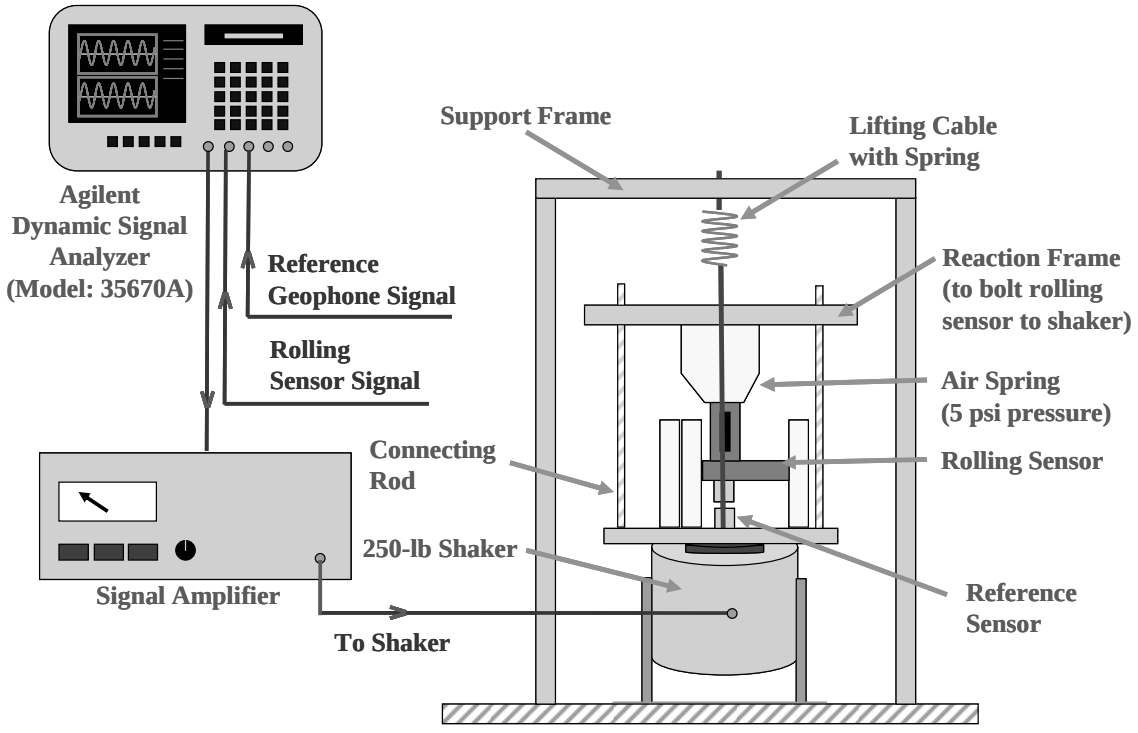

Figure 4.11 Schematic Illustration of the Laboratory Calibration Setup of a Second-Generation Rolling Sensor

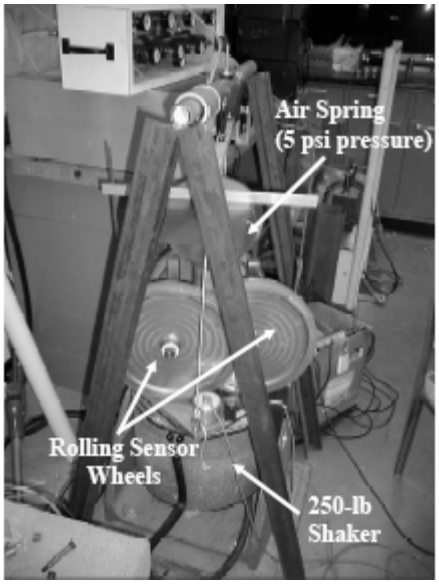

Figure 4.12 Photograph of the Laboratory Calibration Setup of a Second-Generation Rolling Sensor

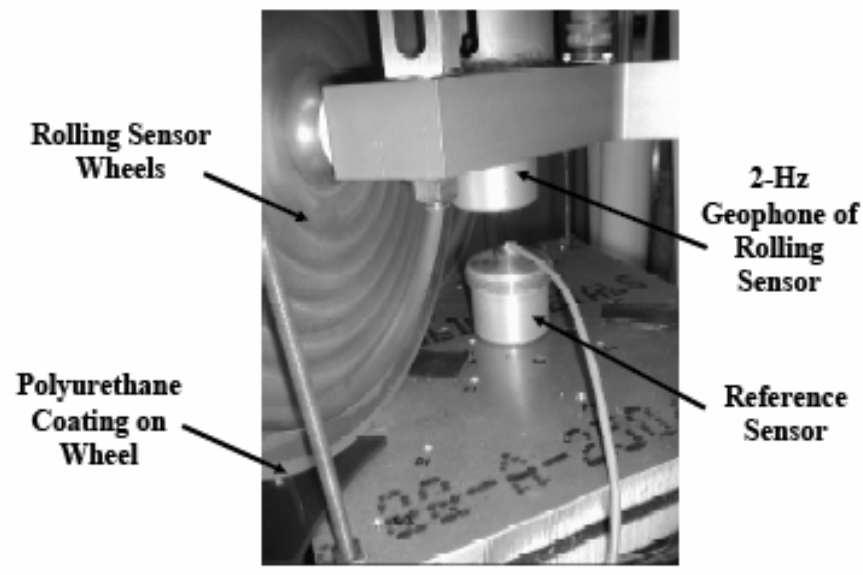

Figure 4.13 Photograph of the Reference Geophone Sensor Used in the Laboratory Calibration Setup Procedure

The laboratory calibration procedure involves placing a rolling sensor on a shake table and monitoring the voltage output of the geophone inside the rolling sensor over a wide range of known shaking levels. The voltage output is a function of the amplitude and driving frequency of the shake table. An Agilent dynamic signal analyzer (Model: 35670A) is used to control and monitor the frequency response of the whole calibration procedure. A swept sine is set to run from 5 to 200 Hz. This frequency range is sufficient to cover the entire frequency range that is of interest to RDD testing. First, the signal analyzer generates the frequency sweep signal that is sent to the signal amplifier. The signal is then amplified by the signal amplifier, and it is used to drive the 250-lb (113-kg) electromagnetic shaker.

The rolling sensor rests on a 0.75-in. (19-mm) thick aluminum plate that is bolted to the central moving core of the electromagnetic shaker. The assumption that the aluminum plate remains rigid during the calibration procedure is made. This assumption means that each rolling wheel has the same excitation motion. The calibration curve of a second-generation rolling sensor with 12-in. diameter rolling wheels and an air spring that was pressurized to 5 psi (34.5 kPa) is shown in Figure 4.14. The calibration curves of the first-generation and second-generation rolling sensors are compared in Figure 4.15. The second-generation rolling sensor has a higher resonant frequency than the first-generation rolling sensor. It also has a slightly flatter calibration curve in the region where the RDD measurements are made.

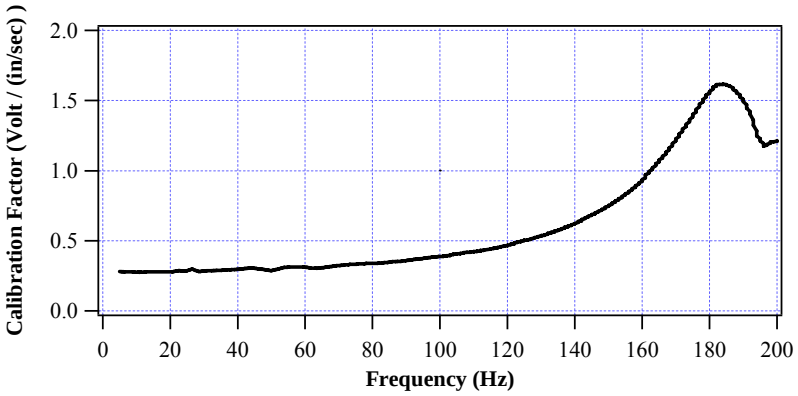

Figure 4.14 Magnitude Response of the Second-Generation Rolling Sensor Measured in the Calibration Setup Shown in Figure 4.12 with a Hold Down Pressure of 5 psi.

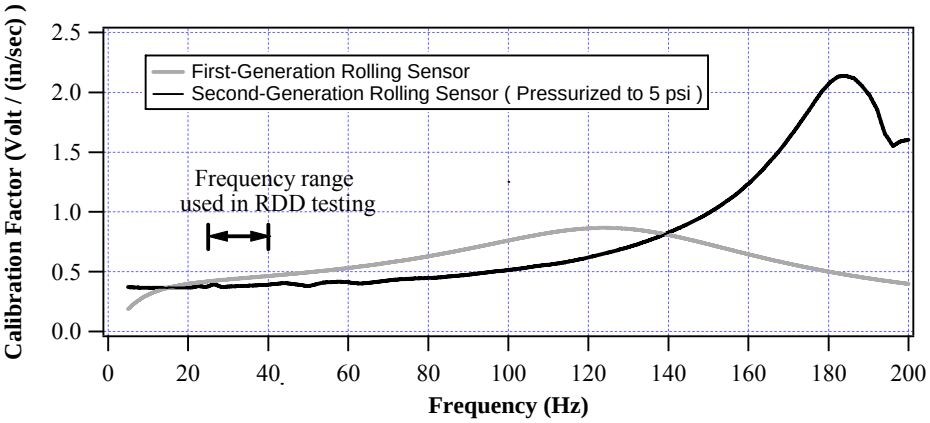

Figure 4.15 Comparison of the First-Generation and Second-Generation Rolling Sensors Calibration Curves

4.4 DESIGN OF THE AIR PRESSURING SYSTEM

Four, second-generation rolling sensors were built, one with 9-in. (229-mm) diameter rolling wheels and three with 12-in. (305-mm) diameter rolling wheels. Each rolling sensor also has an additional hold-down force to maintain coupling with the

pavement surface. A polyurethane air spring is used to provide the required hold-down force.

The air springs on the second-generation rolling sensors were designed to maintain a pressure of roughly 5 psi (34.5 kPa) during RDD testing. Each air spring has a bottom area of 7 in^2 (45 cm^2). A 35-lb-hold-down force (156 N) is generated when the air spring is pressurized at 5 psi (34.5 kPa). To provide the hold-down force for the second-generation rolling sensor, each air spring needs to be pressurized by an external pressure source. The required air pressure can be obtained from the primary air compressor on the RDD truck. The primary air compressor is used mainly for operating the air-brake system and other pneumatic equipment. This air tank maintains a pressure of roughly 90 to 120 psi (621 to 827 kPa). The operating pressure range in the RDD truck implies that a pressure relief valve will open when the pressure reaches 120 psi (827 kPa), and the air compressor will start running when the pressure inside the air tank drops below 90 psi (621 kPa).

To step-down the air pressure from the RDD primary air compressor to the required 5 psi (34.5 kPa) at each rolling sensor, an array of pressure regulators is needed to reduce the air pressure and to maintain it at the correct level throughout RDD testing. A new air pressuring system is used to meet the air pressure requirement of the second-generation rolling sensors. A system diagram of such a new pressuring system is shown in Figure 4.16.

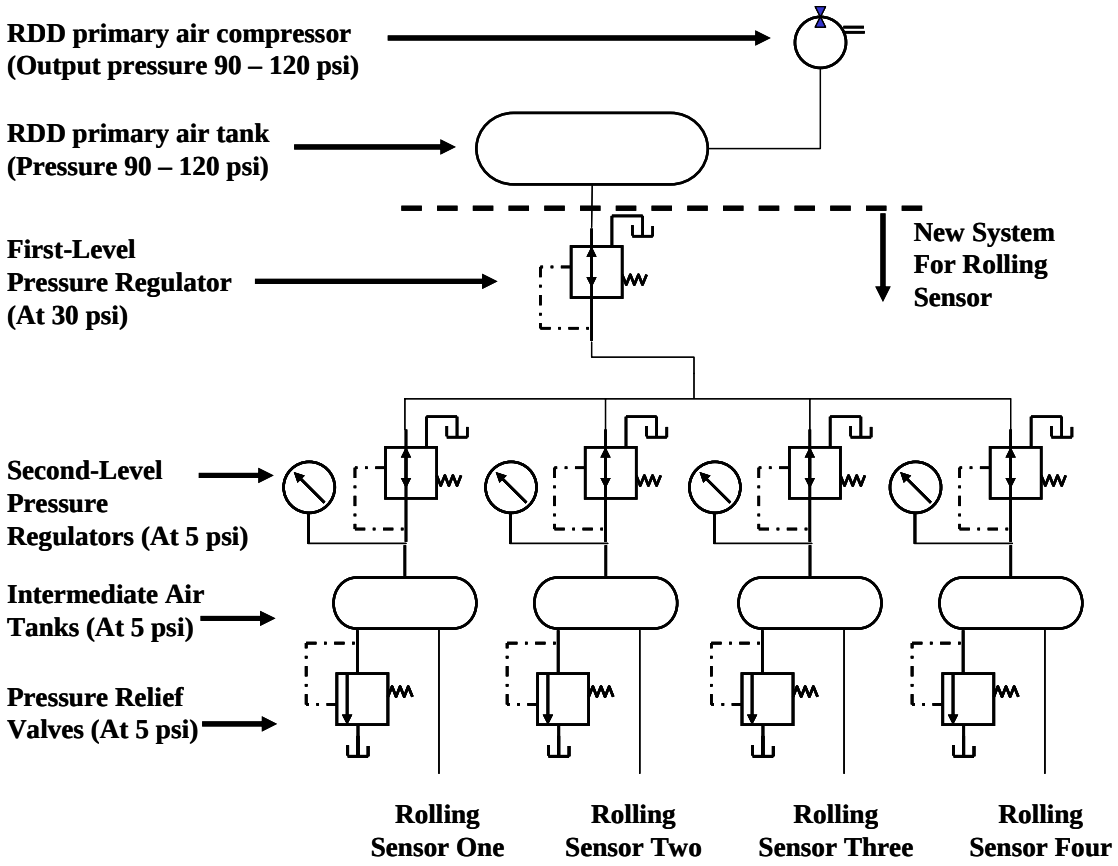

Figure 4.16 Schematic Drawing of the Air Pressuring System from the Primary RDD Air Compressor to Each Second-Generation Rolling Sensor

In the system diagram shown in Figure 4.16, two levels of pressure regulators are required to step-down the primary air compressor pressure from 90 to 120 psi (621 to 827 kPa) to 5 psi (34.5 kPa) at each air spring. One factor which controls the precision of a pressure regulator is the range of allowable input pressure of the regulator. Manufacturers of pressure regulators often have a selection of models with different input pressure ranges. In other words, a pressure regulator with a smaller input pressure range will have a more precise output pressure level in comparison with a pressure regulator with a larger input pressure range. Therefore, pressure regulators in a two-stage reduction system were

chosen so that the precision of the output pressure level is not limited by the range of pressure between the main air compressor and the air springs of the rolling sensors.

The first stage pressure regulator reduces the main air-compressor pressure to around 30 psi (207 kPa). Then the output air pressure is distributed to four individual second stage pressure regulators. There are four pressure regulators in the pressure system that has been designed and constructed for the second-generation rolling sensors. Pneumatic Precision Regulators from Fairchild, Inc. (Model 10 Series) were chosen. Each one of these pressure regulators has an output pressure between 0 and 10 psi (0 and 69 kPa) and is located between the first-stage pressure regulator and the intermediate air tanks. The sole purpose of these pressure regulators is to reduce the input air pressure of 30 psi (207 kPa) to the output air pressure of 5 psi (34.5 kPa). For practical purposes, these pressure regulators are presently mounted on a pressure panel box with an individual pressure gauge to monitor the pressure of each air spring. The pressure panel box is shown in Figure 4.17. The pressure panel box and the intermediate air tanks are also shown in Figure 4.9.

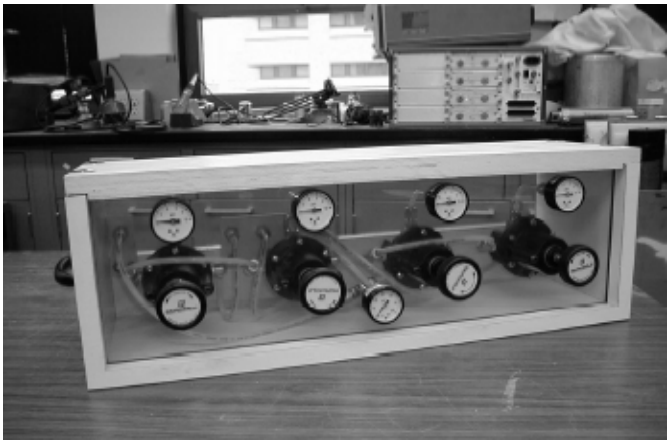

Figure 4.17 Photograph of the Pressure Panel Box Used to Provide a Constant 5 psi (34.5 kPa) Pressure to Each Second-Generation Rolling Sensor

Intermediate air tanks are connected downstream of the second-level pressure regulators. The intermediate air tanks act as buffer zones to minimize the change of pressure inside each air spring when the volume of the air spring changes due to changes in the pavement profile. Pressure fluctuations inside the air spring are further discussed in the next section. Each intermediate air tank is connected to the air spring and a pressure relief valve is also fitted on each intermediate air tank to prevent any accidental pressure surge that can damage the polyurethane air springs. These pressure relief valves are the poppet-type relief valve, and the relief pressure setting is controlled by turning the top cap, which changes the length of a calibrated compression spring. A photograph of a prototype towing frame, pressure system, and two second-generation rolling sensors is shown in Figure 4.18. This prototype towing frame can only support two rolling sensors.. To support four rolling sensors, a towing frame and pressure system would be about two times greater in length and have four intermediate air tanks.

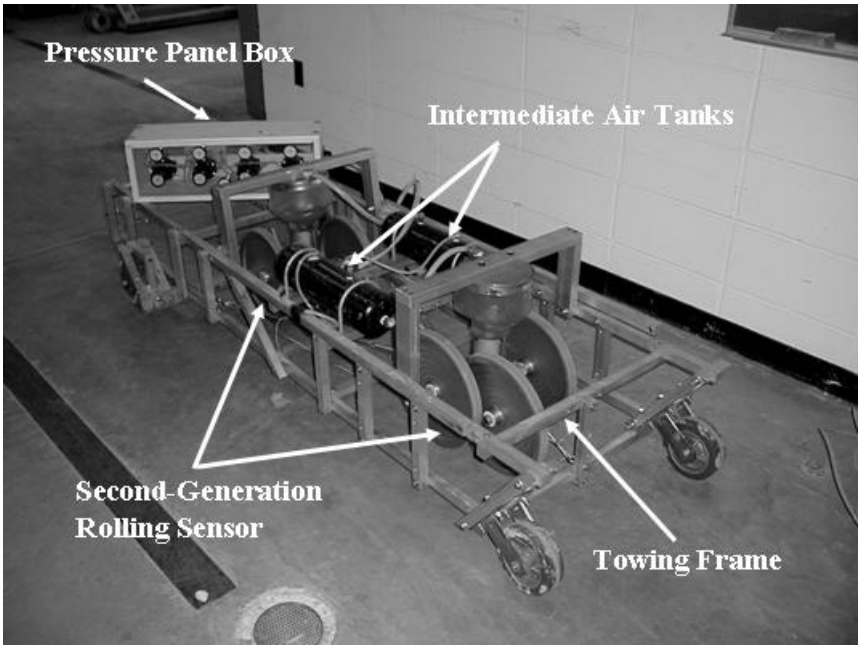

Figure 4.18 Photograph of a Prototype Towing Frame and the Pressuring System that Supports Two Second-Generation Rolling Sensors

4.4.2 Minimizing Hold-Down Pressure Fluctuation

The second-generation rolling sensors rely on the applied hold-down force to maintain coupling with the pavement surface at higher testing speeds. The hold-down pressure within the air springs can adversely influence the maximum testing speed achievable by the second-generation rolling sensors. There are many factors that can cause pressure fluctuations inside the air springs. Some of these factors are: (1) pressure variability that is caused by fluctuations in the supply pressure, (2) volume change of the compressed air inside the air springs due to pavement surface-profile variations, and (3) any air leakage along the pressure lines. Each of these factors is discussed below, and features of the pressure system are also described.

First, the supply pressure of the system will never be constant. The pressure regulators use the balanced-force principle to regulate the output pressure, and these regulators have a small output pressure range of 1 to 10 psi (6.9 to 69 kPa). This type of regulator has a calibrated compression spring inside which connects to the top of a diaphragm. This compression spring controls the output pressure by balancing the forces that act on both sides of the diaphragm. Furthermore, any excessive pressure will bleed to the atmosphere through a pressure-relief port. The accuracy of the output pressure depends on the response of the compression spring, and a softer spring is used for lower-pressure- range regulators. The length of a soft spring displaces more than a stiff spring under a given pressure increment, and more displacement often means more control on the accuracy of the output pressure.

Second, Boyle's Law states that there is a fixed relationship between the pressure and the volume. The pressure of a gas decreases as the volume of that gas increases. Boyle's Law can be represented by:

$$p\,V = kT \qquad (4.3)$$

where

p = pressure of gas,
V = volume of gas,
k = constant, and
T = temperature of gas.

As a second-generation rolling sensor rolls along the pavement, the varying profile of the pavement surface can change the overall height of the rolling sensor. This change in height occurs from the compression or extension of the air spring that is located at the top of each rolling sensor. As the rolling sensor rolls across an overlay section that has severe rutting distress, the height of the rolling sensor will increase and therefore also increase the gas volume of the air spring. This change will correspondingly decrease the pressure inside the air spring, according to Boyle's Law. Since it is impossible to predict how the volume of the air spring will change, an intermediate air tank is installed for each sensor to compensate for air-spring pressure fluctuations.

These intermediate air tanks are made from a 4-in. (102 mm) diameter steel pipe section. These immediate air tanks have two functions. The primary function is to provide sufficient volume of air to the air-spring. Due to the space limitation underneath the RDD vehicle, the air-spring located at the top of each rolling sensor does not have sufficient volume of air to be a very soft (or compliant) cushion for noise attenuation. The secondary function of these air-tanks is to act as a buffer zone downstream of each second-stage pressure regulator (i.e. maintaining constant hold-down pressure within the air-spring). Two intermediate tanks were installed at this time because only two rolling sensors have been installed; each compensates for the pressure fluctuations in each rolling sensor. These tanks are conveniently located on the towing frame that is in the closest position to the associated rolling sensor. By providing a large volume buffer, it is

expected that any change in the air-spring volume will not significantly affect the pressure within each air spring. Furthermore, the air passage between each rolling sensor and the corresponding intermediate air tank are provided using 0.5-in. (12.7-mm) diameter polyethylene lines. This size line is larger in diameter than the air lines for the rest of the pressurizing system. By locating an intermediate air tank close to each rolling sensor and by having larger diameter air lines, it is possible to achieve nearly unrestricted flow for compensating any air-spring pressure fluctuations.

Third, at the current configuration, a pressure regulator is used to regulate the pressure of each air spring. There are two main reasons for this configuration which are: (1) to allow the testing crew to monitor the pressure of each air spring, and (2) to provide continuous operation of the other rolling sensors if one of them experiences problems in the field. Furthermore, this system can easily be re-configured so that a single regulator can be used to control more than one rolling sensor. This arrangement is useful if there are air leaks within the pressure system during the field testing, and this configuration provides a potential backup system.

4.5 FIELD CALIBRATION OF THE ROLLING SENSOR

As discussed in the previous section, each rolling sensor was carefully calibrated in the laboratory. However, it is a good practice to perform field calibration at the beginning of the RDD testing. This practice ensures that each rolling sensor is performing properly and provides a useful comparison between the laboratory and field calibration curves. Ideally, the laboratory and field calibration curves should match. Therefore, any discrepancy should be investigated before the RDD testing. In this section, the field calibration equipment and setup procedure are presented using the second-generation rolling sensor.

At the current RDD configuration, two sizes of second-generation rolling sensors are used: (1) a rolling sensor with 9-in. diameter wheels, and (2) rolling sensors with 12-in. diameter wheels. The rolling sensor with 9-in. diameter wheels is located mid-way between the loading rollers, and this smaller size rolling sensor is necessary because of space limitations of the current RDD configuration.

The field calibration setup is simple and can be performed with ease in the field. The field calibration setup is shown in Figure 4.19. It involves fixing a small metal plate to the pavement surface using "fast-set" epoxy, where a precisely calibrated reference transducer is screwed to this plate. A high-precision accelerometer (Wilcoxon 736T) was selected to measure the motion on the pavement surface. The following are the steps of the calibration procedure.

1. setup rolling sensor array in the usual manner
2. attach the reference transducer to the pavement surface
3. adjust the pressure regulator so that the pressure in the air-spring is at the desired level.
4. adjust the static force to ensure that it provides sufficient hold-down force for the loading rollers. Sufficient static force is needed to provide good coupling between the loading roller and ensure that a good dynamic waveform is measured.
5. perform swept sines over a range of frequencies (typically between 20 to 70 Hz).
6. Record the time histories from each rolling sensor and reference sensors. This recording is done using the on-board data acquisition system of the

RDD. Therefore, no additional data acquisition hardware is needed to carry out the field calibration procedure.

7. Perform post-processing on the recorded time histories where the frequency response is computed in the swept sine frequency range.

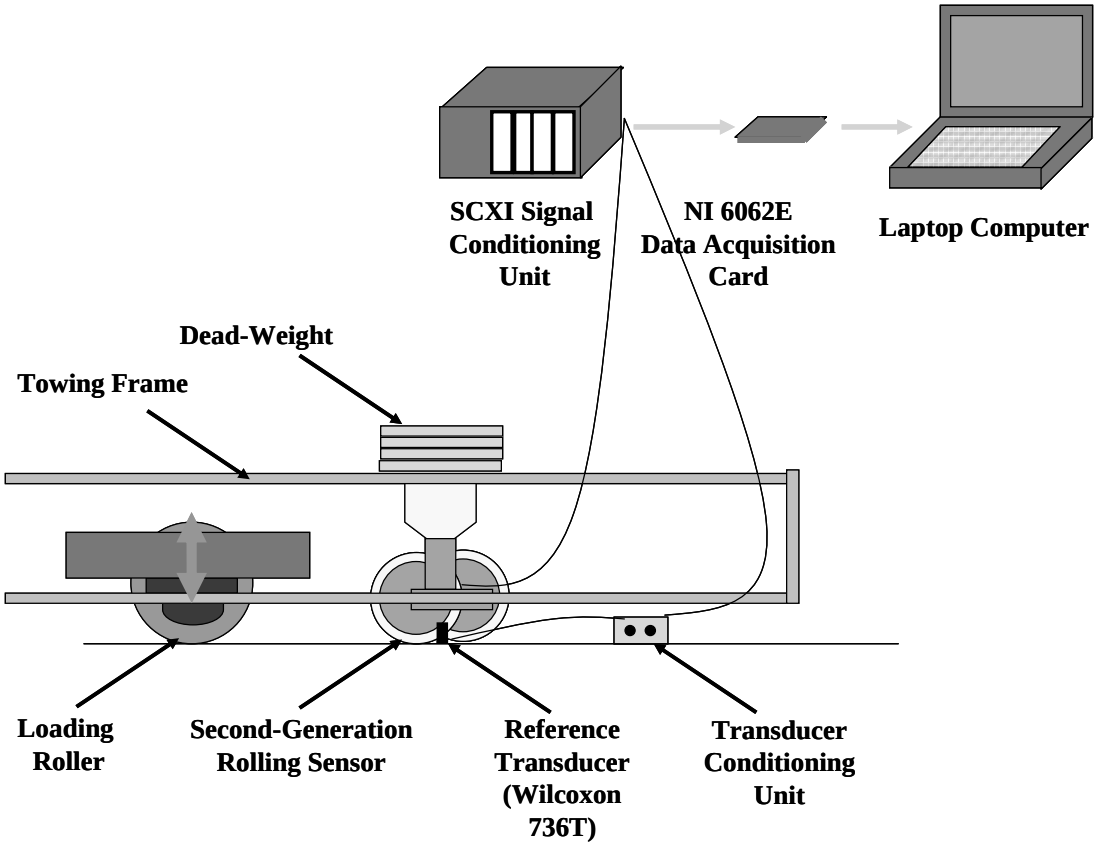

Figure 4.19 Field Calibration Equipment Setup

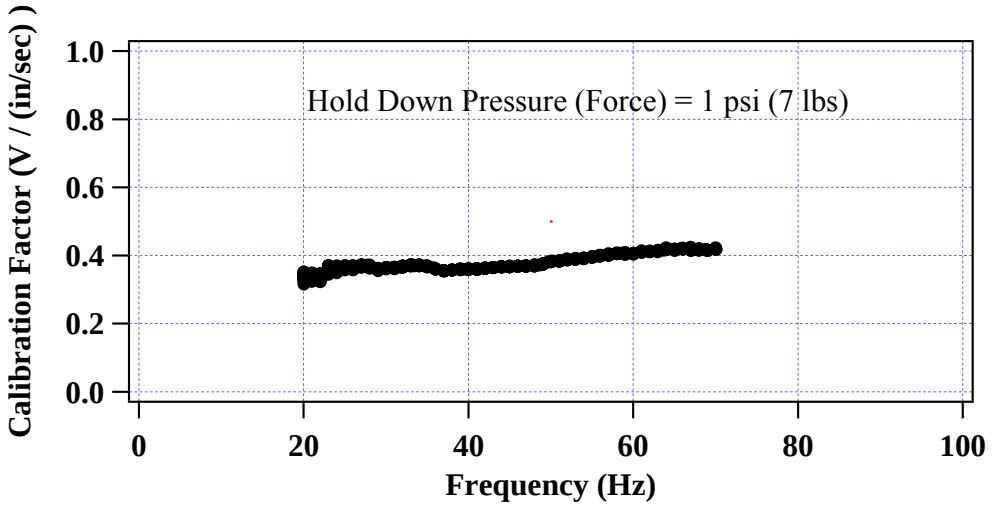

Figure 4.20 Field Calibration Curve for Rolling Sensor with 12-in. Diameter Wheel (Air-Spring Pressurized to 1 psi)

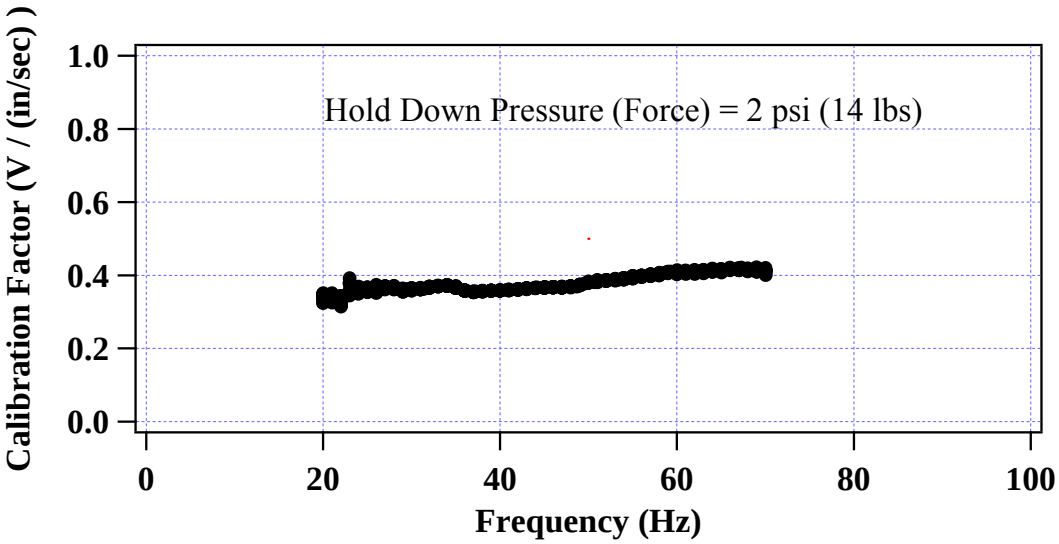

Figure 4.21 Field Calibration Curve for Rolling Sensor with 12-in. Diameter Wheel (Air-Spring Pressurized to 2 psi)

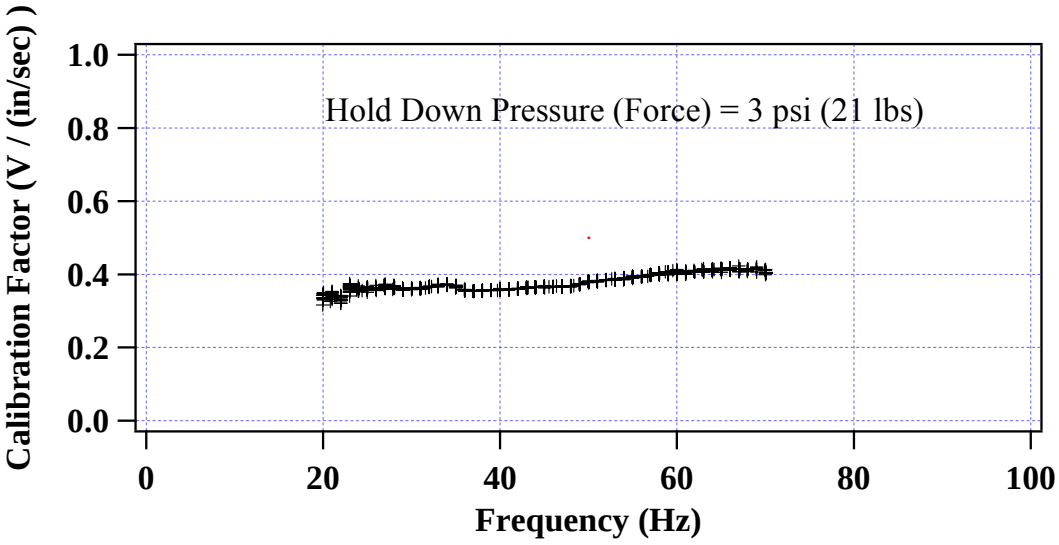

Figure 4.22 Field Calibration Curve for Rolling Sensor with 12-in. Diameter Wheel (Air-Spring Pressurized to 3 psi)

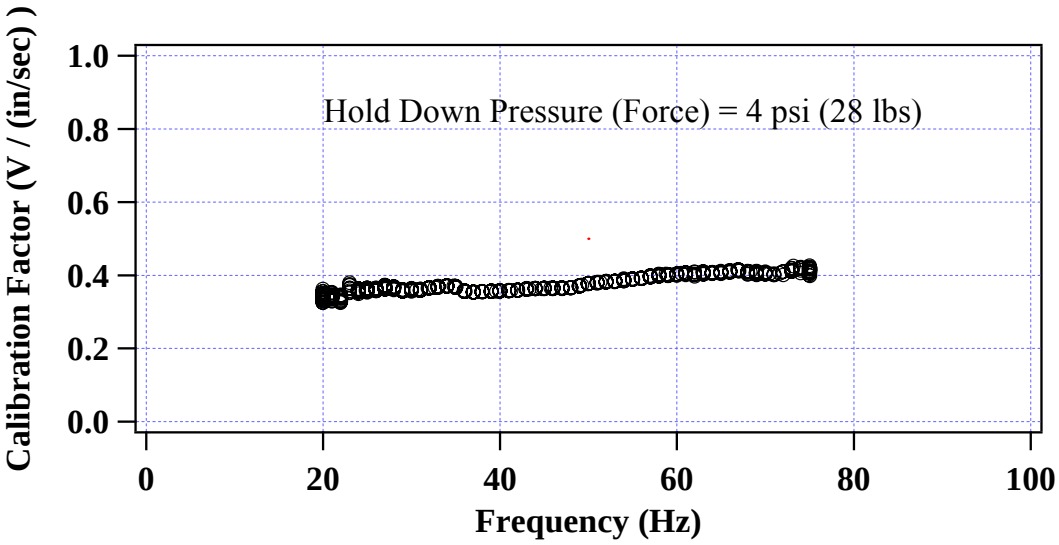

Figure 4.23 Field Calibration Curve for Rolling Sensor with 12-in. Diameter Wheel (Air-Spring Pressurized to 4 psi)

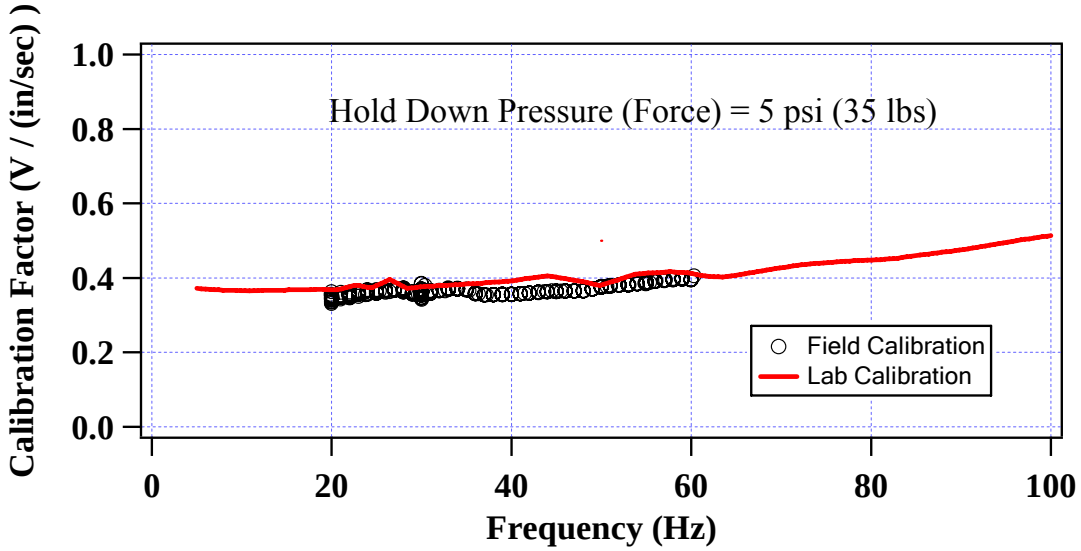

Figure 4.24 Field and Laboratory Calibration Curves for Rolling Sensor with 12-in. Diameter Wheel (Air-Spring Pressurized to 5 psi)

To better understand how the pressure inside the air-spring influence the calibration curves of the second-generation rolling sensor, a series of field calibration tests with different air-spring pressure were carried out. The field calibration curves are presented between Figures 4.20 and 4.24. It was found that the calibration curve was not significantly influenced by the pressure inside the air-spring. This is especially true in the typical RDD operating frequency range (i.e. 20 to 40 Hz). In addition, the laboratory calibration curve in Figure 4.15 is plotted together with the field calibration curve shown in Figure 4.24. Both calibration curves are very similar in the typical RDD operating frequency range.

4.6 NOISE ATTENUATION CHARACTERISTICS OF AIR-SPRING

At the current configuration, the second-generation air-spring is rigidly connected to the RDD towing frame through the air-spring, it is important to understand the noise

attenuation characteristic of the air-spring. If the air-spring performs poorly and vibration noise from the towing frame becomes excessive, the ability of the rolling sensor to measure the pavement surface deflections accurately can be impaired. In this section, the air-spring noise attenuation characteristics were evaluated in both the laboratory and field environment. The laboratory and field evaluation studies used different sources to simulate noise vibration. There are two main differences between the laboratory and field evaluation studies as follows.

1. In the field evaluation study, the dynamic loading system of the RDD was used as the source. Any arbitrary waveform can be generated by the RDD loading system. However, to better simulate the vibration from the RDD, swept sine waveforms were applied and transmitted to the top of the towing frame through two aluminum bars. Also, the towing frame was connected to the RDD truck as it would be during actual RDD testing.
2. In the laboratory evaluation study, a rubber mallet hammer was used as the source. The type of vibration that is generated by a rubber mallet hammer is a wide-band type noise. The air-spring was not excited by a single frequency at any instance, instead, a wide range of frequencies were applied as an impact force. The shortcoming of this set-up is that the frequency content of each impact varies and the result is not repetitive.

4.6.1 Field Evaluation of Noise Transmission through the Air Spring

The field evaluation study was designed to focus on the vibration noise created by the RDD at the RDD operating frequency. This noise is believed to be the primary source of noise which gets transmitted through the air-spring to the rolling sensor. An equipment setup used to perform this field evaluation study is shown in Figure 4.25. Also, this type of noise is the most detrimental due to the fact that it is located close to the actual RDD

operating frequency. If this noise component becomes excessive, it would be extremely challenging for the digital filter to distinguish between the noise and the actual RDD signal (i.e. pavement surface deflection). On the other hand, other noise does exist that is outside the RDD operating frequency range. For example, the low-frequency movement of the towing frame caused by the changing longitudinal pavement profile. Since the RDD loading system is not very good at applying force at frequencies that are outside the range of 20 to 100 Hz, a laboratory evaluation study was carried out to try and cover this gap. The vibration noise that is transmitted through the air-spring is shown in Figures 4.26 and 4.30. A term known as the attenuation ratio, is used to quantify the decrease in the acceleration magnitude as the vibration noise travels from the air-spring to the main body of the rolling sensor. This is simply the ratio between the two recorded magnitudes. The vertical axis in each figure is the attenuation ratio which is defined as the ratio between the acceleration measured in the frame and the ground.

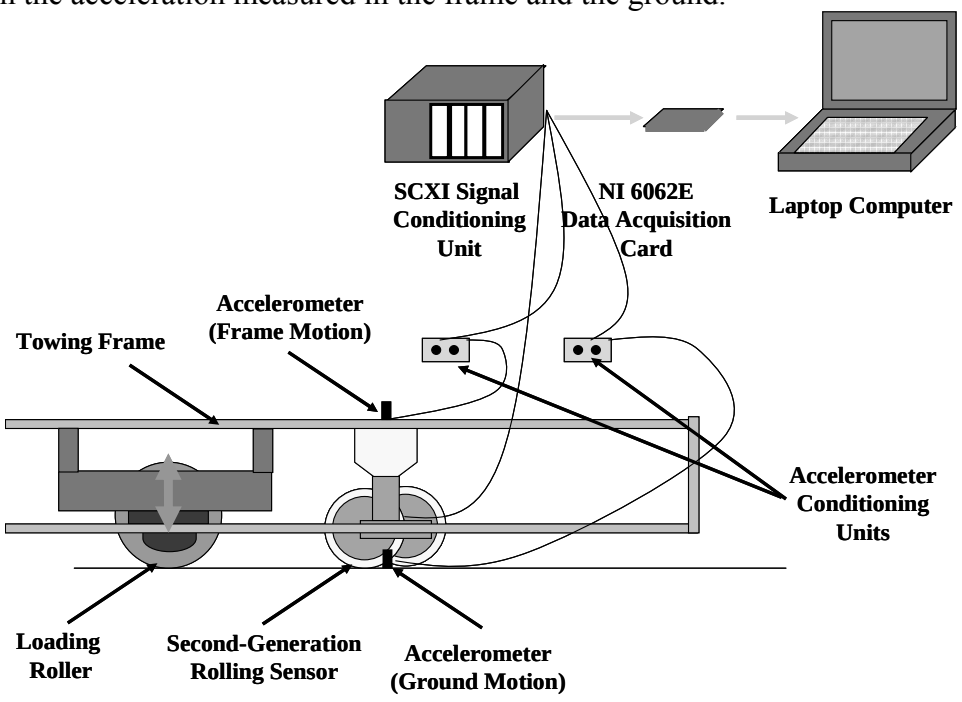

Figure 4.25 Equipment setup used in the Field Evaluation Study on Air-Spring Noise Attenuation Characteristics

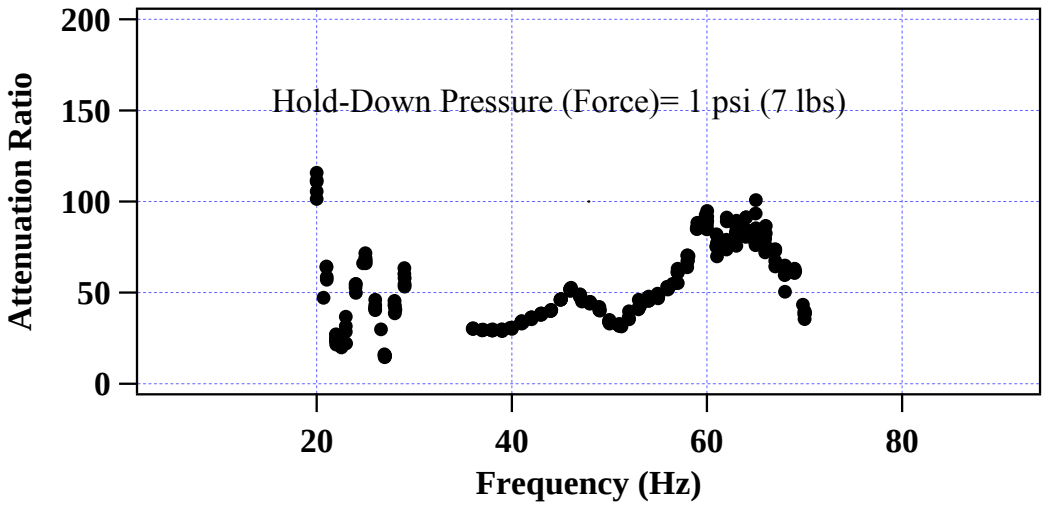

Figure 4.26 Attenuation Ratios at Different Frequencies for Rolling Sensor with 12-in. Diameter Wheels (pressurized at 1 psi)

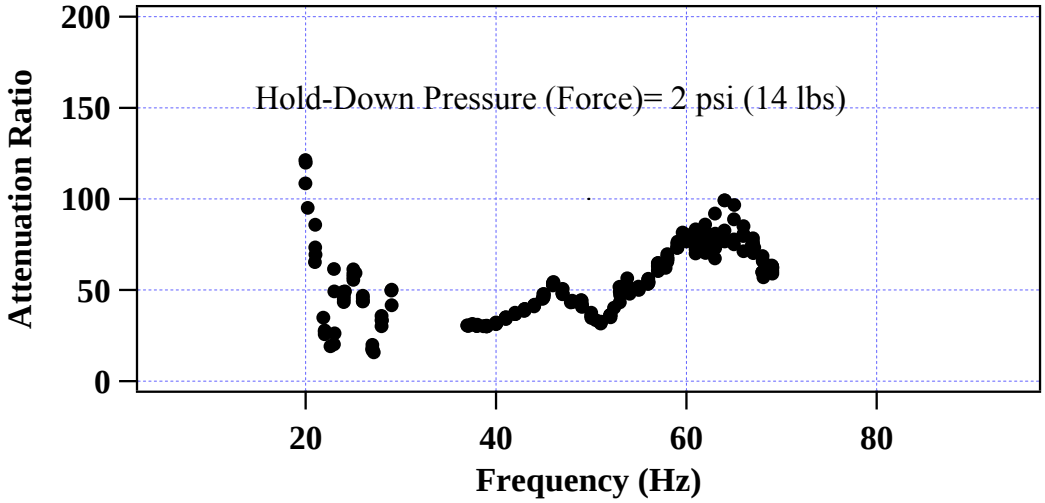

Figure 4.27 Attenuation Ratios at Different Frequencies for Rolling Sensor with 12-in. Diameter Wheels (pressurized at 2 psi)

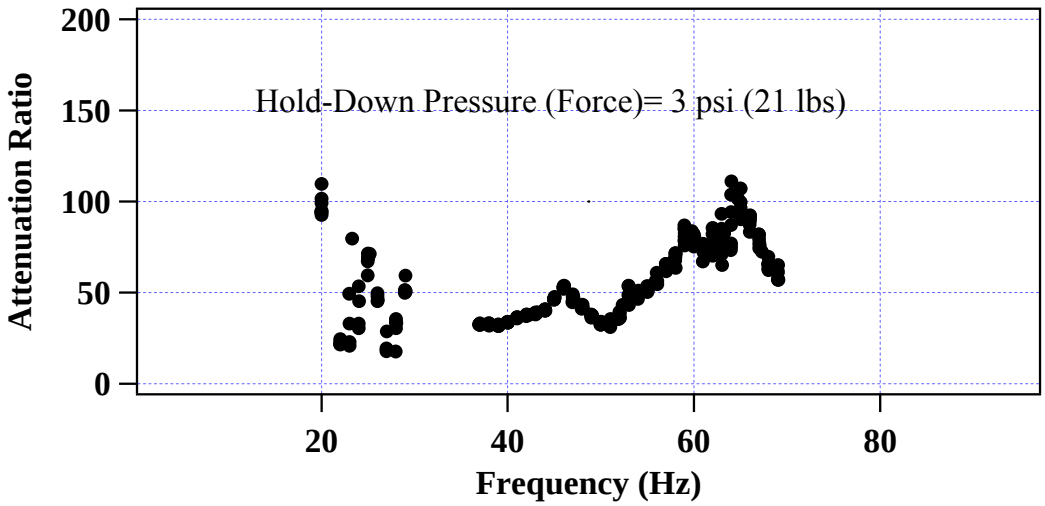

Figure 4.28 Attenuation Ratios at Different Frequencies for Rolling Sensor with 12-in. Diameter Wheels (pressurized at 3 psi)

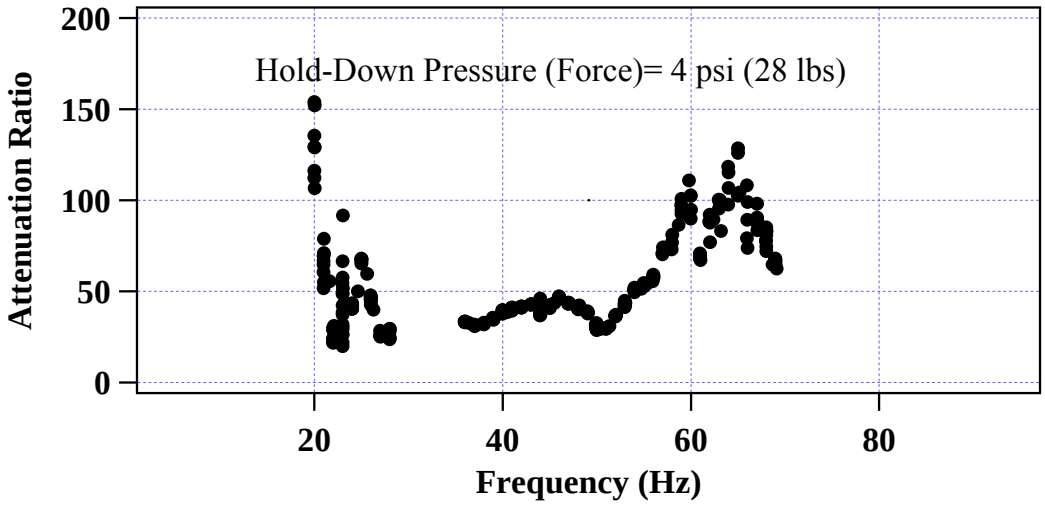

Figure 4.29 Attenuation Ratios at Different Frequencies for Rolling Sensor with 12-in. Diameter Wheels (pressurized at 4 psi)

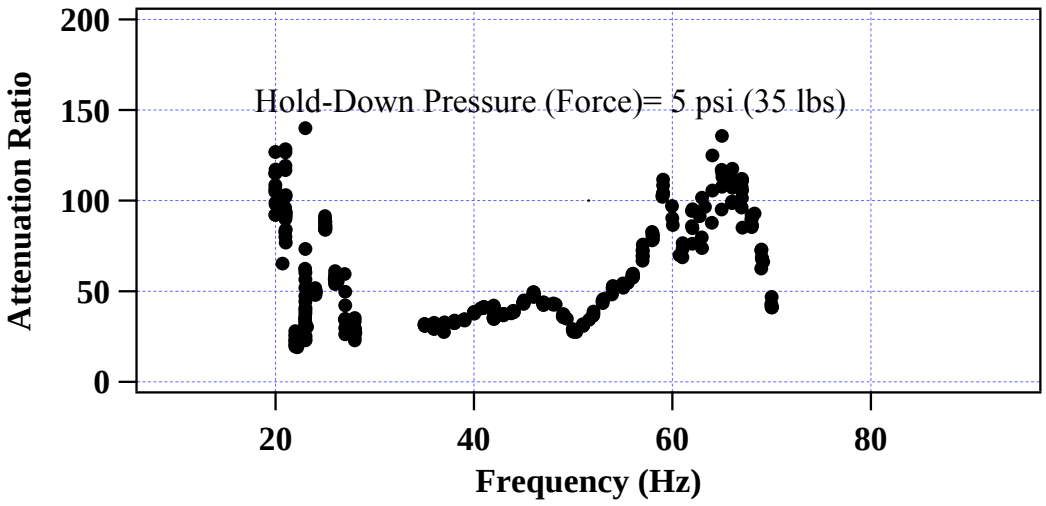

Figure 4.30 Attenuation Ratios at Different Frequencies for Rolling Sensor with 12-in. Diameter Wheels (pressurized at 5 psi)

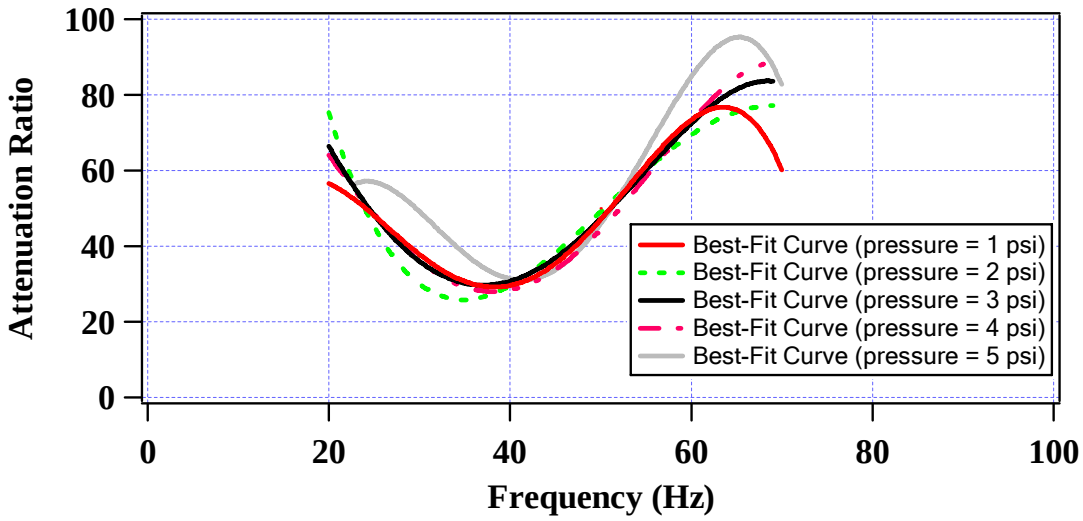

Figure 4.31 Best-Fit Trends of the Attenuation Ratios in the Frequency Domain at Different Air-Spring Pressures (1 to 5 psi)

A curve fitting procedure was then applied to generalize the trends between the attenuation ratio and frequency at different air-spring hold-down pressure as shown in Figure 4.31. All the attenuation curves have similar shape in the frequency domain, and the lowest attenuation ratio is approximately 1:25. It was surprising to find out that the pressure inside the air-spring does not have a significant effect on the attenuation ratio. Also, the air-spring has higher attenuation ratios at frequencies outside the typical RDD operating frequency than within the RDD operating frequency range.

4.6.2 Laboratory Evaluation of Noise Transmission through the Air Spring

To evaluate the noise isolation performance of the air spring, two identical accelerometers, Model 736T by Wilcoxon, Inc., were attached above and below the air spring. Then an impact force was applied using a rubber mallet hammer. The output signal from each accelerometer was recorded using an Agilent dynamic signal analyzer, Model 35670A. A photograph of the noise evaluation setup is shown in Figure 4.32. The time histories from the two accelerometers are shown in Figure 4.33. The difference in acceleration after the impact wave travels through the air spring (pressurized at 5 psi, which is equivalent to a 35-lb hold-down force) has a ratio of approximately 1:60. This is equivalent to a measurement error of 0.17 mils due to noise transmission through the air-spring when the rolling sensor is tested on a pavement with an average deflection of 10 mils. Therefore, the air spring is believed to sufficiently reduce noise that might be transmitted to the rolling sensor from the towing frame.

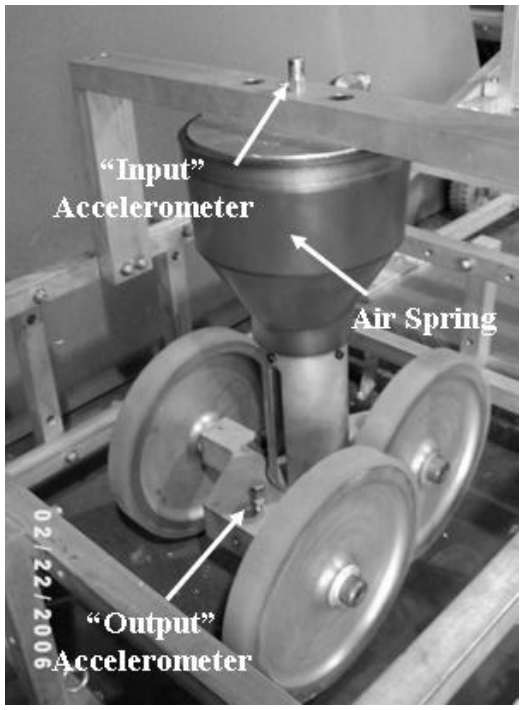

Figure 4.32 Photograph of the Laboratory Setup Used to Evaluate the Noise Isolation Performance of the Air Spring

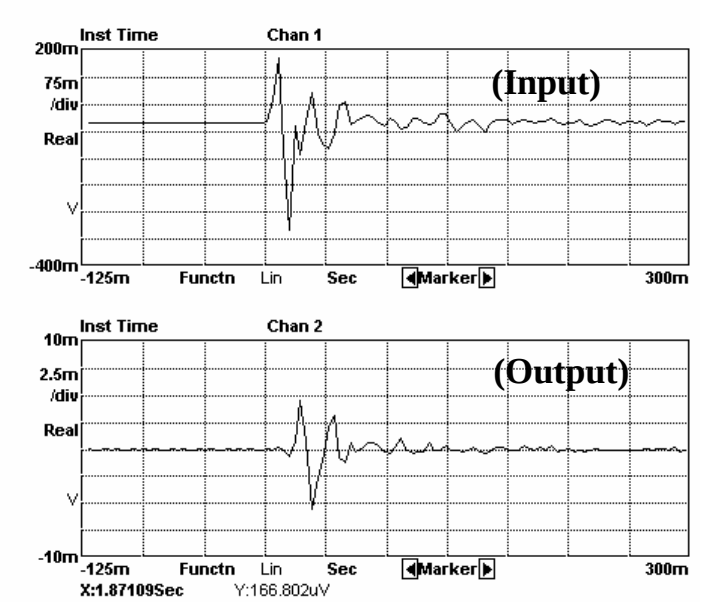

Figure 4.33 Output from Accelerometers Located Above (Input) and Below (Output) the Air Spring

4.7 SUMMARY

In this chapter, the different design considerations for developing second-generation rolling sensors are presented. The development of the second-generation sensors is then presented. The primary objective of this new rolling sensor is to increase the RDD testing speed from 1 to 3 mph (1.6 to 4.8 km/hr). The secondary objective of this new rolling sensor is to reduce the noise levels in the rolling sensor measurements relative to noise levels present in the first-generation rolling sensors.

During the course of this study, a total of two rolling sensor designs were conceptualized. The second design which uses an air-spring to provide a hold-down force to the rolling sensor was used. Prototypes sensors were constructed according to the second-generation specifications. The prototypes include second-generation rolling sensors with either 9-in. diameter or 12-in. diameter wheels. All prototype rolling sensors discussed herein were calibrated in the laboratory. This calibration involved exciting the sensors on a platform that was driven dynamically by a electro-hydraulic dynamic shaker. The movement of the platform represented dynamic movements on a pavement. In addition, a field calibration procedure was developed to calibrate the rolling sensors in the field. In this case, the pavement was driven dynamically using the RDD hydraulic loading system and an independent measurement of the pavement movement was also performed. It was concluded that this design has accomplished both objectives of this study.

Chapter 5 Field Testing Using the Second-Generation Rolling Sensor

5.1 INTRODUCTION

Development of the second-generation rolling sensor is presented in Chapter 4. Second-generation rolling sensors with 9-in. and 12-in. diameter wheels were built. In this chapter, results collected along different types of pavement using these second-generation rolling sensors are presented. The second-generation rolling sensor has the following major improvements over the first-generation rolling sensor:

1. the overall rolling noise across the Nyquist frequency band is reduced. More importantly, the rolling noise near the RDD operating frequency (20 – 40 Hz) is significantly lower.
2. the rolling sensor stays coupled with the pavement surface when traveling at speeds up to 3 mph (4.4 fps).

In Chapter 3, the effect of rolling noise on the RDD measurements is discussed. The testing speed, pavement type and level of road roughness affect the rolling noise characteristics. As a result, the digital filter specification that is used in the RDD data analysis procedure should be changed accordingly to reflect the change in rolling noise characteristics.

Since one of the objectives in the design of the second-generation rolling sensor is to increase the testing speed, rolling noise level will increase with increasing testing speed. Another important improvement is to reduce the rolling noise measured when the RDD is tested along different types of pavement. The following two aspects were considered when evaluating the performance of the second-generation rolling sensors:

1. the level and the characteristics of the rolling noise, and
2. the ability for the rolling sensor to stay in contact with the pavement surface when tested at different speeds (i.e. speeds of 1, 2, and 3 mph).

The results of different test trials using the second-generation rolling sensors along different types of pavements were evaluated, and the results are presented in this chapter.

5.2 OVERVIEW OF FIELD PERFORMANCE EVALUATION

The performance of the second-generation rolling sensor was evaluated along four different types of pavements. This performance evaluation is presented to illustrate the improvements that the second-generation rolling sensor has over the first-generation rolling sensor. The four types of pavements that were tested are as follows:

1. **Flexible Pavement** - Texas Accelerated Pavement Testing (TxAPT) Facility, Austin, TX. (extremely smooth surface, not opened to traffic),
2. **Flexible Pavement** - Thin Asphalt Concrete (AC) surface with a granular base adjacent to the TxAPT site,
3. **Rigid Pavement** – Loop 610 at Houston, Texas, Continuously Reinforced Concrete (CRC) Pavement with top part milled off (extremely rough surface), and
4. **Rigid Pavement** – Loop 610 at Houston, Texas, CRC Pavement currently under rehabilitation (no milling was performed).

In addition to the regular RDD deflection collection procedure, the rolling sensor array was also towed along the pavement surface with no dynamic force applied by the RDD. Time histories collected using this technique should only contain the rolling noise

component, which provides a baseline for evaluating the rolling noise with no influence from the RDD hydraulic dynamic loading system.

5.3 FLEXIBLE PAVEMENT - TXAPT FACILITY

The TxAPT facility is located inside the Prickle Research Center (PRC) at the University of Texas at Austin. It is a test facility that was originally built for the Texas Mobile Load Simulator (TxMLS), which is used to study the level of rutting and damage that are caused by the continuous loading of the TxMLS machine. This test site was built with high-quality construction workmanship and has never been open to traffic. This pavement represents the ideal case of the smoothest pavement on which an RDD deflection profile is likely to be collected. A photograph of the TxAPT site is shown in Figure 5.1. The pavement cross-section of the TxAPT site is shown in Figure 5.2. A series of test runs were performed along the east shoulder of the TxAPT site using the second-generation rolling sensors. Both the 9-in. and 12-in. diameter rolling sensors were used. Furthermore, deflection profiles were collected under different testing speeds: 1, 2 and 3 mph and at two different air-spring pressure levels (3 and 5 psi). A summary of the different test runs along the TxAPT site is presented in Table 5.1. Lastly, time histories were collected at different testing speeds with no dynamic load applied.

5.3.1 Rolling Noise Baseline

The idea of establishing a baseline for rolling noise measurement is illustrated in Figures 5.3 and 5.4. In Figure 5.3, the records were collected with RDD dynamic loading applied to the pavement. The forcing signal at the RDD operating frequency of 35 Hz is clearly identified in the frequency domain, and information pertaining to the pavement surface deflection only shows up at this frequency. Selected time histories with the same level of RDD deflection signal (i.e. V_{signal} = 0.3 V) under a 35-Hz sinusoidal dynamic

peak-to-peak load of ± 3 kips (± 13.3 kN) was chosen for a more compatible comparison. Any other energy will be treated as rolling noise in the study. As expected, the noise spectrum change characteristics and increases in amplitude as the testing speed increases. Also, the rolling noise in the higher frequency range (i.e. frequencies above the typical RDD operating frequency) also increases more rapidly as the test speed increases. Similar conclusion was obtained by Bay (1997) with simulation of rolling sensor traveling over a synthesized pavement surface at different speeds. It is also important to note that the first and second harmonics can clearly be identified when analyzing the 1 mph data in the frequency domain as shown in Figure 5.3(a). But these harmonics are masked by the rolling noise envelope as the envelope increases in magnitude with increasing testing speed (shown in Figures 5.3(b) and 5.3(c).

Up to this point, it has always been assumed that all the energy at the RDD operating frequency (i.e. 35 Hz) is due to the pavement surface deflection. However, this is not necessarily true as the frequency spectra shown in Figure 5.4 indicate that energy does exist at 35 Hz even when no RDD dynamic loading is applied. Also, it is important to evaluate whether the current second-generation rolling sensor configuration (i.e. connections between the RDD vehicle, towing frame, and rolling sensor) is sufficient to isolate the rolling sensor from the vibration on the RDD loading platform. Statistical analysis on the FFT spectra collected with RDD dynamic loading, and no RDD dynamic loading are shown in Tables 5.2 and 5.3, respectively. Comparison between the statistical parameters obtained on the FFT spectra in Figures 5.3 and 5.4 are shown in Figure 5.5. Based on the results shown in Figure 5.5, the following comments can be made:

1. In general, the magnitude of the rolling noise increases with increasing speed at all three frequency bands analyzed: (i) 0 – 128 Hz, (ii) 0 – 34 Hz, and (iii) 36 – 100 Hz.

2. The FFT spectra collected with RDD loading has more variability in the magnitude of the rolling noise (i.e. indicated by higher standard deviation values) than when the FFT spectra were collected with no RDD loading,
3. Two-tailed Student T-Test was performed on both sets of data. With the consideration that the standard deviation (σ) is fairly large relative to the mean value (μ) for both cases (i) with RDD loading and (ii) without RDD loading. It was found that statistically there is no difference between the values obtained in both cases with an alpha value (α) of 0.05. Based on this information, it can be concluded that the current rolling sensor configuration is sufficient to isolate the rolling sensor from the RDD loading platform. Furthermore, a rolling noise baseline can be estimated when no RDD loading was applied. This baseline will help to understand the rolling noise characteristics under no RDD loading condition, and is a good indicator for the level of rolling noise that exists at and around a chosen RDD operating frequency.

Information about the energy in the vicinity of the RDD operating frequency can be equally important because these energy characteristics will control the required primary lobe bandwidth of the chosen digital filter for analyzing the RDD data. However, it is important to note that the noise energy at the RDD operating frequency and in the vicinity of the RDD operating frequency is usually small in comparison to the RDD deflection signal. It is important to note that every 20 dB is equivalent to a factor of 10 in the arithmetic scale. Typical ratios between the RDD deflection signal and the surrounding noises are between 30 dB to 50 dB (i.e. RDD deflection signal are usually 31.6 to 316 times larger than the surrounding noise) when measured using the first-generation rolling sensor at Sensor #1 location at testing speed of about 1 mph (1.6

km/hr). These ratios were obtained from many different project-level studies collected on different highways and airport pavements as presented in Chapter 3. There are only very limited deflection data collected using the second-generation rolling sensor (with 12-in. diameter wheels). But it was found that a SNR between 30 to 40 dB (i.e. RDD deflection signal is 31.6 to 100 times larger than the surrounding noises) was obtained using the second-generation rolling sensor when tested along the TxAPT site.

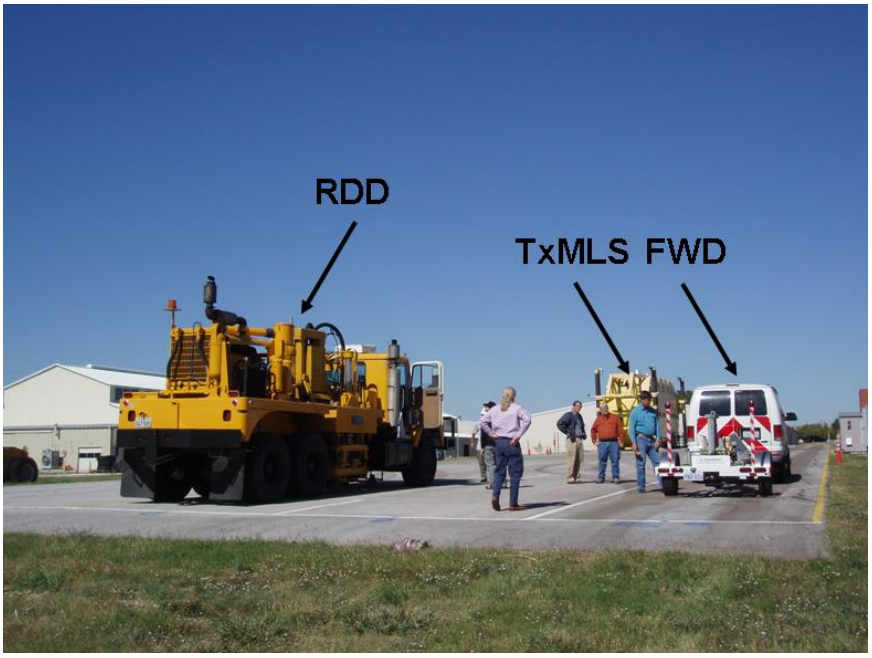

Figure 5.1 Photograph of the RDD, FWD and TxMLS on the TxAPT Test Site.

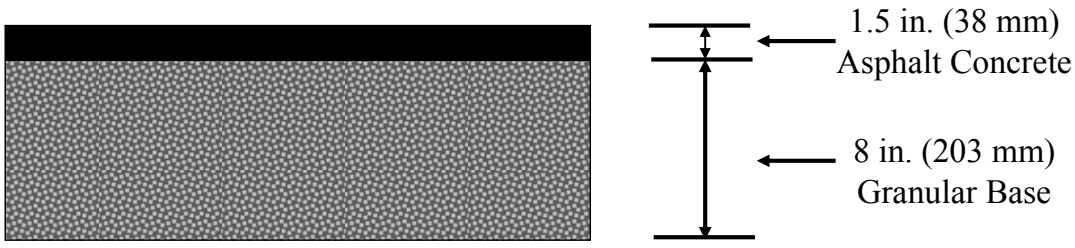

Figure 5.2 Pavement Cross-Section of the TxAPT Test Site.

Table 5.1 RDD Testing Matrix along the TxAPT Site Using the Second-Generation Rolling Sensor

	Hold-Down Pressure (Force)		
	0 psi (0 lbs)	3 psi (21 lbs)	5 psi (35 lbs)
Avg. Testing Speed (mph)	1	1	1
	2	2	2
	3	3	3

Second-Generation Rolling Sensor (9-in. Diameter Wheels)

	Hold-Down Pressure (Force)		
	0 psi (0 lbs)	3 psi (21 lbs)	5 psi (35 lbs)
Avg. Testing Speed (mph)	1	1	1
	2	2	2
	3	3	3

Second-Generation Rolling Sensor (12-in. Diameter Wheels)

Table 5.2 Results of Statistical Analysis Performed on RDD Data shown in Figure 5.3

	Frequency Ranges Used for Statistical Analysis					
	0 - 128 Hz		0 - 34 Hz		36 - 100 Hz	
Average Speed (mph)	Mean (μ)	St. Dev. (σ)	Mean (μ)	St. Dev. (σ)	Mean (μ)	St. Dev. (σ)
1	-54.9	15.3	-48.2	9.1	-61.9	10.2
2	-40.4	17.3	-35.5	9.4	-43.5	9.5
3	-34.8	15.3	-38.0	8.72	-36.0	8.3

Table 5.3 Results of Statistical Analysis Performed on RDD Data shown in Figure 5.3

	Frequency Ranges Used for Statistical Analysis					
	0 - 128 Hz		0 - 34 Hz		36 - 100 Hz	
Average Speed (mph)	Mean (μ)	St. Dev. (σ)	Mean (μ)	St. Dev. (σ)	Mean (μ)	St. Dev. (σ)
1	-53.4	10	-45.1	7.3	-52.5	7
2	-45	11.3	-39.8	5	-40.8	5.9
3	-40.5	10.8	-40.6	6.6	-35.1	5.5

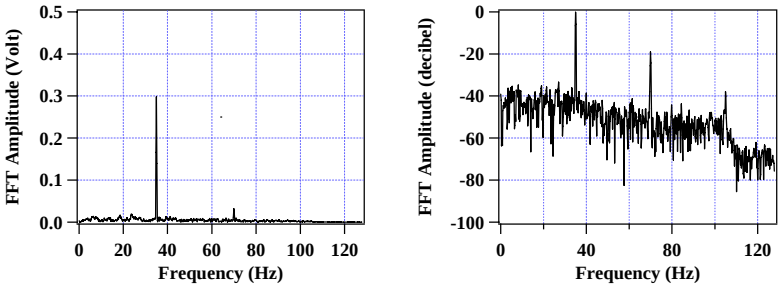

(a) Average Speed = 1 mph

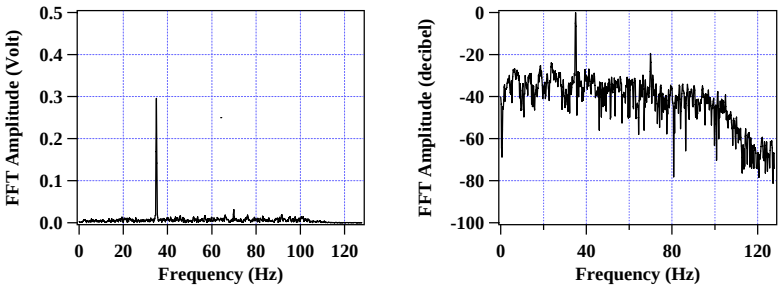

(b) Average Speed = 2 mph

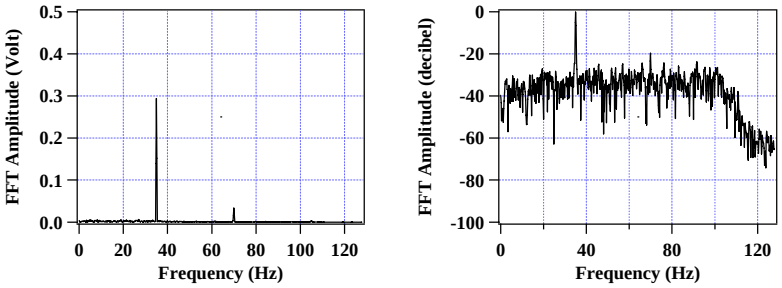

(c) Average Speed = 3 mph

Figure 5.3 Second-Generation Rolling Sensor Measurement at Various Average Test Speed Presented In the Frequency Domain; 12-in. Diameter Rolling Sensor, 5 psi Hold-Down Pressure, and RDD Operating at 35 Hz and 3 kips of Peak Dynamic Load.

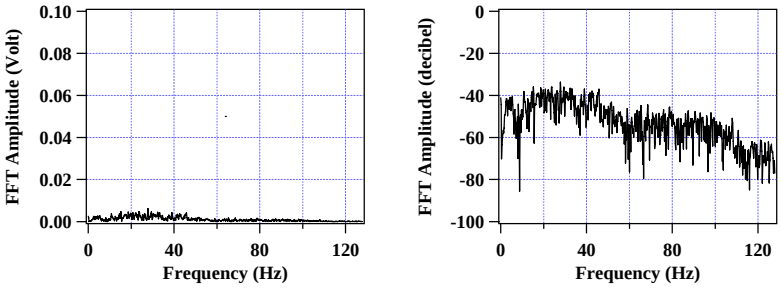

(a) Rolling Noise Baseline – Average Speed = 1mph

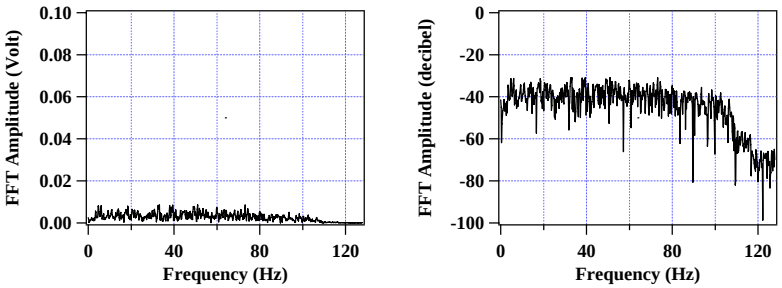

(b) Rolling Noise Baseline – Average Speed = 2mph

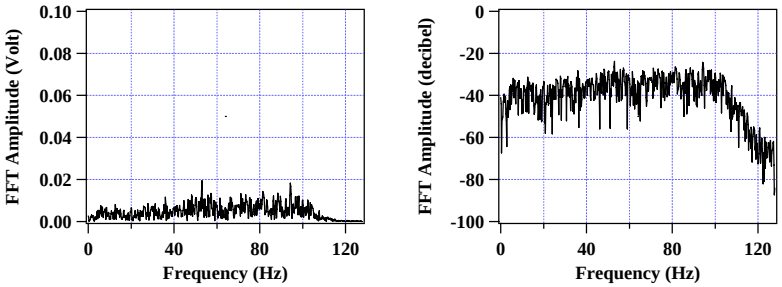

(c) Rolling Noise Baseline – Average Speed = 3mph

Figure 5.4 Second-Generation Rolling Sensor Measurement at Various Average Test Speed with No RDD Dynamic Loading Presented In the Frequency Domain; 12-in. Diameter Rolling Sensor, 5 psi Hold-Down Pressure, and no RDD Dynamic Loading Applied.

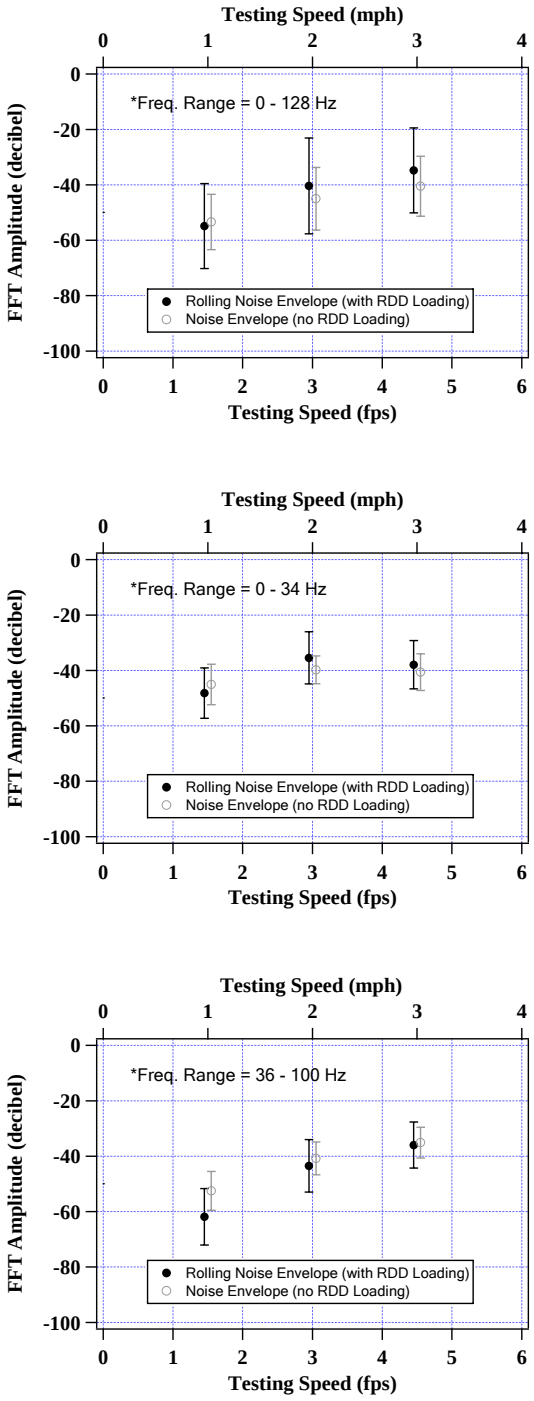

Figure 5.5 Comparison of Statistical Analysis Results for the Cases: (i) with RDD Dynamic Loading, and (ii) with no RDD Dynamic Loading, along the TxAPT Site.

An accelerometer was attached to each second-generation rolling sensor to monitor the vertical acceleration of the rolling sensor during RDD testing. The negative acceleration that the rolling sensor experience at different testing speeds indicates the coupling performance of the rolling sensor during RDD testing. Time histories of the rolling sensor and accelerometer for the 9-in. and 12-in. diameter rolling sensors are shown in Figures 5.6 and 5.7, respectively. No RDD dynamic load was applied when these time histories were collected, and this information provides a baseline for the estimation of the rolling-noise magnitude, distribution of energy in the frequency domain, and the coupling performance of the rolling sensor without the influence of the RDD dynamic load.

The acceleration time histories shown in Figures 5.6 and 5.7 are used to evaluate the coupling performance of the second-generation rolling sensors. Theoretically, with an air-spring hold-down pressure of 5 psi (i.e. equivalent to 35-lbs hold-down force), the negative acceleration should be less than -2.5 g for the majority of the time. The acceleration time histories shown in Figures 5.6 and 5.7 comprised primarily of a 35-Hz sinusoidal acceleration function and only the peak values are of importance. Therefore, for easy visualization, acceleration envelopes such as those shown in Figures 5.8 and 5.9 can be used to represent the acceleration time histories for the 9-in. and 12-in. diameter rolling sensor, respectively. With only a few exceptions along the time record, it was found that both the 9-in. and 12-in. diameter rolling sensors have negative acceleration values less than -2.5 g at testing speeds of 1, 2, and 3 mph. This measurement indicated that the rolling sensor stays coupled with the pavement during testing. The few exceptions shown in the envelope are mostly likely to be caused by the high instantaneous acceleration when the rolling sensor rolls from one high point along the pavement to the other. Because these high accelerations only happen over a very short

period of time, the influence of this to the deflection measurement is not significant. There are other reasons that are listed as follows:

1. accelerometer is more sensitive to high frequency components,
2. accelerometer is not attached directly above the 2-Hz geophone, and
3. the rolling sensor does not behave as a rigid body at high frequency range.

The following general observations can be made:

1. The acceleration envelopes increase in magnitude with increasing test speed,
2. By having 12-in. diameter rolling wheels, the acceleration envelopes are consistently lower than with the rolling sensor with 9-in. diameter rolling wheels. However, according to the numerical simulation study done by Bay (1997), the benefit of using larger diameter wheels will diminish as the diameter increases, and
3. The measured acceleration envelopes are lower than the theoretical limiting acceleration value of -2.5 g for the majority of the time.

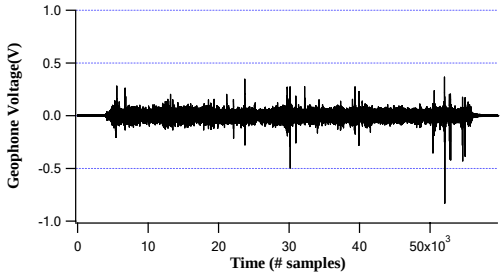

(a) Rolling Sensor Output – 1 mph

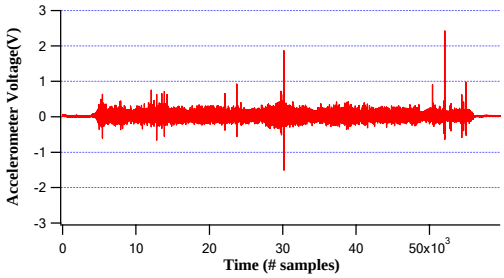

(b) Accelerometer Output – 1 mph

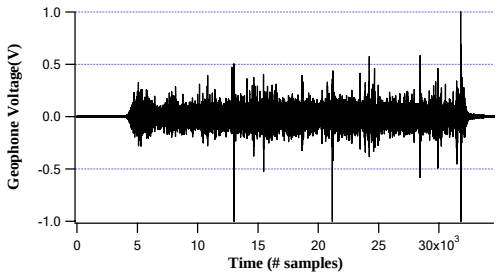

(c) Rolling Sensor Output – 2 mph

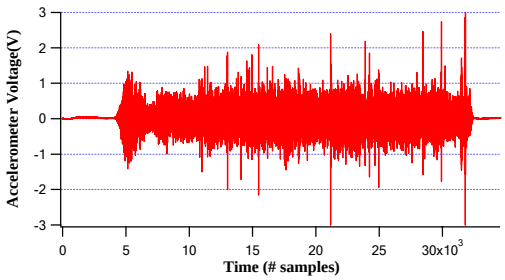

(d) Accelerometer Output – 2 mph

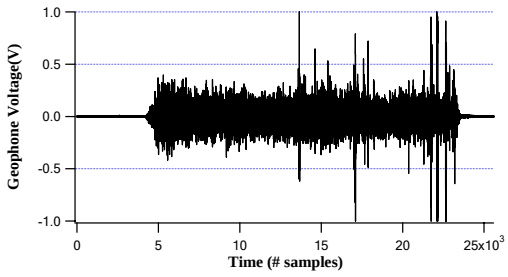

(e) Rolling Sensor Output – 3 mph

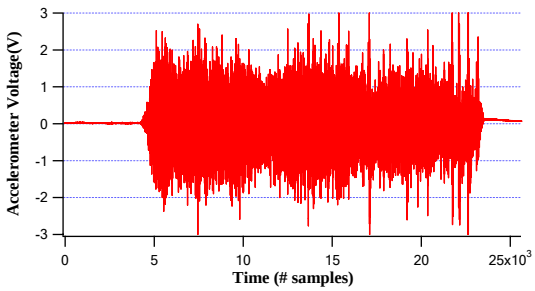

(f) Accelerometer Output – 3 mph

Figure 5.6 9-in. Diameter Second-Generation Rolling Sensor and Accelerometer Outputs Collected Along the TxAPT Site with no RDD Dynamic Load

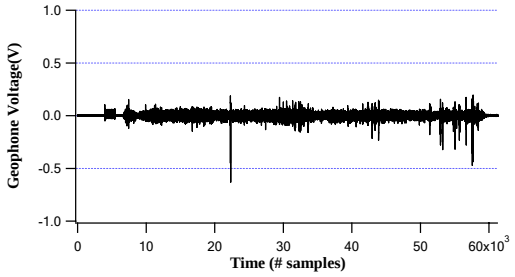

(a) Rolling Sensor Output – 1 mph

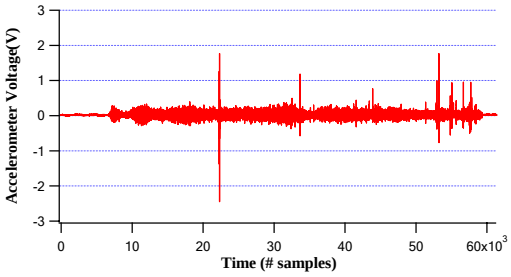

(b) Accelerometer Output – 1 mph

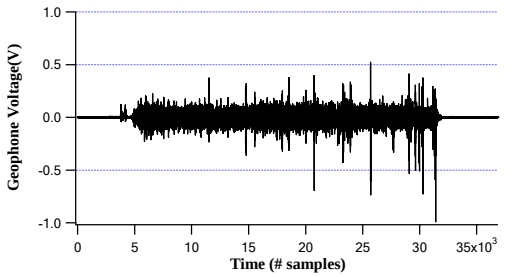

(c) Rolling Sensor Output – 2 mph

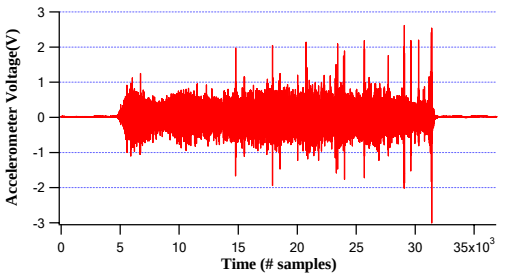

(d) Accelerometer Output – 2 mph

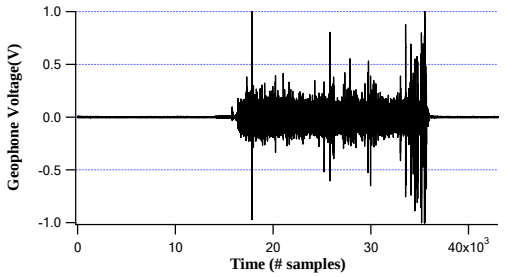

(e) Rolling Sensor Output – 3 mph

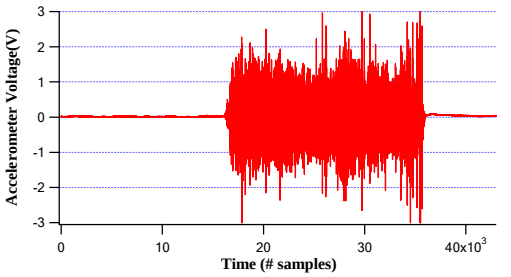

(f) Accelerometer Output – 3 mph

Figure 5.7 12-in. Diameter Second-Generation Rolling Sensor and Accelerometer outputs Collected Along the TxAPT Site with no RDD Dynamic Load

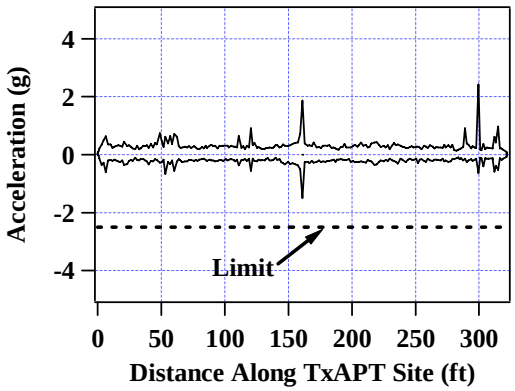

(a) Average Speed 1 mph

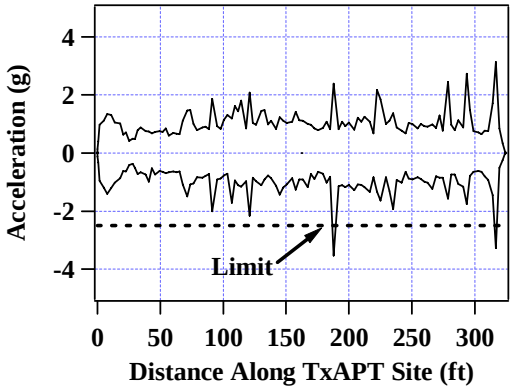

(b) Average Speed 2 mph

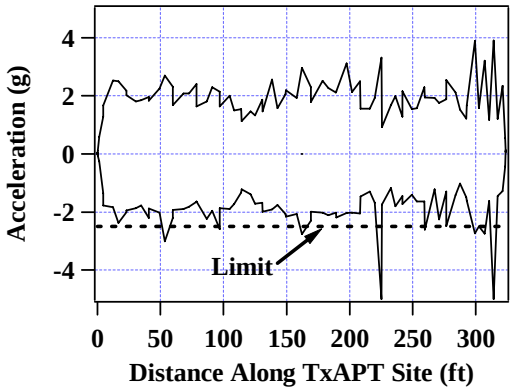

(c) Average Speed 3 mph

Figure 5.8 Acceleration Envelope Collected at Speeds of 1, 2, and 3 mph Along the TxAPT Site Using the 9-in. Diameter Second-Generation Rolling Sensor with no RDD Dynamic Load.

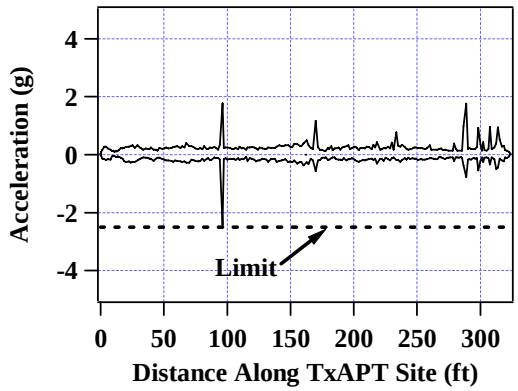

(a) Average Speed 1 mph

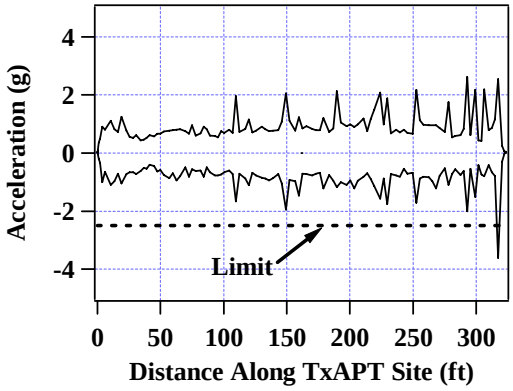

(b) Average Speed 2 mph

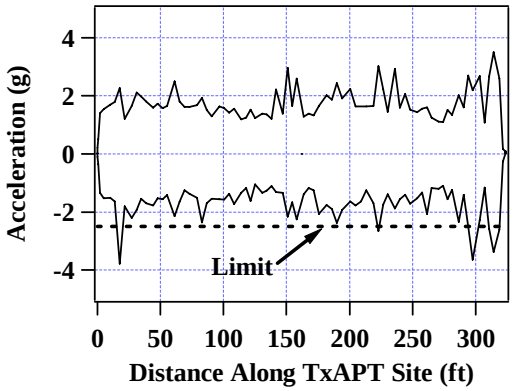

(c) Average Speed 3 mph

Figure 5.9 Acceleration Envelope Collected at Speeds of 1, 2, and 3 mph Along the TxAPT Site Using the 12-in. Diameter Second-Generation Rolling Sensor with no RDD Dynamic Load.

5.3.2 Distribution of Rolling Noise in the Frequency Domain

The next factor to be considered is the distribution of the measured rolling noise energy in the frequency domain. Ideally, if an infinitely sharp filter can be used to extract information from the rolling sensor time histories, then the only rolling noise component that is of concern would be the one at precisely the RDD operating frequency. However, this digital filtering approach would not be feasible because an infinitely sharp filter requires an infinitely long time record, which would have a very poor and unacceptable time resolution for RDD measurement application. As a result of this practical issue, all digital filters presented herein have a finite pass band. These digital filters will usually center about the chosen RDD operating frequency and will not be very good at attenuating noise that is close to the RDD operating frequency. In fact, the design parameter of the rolling sensor is also controlled by the performance of the chosen digital filter. In short, the lower the rolling noise energy is around the operating frequency range in which the digital filter needs to resolve, the better accuracy the RDD deflection measurement be.

The average noise energy located between 20 and 40 Hz for the 9-in. and 12-in. second-generation rolling sensors are shown in Figures 5.10 and 5.11, respectively. These data were collected with no RDD dynamic load applied and an air-spring hold-down pressure of 5 psi (i.e. 35-lbs) was applied. These data represent the baseline rolling noise level in the vicinity of the operating frequency in which the RDD digital filter's primary lobe intercepts. Based on these results, the following observations can be made:

1. The rolling noise level increases with increasing test speed,
2. For 9-in. diameter rolling sensor, the average noise level increases from 0.002 to 0.0045 V when testing speeds increased from 1 to 3 mph,

3. For 12-in. diameter rolling sensor, the average noise level increases slightly less than the measurements observed using the 9-in. diameter rolling sensor. The average noise level increases from 0.002 to 0.003 when testing speeds increased from 1 to 3 mph,
4. The key point is that even though the noise level obtained from 9-in. diameter rolling sensor is higher than the noise level obtained from 12-in. diameter rolling sensor. A noise level of 0.0045 V is still very small in comparison to a typical RDD deflection signal of 0.3 V (i.e. SNR of 66 times),
5. The rate of change of the measured rolling noise (with increasing testing speed) is small when tested along the TxAPT site, which is a very smooth pavement that has never been open to traffic, and
6. The typical ratio between the RDD signal and the surround noise between 20 and 40 Hz is around 30 – 40 dB (i.e. 31.6 to 100 times).

In terms of minimizing the rolling noise in the vicinity of the RDD operating frequency, Figures 5.10 and 5.11 indicated that there is only a small benefit in using the second-generation sensor with 12-in. diameter rolling wheels. This conclusion can be explained by the fact that the TxAPT site is a very smooth pavement which has never been open to traffic. The surface roughness dimension is insignificant in comparison with the diameter of the 9-in. or 12-in. diameter rolling wheels that support the rolling sensors. However, this type of pavement surface roughness is uncommon for in-service pavements, and when RDD deflection profiles need to be collected on pavement surface with extreme roughness, the benefit of having larger diameter rolling wheels becomes apparent as is discussed in Section 5.4.

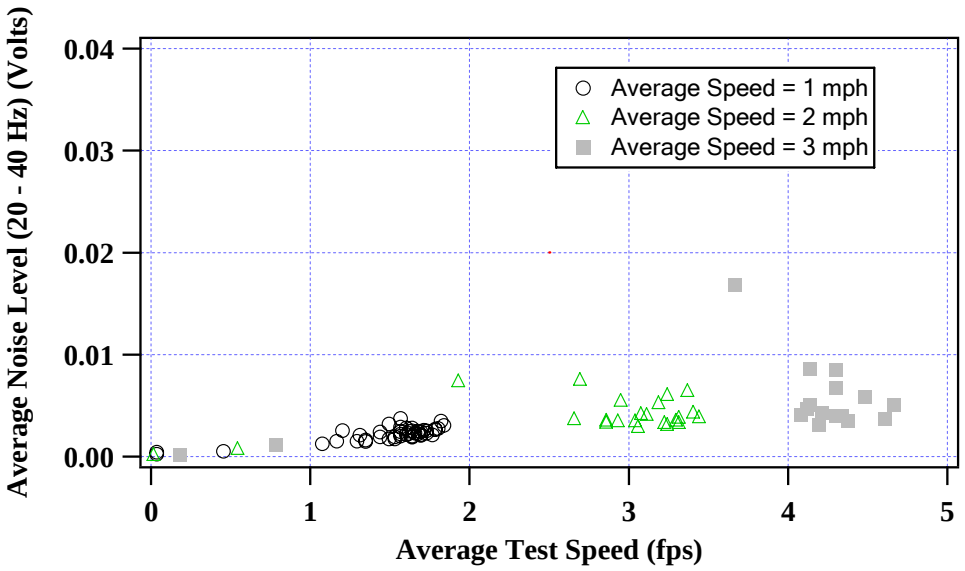

Figure 5.10 Average Noise Level Between 20 and 40 Hz Collected Using the 9-in. Diameter, Second-Generation Rolling Sensor Along the TxAPT Site

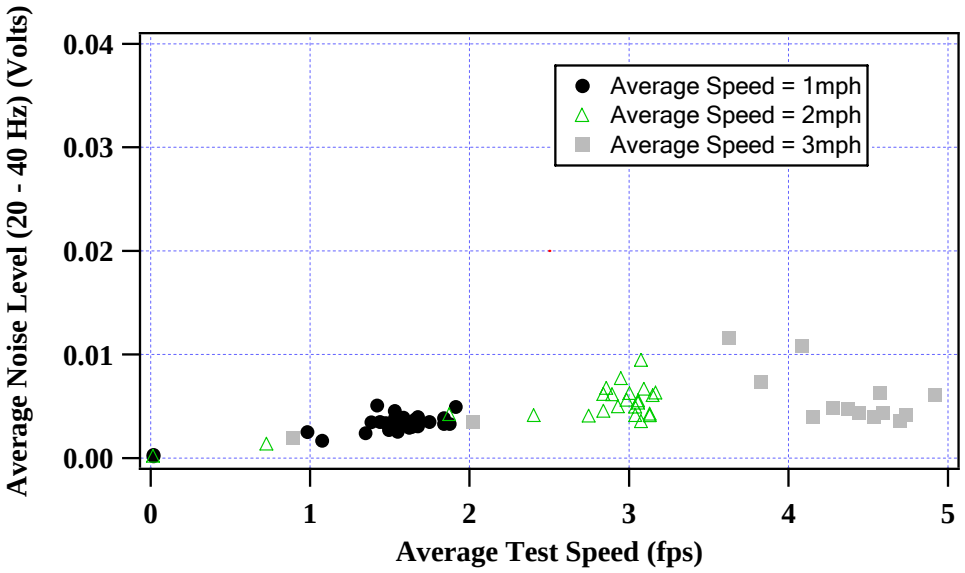

Figure 5.11 Average Noise Level Between 20 and 40 Hz Collected Using the 12-in. Diameter, Second-Generation Rolling Sensor Along the TxAPT Site

RDD continuous deflection profiles collected along the TxAPT test site are shown in Figures 5.12 and 5.15. These deflection profiles were collected using the second-generation rolling sensors with 9-in. and 12-in. diameter rolling wheels. The air-spring was pressurized to 5 psi (approximately 35-lbs of hold-down force) when the deflection profiles shown in Figures 5.12 and 5.13 were collected. A lower air-spring pressure of 3 psi (approximately 21-lbs of hold-down force) was used when the deflection profiles shown in Figures 5.14 and 5.15 were collected. It was found that the deflection profiles collected at different speeds and rolling sensor configurations are similar in trend. The deflection profiles measured using the 9-in. rolling sensor is consistently lower than the deflection profiles measured using the 12-in. rolling sensor. The main reason is because by the time the 12-in. rolling sensor were replaced with the 9-in. rolling sensor, the surface temperature of the TxAPT site increases from 26^{o}C to 35^{o}C. Therefore, the deflection profiles obtained using the 12-in. rolling sensor were measured when the pavement was at a higher temperature. This difference in temperature can cause change in the pavement deflection characteristics in this thin AC pavement (i.e. reduce modulus and increase measured deflection), which explains the difference in deflection profiles collected using the 9-in. and 12-in. rolling sensors.

FWD deflection basins were also collected at a 5-ft spacing along the TxAPT test pad on October 25th, 2005. The FWD deflection measurements are shown in Figure 5.16. The deflection trend along the pavement section measured by the FWD and the RDD devices agrees well. This is most easily seen by comparing the RDD deflection values with the FWD sensor #2 (W1) value. This comparison is shown in Figure 5.17. With the consideration that the deflection basins collected using a single loading area (i.e. FWD) and a double loading area (i.e. RDD) are different on a thin flexible pavement such as the one in the TxAPT test site. Nevertheless, both the RDD and the FWD identified a sudden

decrease in deflection at the station mark of 200, which corresponds to the location where there is a transition in the type of base material that was used to construct the TxAPT site.

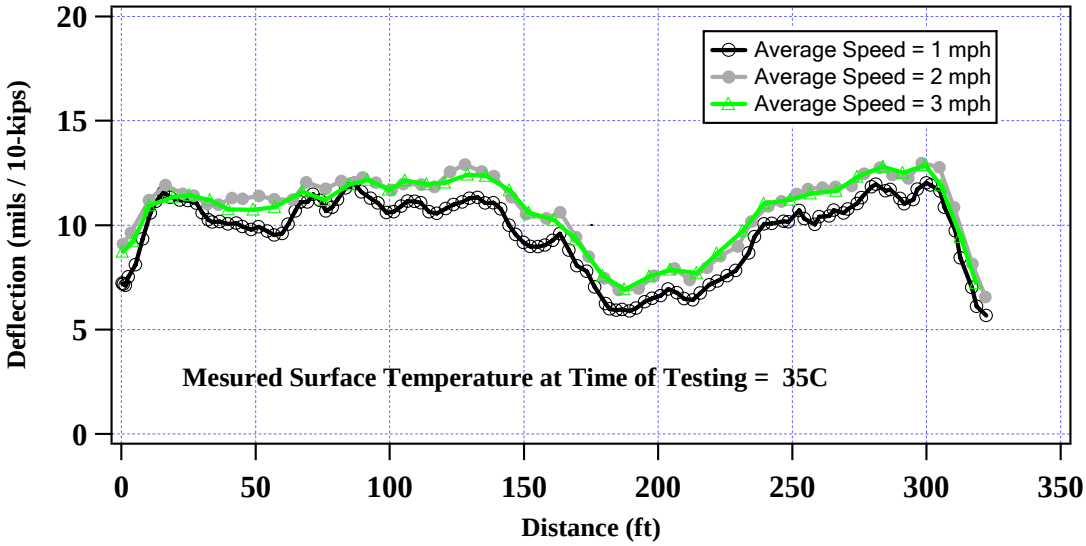

Figure 5.12 RDD Deflection Profiles Collected Along the TxAPT Site Using the 12-in. Diameter Second-Generation Rolling Sensor (5 psi Hold-Down Pressure in Air-Spring) at 1, 2, and 3 mph.

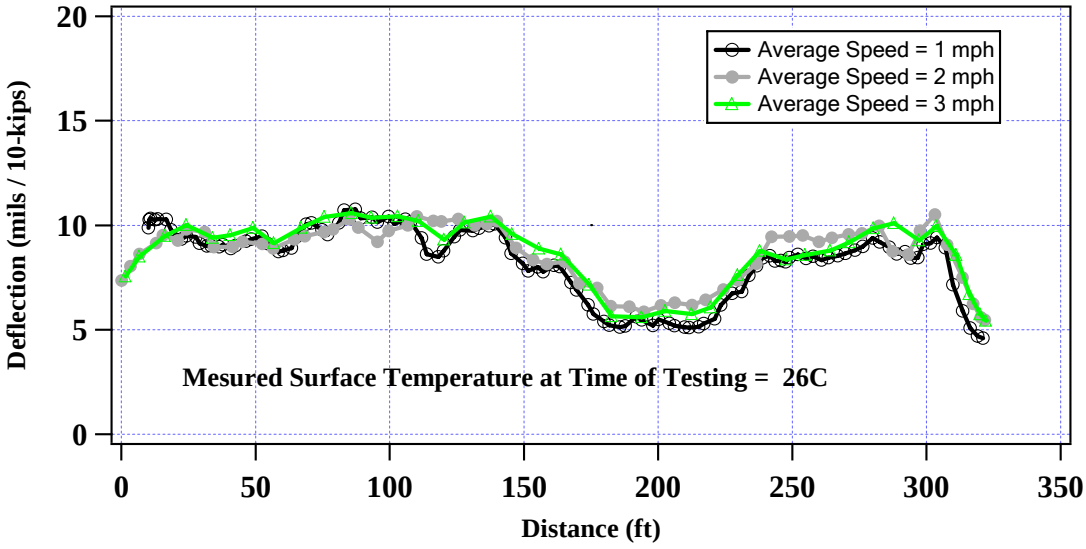

Figure 5.13 RDD Deflection Profiles Collected Along the TxAPT Site Using the 9-in. Diameter Second-Generation Rolling Sensor (5 psi Hold-Down Pressure in Air-Spring) at 1, 2, and 3 mph.

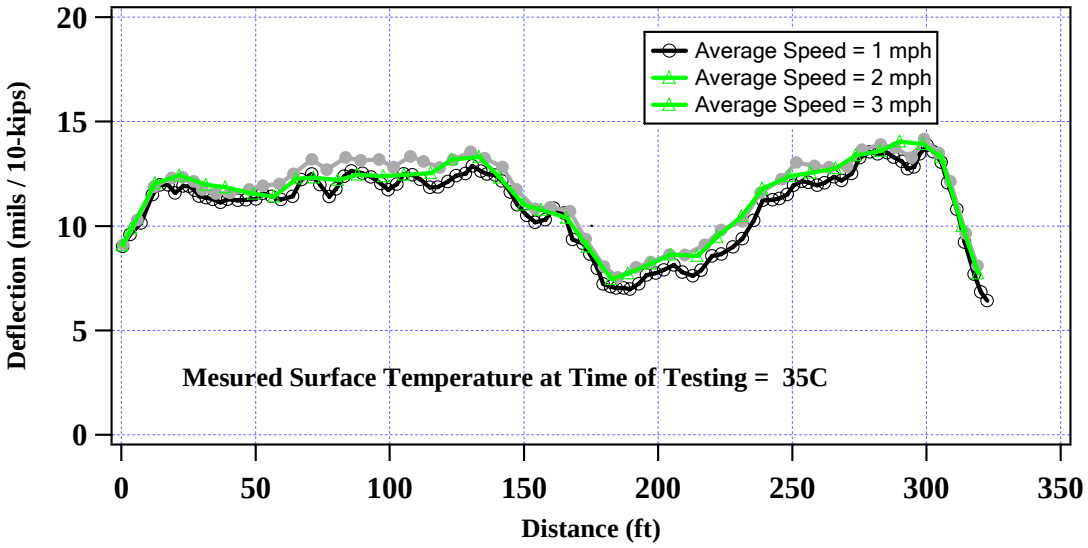

Figure 5.14 RDD Deflection Profiles Collected Along the TxAPT Site Using the 12-in. Diameter Second-Generation Rolling Sensor (3 psi Hold-Down Pressure in Air-Spring) at 1, 2, and 3 mph.

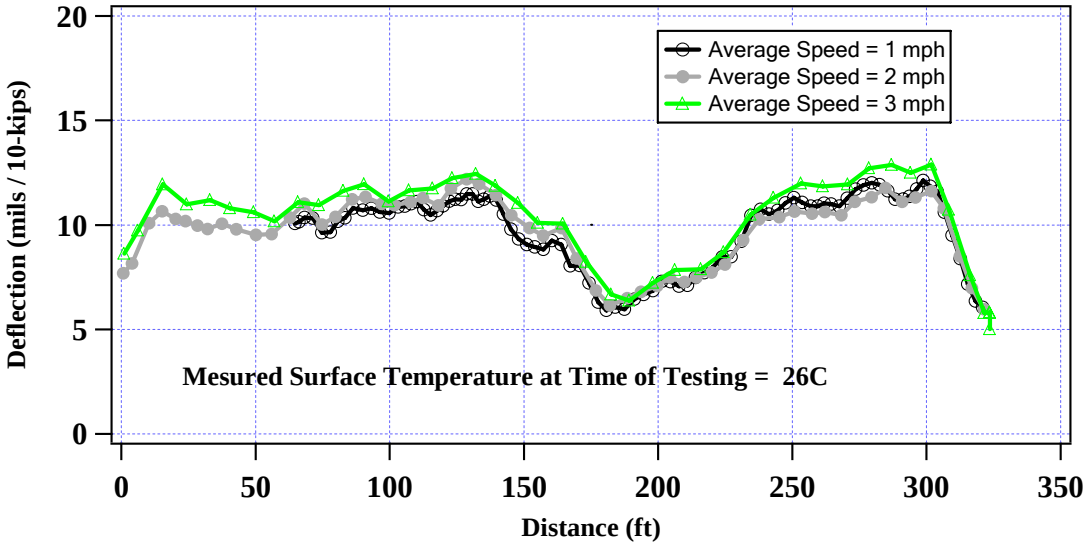

Figure 5.15 RDD Deflection Profiles Collected Along the TxAPT Site Using the 9-in. Diameter Second-Generation Rolling Sensor (3 psi Hold-Down Pressure in Air-Spring) at 1, 2, and 3 mph.

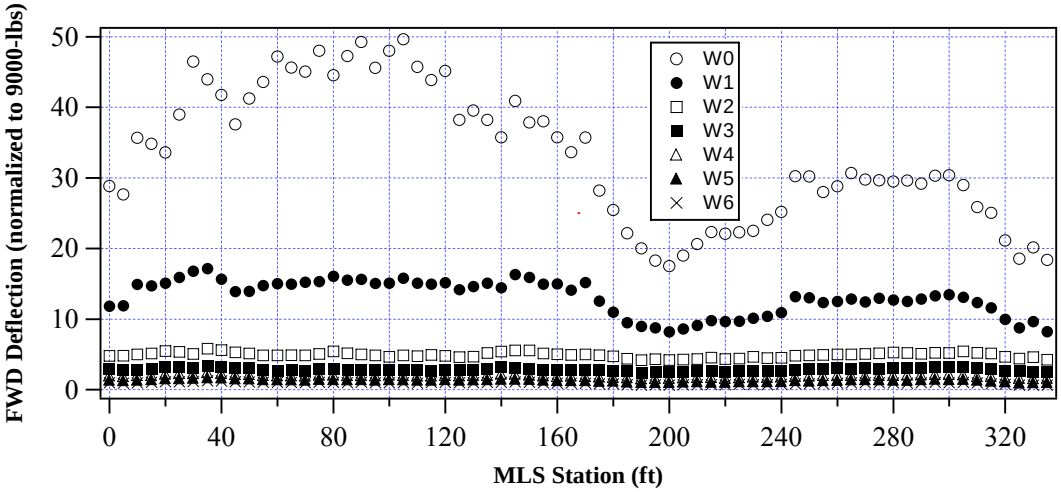

Figure 5.16 FWD Deflection Profile Collected Along the TxAPT Site on October 25, 2005.

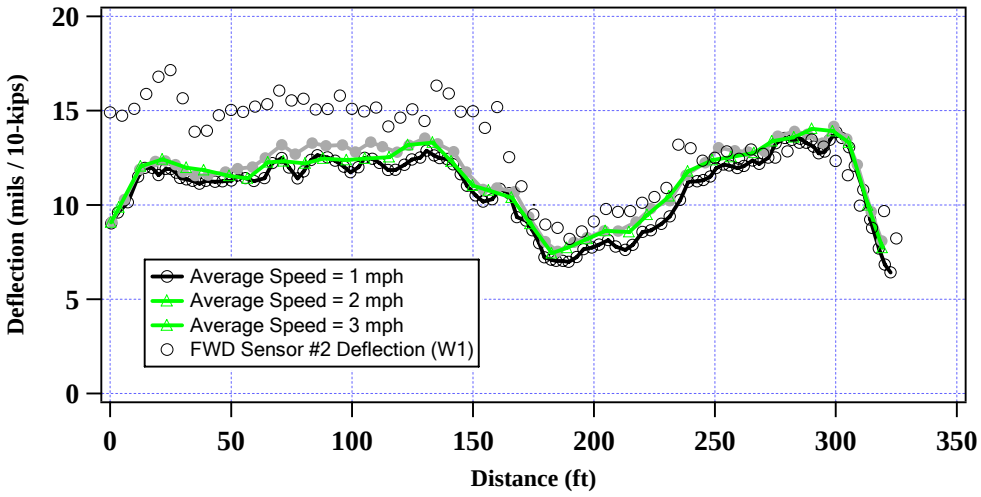

Figure 5.17 Comparison of FWD Deflections and RDD Deflection Profiles Collected Along TxAPT Site on October 25, 2005

5.4 FLEXIBLE PAVEMENT – THIN AC SURFACE OVER GRANULAR BASE

A flexible pavement that is adjacent to the TxAPT facility was also selected for this roughness comparison study. This flexible pavement has a thin AC surface at the top with granular base material underneath. The road has been subjected to light traffic load which consisted primarily of shuttle buses and other small university vehicles. Low-level rutting and longitudinal cracking as shown in Figure 5.18 was found along the pavement test site.

Figure 5.18 Photograph of RDD Testing Along a Flexible Pavement at Pickle Research Campus.

5.4.1 Deflection Measurement

Deflection profiles were collected at different testing speeds along this flexible pavement using the first-generation and second-generation rolling sensors. The rolling sensor signals in the frequency domain for test speeds of about 1 mph and 3 mph are shown in Figures 5.19 and 5.20, respectively.

The following observations can be made:

1. The rolling noise increases with increasing testing speed,
2. At testing speed of 1 mph, the second-generation rolling sensor has a noise floor of -35 dB (in the 20 – 40 Hz frequency range), which is lower than the noise floor measured using the first-generation rolling sensor of -28 dB,
3. At testing speed of 1 mph, the SNR for the first- and second-generation rolling sensors are 28 dB and 35 dB, respectively. At testing speed of 3 mph, the SNR for the first- and second-generation rolling sensors are 24 dB and 32 dB respectively. This indicates that the second-generation rolling sensor (with 12-in. diameter wheels) when tested at 1 mph along this flexible pavement has comparable SNR as when the first-generation rolling sensor was used at 1 mph,
4. The rolling noise level in the higher frequency range increases disproportionately with increasing test speed, and
5. The rolling noise characteristics are different once the sensor decouples from the pavement surface.

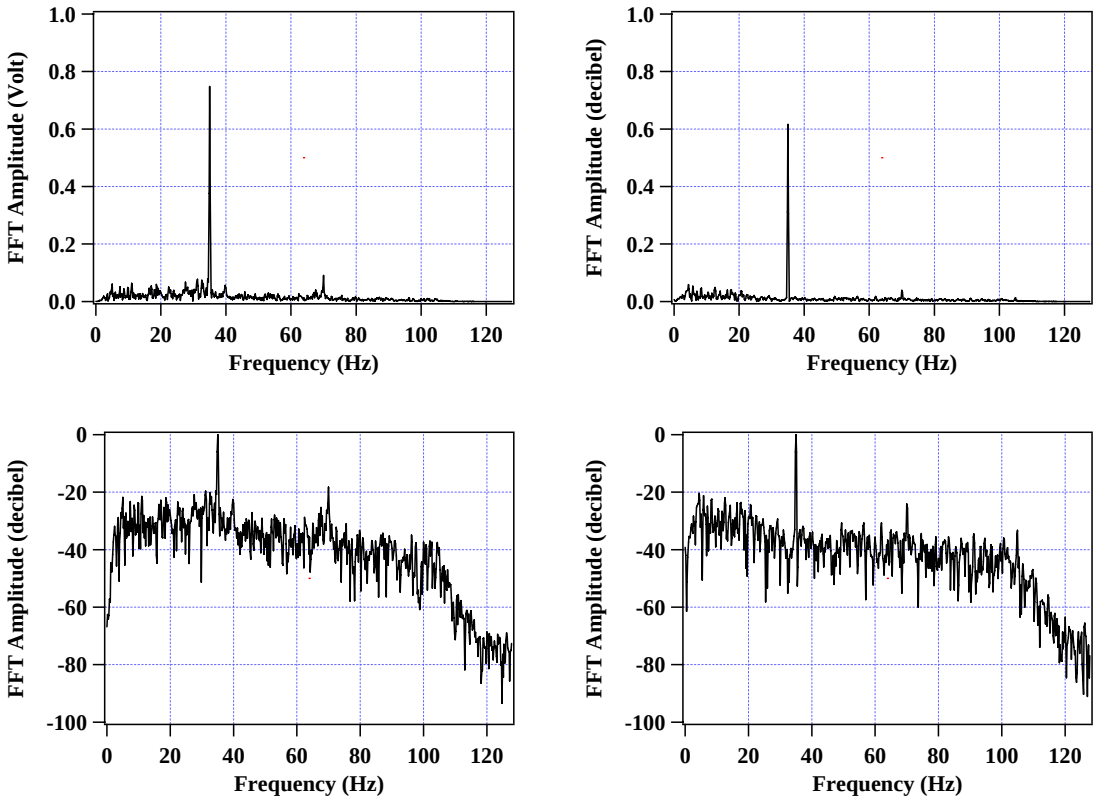

(a) First-Generation Rolling Sensor (6-in. Rolling Wheels)

(b) Second-Generation Rolling Sensor (12-in. Rolling Wheels)

Figure 5.19 FFT Spectra Collected Using First-and Second-Generation Rolling Sensors (with 12-in. Diameter Wheels) at an Average Speed of about 1 mph (peak-to-peak dynamic force of ± 5 kips, 5 psi Pressure in Air-Spring).

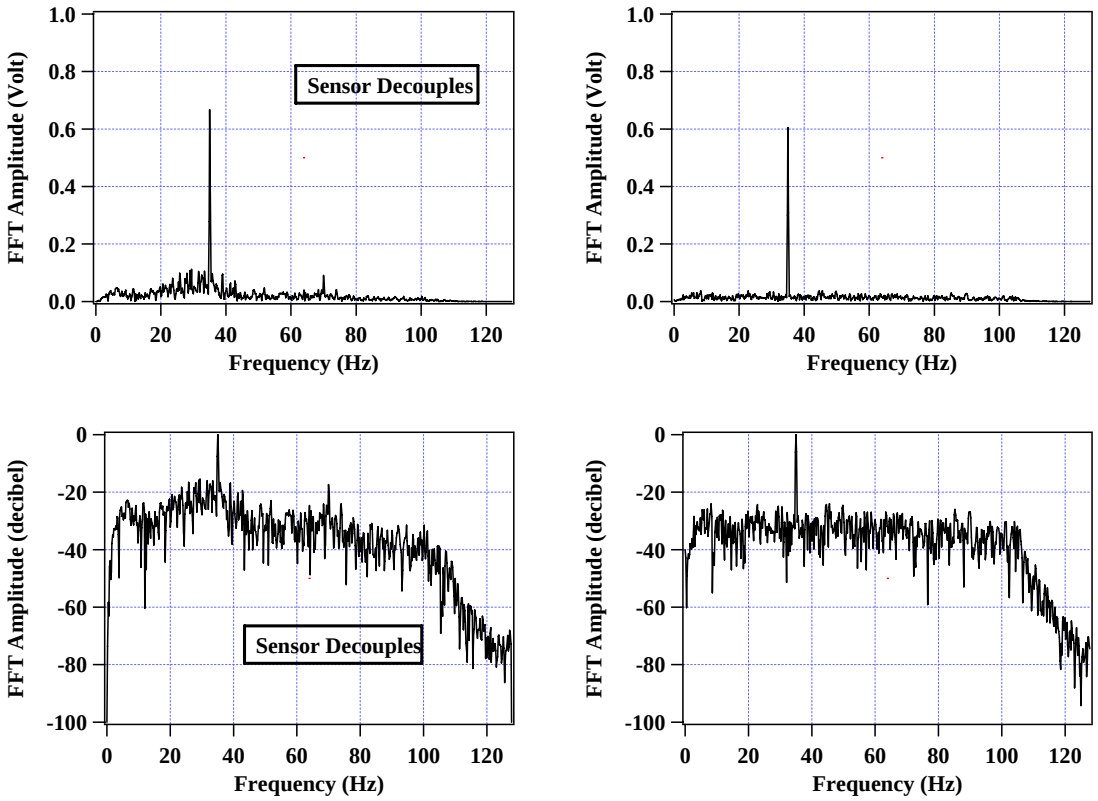

(a) First-Generation Rolling Sensor (6-in. Rolling Wheels)

(b) Second-Generation Rolling Sensor (12-in. Rolling Wheels)

Figure 5.20 FFT Spectra Collected Using First-and Second-Generation Rolling Sensors (with 12-in. Diameter Wheels) at an Average Speed of about 3 mph (peak-to-peak dynamic force of ± 5 kips, 5 psi Pressure in Air-Spring).

5.4.2 Noise Measurement

Other than collecting deflection profiles using the first- and second-generation rolling sensor at different speeds, rolling noise of each rolling sensor was also collected along this section of pavement to provide an accurate estimate of the rolling noise level. The rolling noise was measured by driving the RDD at a desired speed with no RDD dynamic loading applied to the pavement surface. As explained in Section 3.3, the rolling noise which exists in close proximity to the chosen RDD operating frequency would be

the most detrimental in terms of resolving accurate deflection amplitudes using digital filtering techniques.

For the purpose of comparison, the pure rolling noise collected along a rough pavement such as the Loop-610N, Houston is compared with the rolling noise collected along this flexible pavement at PRC. The data collected using the first-generation rolling sensor, second-generation rolling sensor with 9-in. wheels, and second-generation rolling sensor with 12-in. wheels are shown in Figures 5.21, 5.22 and 5.23, respectively.

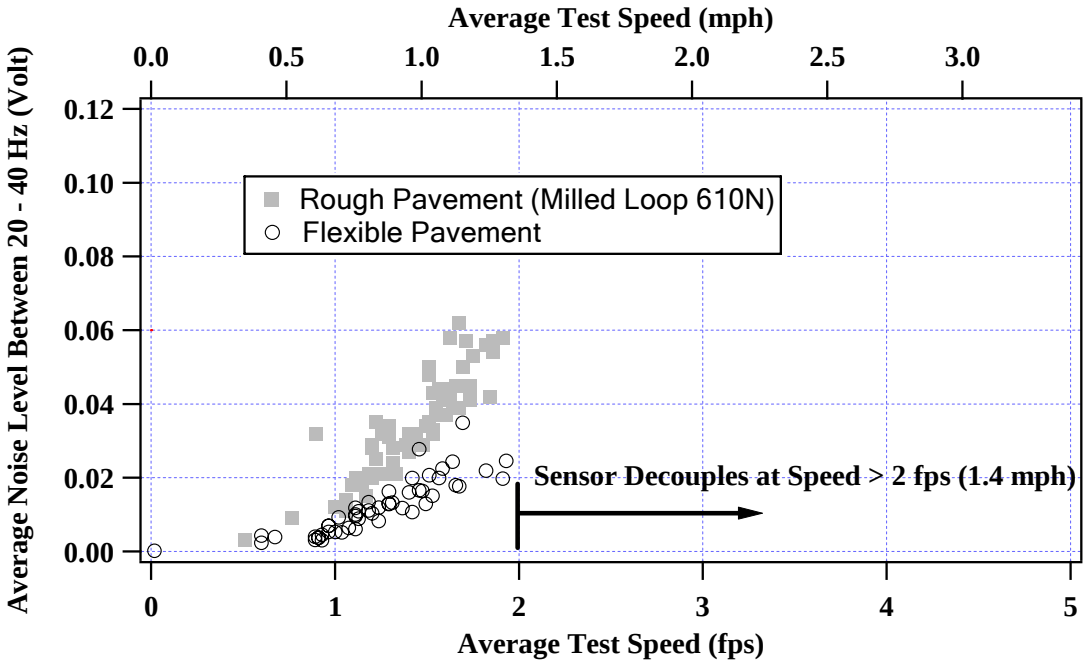

Figure 5.21 Comparison of Rolling Noise Around the RDD Operating Frequency Range Collected Along a Rough Pavement and a Flexible Pavement using the First-Generation Rolling Sensor (6-in. Diameter Wheels)

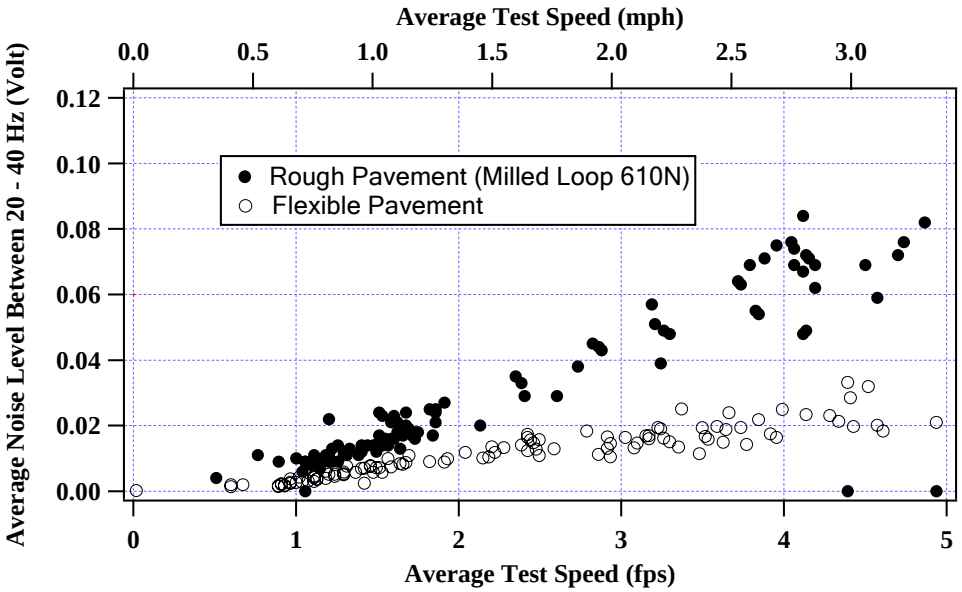

Figure 5.22 Comparison of Rolling Noise Around the RDD Operating Frequency Range Collected Along a Rough Pavement and a Flexible Pavement using the Second-Generation Rolling Sensor (9-in. Diameter Wheels); with 5 psi Hold-Down Pressure in Air-Spring.

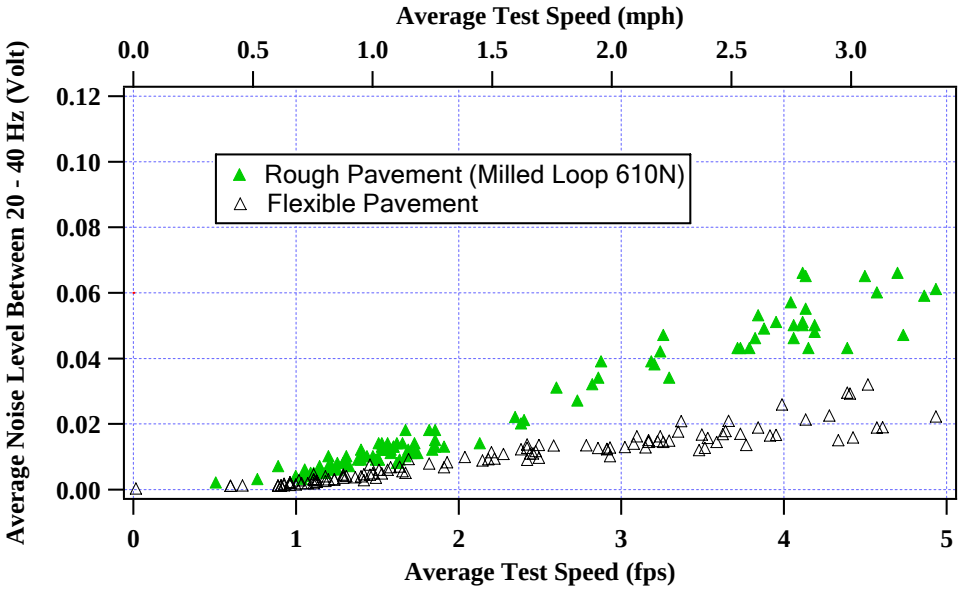

Figure 5.23 Comparison of Rolling Noise Around the RDD Operating Frequency Range Collected Along a Rough Pavement and a Flexible Pavement using the Second-Generation Rolling Sensor (12-in. Diameter Wheels); with 5 psi Hold-Down Pressure in Air-Spring.

By comparing the rolling noise measured along a rough pavement with a flexible pavement using different rolling sensors, the following observations are made:

1. The general trend for the rolling noise around the RDD operating frequency range increases nearly linearly with increasing speed.
2. The pavement roughness is an important factor which influences the level of rolling noise measured. The results indicated that a particular rolling sensor will measure a higher level of rolling noise when rolled along a rough pavement than a smooth pavement. The rolling noise level measured between 20 and 40 Hz at a testing speed of 1 mph is shown in Table 5.4 for all three sensors rolled along a rough and a flexible pavement. The data confirms that the rolling noise increases with increasing pavement roughnesses. Also, the rolling noise decreases with increasing size of the rolling wheels.
3. Other than the pavement roughness, the rate of increase of rolling noise is also dependent upon the rolling sensor used. The rate of change decreases with increasing diameter of the rolling wheels. Therefore, the different types of rolling sensors can be ranked as follows with increasing performance in terms of attenuating rolling noise near the RDD operating frequency range:
    a. First-generation rolling sensor (6-in. diameter wheels)
    b. Second-generation rolling sensor (9-in. diameter wheels)
    c. Second-generation rolling sensor (12-in. diameter wheels)
4. The rolling noise level has more scattering when the rolling sensors were rolled along a rough pavement surface than along a smooth pavement.

Table 5.4 Average Noise Level Between 20 – 40 Hz at a Testing Speed of 1 mph for Different Rolling Sensor Configurations

	Average Noise Level between 20 - 40 Hz at Testing Speed of 1 mph (Volt)	
Sensor	Rough Pavement (Loop 610N)	Flexible Pavement (PRC)
First-Generation 6-in.	0.032	0.016
Second-Generation 9-in. Wheels; 5 psi Hold-Down Pressure	0.014	0.007
Second-Generation12-in. Wheels; 5 psi Hold-Down Pressure	0.01	0.004

5.4.3 Comparison of Deflection Profiles

Three trial runs at 1, 2, and 3 mph were made using the RDD to collect deflection profiles along the flexible pavement. In each trial run, three different rolling sensors were used to collect individual deflection profiles. An accelerometer was attached on the main body of each rolling sensor to monitor the acceleration level experienced by each rolling sensor during the entire testing. A photograph showing the rolling sensor array configuration is presented in Figure 5.24. The different types of rolling sensors used are listed as follows:

1. Second-Generation Rolling Sensor with 9-in. Diameter Wheel,
2. Second-Generation Rolling Sensor with 12-in. Diameter Wheel, and
3. First-Generation Rolling Sensor with 6-in. Diameter Wheel.

The deflection profiles collected using the second-generation rolling sensor with 9-in. diameter wheels at testing speeds of 1, 2 and 3 mph are shown in Figure 5.25. Also included in this figure is the acceleration levels measured for each trial run on the right

axis. These acceleration levels can be compared with the theoretical maximum acceleration levels shown in Table 5.5.

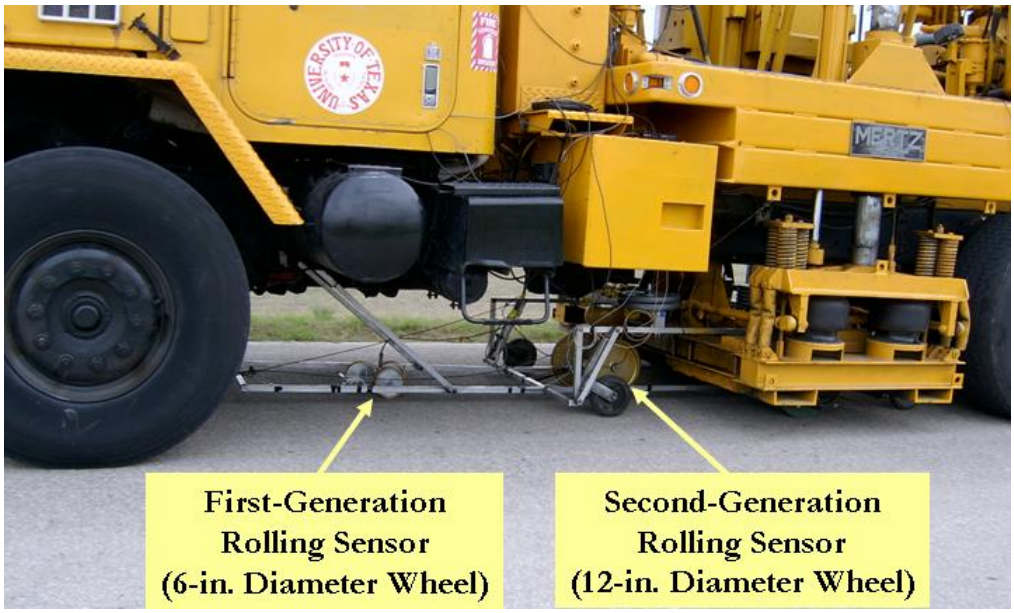

Figure 5.24 Photograph Showing RDD Rolling Sensor Array Used During Trial Testing Along a Flexible Pavement at PRC.

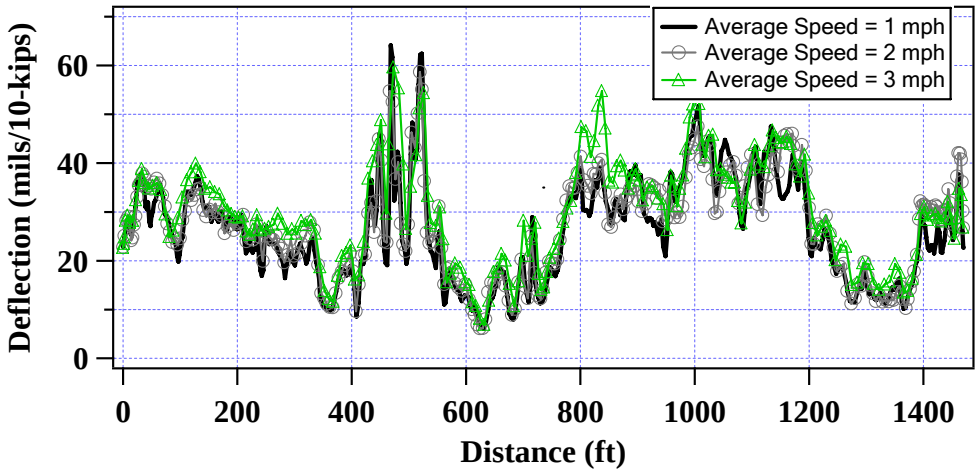

Figure 5.25 Sensor #1 Deflection Profiles Collected Along the Flexible Pavement at PRC at 1, 2, and 3 mph; Second-Generation Sensor with 9-in. Diameter Wheels.

Table 5.5 Theoretical Maximum Acceleration with Different Levels of Hold-Down Pressures in Air-Spring

Additional Hold-Down Pressure (psi)	Additional Hold-Down Force (lbs)	Maximum Allowable Acceleration (g)
0	0	1
1	7	1.3
2	14	1.6
3	21	1.9
4	28	2.2
5	35	2.5

* Calculation Based on Eqn. 5.2

Similar deflection and acceleration profiles measured with the second-generation rolling sensor with 12-in. diameter wheels are shown in Figures 5.27 and 5.28. The deflection and acceleration profiles measured with the first-generation rolling sensor with 6-in. diameter wheels are shown in Figures 5.29 and 5.30.

Based on the data presented in Figures 5.25 to 5.30, the following observations are made:

1. The acceleration level experienced by each rolling sensor increases with increasing test speed,
2. Both the second-generation rolling sensors with 9-in. diameter wheels and 12-in. diameter wheels were able to collect deflection profiles at 3 mph,
3. The deflection profiles collected using different rolling sensors can not be compared directly because they were installed at different offset distances from the two loading rollers. Even though the rolling sensors can be reconfigured and tested at the same offset distance, but then the rolling sensors will not be tested under the identical testing conditions (e.g. pavement temperatures and testing speeds), and

4. Both the deflection and acceleration profiles collected using the first-generation rolling sensor at testing speeds of 2 and 3 mph indicated that this sensor uncouples from the pavement surface, and therefore is not capable of making accurate deflection measurements at speeds of 2 and 3 mph. This is best illustrated by comparing all three profiles at 1, 2 and 3 mph (i.e. such as Figure 5.29). The deviation of the measured deflection profile collected at 1, 2 and 3 mph shows that the first-generation rolling sensor decouples from the pavement at higher testing speeds, and
5. The second-generation rolling sensor with 12-in. diameter wheels shows the best agreement between the deflection profiles collected at 1, 2, and 3 mph, which is shown in Figure 5.27.

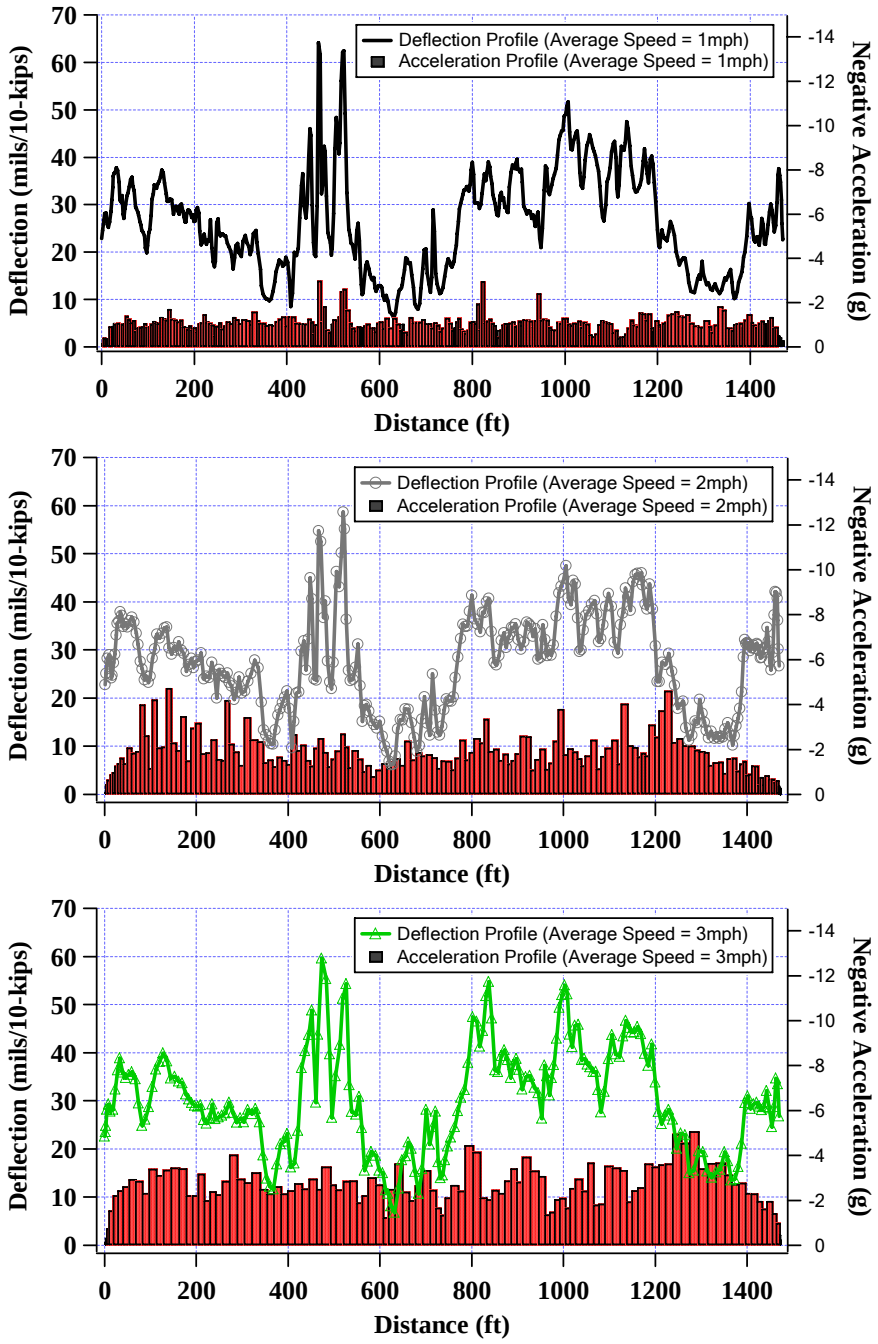

Figure 5.26 Sensor #1 Deflection and Sensor Acceleration Profiles Collected Along the Flexible Pavement at PRC at 1, 2, and 3 mph; Second-Generation Sensor with 9-in. Diameter Wheels

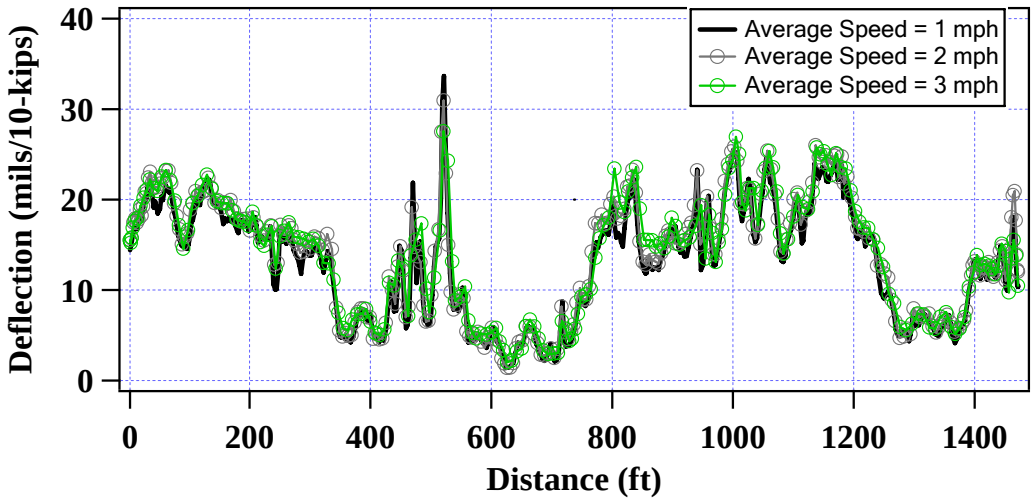

Figure 5.27 Sensor #2 Deflection Profiles Collected Along the Flexible Pavement at PRC at 1, 2, and 3 mph; Second-Generation Sensor with 12-in. Diameter Wheels.

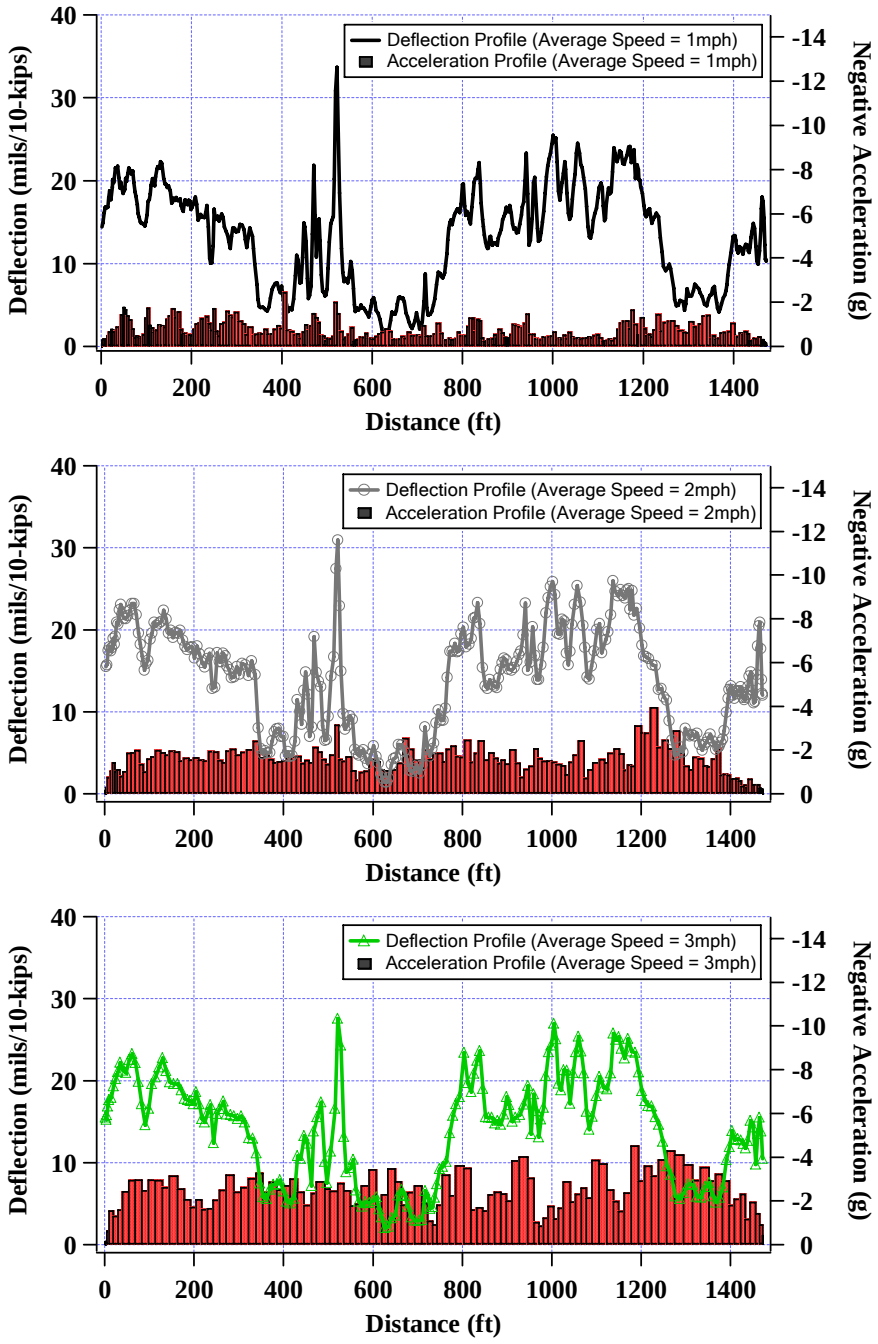

Figure 5.28 Sensor #2 Deflection and Sensor Acceleration Profiles Collected Along the Flexible Pavement at PRC at 1, 2, and 3 mph; Second-Generation Sensor with 12-in. Diameter Wheels.

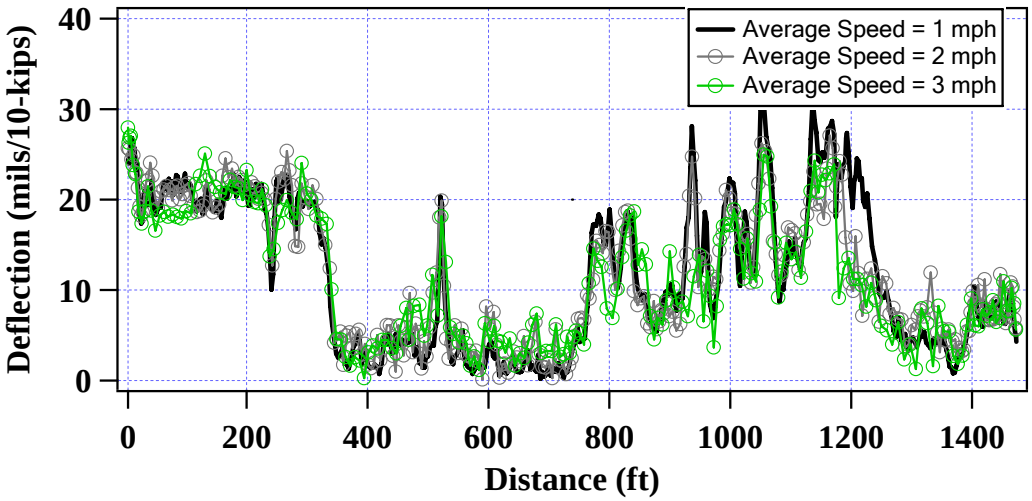

Figure 5.29 Sensor #3 Deflection Profiles Collected Along the Flexible Pavement at PRC at 1, 2, and 3 mph; First-Generation Sensor with 6-in. Diameter Wheels.

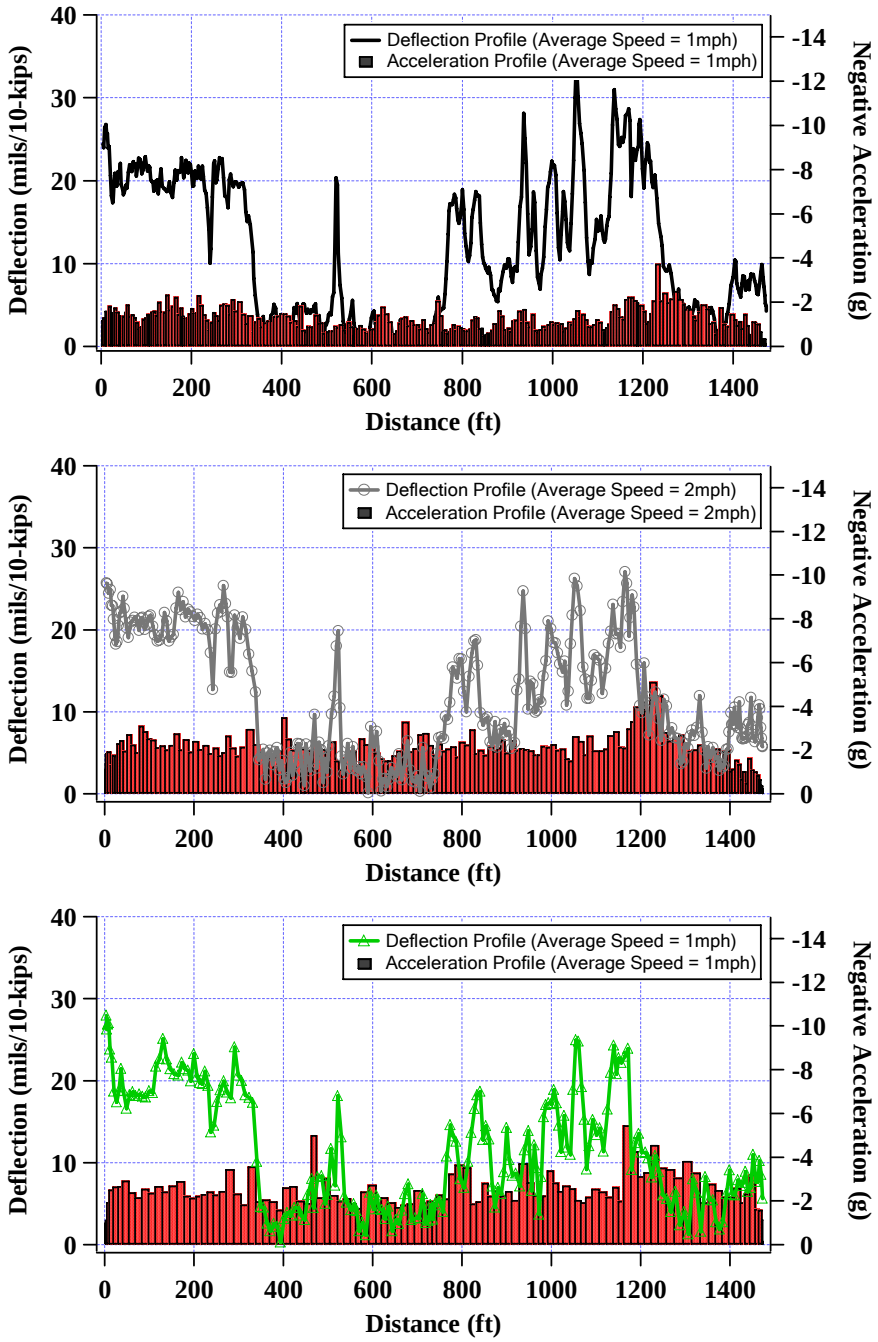

Figure 5.30 Sensor #3 Deflection and Sensor Acceleration Profiles Collected Along the Flexible Pavement at PRC at 1, 2, and 3 mph; First-Generation Sensor with 6-in. Diameter Wheels.

5.4.4 Theoretical Maximum Acceleration

As mentioned earlier, theoretical simulations on rigid wheels rolling over synthetic pavement surface was done by Bay (1997). Based on the theoretical simulation, an equation which governs the RDD testing speed was derived. This equation is:

$$\frac{1}{r}V^2 + \frac{2}{3}v_{p,\max}(2\pi f_0)^2 \le 1g \qquad (5.1)$$

where r = rolling sensor wheel radius (3 in.),
V = testing velocity along the pavement,
$v_{p,max}$ = peak vertical pavement displacement, and
f_o = RDD operating frequency

The expected acceleration of the rolling sensor when rolling over a pavement is represented by left hand side (LHS) of the equation. The available acceleration to resists the negative acceleration of the rolling sensor is represented by the right hand side (RHS) of the equation, which is the weight of the rolling sensor for the case of first-generation rolling sensor. In the second-generation rolling sensor, an additional hold-down force (F_{hd}) is provided on top of the weight from the rolling sensor. This additional hold-down force is the main factor which allows the second-generation rolling sensor to achieve a higher testing speed. With the addition of this hold-down force provided by the air-spring located at the top of the second-generation rolling sensor, Eq. 5.1 becomes:

$$\frac{1}{r}V^2 + \frac{2}{3}v_{p,\max}(2\pi f_0)^2 \le 1g + \frac{F_{hd}}{W_{sensor}} \qquad (5.2)$$

where r = rolling sensor wheel radius (3 in.),
V = testing velocity along the pavement,
$v_{p,max}$ = peak vertical pavement displacement,
f_o = RDD operating frequency,
F_{hd} = hold down force from air-spring, and
W = weight of rolling sensor.

5.5 RIGID PAVEMENT – LOOP 610, MILLED, ROUGH SURFACE

This rigid pavement is a test site along Loop 610 north in Houston. The surface of the CRCP has been milled which has exposed the large aggregates in the CRCP. This pavement is the roughest road that the RDD is likely to test. A photograph of the RDD with the first- and second-generation rolling sensors at this test site is shown in Figures 5.31 and 5.32.

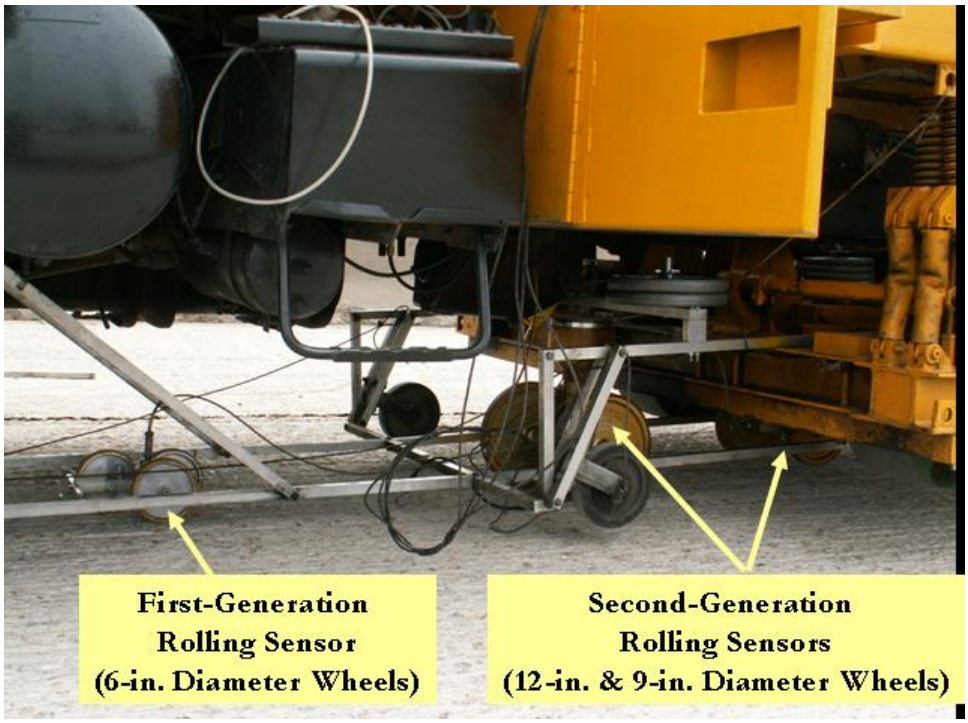

Figure 5.31 Photograph of the RDD on a Milled CRCP along Loop-610, Houston.

Figure 5.32 Testing on Rough CRCP with 12-in. Diameter Wheels.

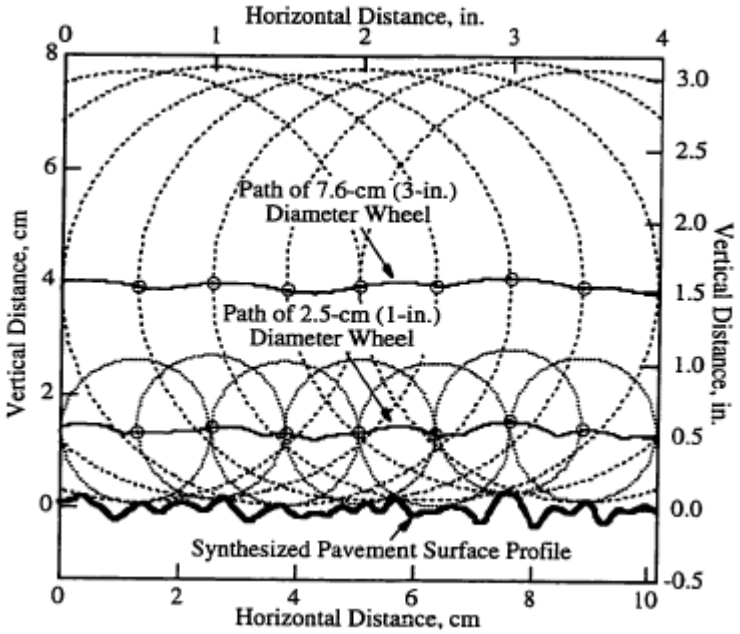

Figure 5.33 Paths of 2.5-cm (1-in.) and 7.6-cm (3-in.) Diameter Rigid Wheels Over a Synthesized Surface of a Rough Pavement (from Bay, 1997).

A simulation study of a rigid wheel traveling over a synthesized rough pavement surface was performed by Bay in 1997. Results from the simulation study are shown in Figures 5.33 and 5.34. These results indicated that the displacement of the rolling sensor when rolling over a given roughness decreases as larger diameter wheels are used. Larger-diameter wheels also decrease the acceleration level that is experienced by the rolling sensor. The results show that by using wheels of 6-in. diameter, the dynamic vertical displacement is significantly less than when using a wheel of 1-in. diameter wheel. Then, as the wheel diameter increases further, the dynamic displacement only decreases gradually at a reduced rate.

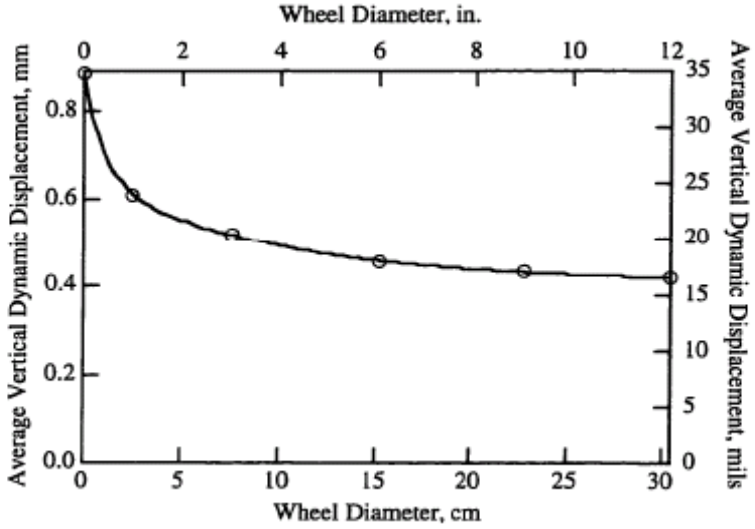

Figure 5.34 Average Vertical Displacement of Wheels with Various Diameters Rolling Over the Synthesized Pavement Surface (from Bay, 1997).

So far, the benefit of having larger-diameter wheels has been limited to results obtained from Bay's simulation study. Over the past decade, all RDD testing has been performed using the first-generation rolling sensors which have 6-in. diameter wheels. In recent testing performed along a rough CRCP surface that is located at Loop 610N,

Houston, data have been collected that demonstrate the benefit of having larger diameter rolling wheels.

Acceleration time histories were collected to monitor the motion of the different rolling sensors as the array rolled along the rough surface of Loop 610N. These time histories were collected at a testing speed of about 2 mph (3.2 km/hr), each four-seconds long, are shown in Figure 5.35. Since this particular set of data was collected to observe the performance of the rolling sensor on rough concrete pavement, no sinusoidal RDD dynamic load was applied. Each acceleration time history is characterized by having large positive acceleration spikes. These spikes are caused by the upward acceleration as the rolling wheel rides from one high point to the next high point along the rough pavement surface. As expected, the number of high positive spikes decreases as the rolling wheel diameter increases. But more importantly, the level of negative acceleration also decreases with increasing rolling wheel diameter. The negative acceleration is the primary factor which leads to the decoupling of the rolling sensor from the pavement surface, therefore invalidating the deflection measurement.

Based on the acceleration time histories shown in Figure 5.35, the following observations are made:

1. the acceleration time histories collected at a testing speed of 2 mph using the first-generation rolling sensor is different from the time histories collected using the second-generation rolling sensor. The negative acceleration values recorded on the first-generation rolling sensor approaches a limiting value of -1g, which indicates that the sensor decouples from the pavement surface. This limiting acceleration value cannot exceed -1g even if the first-generation rolling sensor travels at speed higher than 2 mph. This is because physically the first-generation

sensor can only provide -1g. As soon as the rolling sensor lost contact with the pavement surface, the acceleration value will be independent of the testing speed until the rolling sensor hits the next high point on the pavement.

2. the magnitude of the positive acceleration spikes are not representative indicators of the coupling condition of the rolling sensor. These high spikes were caused by the upward impact as the rolling sensor pivoting from one high point to the next high point on the pavement surface.
3. the magnitude of the negative acceleration spikes which occurs immediately after the positive acceleration spikes are also caused by the impact of the rolling sensor when riding from one high point to another high point. These spikes may exceed the theoretical limiting acceleration value, but this is not of major concern because this high negative acceleration only happens over very short time duration.
4. the acceleration time history will become asymmetric when the rolling sensor lost contact with the pavement surface. This can be seen in the acceleration time history collected using the first-generation rolling sensor at a testing speed of 2 mph.

Histograms of the number of positive and negative spikes are shown in Figures 5.36 and 5.37, respectively. It was found that both second-generation rolling sensors behave differently from the first-generation rolling sensor. There are more positive spikes identified in the acceleration record obtained from the second-generation rolling sensor than from the first-generation rolling sensor. This can be explained by the increased in high points that the first-generation rolling sensor need to ride over at a testing speed of 2 mph. Furthermore, the 9-in. diameter rolling sensor has more positive spikes than the 12-

in. diameter rolling sensor, which represents the benefits of having a larger diameter rolling wheels.

The acceleration histories collected from the three rolling sensors are useful to detect if the rolling sensor decouples from the pavement surface. The limiting acceleration for the first-generation rolling sensor is -1g, while the limiting acceleration for the second-generation rolling sensor is -2.5g.

Based on the histogram of the negative acceleration, it can be seen that the first-generation rolling sensor only experiences accelerations up to -1g. The surface deflection should be invalidated when the first-generation rolling sensor exceeds -1g. The first-generation rolling sensor will approach a limiting of -1g and will not go over this because at this stage, the rolling sensor will be bouncing from a high point to the next high point, which can be visualized as "flying" above the pavement surface. Therefore, the acceleration becomes independent of the traveling speed and the surface deflection.

In contrast, both second-generation rolling sensors do not have negative acceleration spikes that are in excess of the limiting acceleration of -2.5g. This implies that the second-generation rolling sensor remains in contact with the pavement surface even in a pavement that is as rough as this milled off rigid pavement. This characteristic represents an important advantage of the second-generation rolling sensor over the first-generation rolling sensor.

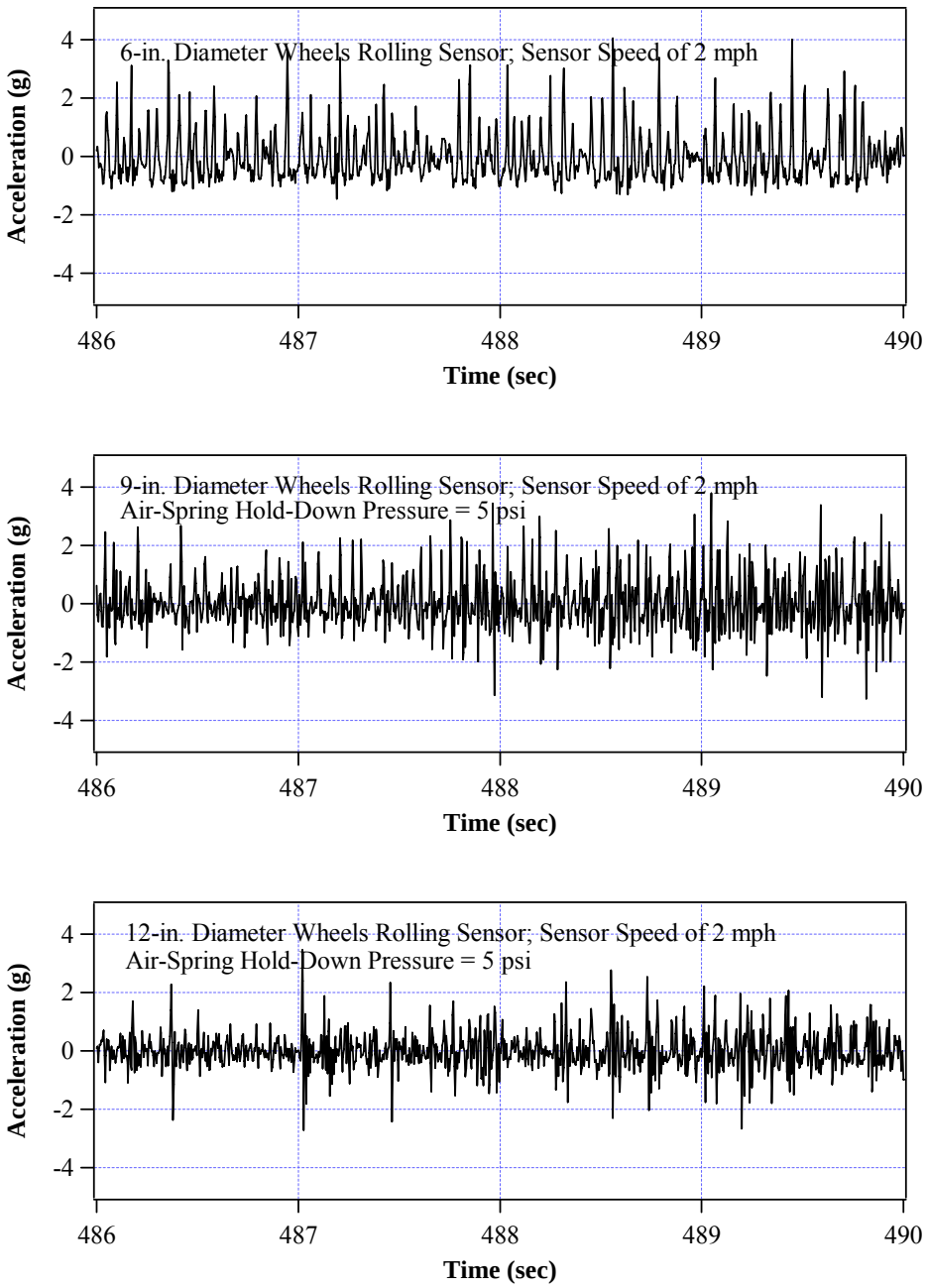

Figure 5.35 Acceleration Time Histories of Rolling Sensors: (a) First-Generation 6-in. Diameter Wheels, (b) Second-Generation 9-in. Diameter Wheels and (c) Second-Generation 12-in. Diameter Wheels Rolling Sensors along the milled-off CRCP.

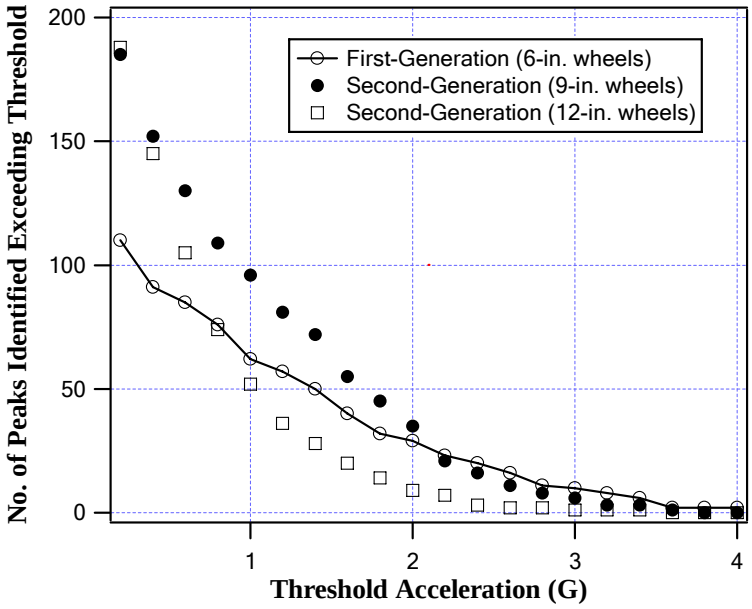

Figure 5.36 Histogram of the Number of Positive Spikes

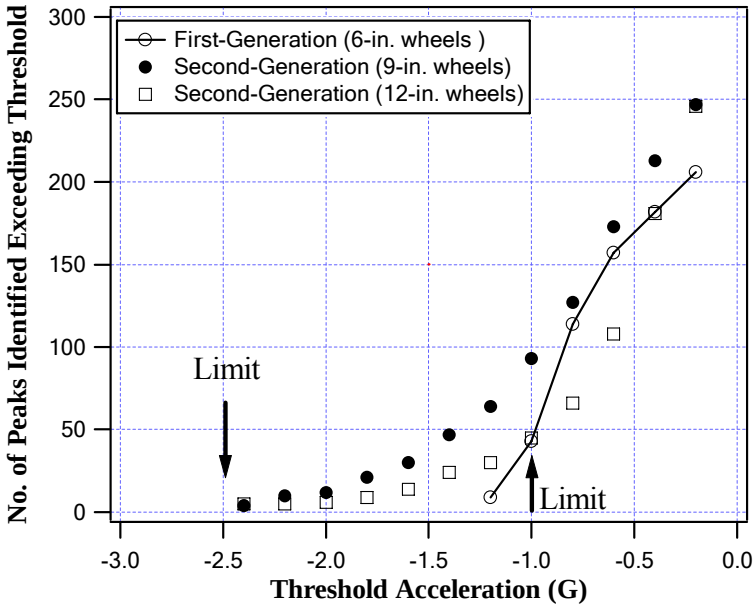

Figure 5.37 Histogram of the Number of Negative Spikes

5.5.2 Analysis in the Frequency Domain

In the second part of the roughness study, the frequency responses of the first- and second-generation rolling sensors were investigated. As discussed in the RDD noise evaluation study presented in Chapter 3, it was found that the region around the RDD operating frequency range is the range that most influences the accuracy of the RDD measurement. More specifically, it becomes more difficult to resolve the dynamic signal at the operating frequency (which represents the dynamic pavement surface deflection) if the rolling noise component is excessive and is concentrated near the RDD operating frequency range. To study this effect, the FFT spectra were computed from the signals collected in each of the three rolling sensors. Figures 5.38 through 5.40 show the average FFT energy which is near the RDD operating frequency range (20 – 40 Hz). It is clear that the first-generation rolling sensor has the highest noise among the three rolling sensors. Furthermore, the magnitude increases with the increasing test speed. Also, the second-generation rolling sensor with the 12-in. diameter rolling wheels has less rolling noise than the sensor with 9-in. diameter rolling wheels. The average FFT energy near the RDD operating frequency range as shown between Figures 5.38 through 5.40 can be plotted in the decibel (dB) scale as shown in Figures 5.41 to show the reduction in rolling noise in the vicinity of RDD operating frequency range for different first- and second-generation rolling sensors.

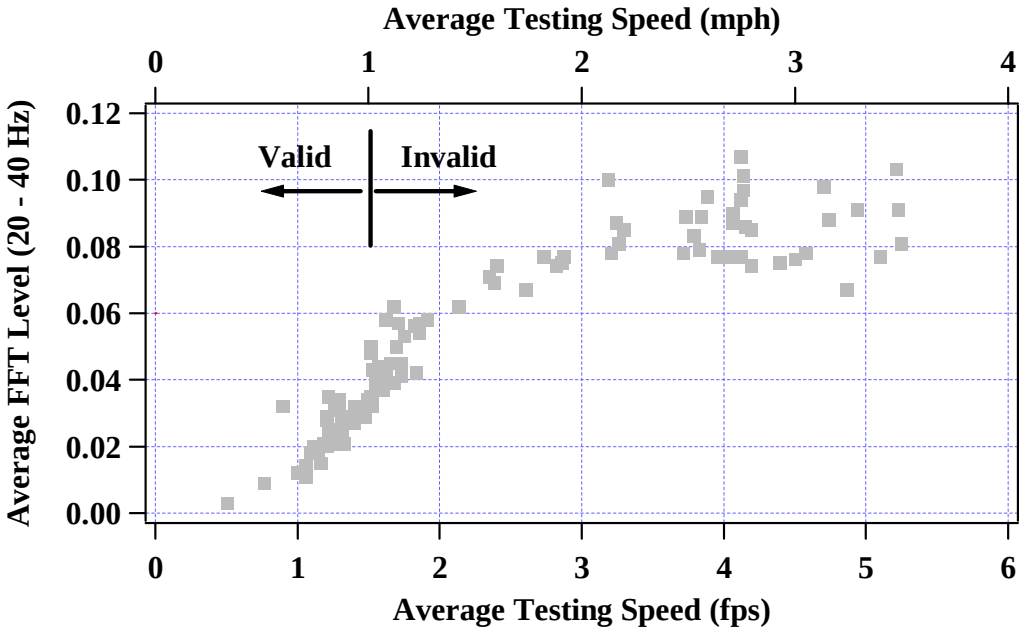

Figure 5.38 Average FFT Amplitude Between 20 and 40 Hz Collected Using First-Generation Rolling Sensor (6-in. Diameter Wheels) on Milled CRCP Section Along Loop 610N.

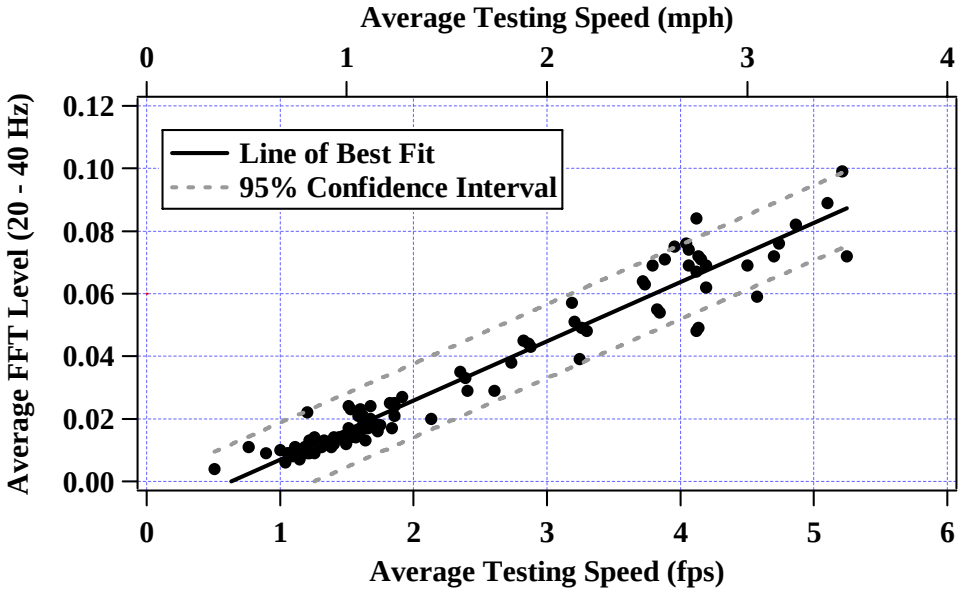

Figure 5.39 Average FFT Amplitude Between 20 and 40 Hz Collected Using Second-Generation Rolling Sensor (9-in. Diameter Wheels; 5 psi Hold-Down Pressure) on Milled CRCP Section Along Loop 610N.

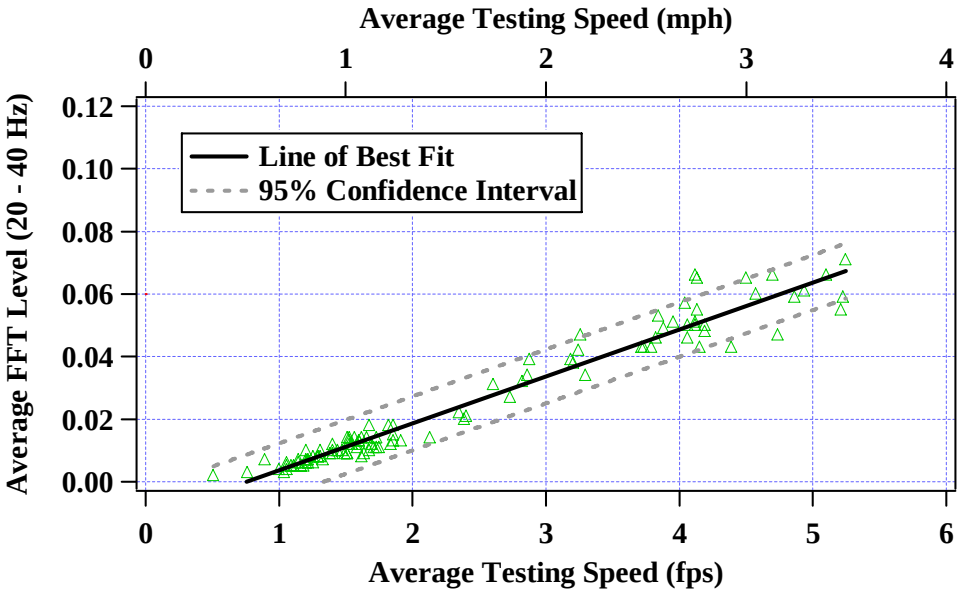

Figure 5.40 Average FFT Amplitude Between 20 and 40 Hz Collected Using Second-Generation Rolling Sensor (12-in. Diameter Wheels; 5 psi Hold-Down Pressure) on Milled CRCP Section Along Loop-610.

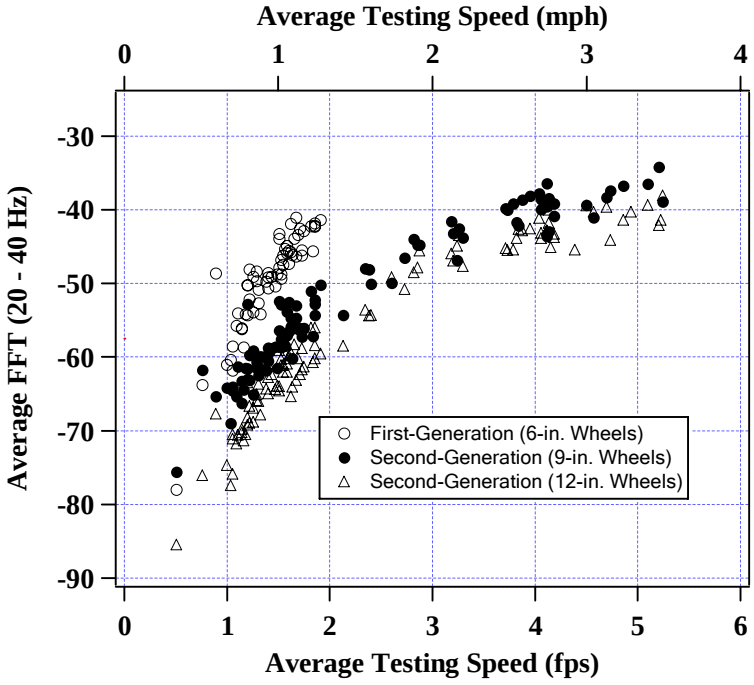

Figure 5.41 Average FFT Level in the Typical RDD Operating Frequency Range for First- and Second-Generation Rolling Sensors (Air-Spring Hold-Down Pressure of 5 psi)

5.6 RIGID PAVEMENT – LOOP 610, CRCP SURFACE

This test site is located along Loop610N in Houston, and the test limits are between the Interstate Highway 45 and US-59 Highway. At the time the data were collected, a rehabilitation project was currently underway which included placement of a new 15-in. CRCP in some selected areas, and surface preparation of parts of the old 9-in. CRCP for an AC overlay. A photograph of the RDD testing along the CRCP surface is presented in Figure 5.42.

The signals collected using the first-generation and second-generation (12-in. diameter rolling wheels; 5 psi hold-down pressure in the air-spring) when tested at speeds of 1 mph and 3 mph were shown in Figures 5.43 and 5.44, respectively. As before, it was found that the noise increases with increasing speed. But, the second-generation rolling sensor has less noise than the first-generation rolling sensor when both rolling sensors were tested at the same speed. At a testing speed of 1 mph, SNR of 20 dB and 30 dB was obtained for the first- and second-generation rolling sensor, respectively. At a testing speed of 3 mph, SNR of 10 dB and 18 dB was obtained for the first- and second-generation rolling sensor. It was found that the first-generation rolling sensor (at 1 mph) and the second-generation rolling sensor (at 3 mph) obtained similar SNR at this pavement site.

The signal collected along a rigid pavement can be compared with the signal collected along a flexible pavement in the frequency domain, as previously shown in Figures 5.19 and 5.20. There are two major differences between these two sets of record:

1. At a given forcing level, the amplitude of the signal at the operating frequency collected along a rigid pavement is typically lower than the amplitude of the signal along a flexible pavement.

2. The rolling noise across the frequency spectrum collected along a rough rigid pavement is higher than the rolling noise collected along a flexible pavement.

A 900-ft section of the 9-in. CRCP was selected from the test site where repetitive deflection profiles were collected using both the first-generation and second-generation rolling sensors. These data were collected at different average testing speeds of 1, 2 and 3 mph. The deflection profiles collected from the first- and second-generation rolling sensors at average speeds of 1, 2 and 3 mph are plotted in Figures 5.45 through 5.47, respectively. It was found that the deflection profiles collected using the 12-in. diameter second-generation rolling sensors at speeds of 1, 2 and 3 mph agrees fairly well with the result collected using the first-generation rolling sensor at speed of 1 mph. Some of the discrepancy between these data can be explained by the fact that the difference in foot print between the two sensors, which can became important when data is collected along a concrete pavement with severely deteriorated cracks that are closely spaced. Also, the data were analyzed Bay's filter (same filter resolution), which means that for the dataset that were collected at 3 mph, the deflection profiles will consist of more sparsely spaced points. Furthermore, all three profiles collected using the second-generation rolling sensors at different speeds are shown in Figures 5.48. All three profiles agree very well with each other.

Figure 5.42 Photograph of the RDD Testing Along a CRCP Rehabilitation Project Along Loop 610N, Houston, TX.

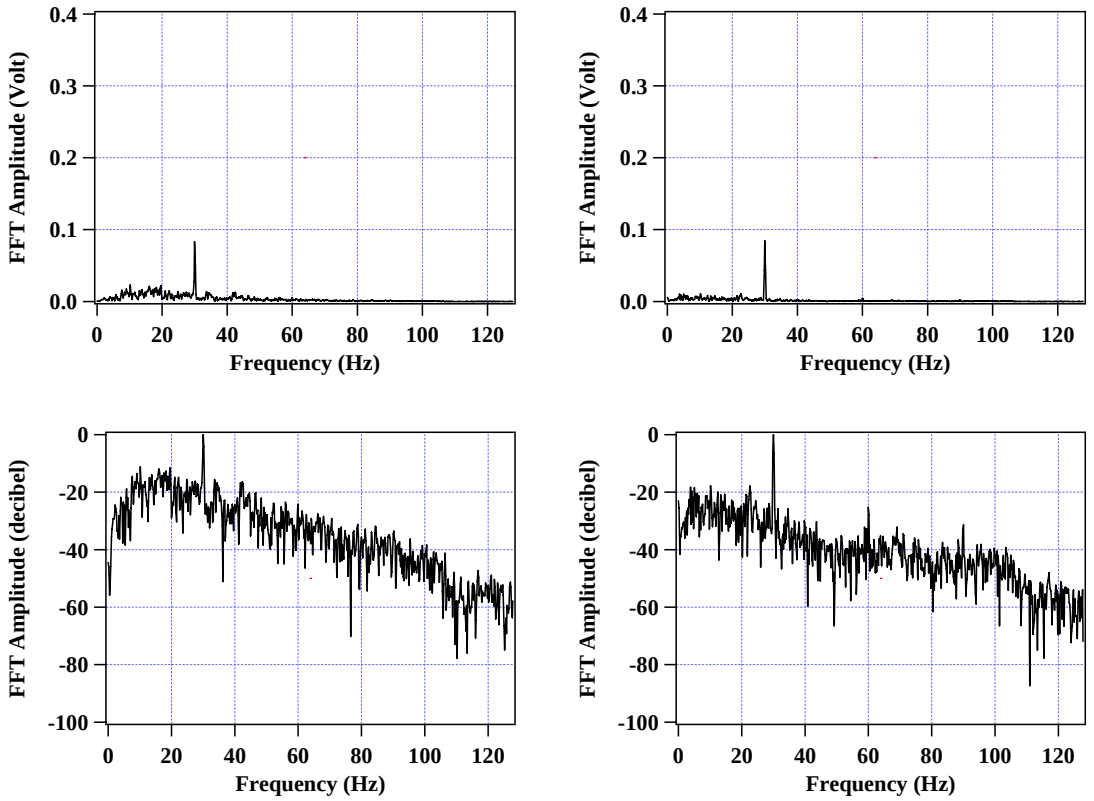

(a) First-Generation Rolling Sensor (6-in. Diameter Wheels)

(b) Second-Generation Rolling Sensor (12-in. Diameter Wheels)

Figure 5.43 FFT Spectra of First-Generation and Second-Generation Rolling Sensor (with 12-in. Diameter Wheels and 5 psi Hold-Down Pressure in Air-Spring) Collected at 1 mph Along Loop610N, near Houston.

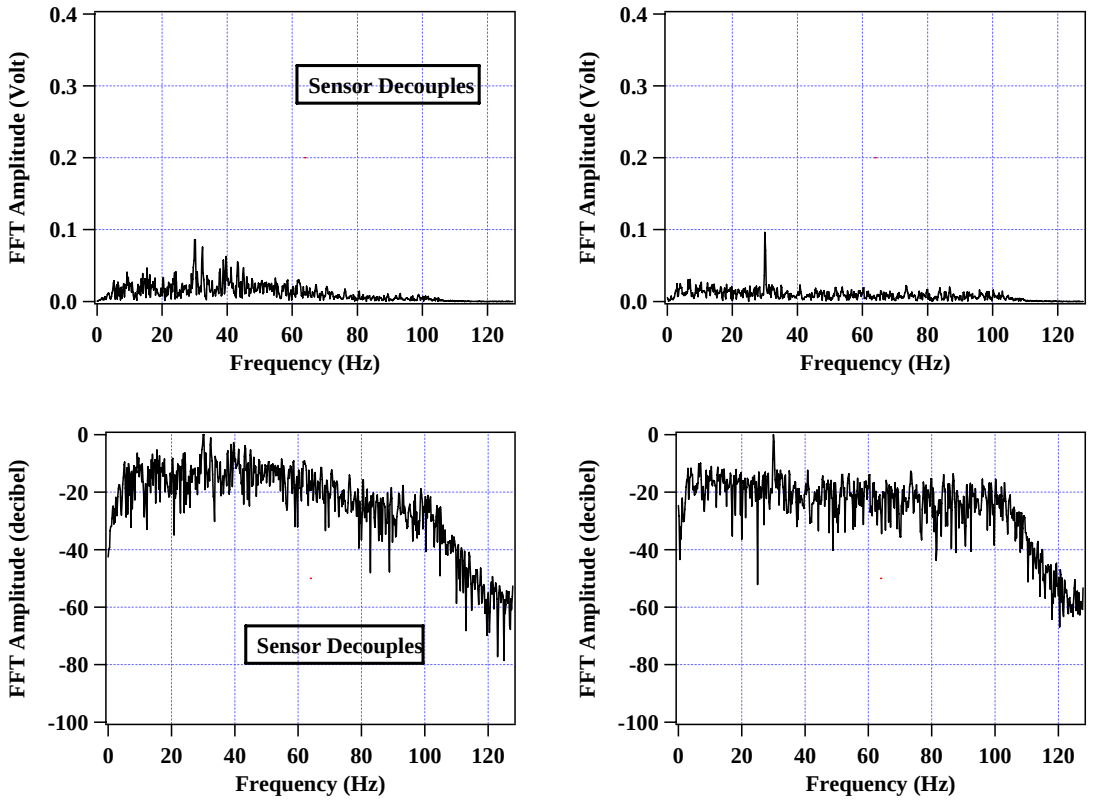

(a) First-Generation Rolling Sensor (6-in. Diameter Wheels)

(b) Second-Generation Rolling Sensor (12-in. Diameter Wheels)

Figure 5.44 FFT Spectra of First-Generation and Second-Generation Rolling Sensor (with 12-in. Diameter Wheels and 5 psi Hold-Down Pressure in Air-Spring) Collected at 3 mph Along Loop610N, near Houston.

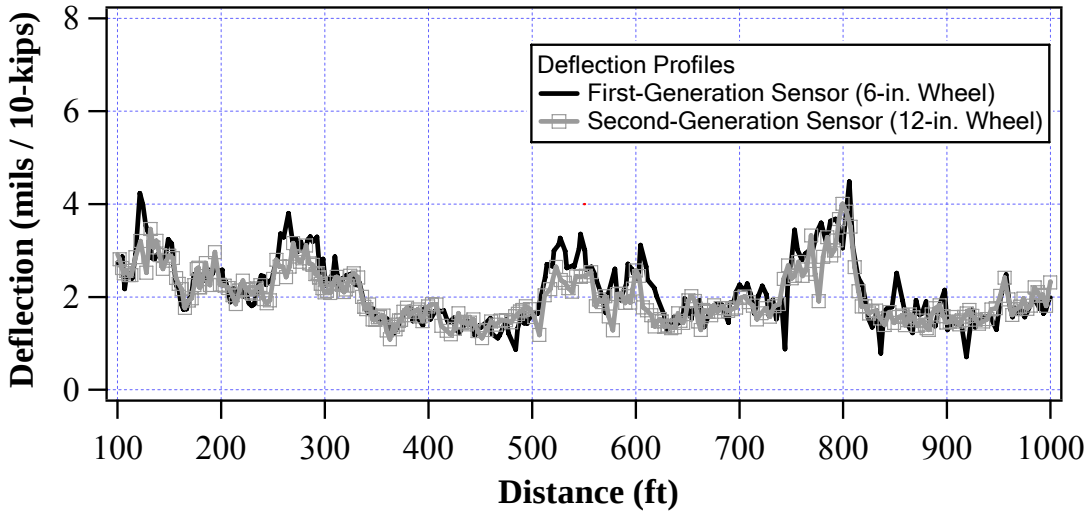

Figure 5.45 Deflection Profile Collected Using the First- and Second-Generation Rolling Sensors (12 in. Diameter Wheels) at an Average Speed of 1 mph; 5 psi Hold-Down Pressure in Air-Spring.

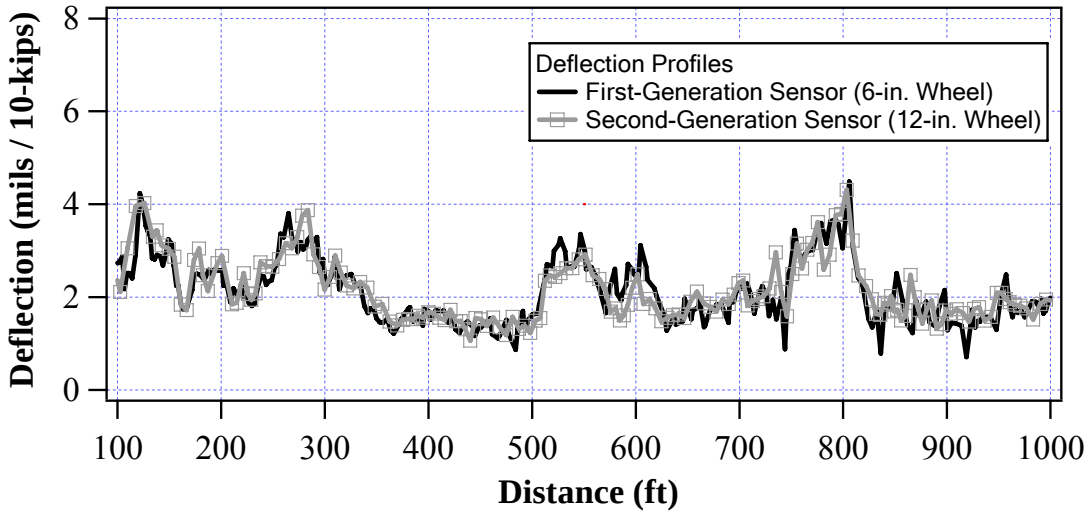

Figure 5.46 Deflection Profile Collected Using the First- and Second-Generation Rolling Sensors (12in. Diameter Wheels) at an Average Speed of 2 mph; 5 psi Hold-Down Pressure in Air-Spring.

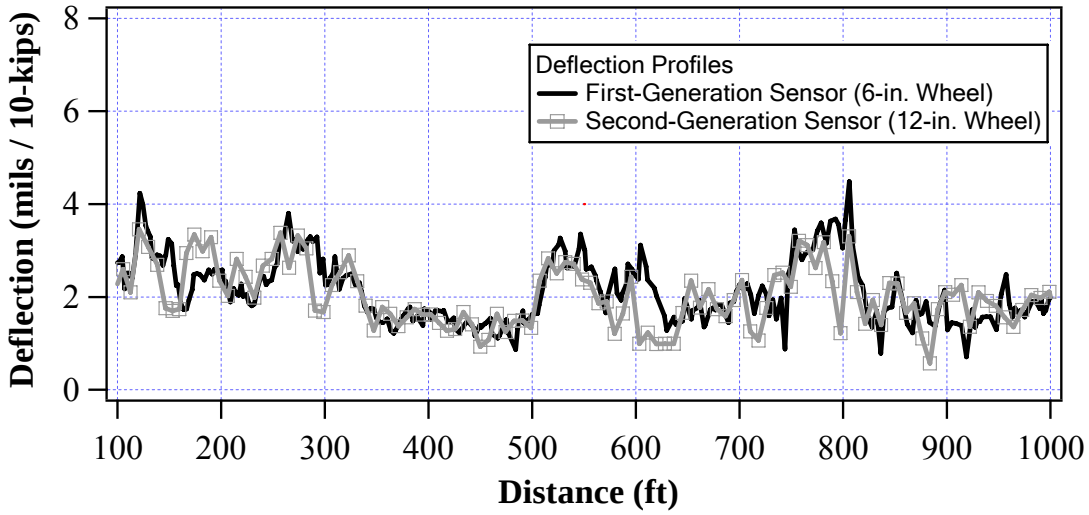

Figure 5.47 Deflection Profile Collected Using the First- and Second-Generation Rolling Sensors (12-in. Diameter Wheels) at an Average Speed of 3 mph; 5 psi Hold-Down Pressure in Air-Spring.

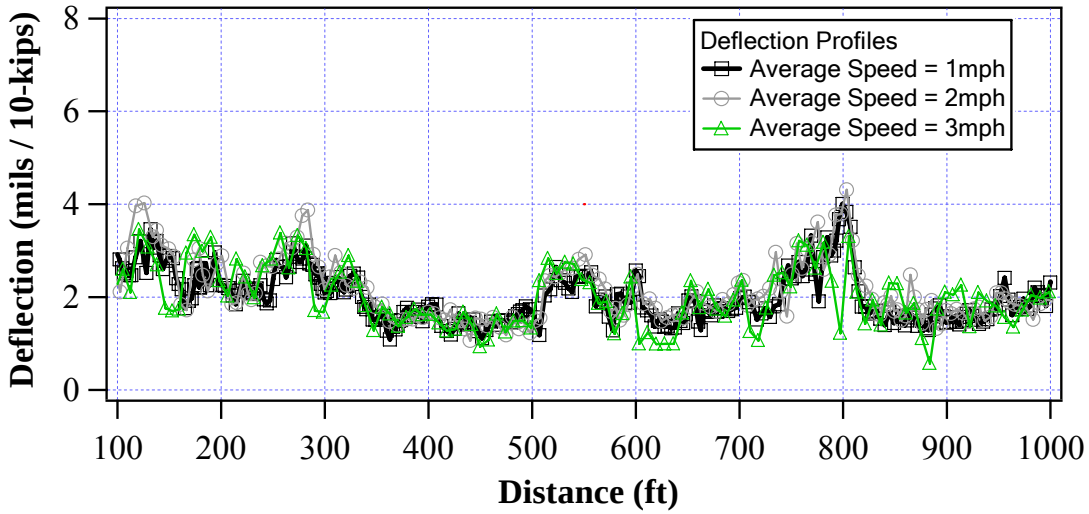

Figure 5.48 Deflection Profiles Collected Using the Second-Generation Rolling Sensors at Average Speeds of 1, 2 and 3 mph.

5.7 SUMMARY

The design and development of the second-generation rolling sensors are discussed in Chapter 4. In this chapter, the performance of these prototype rolling sensors were evaluated in a number of case studies. These case studies were performed using both the first- and second- generation rolling sensors along different pavement types or surfaces.

To evaluate the performance of the rolling sensor when tested along different pavements, deflection and acceleration measurements were made at a range of testing speeds between 1 to 3 mph. The rolling noise was also measured using the second-generation rolling sensor along pavements with different surface roughness. The rolling noise was then compared with the rolling noise collected using the first-generation rolling sensor to quantify the benefits of larger diameter rolling wheels (i.e. 9-in. and 12-in. diameters).

It was found that the pavement roughness significantly affects the measured noise levels (i.e. especially in the frequency range near the RDD operating frequency), and the benefit of having larger diameter rolling wheels is more apparent along pavement with high roughnesses (i.e. The second-generation rolling sensor is able to obtain measurement with lower level of rolling noise than with the first-generation rolling sensor at the same testing speed. This point is especially true on pavements with very rough pavement textures). It is important to note that the second-generation rolling sensor (with 12-in. diameter wheels traveling at 3 mph) did not exceed the theoretical maximum acceleration level of -2.5 g (i.e. stay coupled with the pavement surface) even on the milled concrete surface with unusually high surface roughnesses. By comparing deflection profiles collected using both the first- and second-generation rolling sensors at different pavement test sites, it was concluded that the deflection measurements made

using the second-generation rolling sensors at 3 mph are comparable with the deflection measurements collected at 1 mph on a range of pavement types. Furthermore, the SNR values are similar when comparing the first-generation rolling sensor testing at 1 mph with the second-generation rolling sensor (with 12-in. diameter rolling wheels) testing at 3 mph.

Chapter 6 Signal Processing Enhancements To The RDD Measurements

6.1 INTRODUCTION

The RDD is used to measure the pavement surface deflection basin under a known applied load. The primary benefit of the RDD is that it measures the surface deflection basin continuously as it rolls along a test path. However, in comparison with other discrete type of deflection testing devices, such as the FWD, more complex analysis is required before the deflection measurements can be obtained.

The FWD releases a drop weight from a known height onto a circular loading pad, and, as a result, applies a dynamic impulsive load to the pavement surface. Then, the stress wave travels to each geophone sensor at different times. There are a number of ways to obtain the FWD deflection basin. The most commonly used method is to pick out the peak deflections measured at each geophone sensor, and combine them to obtain a deflection basin. Both the FWD and RDD use geophones to measure deflections. The geophone is a transducer with output voltage proportional to the measured particle velocity. Since the geophone uses the acceleration of gravity as the reference, it can only measure the dynamic component of the pavement surface motion. A typical RDD time record collected from the rolling sensor is shown in Figure 6.1. During testing, the RDD applies a single-frequency sinusoidal dynamic force to the pavement. In addition to the RDD signal at the operating frequency, rolling sensor measurements also contain significant rolling noise. Therefore, the method that is used to analyze the FWD geophone measurements cannot be applied to pick out the peak deflection from an RDD time record. Nevertheless, the knowledge of the precise operating frequency and the high

signal-to-noise ratio (SNR) at the operating frequency allows the separation of the RDD signal from the rolling noise. Appropriate digital filtering needs to be chosen to isolate the RDD deflection signal from the rolling noise components. The signal can be better represented in the frequency domain. To illustrate this point, consider the power spectrum of the time record shown in Figure 6.1. The power spectrum is shown in Figure 6.2.

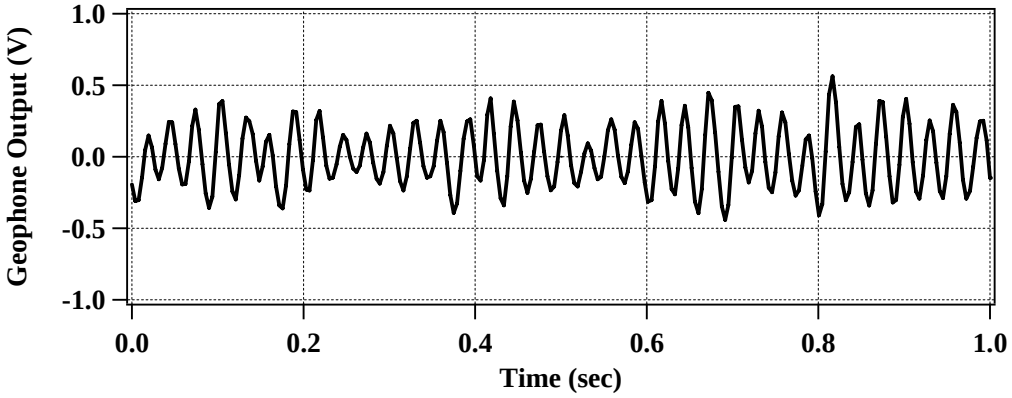

Figure 6.1 Time Record of a Signal Measured by an RDD Rolling Sensor.

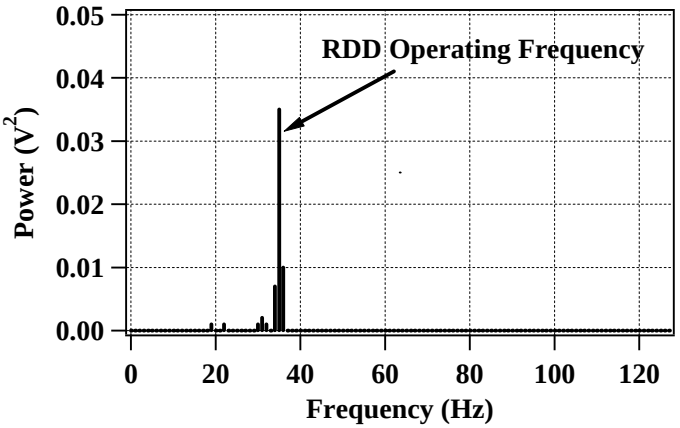

Figure 6.2 Frequency Domain Representation of the RDD Rolling Sensor Time Record Shown in Figure 6.1.

This chapter can be separated into two parts. In the first part, a review of the current signal processing analysis is presented. The short-comings and limitations of the current analysis algorithm are discussed. In the second part, an alternative digital filtering scheme is presented which addresses some of the limitations of the current method.

6.2 CURRENT RDD DATA ANALYSIS PROCEDURES

The current RDD data analysis procedures were developed by Bay (1997). The RDD raw data measurements can be separated into three groups. These groups are: (1) force measurements from load cells, (2) dynamic displacement measurements from rolling sensors, and (3) distance measurements from a distance measuring instrument (DMI). Analysis procedures are needed for both the force and dynamic displacement measurements to remove the noise components that are outside the RDD operating frequency. Due to the very high SNR from the load cells measurements (typical SNR is about 80 dB), choosing an appropriate digital filter is usually not a challenging task. In contrast, the rolling sensor outputs usually have a lower SNR (typical SNR is about 30 to 50 dB) than the load cell measurements, and this lower SNR often governs the digital filter to be used for analyzing the RDD deflection data.

Bay (1997) uses the amplitude demodulation method to calculate the RDD dynamic force applied to and dynamic displacements of the pavement surface. The basic principle of the RDD is to apply single-frequency sinusoidal energy on the pavement surface and measure the dynamic surface displacement at multiple locations using rolling sensors. Changes in the dynamic displacement amplitude envelope reflect changes in the dynamic displacements measured along the pavement surface. A low magnitude envelope normalized to a known applied load indicates a pavement system with high stiffness. On the other hand, a high magnitude envelope indicates a pavement system with low

stiffness. Therefore, the ultimate goal in analyzing the RDD data is to obtain the variation of the amplitude envelopes from the force and displacement signals.

The current analysis procedure is quite similar to the demodulation operation of an amplitude modulation (AM) radio receiver found in every day life. During AM radio transmission, the magnitude f(t) and phase $\phi(t)$ information of the audio transmission were first modulated according to the transmission frequency. Modulation technology helps the radio wave signal to transmit further with less signal degradation. When the radio signal arrives at the AM radio receiver, the audio transmission can be retrieved by applying the amplitude demodulation procedure on the signal. The amplitude demodulation and signal amplification are usually handled by analog electronic circuits inside a radio receiver. For the RDD, a similar procedure was performed using numerical algorithms. These numerical algorithms perform a similar amplitude demodulation procedure, which includes a well designed digital filter to separate the RDD deflection signal from other noise. The analysis procedure that was developed by Bay (1997) is summarized below.

The RDD signal can be represented using Eq. 6.1:

$$g(t) = f(t)\cos(\omega_o t - \phi(t)) + n(t) \qquad (6.1)$$

In this equation, g(t) represents the raw RDD measurement, which contains the magnitude f(t) and phase $\phi(t)$ information that is modulated under the transmission frequency ($\omega 0$). There is also a noise component n(t) that exists within the g(t) signal. The noise component n(t) is assumed to be negligible in the following equation derivation. However, the characteristic of n(t) plays an important role in the digital filter design and the RDD measurement error. The noise characteristics of the rolling sensor measurements are discussed in Chapters 3 and 5. This noise characterization is based on real RDD time records collected along different highways and airport runways.

In an effort to simplify the complexity of the Eq. 6.1, two parameters a(t) and b(t) were introduced. By substituting a(t) and b(t) into Eq. 6.1, Eq. 6.2 can be obtained.

$$f(t)\sin(\omega_o t - \phi(t)) = a(t)\cos\omega_o t + b(t)\sin\omega_o t \tag{6.2}$$

where:
$$f(t) = \sqrt{a^2(t) + b^2(t)}, and \tag{6.3}$$
$$\phi(t) = \arctan\frac{b(t)}{a(t)} \tag{6.4}$$

The Amplitude demodulation method can be performed on the formula in Eq. 6.2 by multiplying Eq. 6.2 with Eq. 6.5. The end result is the amplitude demodulation product.

$$(\cos\omega_c t + i\sin\omega_c t) \tag{6.5}$$

The amplitude demodulation product can be simplified using trigonometric identities. In Eq. 6.6, the amplitude demodulation product contains a summation of terms that has both the DC-part (i.e. 0-Hz) and the AC-part (i.e. $2\omega_o$).

$$\begin{aligned}
&\left(f(t)\sin(\omega_o t - \phi(t))\right)(\cos\omega_o t + i\sin\omega_o t) = \\
&\left(a(t)\cos\omega_o t + b(t)\sin\omega_o t\right)(\cos\omega_o t + i\sin\omega_o t) = \\
&\tfrac{1}{2}a(t) + \tfrac{1}{2}a(t)\cos 2\omega_o t + \tfrac{1}{2}i\,a(t)\sin 2\omega_o t + \\
&\tfrac{1}{2}b(t)\sin 2\omega_o t + \tfrac{1}{2}i\,b(t) - \tfrac{1}{2}i\,b(t)\cos 2\omega_o t.
\end{aligned} \tag{6.6}$$

All the AC terms are trigonometric functions with an angular frequency of $2\omega_o$. Also, the DC terms has half the magnitude as the original audio transmission. Since the primary objective is to retrieve the embedded audio transmission functions f(t) and $\phi(t)$, or the a(t) and b(t) functions as defined in Eq. 6.2. This requires the removal of the AC terms in the amplitude demodulation product. A simple low-pass filter with a cut-off

frequency equal to or less than 2□o can achieve this purpose under a noise-free environment. This is shown in Eqn. 6.7.

$$2\left[\frac{1}{2}a(t)+\frac{1}{2}a(t)\cos 2\omega_o t+\frac{1}{2}i\,a(t)\sin 2\omega_o t+\frac{1}{2}b(t)\sin 2\omega_o t+\frac{1}{2}i\,b(t)-\frac{1}{2}i\,b(t)\cos 2\omega_o t\right]\xrightarrow{L\text{-}P} a(t)+i\,b(t), \tag{6.7}$$

In reality, the RDD raw data collected from load cells and rolling sensors contains noise that distributes across the entire frequency spectrum. However, careful design of the rolling sensors and understanding the characteristics of the rolling noise helps to separate the actual pavement deflection signal from the noise. This careful design is discussed in Chapter 4 where different design issues of the second-generation rolling sensor are discussed.

Flow charts that illustrate the data analysis steps for the load-cell-force measurements and dynamic displacement measurements are shown in Figures 6.3 and 6.4, respectively. There are four load cells mounted on the RDD, and these transducers measure the dynamic force that is applied to the pavement surface. The load cells signals are multiplied by the load cells calibration factors, and then summed to obtain the total dynamic force. Amplitude demodulation is then performed, followed by a 0-Hz notch-pass filter to retrieve the desired DC term in the amplitude demodulation product in the complex domain. Last, the dynamic force $F_D(t)$ is obtained from the a(t) and b(t) functions.

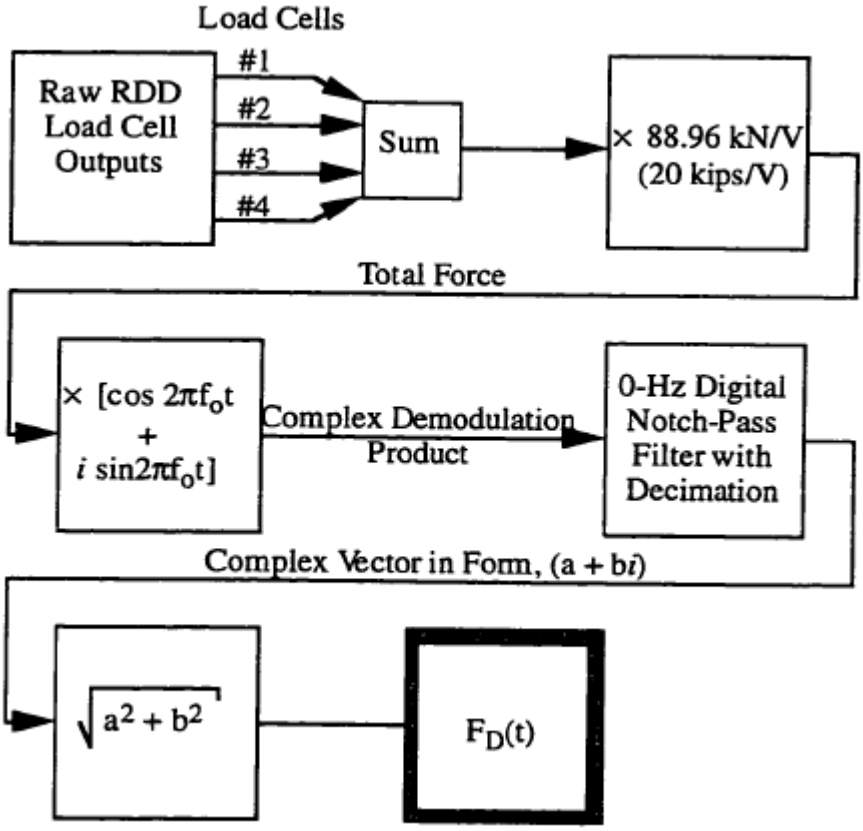

Figure 6.3 Flow Chart of the Steps Used to Calculate the Dynamic Force from the RDD Load Cell Outputs (from Bay, 1997).

Procedures for analyzing the rolling sensor outputs are very similar to the procedures used for analyzing the load cell outputs. After the demodulation product is obtained, an identical 0-Hz notch-pass filter is applied. Since the calibration factor of the rolling sensor varies with frequency, the correct calibration factor for the chosen RDD operating frequency (f_o) is then applied. The voltage output of a geophone transducer measures the vertical velocity of the pavement surface motion. A factor of $1/(2\pi f_o)$ is applied to convert the velocity measurement into a displacement measurement. Lastly, the dynamic displacement $\delta_D(t)$ is obtained from the a(t) and b(t) functions as illustrated in Figure 6.4.

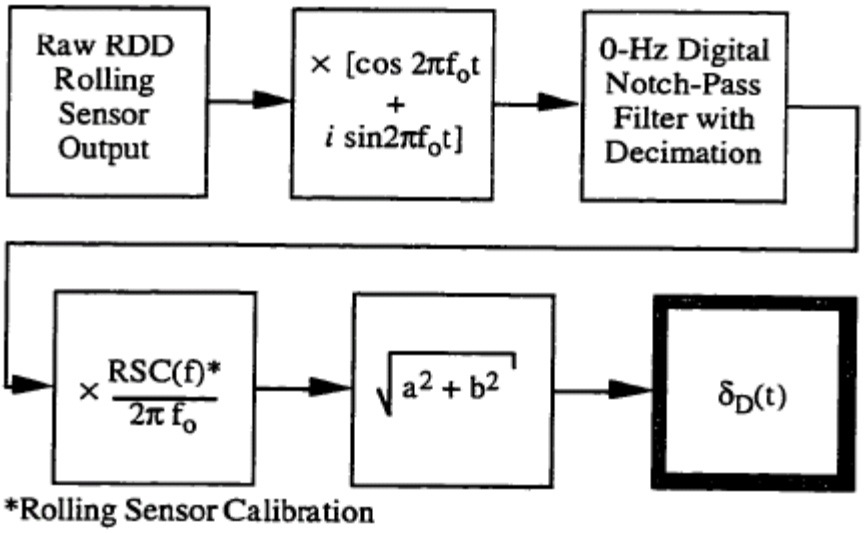

Figure 6.4 Flow Chart of Steps Used to Calculate the Dynamic Displacement From the RDD Rolling Sensor Outputs (from Bay, 1997).

6.3 CURRENT DIGITAL FILTER DESIGN

An overview of the current RDD data analysis procedure is presented above. The design of the digital filter to separate the real signal from other noise components is very important when analyzing the RDD raw data obtained from the load cells and rolling sensors. Therefore, it should be apparent that the performance of the analysis procedure is controlled by the performance of the 0-Hz digital notch-pass filter. The performance of the digital filter has a direct impact on the deflection measurements and error bands of such measurements. Bay (1997) proposed two digital filtering schemes for use in analyzing the RDD raw measurements. First, a composite IIR and FIR filter can be used. Second, a Hamming FIR filter can also be used. Both filters are band-pass filters with a narrow bandwidth centered about 0-Hz. This type of filter is referred to as 0-Hz digital notch-pass filter in Figure 6.4.

The first digital filtering scheme contains a composite filter by cascading an IIR notch-pass filter and an FIR decimating filter. A typical filter response of such filter is shown in Figure 6.5. The IIR notch-pass filter has two identical poles located near the unit circle. The frequency response around 0 Hz of the IIR notch-pass filter with different poles (p) is shown in Figure 6.6. Typical pole values range from 0.8 to 0.975, and the bandwidth of the primary lobe with -20dB attenuation (BW_{20}) decreases with increasing pole value. The relationship between BW_{20} and the poles is shown in Figure 6.7. This relationship can be approximated using Eq. 6.8 as:

$$\frac{BW_{20}}{f_s} = (1 - p) \tag{6.8}$$

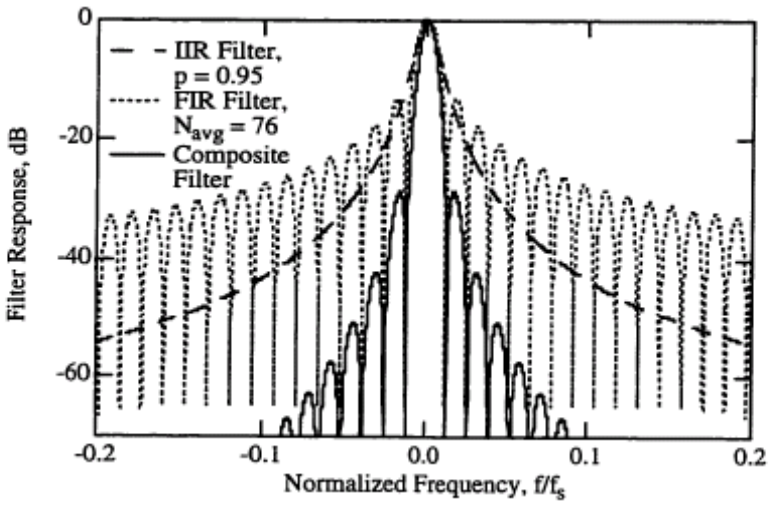

Figure 6.5 Responses of IIR Digital Filter and FIR Averaging Digital Filter and the Composite of the Two Filters (from Bay, 1997).

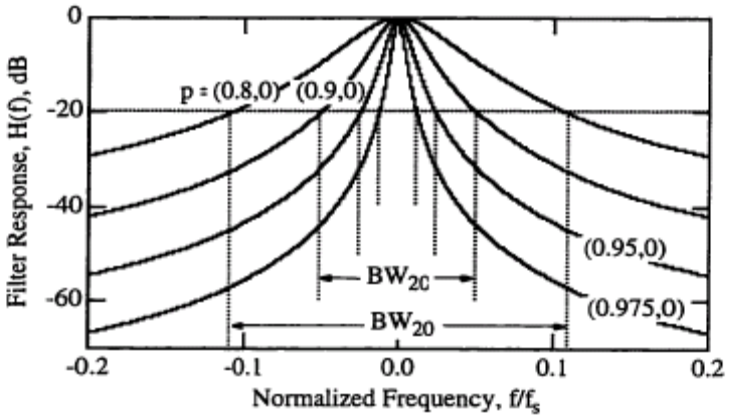

Figure 6.6 Notch-Pass Filter Responses of 0-Hz IIR Digital Notch-Pass Filters (from Bay, 1997).

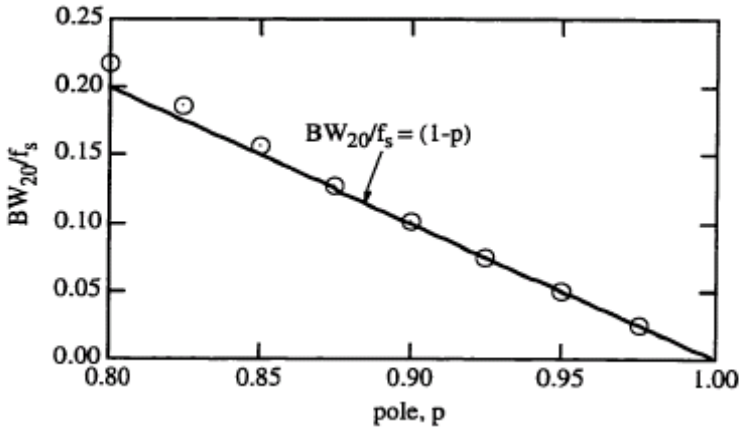

Figure 6.7 Relationship Between BW_{20} and Pole Position for Two-Pole, Notch-Pass Filter (from Bay, 1997).

The settling time of a digital filter is another important consideration in the digital filter design for analyzing RDD raw data. Ideally, the settling time of a filter should be made as short as possible, so that the digital filter has a fast response to rapid changes in the measured pavement deflections. As the test speed of the RDD increases, the settling time requirement becomes more restrictive. Figure 6.8 illustrates the settling time of different 2-pole IIR digital filter with different pole values. In here, the settling time can

be characterize using a t_{90} parameter, which indicates the time it takes for the amplitude of a particular digital filter to settle 90%. Different pole values are plotted in Figure 6.8, and t_{90} increases as the pole value increases. The relationship between t_{90} and p is shown in Figure 6.9, and the relationship can be approximated as:

$$t_{90} = \frac{\frac{3.89}{(1-p)} - 2}{f_S} \tag{6.9}$$

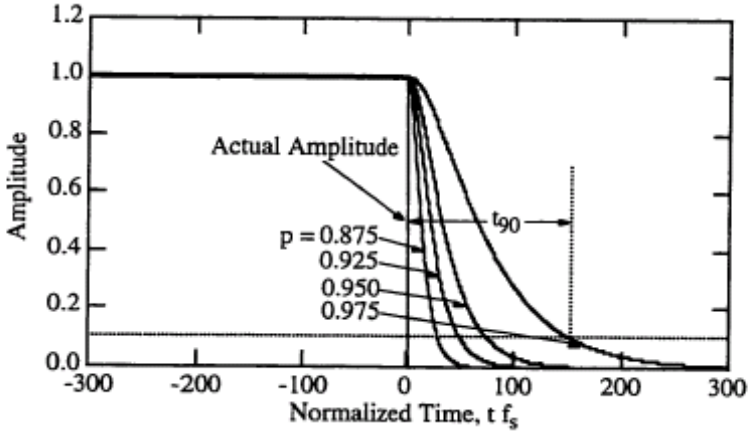

Figure 6.8 Filter Output of Several IIR Digital Filters when subjected to a Step Change in Input Waveform Amplitude (from Bay, 1997)

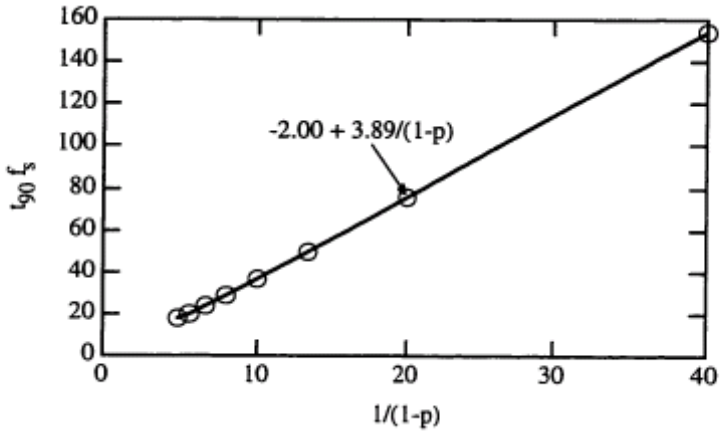

Figure 6.9 Relationship Between Pole Value and Filter Settling Time for 0-Hz Two-Pole Digital IIR Notch-Pass Filter (from Bay, 1997).

6.4 OVERVIEW OF DIGITAL FILTER DESIGN

Digital filters are used in many different applications. Some of the areas where digital filters are commonly used include the following. For examples, areas in the telecommunication, biomedical and electronic industries. When compared with their analog counterparts, digital filters offer many advantages over analog filters. Some of the major advantages are: (1) a digital filter is programmable and can be easily implemented on general-purpose computers or special digital signal processing (DSP) chips, (2) the filter response for a digital filter remains constant over time. This is not necessary true for an analog filter where the filter response is subject to signal drifting and is also dependent on environmental factors such as temperatures, and (3) digital filters are versatile and able to be adapted to changes in the signal characteristics. For instance, a category of digital filter known as adaptive filter, has the ability to change its filter characteristics according to the characteristics of the input signal.

There are two board categories of digital filters. The first one is a finite impulse response (FIR) filter. Once the input signal is set to zero, the filters output signal becomes zero after a finite number of sample times. The mathematical definition of a FIR filter is shown in Eq. 6.10 as:

$$y[n] = \sum_{k=0}^{N} b_k x[n-k] \tag{6.10}$$

The second category of digital filters is an infinite impulse response (IIR) filter. Once the input signal is set to zero, the filter output can be non-zero infinitely. The mathematical definition of an IIR filter is shown in Eqn. 6.11 as:

$$\sum_{i=0}^{M} a_i y[n-i] = \sum_{k=0}^{N} b_k x[n-k] \tag{6.11}$$

where y[n] denotes the output of the filter, x[n] denotes the input of the filter, N denotes the filter order, a_i and b_k are filter coefficients.

Other than the difference in their impulse responses, there are other attributes that differed between the FIR and IIR filters. Some of these attributes are shown in Table 6.1

Table 6.1 FIR Filter Attributes versus IIR Filter Attributes (from NI, 2005)

Attribute	FIR Filter	IIR Filter
Exactly linear phase response possible	Possible	Not possible
Stability	Always stable	Conditionally stable
Fixed-point version	Easy to implement	Can be complicated to implement
Computational complexity	More computations	Fewer computations
Datapath precision typically required	Less precision required	Greater precision required
Zero-input limit cycles[1]	Cannot produce limit cycles	Might produce limit cycles

[1] "Zero-input limit cycle behavior refers to the effect that the output may continue to oscillate indefinitely with a periodic pattern while the input remains equal to zero. And it is a consequence either of the nonlinear quantizers in the feedback loop of IIR filter or of overflow of additions." (Oppenheim and Schafer)

6.5 IMPROVEMENTS TO THE CURRENT DIGITAL FILTER

The current digital filtering scheme uses a composite filter (i.e cascading a 2-pole IIR filter with a FIR-decimating filter). This filter has been used successfully to post-process RDD raw data that were collected in the field over the years. Based on the fact that the RDD hydraulic loading system outputs a fairly clean sinusoidal dynamic force, Bay (1997) designed the current digital filtering scheme based on the knowledge that the RDD deflection signal can be found at precisely the RDD operating frequency (typical operating frequency ranges between 20 and 40 Hz). Furthermore, Bay used the amplitude

demodulation technique to demodulate the RDD signal (i.e. transforms the RDD signal at the operating frequency to 0-Hz). This allows one single digital filter to be used for any chosen RDD operating frequency. This approach has its own benefits and shortcomings as outlined below:

Benefits

1. fairly simple filter with a small number of filter coefficients (i.e. requires less computational power to run, and can often be faster),
2. only one filter is needed for any chosen RDD operating frequency,
3. effectively used to filter out rolling noise in most RDD pavement test sites, and
4. two ways filtering can be carried out to remove the effect of time shift caused by digital filtering.

Shortcomings

1. difficult to visualize the effect that each digital filtering operation has on the raw RDD data (i.e. transformation is performed in the complex domain, and the effect of a 0-Hz filter is difficult to visualize),
2. the 2-pole IIR filter is a symmetric filter with equal attenuation in the positive and negative frequency ranges (i.e an underlying assumption was made indicating that the rolling noise is symmetric about the RDD operating frequency),
3. lacks the flexibility to customize the digital filter according to the need of any particular pavement test site, and
4. not readily implemented using current commercially available Digital Signal Processing (DSP) processors and microcontrollers.

As discussed in the rolling noise study in Chapter 3, more knowledge has been gained regarding the RDD rolling noise characteristics. It was found that the rolling noise can be treated as a random process, and the characteristics are often site specific. In the remainder of this chapter, an alternative digital filtering scheme is proposed to address some of the above shortcomings.

The approach in developing an alternative digital filtering scheme involves the following steps:

1. eliminate the need to apply the amplitude demodulation technique (i.e analysis performed only in the real domain),
2. define a framework for establishing a rolling noise envelope,
3. generates a digital filter to notch-pass the signal at the RDD operating frequency, which satisfies both the frequency and time resolution requirements,
4. obtain the amplitude envelope using the Hilbert transform on the filtered time record, and
5. computes RDD deflection profile after applying the appropriate calibration and unit conversion factors.

6.6 ALTERNATIVE DIGITAL FILTERS FOR RDD ANALYSIS

There are many different ways to design digital filters for RDD applications. As discussed in the previous section, one of the most important components within the RDD analysis is the use of the proper digital filter to isolate the RDD signal from noise that exists at other frequencies.

When designing a digital filter for the RDD, the goal is to come up with a suitable digital filter design that strikes a good balance between the desired frequency resolution

and the time (or spatial) resolution. Since the precise RDD operating frequency is known, ideally the desired digital filter response is a peak filter at the operating frequency. The peak filter should have a sharp transition band that attenuates sufficiently at all other frequencies. However, as the peak filter becomes increasingly narrow and with an increasingly sharp transition, the settling time of this filter also increases. The increase in settling time (time or spatial resolution) is undesirable because it will smear changes in the measured pavement deflections. This characteristic means a filter with a long settling time will react very slowly to changes in the measured pavement deflections, which lacks the ability to correctly identify different localized pavement features (i.e. vicinity of cracks and joints). Unfortunately, an increase in frequency resolution is often at the expense of a slower responding filter design (i.e. poor time resolution). This effect will be more apparent as the testing speed of the RDD increases using the next-generation rolling sensor. In order to maintain the same spatial resolution that the current rolling sensor can achieve (i.e. testing at 1 mph), improvements to the digital filter design becomes a necessity when using the second-generation rolling sensors and testing at higher testing speed.

The tradeoff between the frequency and time resolutions can be characterized using two parameters. First, the time it takes the digital filter to settle to 10% of the original level after the input signal becomes zero. This parameter is denoted as t_{90}. The other parameter that is used to quantify the frequency resolution of the peak filter is the band width at -20 dB attenuation (a factor of 10 in attenuation). This parameter describes how wide the primary lobe is and is an indication of how accurate the digital filter can filter out frequencies other than the RDD operating frequency.

In this section, different digital filter designs are presented. These digital filter design techniques include: (1) zeros-poles placement, (2) peak filter, (3) LP th norm filter, and (4) composite filter.

6.6.1 Filter Design By Placing Zeros and Poles Arbitrarily

One of the most common ad-hocs methods is to design digital filters through trial-and-error placement of zeros and poles. The discussion of this design method is best discussed after presenting the z-transform of an FIR and IIR filter. The z-transform of a FIR and IIR filter is shown in Eqs. 6.12 and 6.13, respectively. The z-transform is a variant form of the Fourier transform that is particularly useful for time-discrete (sampled) functions. This z variable makes the Fourier transform appear as polynomials. The equation for the z variable is shown in Eq. 6.14.

$$H(z) = \sum_{k=0}^{N} b_k z^{-k} = K\prod_{k=1}^{N}(1 - z_k z^{-1}) \tag{6.12}$$

$$H(z) = \frac{\sum_{k=0}^{N} b_k z^{-k}}{1 + \sum_{i=1}^{M} a_i z^{-i}} = K\frac{\prod_{k=1}^{N}(1 - z_k z^{-1})}{\prod_{k=1}^{M}(1 - p_k z^{-1})} \tag{6.13}$$

$$Z = e^{j\omega\Delta t} \tag{6.14}$$

Zeros (z_k) and poles (p_k) refer to roots of the polynomial H(z) shown in Eqs. 6.12 and 6.13. The effect of the pole magnifies the response, while the effect of the zero attenuates the response. By placing the zeros and poles arbitrarily on the z-transform plane, an approximate filter response can be obtained. The 2-pole IIR filter proposed by Bay (1997) is a specific example of this filter design method, where the digital filter only has 2 poles at close proximity within the unit circle (i.e. to obtain a stable filter). The

filter response and the location of two poles within the unit circle is shown in Figures 6.10 and 6.11, respectively.

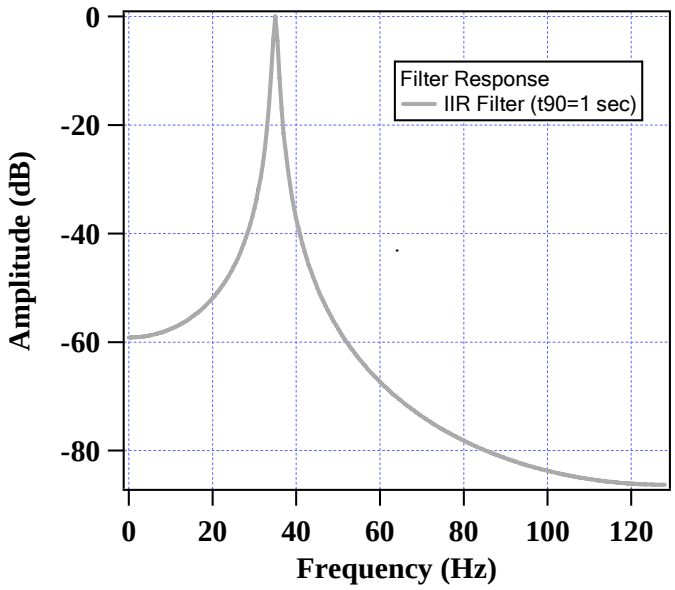

Figure 6.10 Frequency Response of a 2-Pole IIR Filter

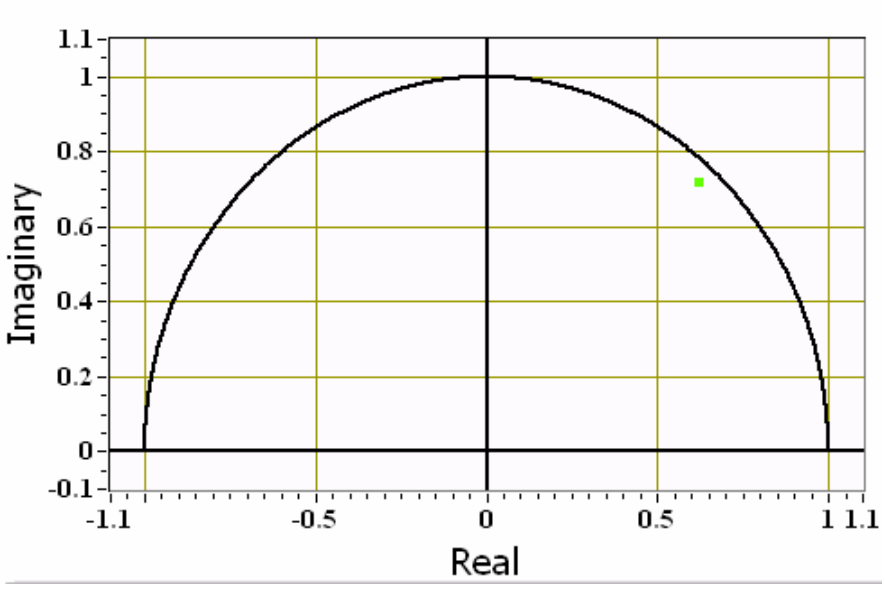

Figure 6.11 Location of Poles Within the Unit Circle

6.6.2 Peak Filter

Another group of filters is known as peak filters. These peak filters are notch-pass filters with narrow pass bands just like the 2-pole IIR filter mentioned earlier. The peak filter usually has high attenuation at the 0 Hz and the Nyquist frequency. While the 2-pole IIR filter uses the location of the poles to define the digital filter characteristics, the peak filter only needs one parameter, known as the Q-factor, to design a filter which will amplify at a single frequency (i.e. in the case, it would be the RDD operating frequency). The Q factor is defined as:

$$Q = \frac{\text{center frequency}}{\text{band width}} \tag{6.15}$$

Since the center frequency is the RDD operating frequency (i.e. fixed), the Q factor will increase with decreasing bandwidth in the pass band. In terms of resolving the amplitude at the operating frequency, the narrower the bandwidth the better. However, a narrower bandwidth (i.e. high Q factor) often results in a filter with a very long settling time (i.e. poor time resolution). The relationship between the Q Factor and the settling time is shown in Figure 6.12.

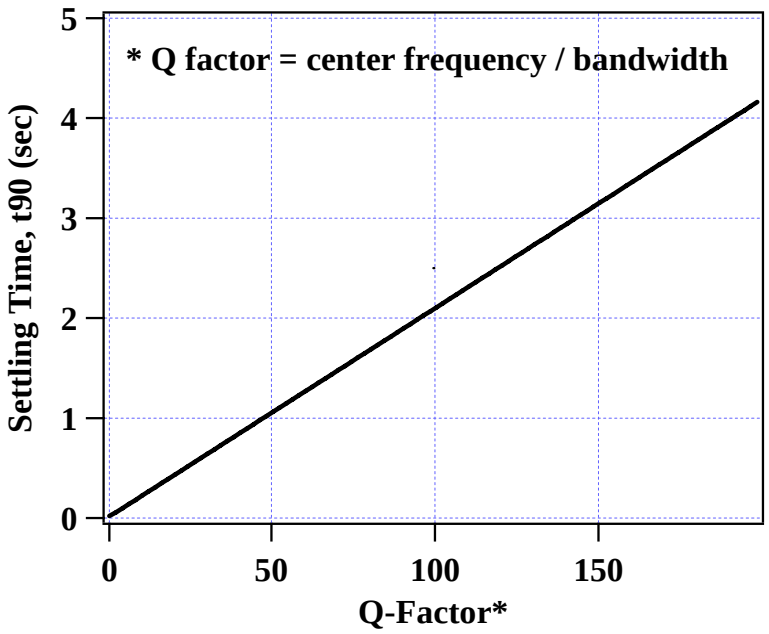

Figure 6.12 Relationship Between Settling Time (t_{90}) and Q Factor

The filter responses and the settling time performance of the peak filter and the 2 pole IIR filter are shown in Figures 6.13 and 6.14, respectively. Selected filters with similar bandwidth at -20 dB attenuation are shown, and the settling times for each filter are also shown. Based on the above results, the following observations can be made:

1. both the IIR filter and the peak filter can be configured to have a pass band with similar sharpness in the frequency response.
2. the IIR filter and the peak filter have different shapes in the stop band zones, and
3. the peak filter generally has poorer time resolution than the IIR filter counterpart.

The simplicity of the peak filter is ideal as a first approach to isolate the RDD signal from surrounding noise. However, the poor time resolution of this filter limits its use for RDD application when compared to a 2-pole IIR filter.

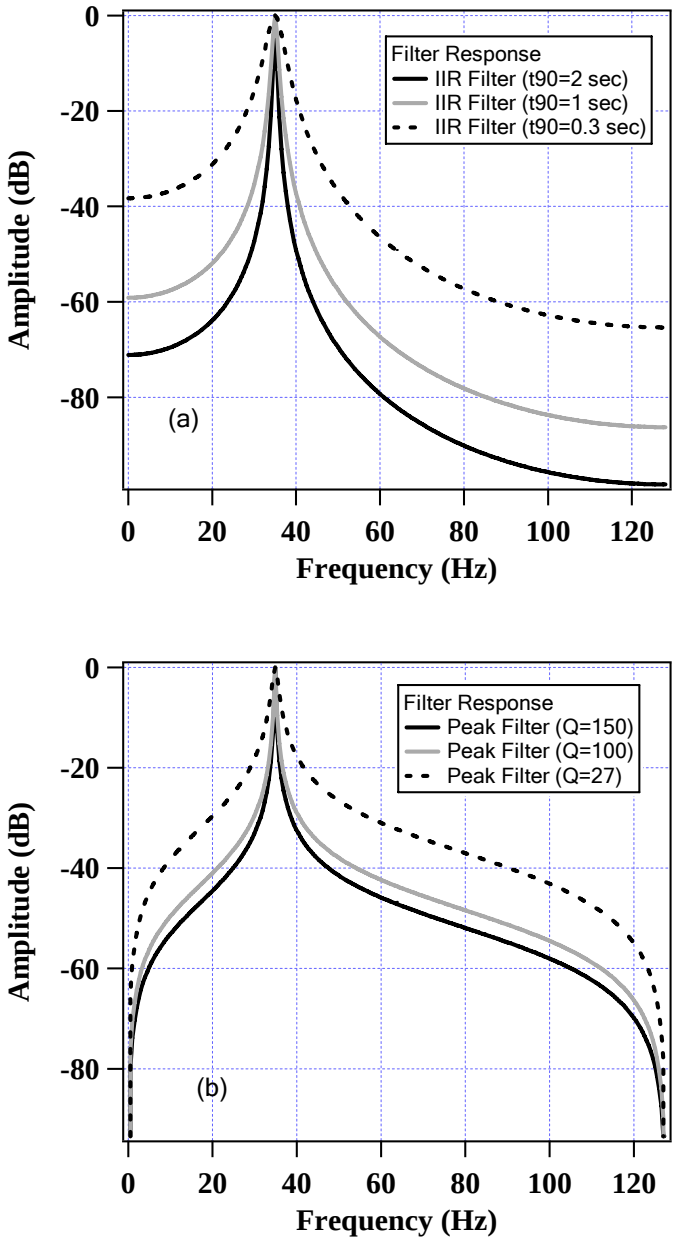

Figure 6.13 Frequency Response: (a) 2-Pole IIR Filter, (b) Peak Filter

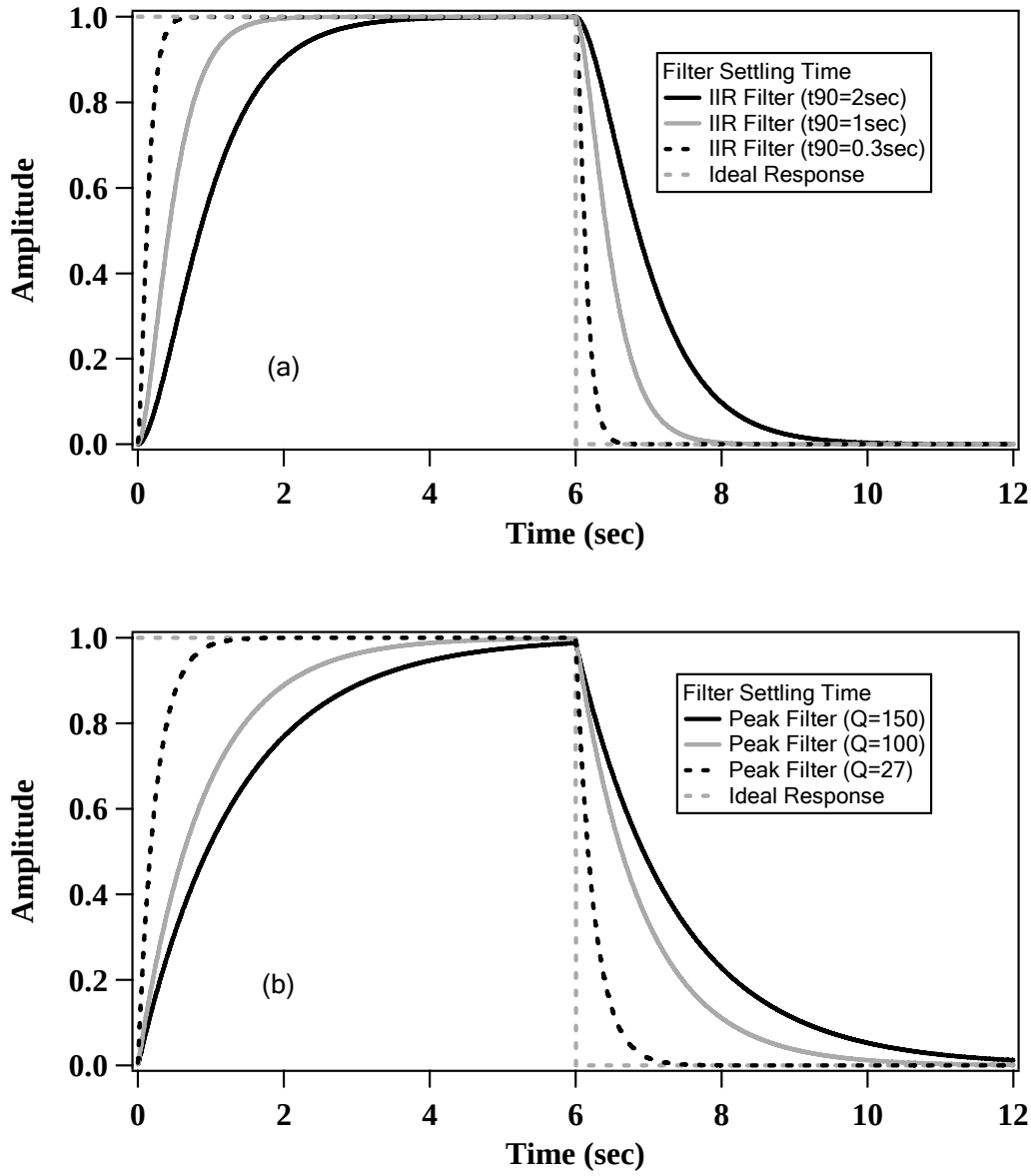

Figure 6.14 Settling Time: (a) 2-Pole IIR Filter, (b) Peak Filter

6.6.3 Least Pth Norm Design Algorithm

Even though both the 2-pole IIR filter and the peak filter can isolate the RDD signal, neither one of them allow the user to custom design the filter specification

according to the need of the data collected at a given RDD site. This limitation can prohibit obtaining an optimal digital filter with the best trade-offs between the frequency and time resolutions. Furthermore, as more information and knowledge are gained in the collected RDD data (e.g. such as the noise distribution and higher order harmonics in the rolling sensor records), this information can be utilized in the design of a digital filter to obtain a more accurate representation of the continuous deflection profile along a highway.

When designing 2-pole IIR filter and the peak filter, the underlying assumption is that the noise amplitude decreases in amplitude as it gets further away from the notch-pass frequency. As shown in Chapter 3, there are times when the distribution of rolling noise does not follow this general trend. When designing a filter with classical design methods, such as Butterworth and elliptic methods, the filter designed is defined as optimal when it meets a certain criterion. With the Least Pth Norm Design Method in the Labview Digital Filter Design Toolkit, the optimal criteria is defined by Eq. 6.16 for designing the minimum and maximum phase digital filter.

$$\|E\|_p = \left(\sum_{i=0}^{L-1} \left(W(i) \left| |H(\omega_i)| - |D(\omega_i)| \right| \right)^p \right)^{\frac{1}{p}} \tag{6.16}$$

where

W(i) = positive weight at the i_{th} frequency point,
H = response of the designed filter,
D = target response,
L = number of frequency points used to perform the calculation, and
p = the pth norm

A number of parameters are required to use the Least Pth Norm Design Algorithm. These parameters are: (1) target frequency response, (2) filter order, number of a[i] and b[k] coefficients, (3) order of norm (p), and (4) pole radius constraint. When p is 2, the Least Pth norm algorithm results in a least squares solution. An increasing p value yields a filter that approaches an equi-ripple magnitude solution, where an equi-ripple solution is obtained when p is 128. The pole radius constraint restricts proximity of poles to the unit circle. The pole radius takes a value between $0 < r \leq 1$. A small pole radius constraint improves the stability of the filter.

By utilizing the Least Pth Norm design algorithms, a filter library was established which contains a range of digital filters with different filter characteristics (both in terms of frequency and time resolutions). These filters are included within the WinRDD digital filter library, as discussed in Chapter 7. The user can choose the appropriate filter which best suits a particular set of data, or the user can redesign a filter using the Least Pth norm filter design algorithm to best fit a particular set of RDD data. These digital filters are grouped as follows:

1. high attenuation in the low frequency range,
2. high attenuation in the high frequency range,
3. short settling time,
4. similar attenuation in the stop band frequencies,
5. narrow primary lobe,
6. wider primary lobe,
7. removing higher order harmonics, and
8. all rounded filter.

6.6.4 Least Pth (LP th) Norm Filter Design: Simulation

As discussed above, a number of input parameters are required to use the LP th norm filter design algorithm. In the first instance, it is not apparent what effects these parameters have on the actual digital filter characteristics. With the current computer processing power, the effects can be better understood using simulations. The approach is to execute the LP th norm filter design algorithm a large number of times. Each time, a random set of input parameters are generated to obtain a digital filter. Then, graphs are plotted between the input parameters to understand the effects on the filter characteristics. Relationship between the different digital filter input parameters and the obtained filter characteristics are shown in Figures 6.15 through 6.19. These results provide a general guideline in choosing the different input parameters for designing a LP th norm filter as discussed below.

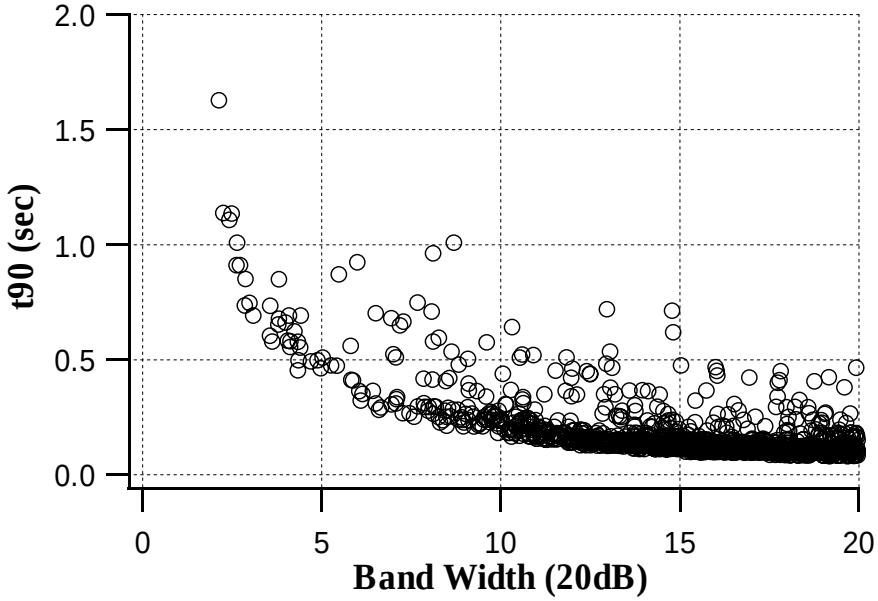

Figure 6.15 Relationship Between Bandwidth at -20 dB and the Settling Time (t_{90})

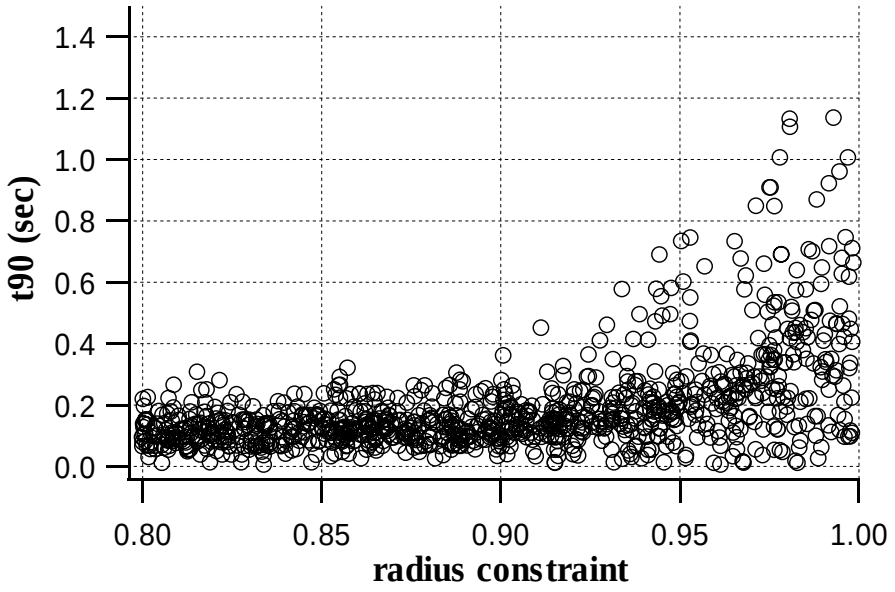

Figure 6.16 Relationship Between Settling Time (t_{90}) and the Radius Constraint

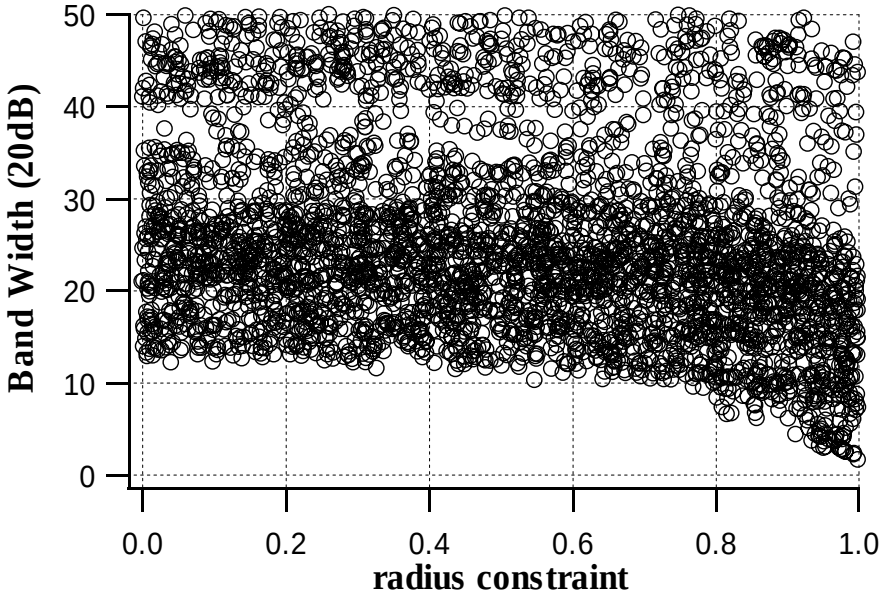

Figure 6.17 Relationship Between Bandwidth at -20dB and the Radius Constraint

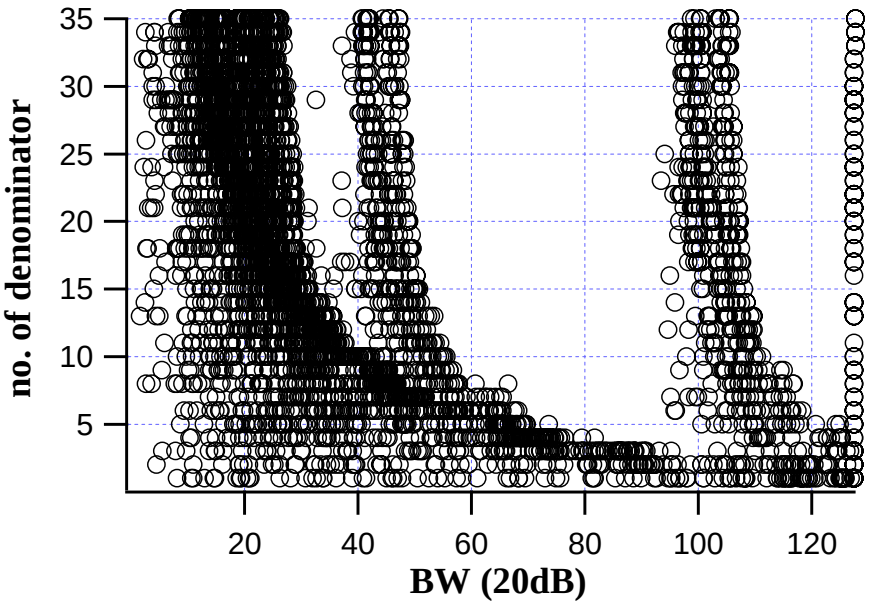

Figure 6.18 Relationship Between the Number of Denominator and the Bandwidth at -20 dB.

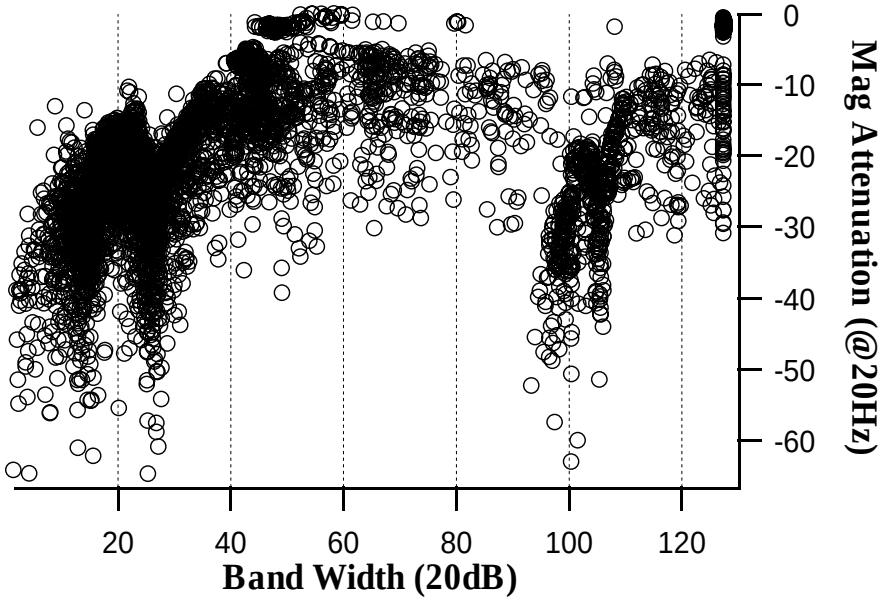

Figure 6.19 Relationship Between Bandwidth at -20dB and Magnitude Attenuation at 20 Hz.

Based on the LP th norm simulation results, the following generalizations can be made to help guide the user in designing LP th norm filters.

1. The settling time, t_{90}, increases sharply as the band width of the primary lobe decreases below 7.5 Hz, as shown in Figure 6.15.
2. The settling time, t_{90}, is primarily governed by the radius constraint value (ranges between 0 – 1.0). The values of t_{90} increases rapidly as the radius constraint increase beyond 0.95, as shown in Figure 6.16.
3. Increasing the radius constraint tends to reduce the bandwidth of the primary lobe, as shown in Figure 6.17.
4. The bandwidth of the primary lobe decreases with the increasing number of y coefficients [denominator coefficients]. As a result, a family of curves between the number of y coefficients and the bandwidth at -20dB attenuation were obtained in Figure 6.18. Each line represents the width of the primary lobe specified as the input to the LPth norm design algorithm.
5. high attenuation at 20 Hz can be obtained with decreasing bandwidth at -20dB, as shown in Figure 6.19.

6.6.5 Alternative Composite Filter: Cascading LP th Norm Filter with FIR Hanning Window Filter

As is illustrated in three examples presented in Section 6.7, an LP th norm filter designed using the technique discussed below can often generate a filter which produces similar results to the composite filter proposed by Bay (1997). However, it was found that by cascading a LP th norm filter with a FIR Hanning Filter, the resulting filter has slightly better performance in terms of primary lobe attenuation, and yet, the time

resolution is comparable with the composite filter proposed by Bay (1997). This filter is called filter Z in this dissertation.

In the case where the SNR is low in the RDD data, an attempt is made to create a filter with a sharper primary lobe and with satisfactory time resolution.

The composite filter that was proposed by Bay (1997) contains two filtering components. First, the 2-pole IIR filter is a filter with a very sharp roll-off in the transition band between the passband and the stopband frequencies. But, this filter alone often does not have enough attenuation in the stopband, especially when there is significant noise in the rolling sensor record at the stopband. Second, the FIR Hamming Decimating Filter is a filter with a similar primary lobe bandwidth as the IIR filter, and yet it has high attenuation (around -80 dB range) in the stopband. When cascading both filters, the resulting frequency response has both the characteristic of a sharp roll-off in the transition band and high attenuation at the stopband frequencies. The frequency response of this composite filter is shown in Figure 6.20.

When designing the new composite filter, the design philosophy used behind filter Z is that a LP th norm filter is designed with sharp roll-off characteristics in the transition band. Yet, instead of increasing attenuation at frequencies further away from the passband frequency (i.e. 2-pole IIR filter), this LP th norm filter has decreasing attenuation at frequencies away from the passband frequency. A filter with this characteristic can only be designed using the design flexibility of the LP th norm algorithm. The key point is that this design often results in a filter with a shorter settling time than a 2-pole IIR filter would have. The justification behind the decreasing attenuation is because this can often be compensated by the high attenuation characteristic in the FIR filter in which it is subsequently cascaded with (i.e. the primary role of the first filter provides the rapid roll-off at the transition band, but not high

attenuation at the stop band). Then, a FIR Hanning filter is chosen to be cascaded with the LP th norm filter instead of the FIR Hamming filter. The Hanning filter is chosen because its rapid drop in the stop band attenuation characteristic is more suitable to compensate for the low attenuation in the stop band provided by the LP th norm filter. The frequency response of this filter Z is shown in Figure 6.21. Then, the comparison between the composite filter and the filter Z in terms of the frequency response and the settling time performance are shown in Figures 6.22 and 6.23, respectively. The comparisons in Figures 6.22 and 6.23 shown that filter Z has the following characteristics:

1. slightly sharper primary lobe than the composite filter,
2. higher attenuation in the stop band frequencies,
3. similar settling time as the composite filter, and
4. a constant time shift in the filter output because filter Z did not use two way filtering as has been done in the composite filter proposed by Bay (1997). However, since the time delay is deterministic, it can be accounted for in the output analysis accordingly.

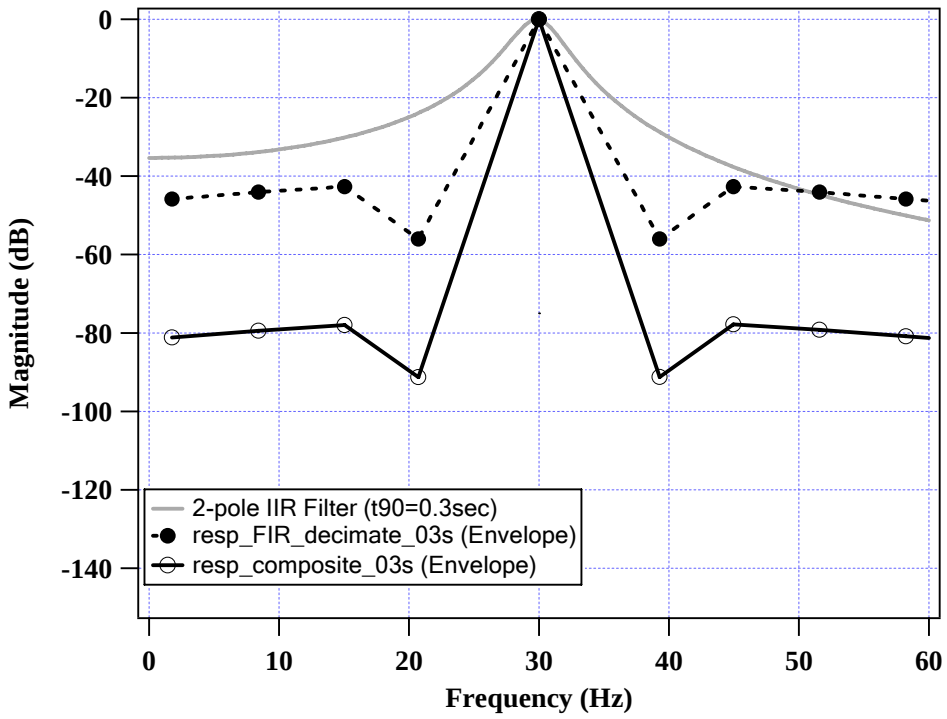

Figure 6.20 Frequency Response of Different Components within the Composite Filter Proposed by Bay (1997)

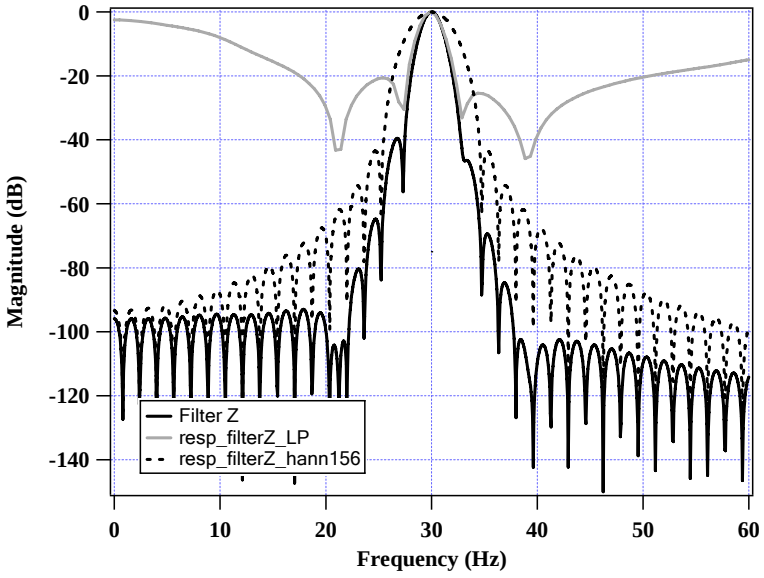

Figure 6.21 Frequency Response of Different Components within the Proposed Filter Z

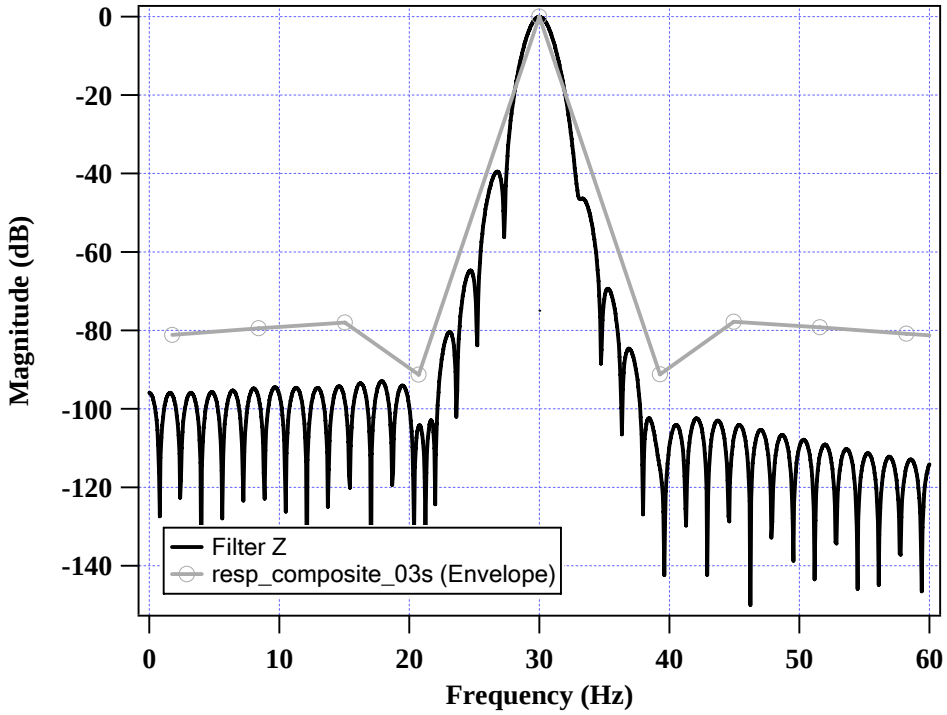

Figure 6.22 Comparison of Frequency Response Between the Proposed Filter Z and the Composite Filter Proposed by Bay (1997)

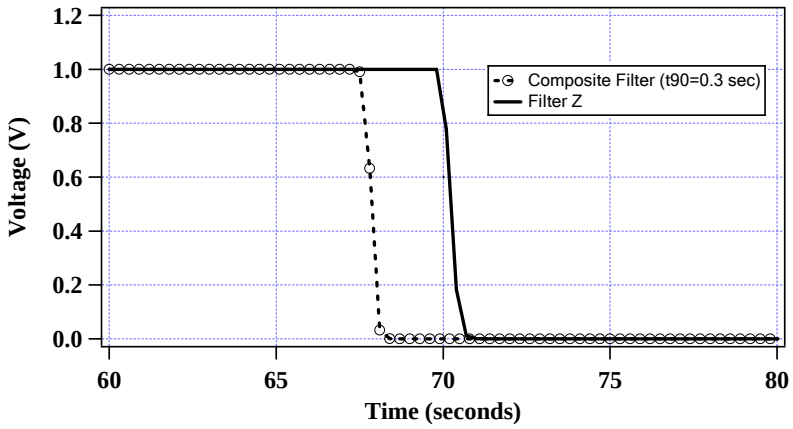

Figure 6.23 Comparison of Settling Time Between the Proposed Filter Z and the Composite Filter Proposed by Bay (1997)

6.7 EXAMPLES ILLUSTRATING AN ALTERNATIVE DATA ANALYSIS METHOD

In this section, the alternative data analysis method is illustrated in this section. The digital filters chosen in these examples are the LP th norm filters designed using the digital filter design technique discussed in Section 6.6.3.

6.7.1 Eliminate The Amplitude Demodulation Technique

An example is provided to illustrate the different steps of this alternative data analysis method. In the current digital filtering scheme, an amplitude demodulation technique is used to shift the RDD operating frequency signal to 0 Hz. Then, only a single digital filter is needed to analyze RDD data collected at different operating frequencies. The proposed filtering scheme eliminates this amplitude demodulation process. Instead, a notch-pass filter at the RDD operating frequency is used to filter out surrounding rolling noise. A digital filter such as the one shown in Figure 6.24 can be used to notch-pass the signal at the RDD operating frequency.

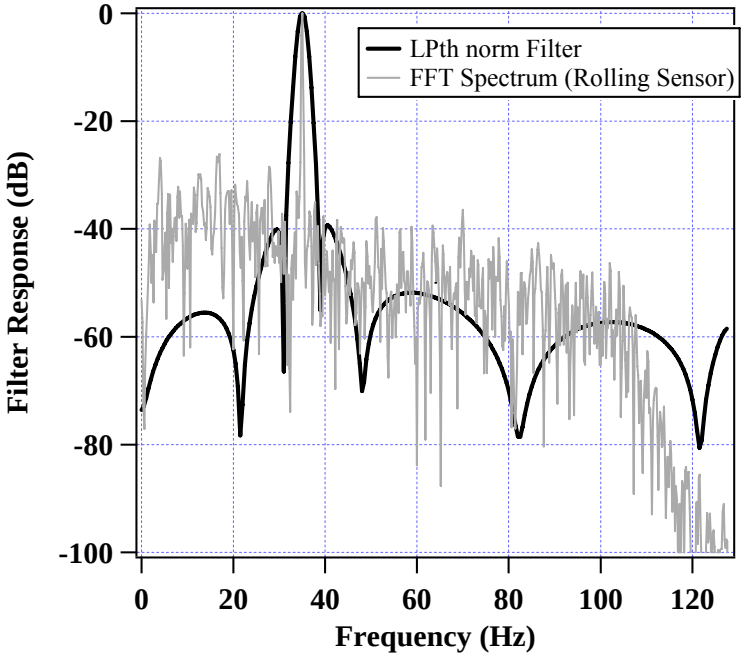

Figure 6.24 FFT Spectrum of Rolling Sensor Measurement and LPth Norm Digital Filter

Since a notch pass filter with a passband centered at the RDD operating frequency is now used, the amplitude envelope of the filtered RDD signal needs to be computed using signal processing technique other than the amplitude demodulation method. One technique which utilizes the property of the Hilbert Transform can be used to compute the amplitude envelope of the signal. This application of the Hilbert Transform is presented in Section 6.7.4. The obvious advantage of eliminating the amplitude demodulation process is that the filtering process can be performed in the real domain. Unlike the amplitude demodulation technique, the amplitude demodulation product requires performing computations in the complex domain. Furthermore, it is easier to visualize the effect of the digital filter (i.e. the user can inspect if the predominant frequency in the filtered time record is at the operating frequency).

6.7.2 Establishing A Rolling Noise Envelope

A time record collected using the second-generation rolling sensor (with 12-in. diameter wheels) is shown in Figure 6.25. This time record is used to illustrate the remaining parts of the filtering process. The time record consists of the predominant 35-Hz RDD operating frequency, and the rolling noise generated as discussed in Chapter 3. The variation of the 35-Hz RDD signal reflects the change in deflections (i.e stiffness) of the pavement system, and the variation of rolling noise level is a function of the testing speed, pavement roughness and deflection levels of the pavement. These factors are expected to change during testing. To illustrate how the characteristics of the collected rolling sensor signal vary with time, six different locations along the time record (indicated as markers A, B, C, D, E, and F in Figure 6.25) have been chosen. The FFT spectra at these various locations were computed as shown in Figure 6.26. Location A was collected before the RDD started to roll (i.e. at stationary position), which represents the case with the absence of rolling noise. It can be seen that the noise floor is very low

around -100 dB at this location. All the other locations were collected when the RDD was rolling along the pavement surface. The FFT spectra for locations B, E, and F were fairly similar in terms of rolling noise levels and distribution characteristics. At location D, the measured deflection is low, resulting in a significantly lower SNR than at any other location. This low SNR usually requires more attenuation in the stopband frequencies to resolve the amplitude at the operating frequency accurately. At location C, the measured deflection is high. However, the shape of the rolling noise distribution has changed somewhat when compared with the other locations. The rolling noise between 5 to 30 Hz is significantly higher when compared with other frequencies.

By analyzing the entire time record in the frequency domain, it is easy to identify the following:

1. an average rolling noise envelope to approximate most of the time records,
2. the average noise level and the average SNR, and
3. areas with particularly high or low measured deflections, and
4. locations where there are changes in the rolling noise spectrum characteristics.

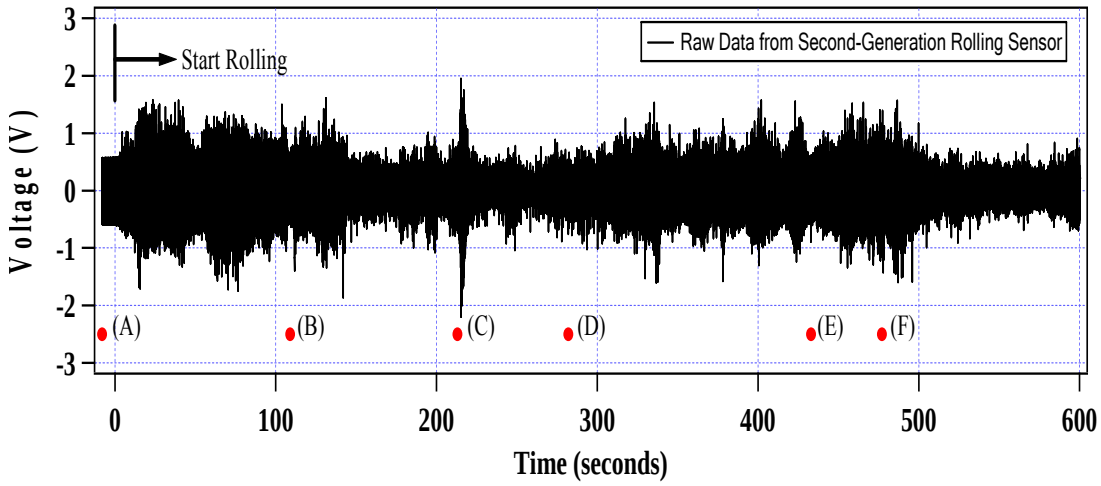

Figure 6.25 Time Record Collected Using Second-Generation Rolling Sensor (12-in. Diameter Wheels) Along A Flexible Pavement at 2 mph (5 psi Hold-Down Pressure in the Air Spring).

All of this information can be useful when choosing the appropriate digital filter and can be helpful in explaining some of the unexpected features found along the RDD deflection profile.

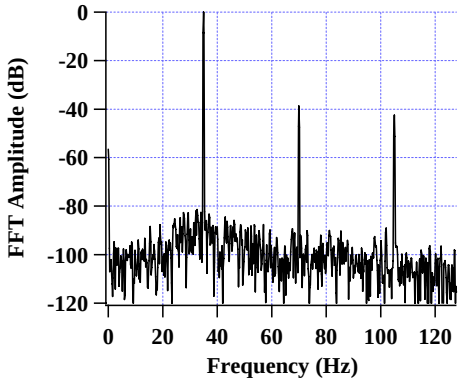

(a) Location A

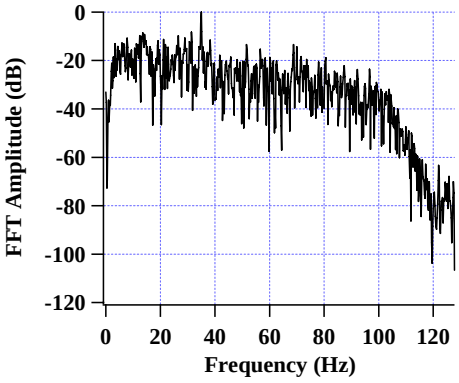

(d) Location D

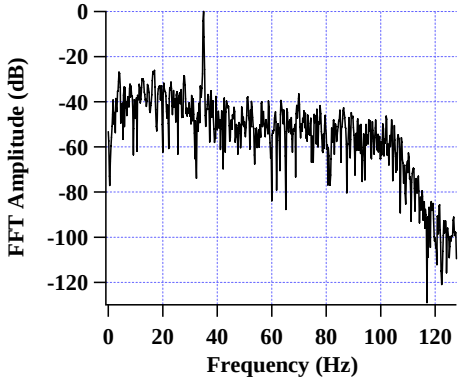

(b) Location B

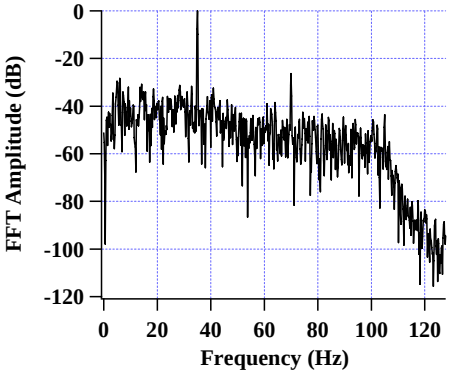

(e) Location E

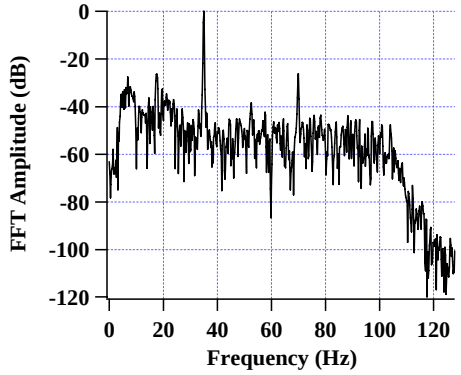

(c) Location C

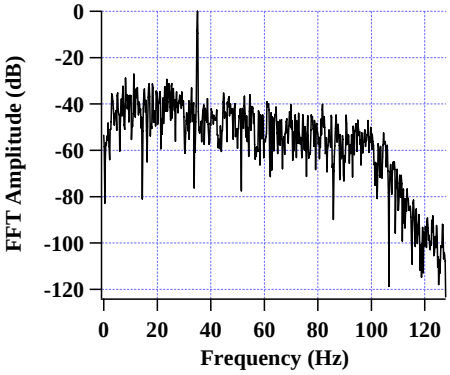

(f) Location F

Figure 6.26 FFT Spectra for Six Selected Locations (Points A to F) Shown in Figure 6.25.

6.7.3 Choosing the Digital Filter

There are different design methods that can be used to improve the digital filter used for analyzing RDD data. The first and the most intuitive approach is by placing zeros and poles arbitrarily on the z-transform plane until the desired filter characteristics are obtained. By knowing the basic effects that zeros and poles have on the filter response, one can easily come up with a reasonable filter design. However, this solution is often far from the optimal solution.

The second approach is to use different filter design algorithms to come up with a digital filter that meets a set of filter specifications. There are many different algorithms available, some of these algorithms generate a peak filter (which only requires one parameter to generate the necessary filter). Other more demanding filters have more flexibility to accommodate different filter specifications, but often require more input parameters and longer computational times to generate the filter coefficients. One such method is the LP th norm algorithm design method which is presented in Section 6.6.

A LP th norm filter is chosen to analyze the time record shown in Figure 6.25. The frequency response of the LP th norm filter is shown in Figure 6.24. The frequency response and the time resolution of this filter are compared with the ones of the current digital filtering scheme (i.e. composite filter), as shown in Figures 6.27 and 6.28, respectively. As mentioned earlier in this chapter, Bay (1997) proposed a composite filter which contains two parts. In the first part, a 2-pole IIR filter. This IIR filter is defined by a pole value (p), which can be related to the filter settling time parameter (t_{90}) using Eq. 6.9. t_{90} ranges between 1 and 2 seconds are typically used. In the second part, a FIR decimating filter which takes the average value of a certain number of points (N_{avg}), and output a single point for every N_{avg} points (i.e. this process is known as decimation). The

N_{avg} value is typically chosen to corresponds to the t_{90} chosen for the IIR filter. The Navg and t_{90} parameters are related to each other:

$$N_{avg} = t_{90} * f_s \qquad (6.17)$$

where t_{90} = time for digital filter to settle 90% of the input amplitude,
N_{avg} = number of points used in the FIR decimating filter, and
f_s = sampling frequency.

By combining the IIR filter and the FIR decimating filter, a filter with very sharp transition and high attenuation at stopband frequencies can be achieved as shown in Figure 6.27.

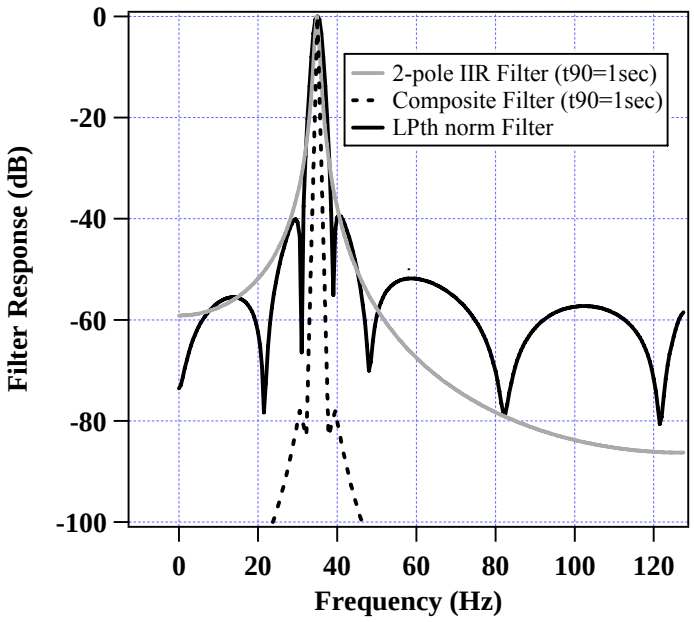

Figure 6.27 Comparison of Frequency Response for Different Digital Filters: (1) 2-pole IIR Filter (t_{90} = 1 sec.), (2) FIR Decimating Composite Filter(t_{90} =1 sec.), and (3) LPth Norm Filter.

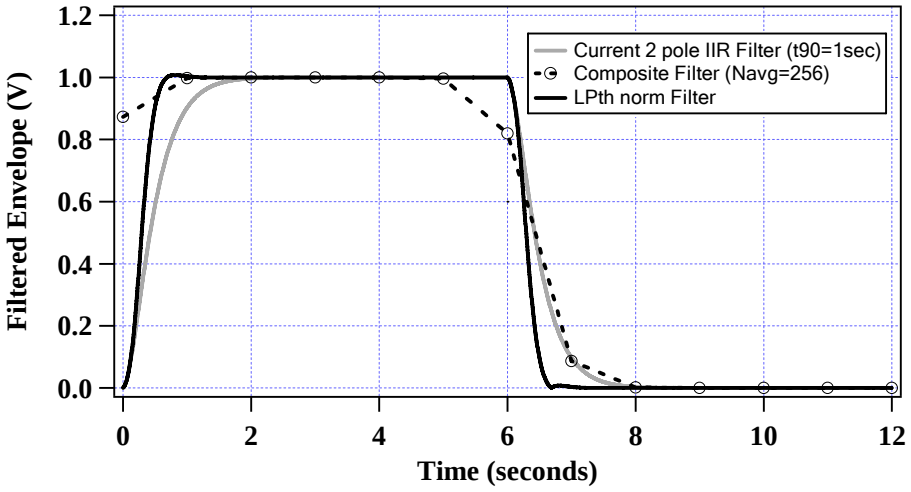

Figure 6.28 Comparison of Time Response for Different Digital Filters: (1) 2-pole IIR Filter (t_{90} = 1 sec.), (2) FIR Decimating Composite Filter (t_{90} = 1 sec.), and (3) LPth Norm Filter.

As shown in Figures 6.27 and 6.28, this LP th norm filter has much better time resolution (ie. spatial resolution) when compared to the current composite filter (with t_{90}=1 sec.). On the other hand, the current digital filter has better frequency resolution than the LP th norm filter presented herein. If the collected rolling sensor time record has very high SNR, then this LP th norm filter, with t_{90} = 0.225 sec., is preferred over the composite filter, with t_{90} = 1 sec. (i.e. the LP th norm filter has more than four times the spatial resolution when compared with the current composite filter). However, if the rolling sensor time record has low SNR, this LP th norm filter may not have enough attenuation to resolve the RDD signal at the operating frequency accurately. The key point is to select the digital filter according to the rolling sensor signal characteristics. An important parameter would be the signal-to-noise ratio (SNR).

Using the current composite filter, a t_{90} value of 0.225 sec. can also be selected instead of the typical 1 sec. value. Then, the current composite filter will have the same

time (or spatial) resolution as the LP th norm filter suggested above. The frequency response and the time resolutions for the 2-pole IIR, composite filter (t_{90}=0.225 sec), and LP th norm filter are shown in Figures 6.29 and 6.30, respectively. Both the composite filter and the LP th norm filter show similar frequency response near the primary lobe, but the composite filter has higher attenuation in the stopband than the suggested LP th norm filter. Since the SNR for this time record is fairly good, the effect that the extra attenuation in the stopband that was provided by the composite filter is negligible, which is shown in the amplitude envelope result that will be shown later in Figure 6.33. It was found that this LP th norm filter can be an alternative filter for used in RDD analysis.

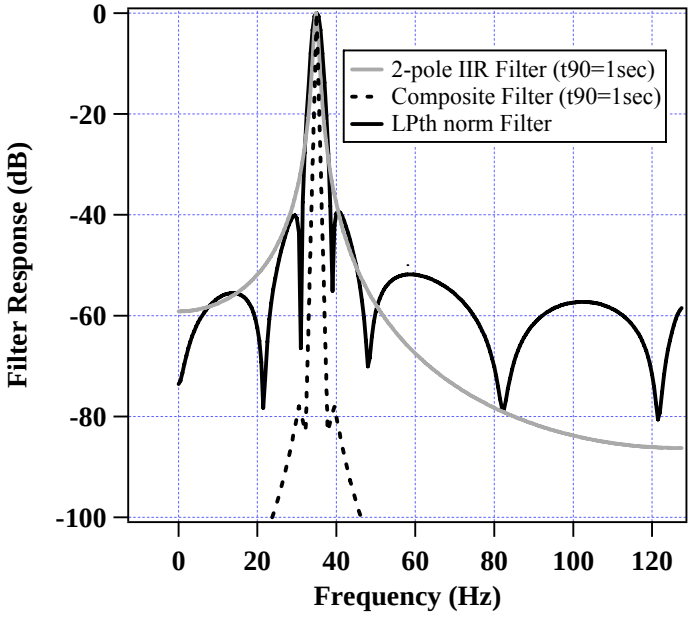

Figure 6.29 Comparison of Frequency Response for Different Digital Filters: (1) 2-pole IIR Filter (t_{90} = 1 sec.), (2) FIR Decimating Composite Filter (t_{90} = 0.225 sec.), and (3) LP th Norm Filter.

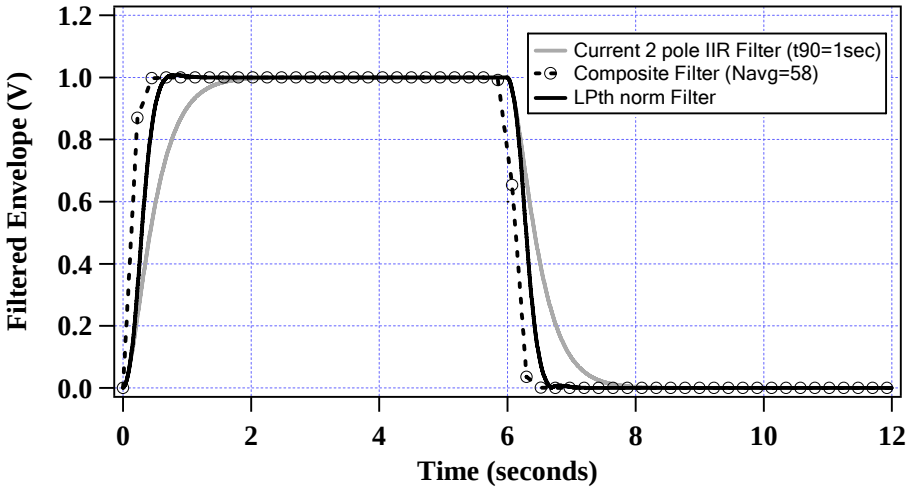

Figure 6.30 Comparison of Time Resolution for Different Digital Filters: (1) 2-pole IIR Filter (t_{90} = 1 sec.), (2) FIR Decimating Composite Filter (t_{90} = 0.225 sec.), and (3) LP th Norm Filter.

6.7.4 Amplitude Envelope Using Hilbert Transform

Once a digital filtering scheme has been selected, the time record as shown in Figure 6.25 can be filtered using the digital filter. The LP th norm digital filter presented in Figure 6.29 is used to filter the rolling noise components in this time record. The filtered time record is shown in Figure 6.31(a). Using this technique, user can easily inspect the filtered signal to check if the output is indeed at the operating frequency. This is illustrated in an expanded section shown in Figure 6.31(b), where it is very easy to count the number of cycles present in each second.

The primary interest in RDD measurements is to determine the amplitude envelope from the load cells and geophones. Without using the amplitude demodulation technique, one can use the Hilbert transformation to obtain the amplitude envelopes of the signal (Wavemetric, 2004; Bracewell, 1965).

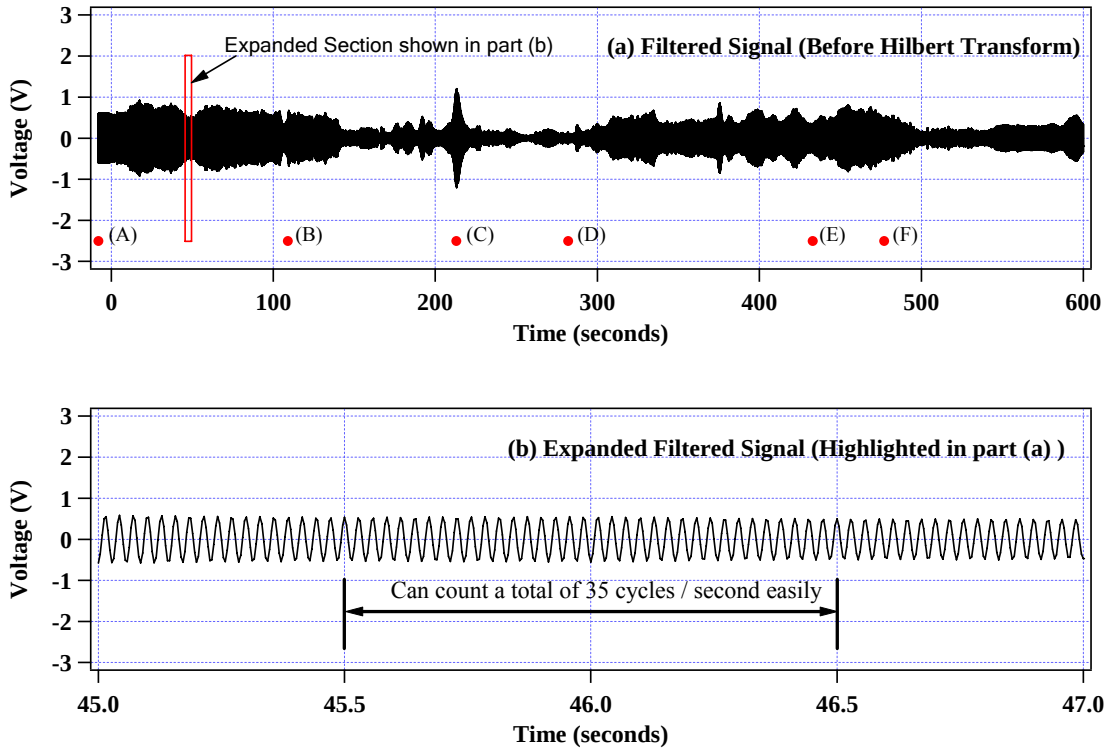

Figure 6.31 Filtered Time Record Collected using the Second-Generation Rolling Sensor (12-in. Diameter) at 2 mph (Raw Time Record Shown in Figure 6.25): (a) Entire Time Record, (b) Expanded Time Record.

The Hilbert transform F(t) of a function f(x) is defined as:

$$F(t) = \frac{1}{\pi} \int_{-\infty}^{\infty} \frac{f(x)}{t - x} dx \qquad (6.18)$$

The Hilbert transform F(t) is also equal to the convolution of $1/(\pi\ t)$ and f(t) as defined as:

$$F(t) = \frac{1}{\pi\ t} * f(t) \qquad (6.19)$$

If y(t) is a real-valued input signal, then the complex time signal can be constructed from the input signal y(t) and its Hilbert transform counterpart h(t) as:

$$Y(t) = y(t) + j\ h(t) \qquad (6.20)$$

The amplitude of the complex time signal Y(t) can be determined by simply expressing Y(t) in polar coordinates, and Eq. 6.20 becomes:

$$Y(t) = A(t) \exp [\, j\, \psi(t)\,] \qquad (6.21)$$

where A(t) = envelope of the complex signal Y(t)

$\psi(t)$ = phase of the complex signal Y(t)

Based on Equations 6.18 to 6.21, the amplitude envelope was obtained by applying the Hilbert transform. The resulting amplitude envelope is shown in Figure 6.32.

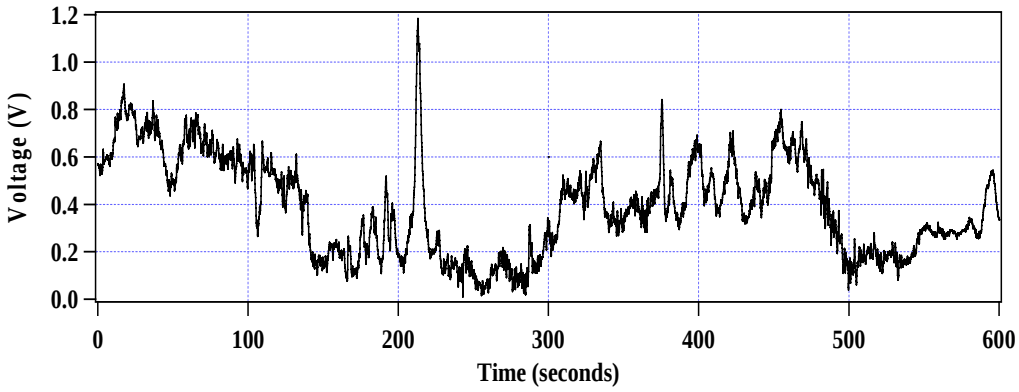

Figure 6.32 Amplitude Envelope of the Rolling Sensor Time Record After Applying a Hilbert Transform.

This process can be repeated for the force measurements from the load cells. Then, the final RDD deflection profile can be computed by applying the appropriate calibration and conversion factors.

6.7.5 Obtaining the Final RDD Deflection Profile

The filtered data using the LP th norm digital filter was shown in Figure 6.32. Then, the same data was also analyzed using the digital filtering scheme developed by Bay(1997). Comparison of the filter output from the LP th norm and Bay's filter is shown

in Figure 6.33. As shown in Figure 6.33, the two filters generate very similar filtered outputs. A residual analysis was performed on the filtered outputs, and the results are shown in Figure 6.34. It was found that the discrepancy between the two digital filter schemes on this particular rolling sensor time record is insignificant. Therefore, it is concluded that either filter can be used in this case.

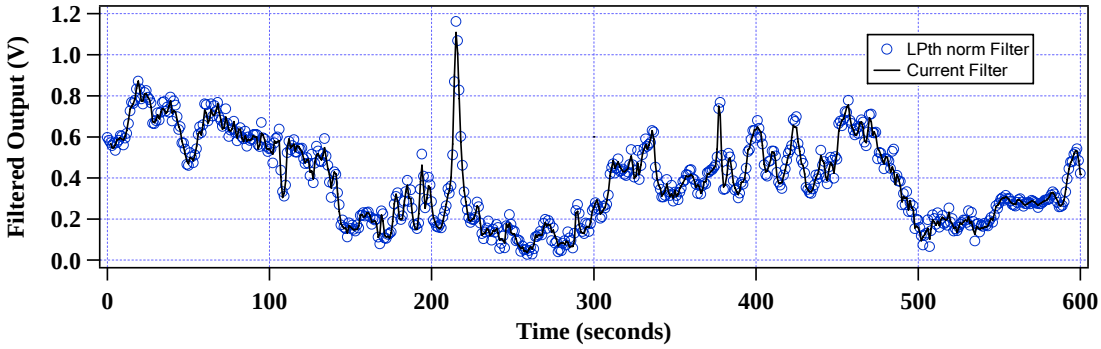

Figure 6.33 Comparison of the Rolling Sensor Amplitude Envelopes Obtained Using the LPth Norm Filter and the Composite Filter (Original Time Record shown in Figure 6.25).

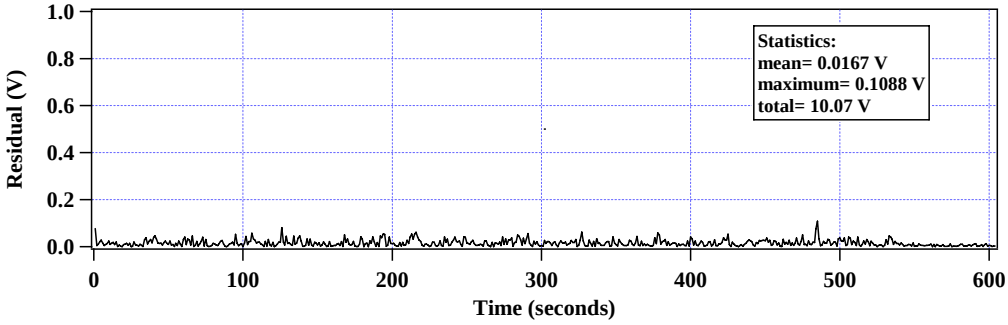

Figure 6.34 Residual Analysis Between the Amplitude Envelopes Obtained Using Different Digital Filtering Schemes.

6.7.6 Improving Spatial Resolution of RDD Deflection Profiles

In Figure 6.33, it was shown that both the LP th norm filter and the current composite filter produced comparable results when reported at the same spatial resolution. However, since the LP th norm filter has a much lower t_{90} value of 0.225, the reported deflection profile can be presented with a higher spatial resolution which corresponds to the t_{90} value of the filter (i.e. in this particular case, approximately 4 times the resolution can be obtained using the LP th norm filter than the current composite filter). Yet, the deflection values do not show significant difference A shorter section along the deflection profile shown in Figure 6.35 were selected and presented in detail as shown in Figure 6.36.

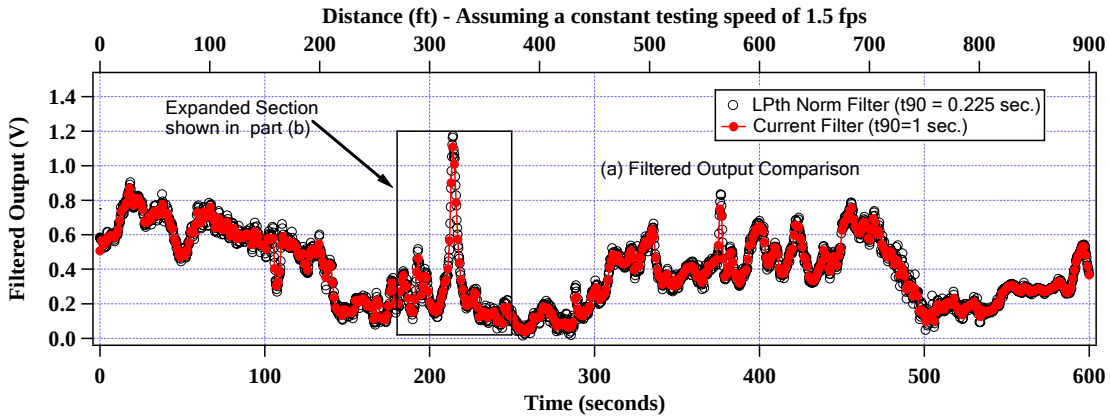

Figure 6.35 Comparison of the Deflection Profiles Obtained Using the LPth Norm Filter (t_{90} = 0.225 sec) and the Current Composite Filter (t_{90} = 1 sec).

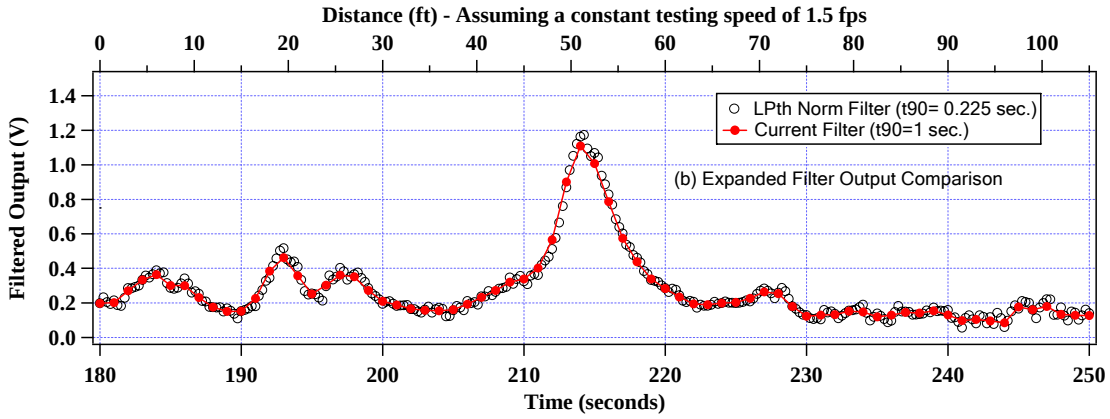

Figure 6.36 Comparison of the Expanded Deflection Profiles (Shown in Figure 6.35) Using the LP th Norm Filter (t_{90} = 0.225 sec) and the Current Composite Filter (t_{90} = 1 sec).

6.8 CASE STUDY: RUNWAY GRAYSON COUNTY AIRPORT

The filtering technique presented in details in Section 6.7 was used on a time record collected along the runway of Grayson County Airport, Texas. A time record collected using the first-generation rolling sensor (testing speed of about 1 mph) is shown in Figure 6.37. To investigate changing rolling noise characteristics along the time record, selected locations labeled as A, B, C, D, E, and F in the time record were studied FFT spectra were calculated for each of the six locations. These spectra are shown in Figure 6.38. Based on the FFT spectra, it was found that the time record collected at this location contains significant higher order harmonics. The harmonics are represented by spikes above the rolling noise envelope at frequencies of 70 and 105 Hz. All five test locations between A and E show similar signal-to-noise ratios and the rolling noise envelope decreases with increasing frequency. The FFT spectrum collected at location F appears to be different from the others. It has another fundamental frequency at around 18 Hz, and also contains higher order harmonics. Furthermore, the rolling noise envelope is also relative flat across the frequency band. Possible causes include the towing

condition of the rolling sensor and pavement surface characteristics near around location F. More study is needed to explain this abnormality.

As mentioned earlier, the RDD data were filtered using a set of analog filters which is set with a cutoff frequency of 100 Hz. The effect of this is shown in all the FFT spectra which have a rapid drop in amplitude at frequencies beyond 100 Hz. Based on the knowledge gained in this FFT analysis, a LP th norm filter with the following characteristics should be used for this site.

1. High attenuation should be focused in the low frequency range (i.e 0 – 30 Hz).
2. High attenuation should also be focused at the locations where higher order harmonics were found (i.e. 70 Hz and 105 Hz).
3. The filter attenuation can be very low at frequencies beyond the cutoff frequency of 100 Hz.

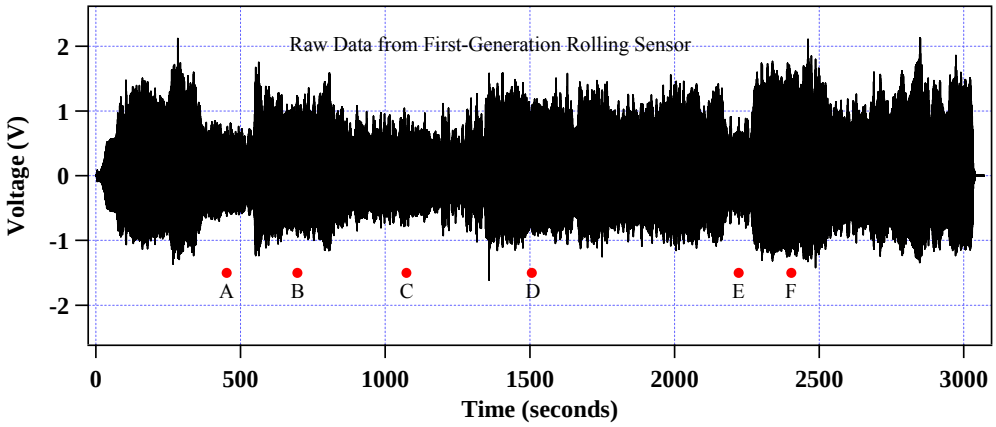

Figure 6.37 Raw Time Record Collected Using First-Generation Rolling Sensor Along Runway at Grayson County Airport

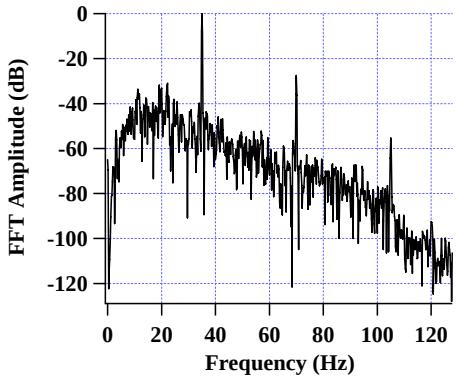

(a) Location A

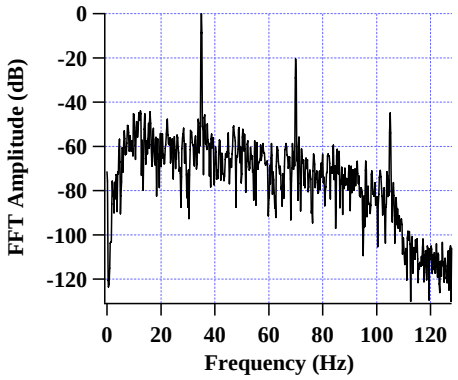

(d) Location D

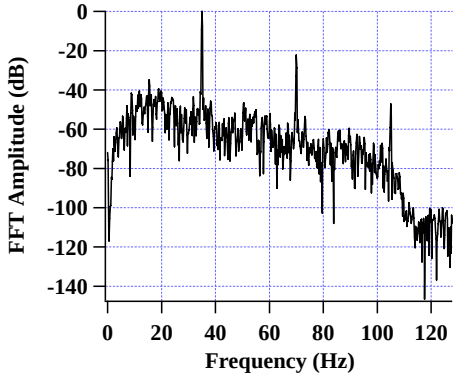

(b) Location B

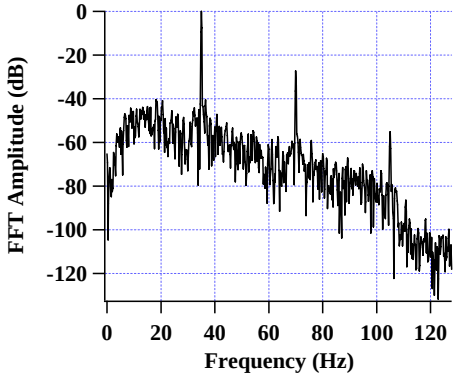

(e) Location E

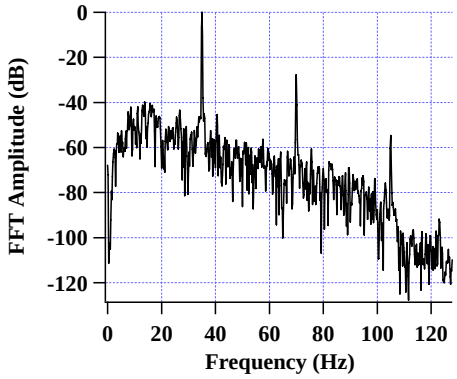

(c) Location C

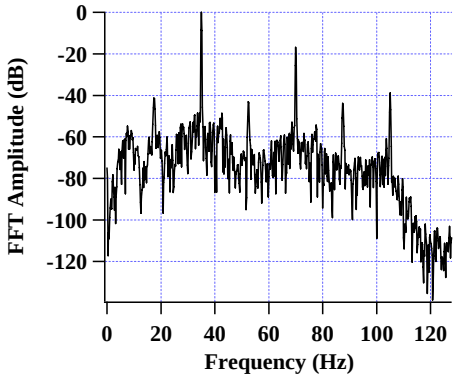

(f) Location F

Figure 6.38 FFT Amplitude Spectrum at Locations A through E Shown in Figure 6.37.

A LP th norm filter with the above characteristics were designed accordingly. The frequency response of this filter is shown in Figure 6.39. It is characterized by high attenuation at areas where it is most needed for this time record. Yet, the settling time performance that is faster than a typical composite filter (with t_{90}=1 sec). The settling time performance between the LP th norm filter presented in Figure 6.39 and a composite filter (Bay 1997) with t_{90} value of 1 sec are shown in Figure 6.40.

When comparing the filtered results between the two filters, the amplitude envelopes from each filter need to be compared (as shown in Figure 6.41). It was found that both filters produced very similar results. Last, a residual analysis is shown in Figure 6.42. This analysis indicates that the average difference between the filtered outputs is around 0.01V. This level of accuracy can be transformed to approximately 0.1 mils (at 35 Hz), which is usually accurate enough for the purposes of collected RDD deflection profiles.

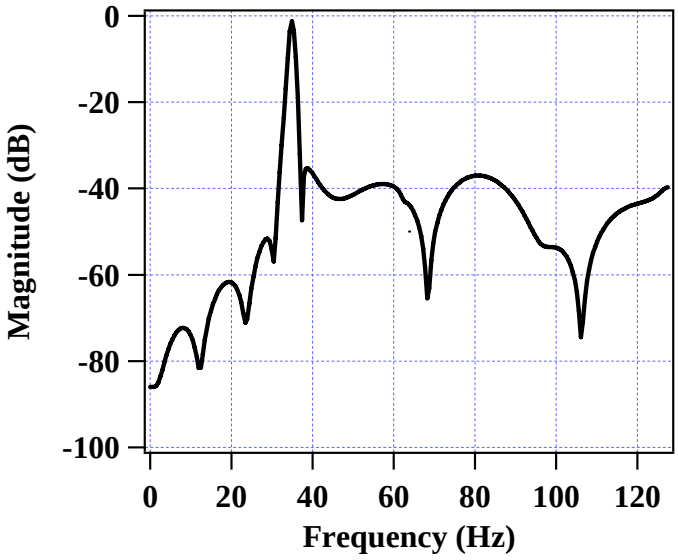

Figure 6.39 Frequency Response of a LP th Norm Digital Filter.

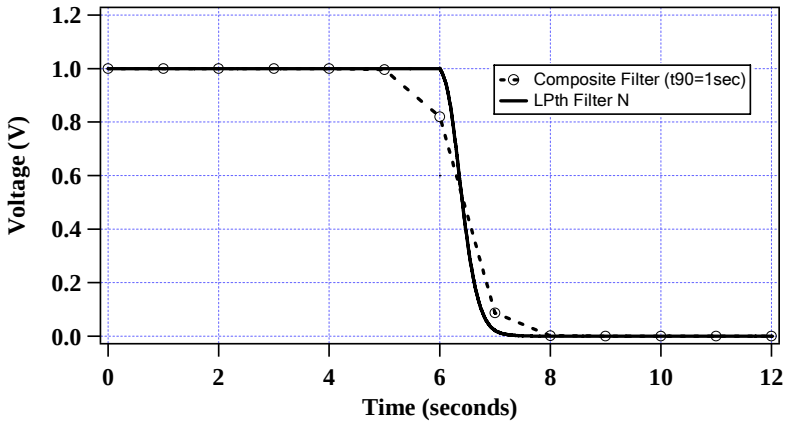

Figure 6.40 Comparison of Settling Time Performance between a LP th Norm Filter and a Composite Filter (t_{90} = 1sec).

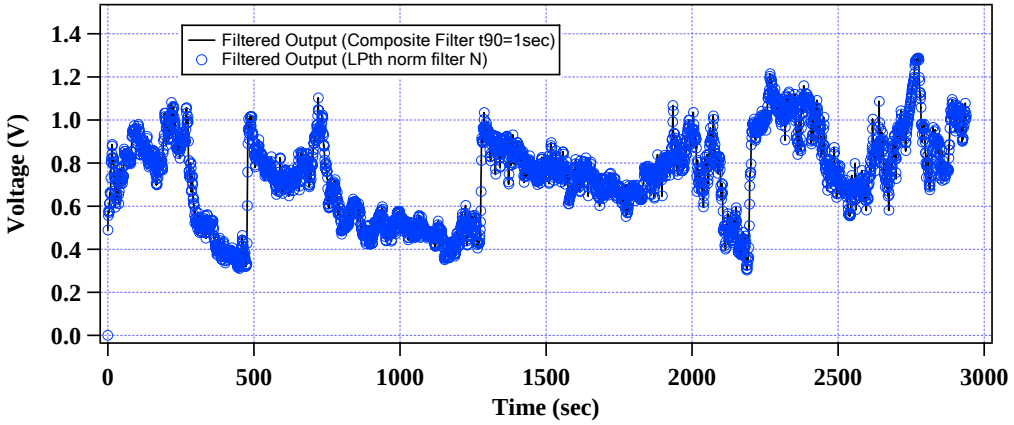

Figure 6.41 Rolling Sensor Amplitude Envelopes Obtained Using the LPth Norm Filter and the Composite Filter (t_{90} = 1 sec) at Grayson County Airport.

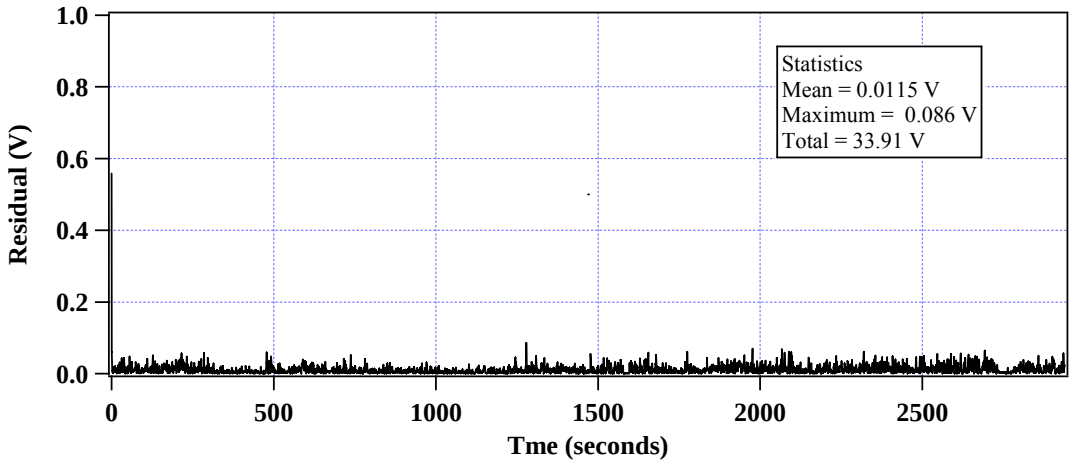

Figure 6.42 Residual Analysis Between the Amplitude Envelopes Obtained Using Different Digital Filtering Schemes (Grayson County Airport)

6.8.2 Improve Spatial Resolution of RDD Deflection Profiles

In Figure 6.41, it was shown that both the LP th norm filter and the current composite filter produced comparable results when reported at the same spatial resolution. However, since the LP th norm filter has a much lower t_{90} value of 0.73, the reported deflection profile can be presented with a higher spatial resolution which corresponds to the t_{90} value of the filter, as shown in Figure 6.43. Yet, the deflection values do not show significant difference. A shorter section along the deflection profile shown in Figure 6.43 were selected and presented in detail as shown in Figure 6.44.

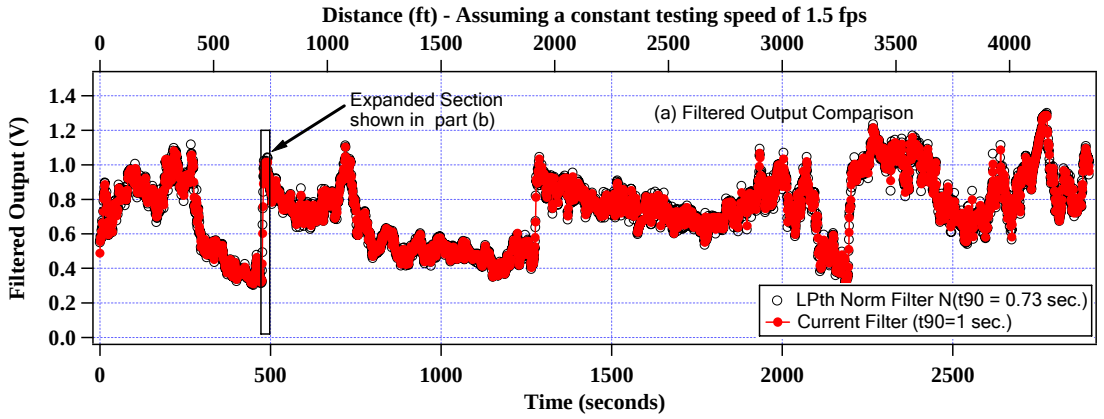

Figure 6.43 Comparison of the Deflection Profiles Obtained Using the LP th Norm Filter (t_{90} = 0.73 sec) and the Current Composite Filter (t_{90} = 1sec).

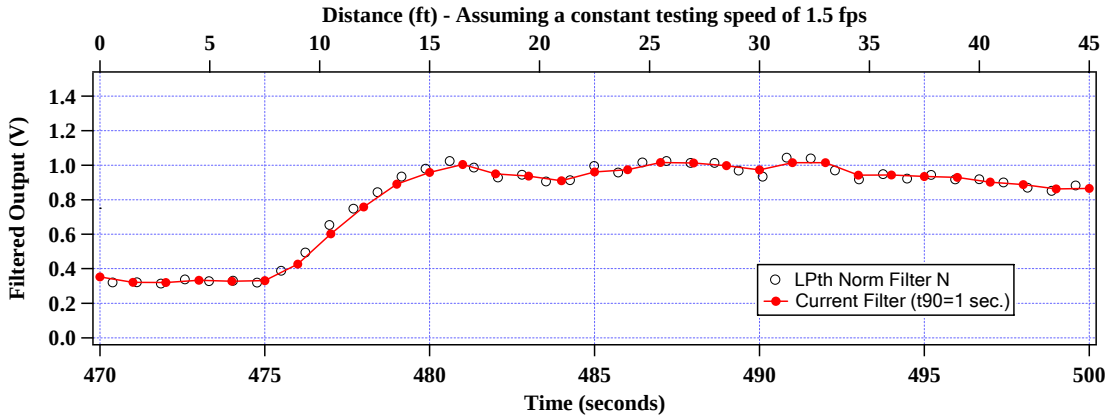

Figure 6.44 Comparison of the Expanded Deflection Profiles (Shown in Figure 6.43) Using the LP th Norm Filter (t_{90} = 0.73 sec) and the Current Composite Filter (t_{90} = 1 sec).

6.9 CASE STUDY: FORT WORTH MEACHAM AIRPORT

Another data-analysis example using RDD data collected along the runway at the Fort Worth Meacham Airport is presented in this section. This record was collected using the first-generation rolling sensor along a Jointed Concrete Pavement (JCP) at a testing speed of about 1 mph. The raw time record is shown in Figure 6.45. Again, six locations

(A,B,C,D,E, and F) were selected. The FFT spectra for all six locations are shown in Figure 6.46. When the FFT spectra at this site are compared with the ones previously shown in Figure 6.38, it was found that the rolling noise envelope are relative flat at the Fort Worth Meacham Airport (i.e indicating that equal attenuation in all stop bands is required). Also, at this airport, one can see that the signal-to-noise ratio (SNR) varies a lot along the time record (Figure 6.46). Locations A and C have high SNR, while the rest have a relatively low SNR. Because the pavement texture and condition were not one of the factors being studied during the time when this record was collected, the reason for this variation in SNR is not fully understood. Nevertheless, it is important to identify the areas with changing SNR, as this would result in different accuracies in the calculated deflections that can be produced with a digital filter. (i.e. the higher SNR requires a filter with less attenuation in the stopband and a wider primary lobe maybe acceptable). Based on these observations, a LP th norm filter with the following characteristics is recommended:

1. a filter with equal attenuation in the stopband,
2. high attenuation is not need at frequencies beyond the cutoff frequency of 100 Hz, and
3. a filter with a relatively sharp primary lobe is required to accurately isolate the RDD signal from the high rolling noise environment.

A LP th norm filter which satisfies the above requirements is shown in Figure 6.47. This filter has sharp roll-off at the transition band and equal attenuation in the stopband. The settling time performances between this LP th norm filter and the composite filter with t_{90} of 1 second are shown in Figure 6.48. The trade-off for having a filter with sharp roll-off and high attenuation is the longer filter settling time as shown in Figure 6.48. The amplitude envelopes obtained using the LP th norm filter and the

composite filter is shown in Figure 6.49. The discrepancy between the two envelopes were also analyzed and shown in Figure 6.50. It was found that the mean residual between these two filters is 0.0057 V, which is equivalent to a difference in deflection of 0.057 mils (at 35 Hz).

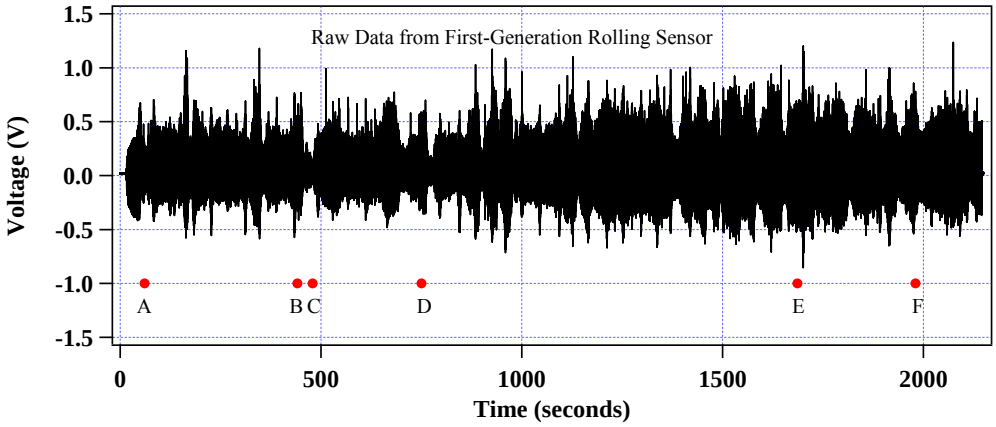

Figure 6.45 Raw Time Record Collected Using First-Generation Rolling Sensor Along the Runway at Fort Worth Meacham Airport(Testing Speed of 1 mph with 6-in. Diameter Rolling Wheels).

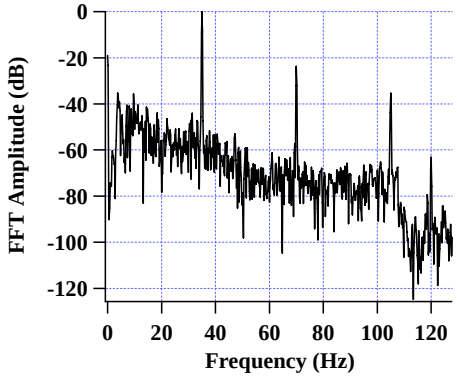

(a) Location A

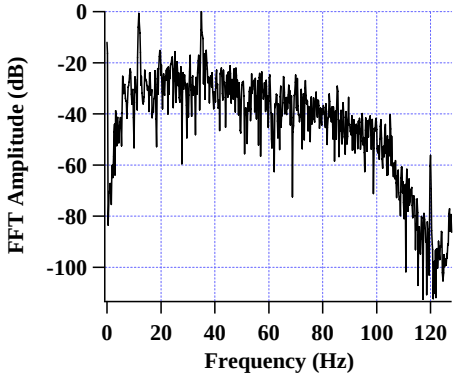

(d) Location D

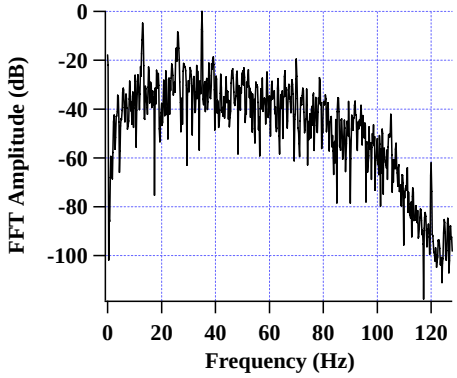

(b) Location B

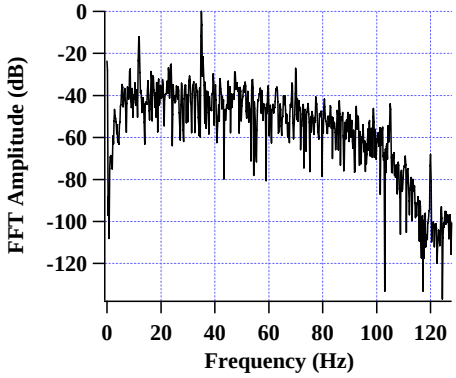

(e) Location E

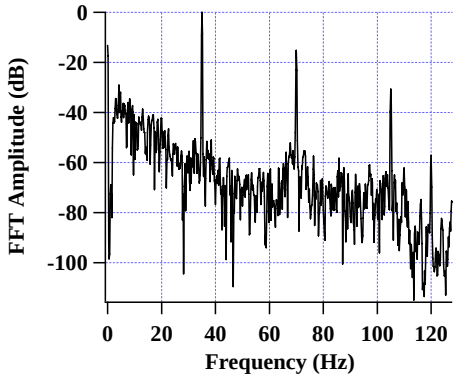

(c) Location C

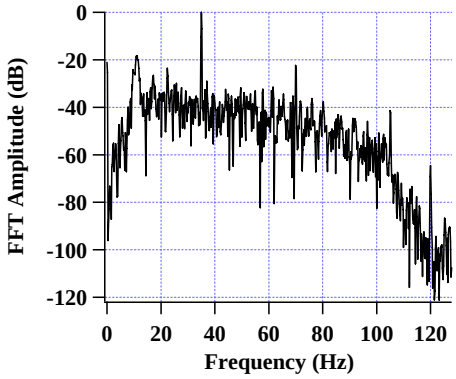

(f) Location F

Figure 6.46 FFT Amplitude Spectra at Selected Locations (Locations A to F) shown in Figure 6.41.

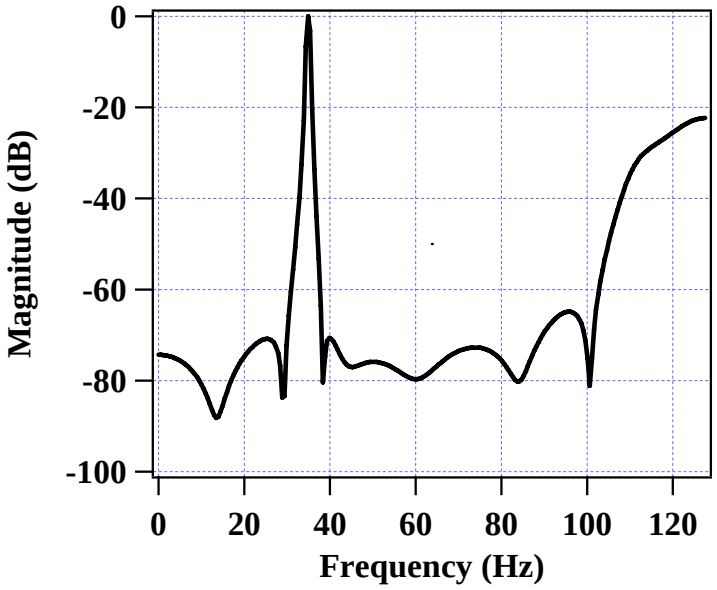

Figure 6.47 Frequency Response of a LPth Norm Digital Filter Used to Analyze the RDD Data Collected at Fort Worth Meacham Airport.

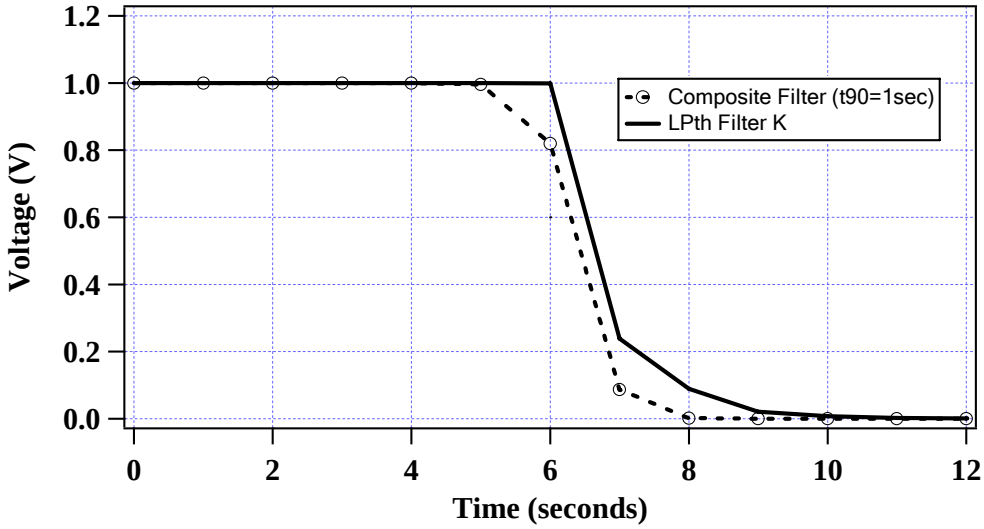

Figure 6.48 Comparison of Settling Time Performance between a LPth Norm Filter and a Composite Filter (t_{90}=1sec) (Fort Worth Meacham Airport).

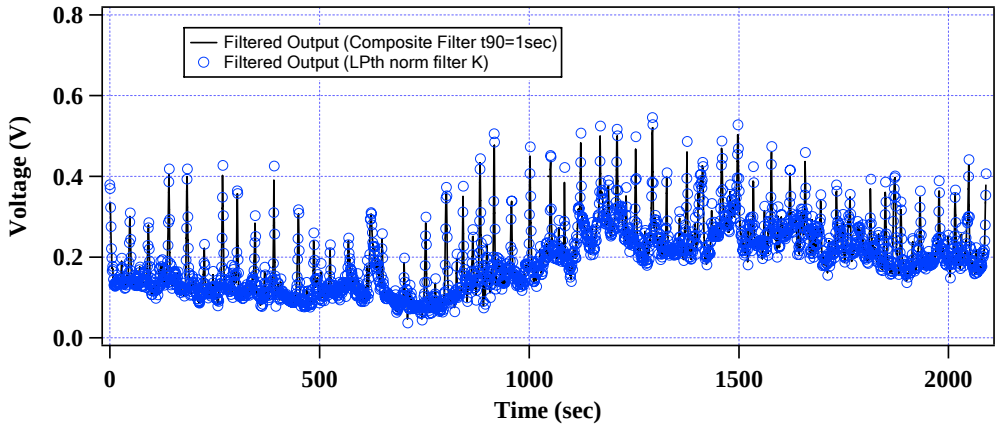

Figure 6.49 Amplitude Envelopes Obtained Using the LPth Norm Filter and the Composite Filter (t_{90} =1 sec)(Fort Worth Meacham Airport)

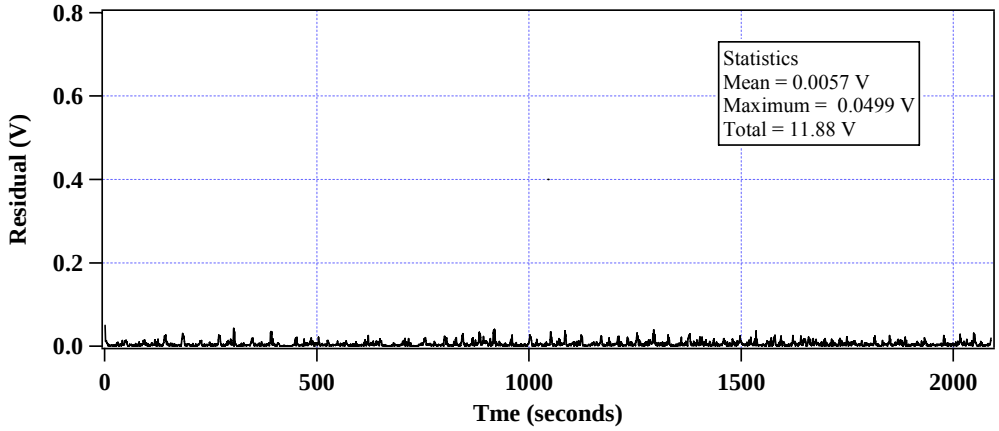

Figure 6.50 Residual Analysis Between the Amplitude Envelopes Obtained Using Different Digital Filtering Schemes (Fort Worth Meacham Airport).

6.10 SUMMARY

To obtain the pavement surface deflection from the RDD raw data, an analysis method is required to retrieve the RDD signal from the noisy time record collected with the rolling sensors. The principle behind the current analysis method involves applying a digital filter with a relatively narrow pass-band, which isolates the signal at the RDD operating frequency from noise located at other frequencies. The design of such a digital filter is a crucial component in the RDD analysis method. The properties of the digital filter have a direct impact on the accuracy and spatial resolution of the reported RDD deflection profile. In the first part of this chapter, a brief summary of the current analysis method that was developed by Dr. James A. Bay (Bay, 1997) is presented.

In the second part of the chapter, alternative digital filters that can be used to analyze RDD data are proposed. These digital filters are designed using the LP th norm filter design method, which has the flexibility to produce filters with specific filter characteristics (i.e. the desired attenuation of the filter across the Nyquist frequency band is specified by the user). Such design flexibility allows the digital filter to be designed according to the characteristics of the collected RDD data. Data collected from three different pavement test sites were used to compare the results collected using both the current and the proposed data analysis method. In some situations, it was found that similar deflection profiles can be obtained using the LP th norm digital filters. These digital filters often have a smaller t_{90} values, which translates to improved time (and spatial) resolution.

Chapter 7 Data Analysis Software – WINRDD

7.1 INTRODUCTION

The raw RDD data consists of three different types of measurements: (1) load cell measurements, (2) rolling sensor (geophone) measurements, and (3) distance measuring instrument (DMI) measurements. The details of these transducers were discussed by Bay (Bay, 1997). The basic principle of the RDD is to apply a static and a sinusoidal dynamic force at a single operating frequency to the pavement while the RDD rolls along the pavement section. In the meantime, an array of rolling sensors is towed along the pavement surface to collect continuous deflection profiles. For each hour of RDD testing, approximately 60 MB of raw data are collected, and the collected time measurements are often noisy if inspected visually in the time domain. In particular, the measurements from the rolling sensors are often illegible to users in the time domain.

Over the last decade, the RDD raw measurements were post-processed using an analysis routine written by Dr. James Bay in the Wavemetric Igor Pro environment. This analysis routine will be called IgorRDD in the context of this chapter. There are a number of limitations in this IgorRDD program that are listed as follows:

1. limited interactive user interface capability to inspect the measured waveform,
2. limited capability to carry out frequency analysis on the measured waveform,
3. only one digital filtering scheme to use,
4. cannot readily integrate with the National Instrument (NI) data acquisition system, and

5. no ability to distribute the program as a stand-alone executable file.

The methodology to estimate rolling noise from field RDD measurements was presented in Chapter 3. Other filtering techniques which can be used are presented in Chapter 6. These improvements are incorporated into the WinRDD program, and will help users to interpret the RDD data and to use some of the new filtering techniques presented earlier. In the WinRDD v.1.0 program, some of the new features include the following:

1. provides an easy and user-friendly interface which allows the user to inspect any part of the measured waveforms interactively,
2. allows the user to carry out different kinds of frequency analysis to evaluate the waveform properties in the frequency domain,
3. provides a number of standard digital filtering schemes for the user to choose from,
4. provides the user with the ability to define a rolling noise envelope (spectrum) which approximates the actual rolling noise characteristic specific to a particular project and portion of the pavement. Then, a tool is provided for the user to input the required filter specifications and to generate the desired digital filtering scheme,
5. this software was written using National Instrument (NI) Labview G programming language and allows readily integration with the existing NI data acquisition system,
6. acts as a shell for IgorRDD, which allows users to analyze the RDD data using IgorRDD from within WinRDD. (Note: the earlier version of IgorRDD and Wavemetric Igor Pro software are needed), and

7. the program can be distributed as a stand-alone executable program (i.e. users are not required to install any additional commercial software to use WinRDD).

7.2 WINRDD PROGRAM STRUCTURE

When the program is first started, the main window of WinRDD will appear. A screenshot of the WinRDD window is shown in Figure 7.1. There are basically four steps in analyzing RDD data in WinRDD. These steps are listed as follows:

1. Read RDD Data,
2. Interpret RDD Data,
3. Digital Signal Processing (DSP) Design, and
4. Analyze RDD Data.

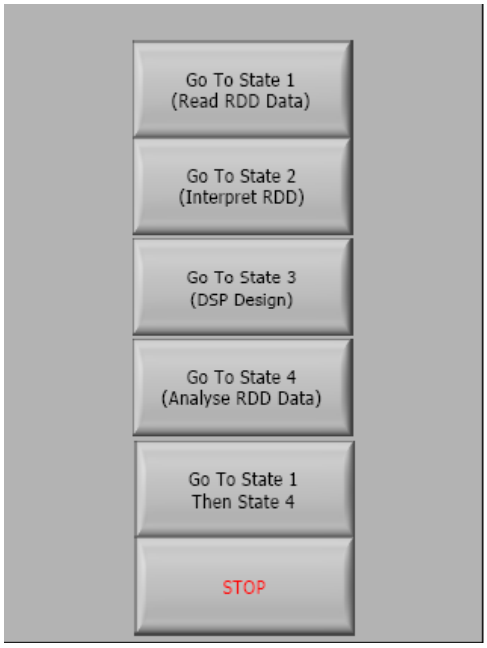

Figure 7.1 Screenshot of the WinRDD Main Window

Users are required to run all four steps to analyze the RDD data. A separate window will appear after the user clicks on one of the four buttons mentioned above. More information will then be shown that is specific to the step. In Step 1, the raw RDD measurement file will be loaded into the program. In Step 2, a user-friendly interface is shown which allows users to inspect the measured waveform and run different kinds of analysis to identify the important characteristics of the RDD waveform. In Step 3, the user is provided with a number of standard signal processing schemes. Also, a digital filter design tool is provided for the user to design a filter that is specific to a pavement site. In Step 4, the user can either analyze the RDD measurements using the digital filtering scheme decided from Step 3 or the user can execute IgorRDD from the background.

7.3 SUB-WINDOW: READ RDD DATA

A sub-window will appear after the user clicks on the "Read RDD Data" button in the main window. The user will first be asked to input the RDD raw data file to analyze. Then, the sub-window shown in Figure 7.2 will appear. In the IgorRDD program, the user is required to provide the file paths for the two RDD raw data files listed below:

1. Analog File - 1D array (in single floating point format) which contains all nine analog channels that are recorded during RDD signal data acquisition (DAQ), and
2. Counter File - 1D array (in double floating point format) which contains two sets of data: (1) time-stamp from the DAQ system, and (2) distance traveled reported every second from the DAQ on-board digital counter.

Compared to IgorRDD, WinRDD uses a different technique to correlate the distance measurements from the distance encoder with each sampling point (in the time domain), the user no longer needs to provide the counter file.

In the sub-window, six different waveforms are displayed for the user to inspect and verify the accuracy of the retrieved raw RDD data file. These waveforms include:

1. Total force waveform (i.e. combined force from the four RDD load cells),
2. Rolling sensor #1 output waveform,
3. Rolling sensor #2 output waveform,
4. Rolling sensor #3 output waveform,
5. Rolling sensor #4 output waveform, and
6. Distance encoder output (i.e. consists of the digitalized version of the square waveform that was generated from the distance encoder).

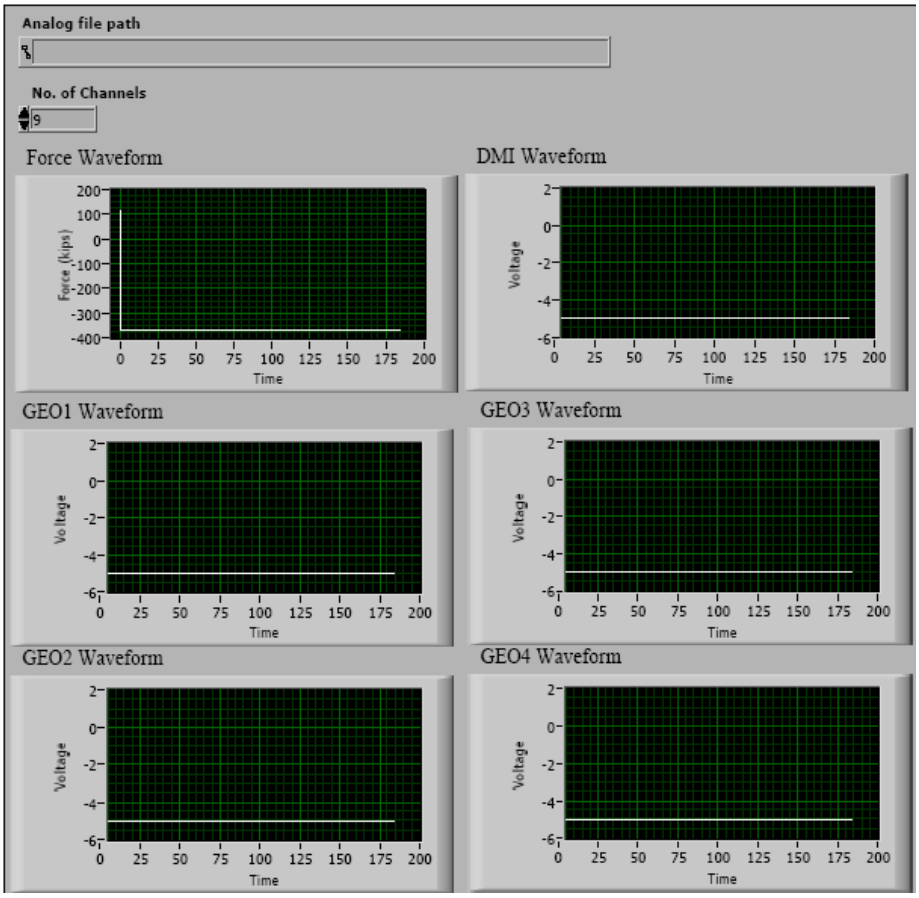

Figure 7.2 Screenshot of the WinRDD Step-1 Window

7.4 SUB-WINDOW: INTERPRET RDD DATA

After the WinRDD program has finished reading the RDD data file, the user is brought back to the main menu. A sub-window appears after the user clicks the "Interpret RDD Data" button in the main window. A sub-window appears as shown in Figure 7.3. In this sub-window, WinRDD is used to perform analysis on the raw RDD data in the frequency domain. The duration of each analysis window can be adjusted accordingly (typically it is set at 5-second intervals). Then, the program marches through the raw RDD data file and presents the following information:

1. time record for each individual load cell and rolling sensor,
2. speed time history,
3. FFT spectrum of the RDD rolling sensor, and
4. average noise level.

As the program marches through the time records, the user can inspect the time records more closely for any abnormalities in the time records. Furthermore, the raw data presented in the frequency domain provides valuable information such as the following:

1. RDD signal level at the operating frequency,
2. general shape of the rolling noise envelope, and
3. presences of higher order harmonics.

As discussed in Chapter 3, the RDD signal and noise characteristics are site specific. The noise characteristics are a function of the testing speed, pavement roughness, and level of deflections. Knowledge from previous testing on pavement sites with similar attributes allows the user to estimate the general trend of the noise envelope. For more accurate analysis, a noise envelope can be created for each section of pavement tested. More specifically, the user has now been given the flexibility to decide a noise envelope in which the measured rolling noise would not be exceeded with a certain probability of confidence. Once the user defines a noise envelope, the noise envelope will appear on top of the FFT spectrum generated from the time record. Then, the program will calculate the percentage of time when the rolling noise will actually exceeded the estimated noise envelope. Based on a trial-and-error approach, the user can create a site-specific noise envelope which represents the rolling noise characteristics of the particular raw data file. The output from this sub-window is used to define the noise envelope,

which is an important component for designing a site-specific digital filtering scheme in the next step of the program.

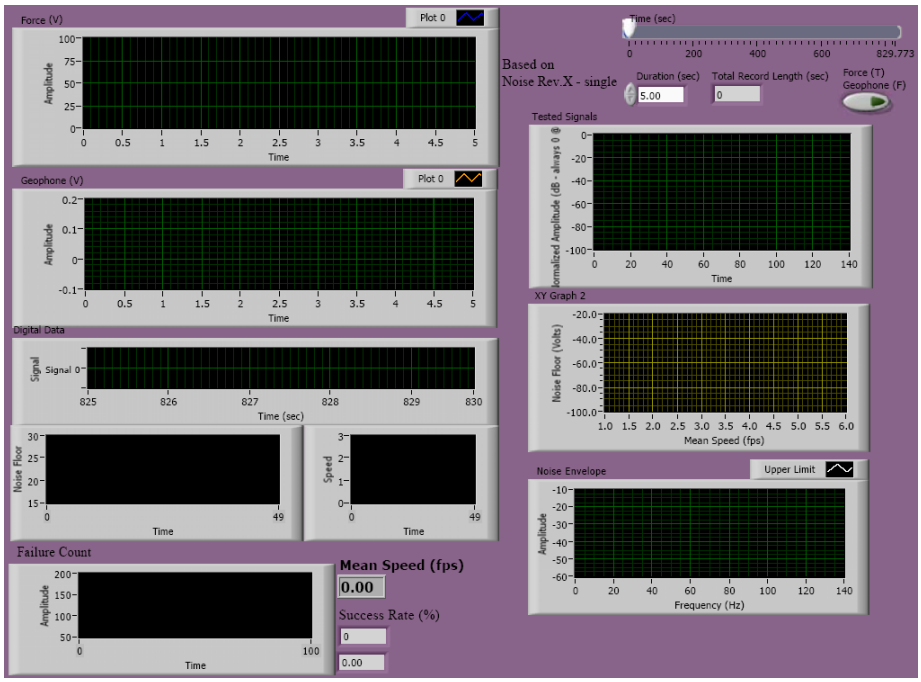

Figure 7.3 Screenshot of the WinRDD Step-2 Window

7.5 SUB-WINDOW: DIGITAL SIGNAL PROCESSING (DSP) DESIGN & DEFLECTION PROFILE OUTPUT

After the WinRDD program has been used to analyze the RDD data file in the frequency domain, the user is brought back to the main menu. A sub-window appears after the user clicks the "DSP Design" button in the main window. The sub-window appears as shown in Figure 7.4. In this sub-window, WinRDD designs the digital filter which is used in the next section to produce the RDD deflection profile output.

Based on the noise envelope from the previous section, the user can calculate the digital filter specifications to achieve a desired attenuation. A number of DSP methods as discussed in Chapter 6 are available:

1. arbitrary zeros and poles placement - ad-hoc approach,
2. peak filter design – only one parameter, Q-factor, is required to design a peak filter,
3. DSP filter library – these are predefined filters which were created based on knowledge from previous RDD test sites, and
4. LP th norm filter design – greater flexibility to allow the user to create different filters which best match any arbitrary frequency response and settling-time response. The simulation study of the effect of different filter parameters is discussed in detail in Chapter 6.

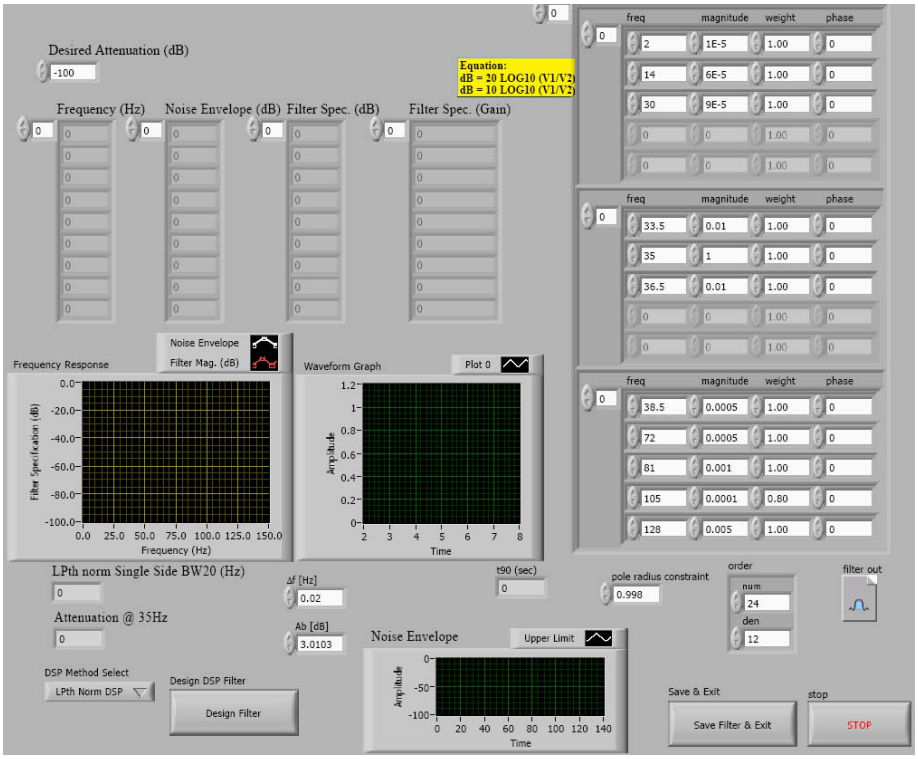

Figure 7.4 Screenshot of the WinRDD Step-3 Window

After the user decides on the filter design method and desired filter specifications, WinRDD creates an appropriate digital filter. Then, the sub-window shown in Figure 7.5

appears. In this sub-window, the filter response of the chosen digital filter is plotted against the noise envelope. The filter response is also plotted in the z-plane using zeros and poles. In addition, the settling time of the filter is shown. These plots allow the user to inspect whether the filter meets both the frequency and time resolution requirements for analyzing the particular RDD data file. If the filter does not meet the requirements, the user will be brought back to the previous sub-window shown in Figure 7.4 and is allowed to change the filter parameters. After a few iterations, the user finalizes the desired filters and this filter is used in the next section where the RDD data are analyzed using this filter. Finally, the RDD deflection profiles are shown in the sub-window shown in Figure 7.6.

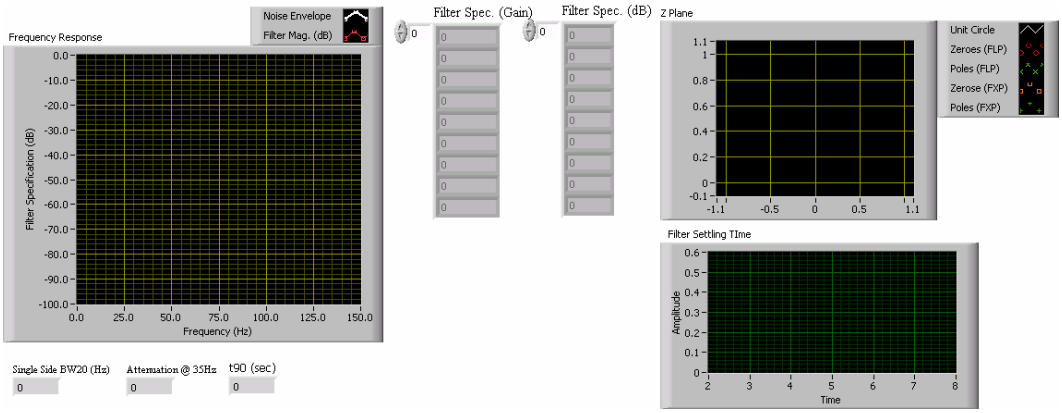

Figure 7.5 Screenshot of the WinRDD DSP Filter Analysis Results Window

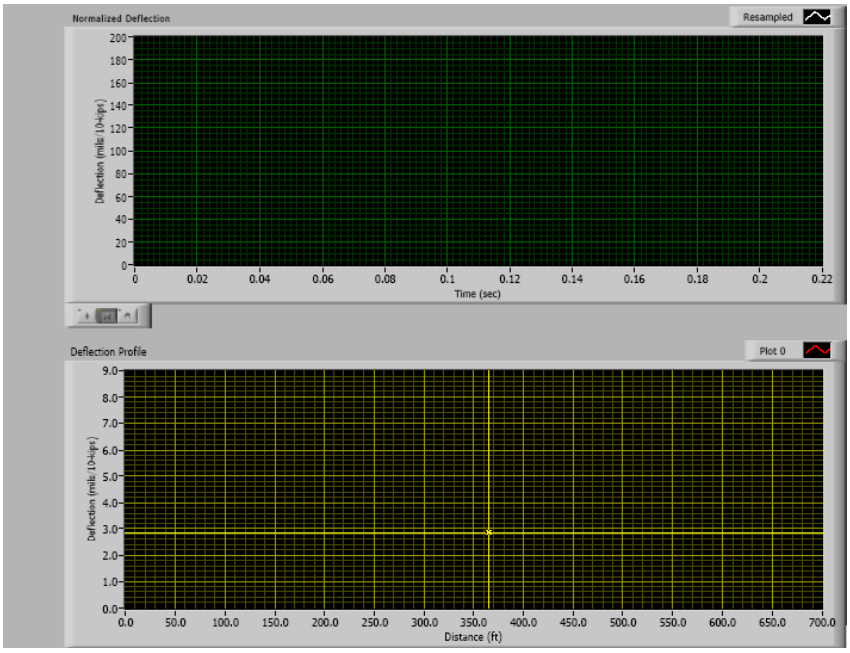

Figure 7.6 Screenshot of the WinRDD Step-4 Window

7.6 SUMMARY

A software program called WinRDD was developed and a brief summary which illustrates the functionality of this software is presented in this chapter. The primary purpose of WinRDD is to incorporate improvements in the RDD analysis method discussed in Chapters 3 and 6. Furthermore, the user interfaces of this software have been greatly improved when compared to the previous RDD analysis program.

Chapter 8 Summary, Conclusions, and Recommendations

8.1 SUMMARY

The findings of a three-part study to further improve the Rolling Dynamic Deflectometer (RDD) are presented in this dissertation. The first part involved the development of second-generation rolling sensors. Key benefits of these new rolling sensors are: (1) increased testing speed from 1 to 3 mph (1.6 km/hr to 4.8 km/hr), and (2) reduced level of rolling noise during RDD measurements. Prototypes of the second-generation rolling sensors were built and tested in a number of field trials. These field trials used the second-generation rolling sensors to collect deflection profiles along different types of pavements over a range of testing speeds between 1 to 3 mph (1.6 to 4.8 km/hr). The details on the design of the second-generation rolling sensor are presented in Chapter 4. Then, results collected from the different field trials are presented in Chapter 5.

The second part of the study focuses on characterizing the rolling noise collected along different highway and airport pavements. A total of 46 different highway and airport test sites that were collected over the last seven years were evaluated to systematically investigate the factors which affect rolling noise in the signals collected with rolling sensors. Some of the factors which were found to affect the rolling noise characteristics are: (1) deflection levels, (2) pavement surface roughness, and more importantly (3) testing speed. Through better understanding of the rolling noise characteristics, better rolling sensors can be designed to reduce measurement noise, and customize digital filters can be used to resolve the RDD signal in the surrounding noise.

The discussion pertaining to RDD rolling noise is discussed in Chapter 3. Due to the complexity and random nature of rolling noise measurements, a simplified rolling noise envelope is proposed to model the rolling noise in the frequency domain. Such a noise envelope allows estimation of the rolling noise over a wide range of pavements, which were also discussed in Chapter 3.

The third part of this study involved improving the data analysis method for RDD testing. A brief summary of the current analysis method that was developed by James A. Bay (Bay, 1997) is included in the first part of Chapter 6. This current analysis method utilizes the amplitude demodulation technique to transform the RDD signal to 0 Hz. Then, a composite filter consisting of a 2-pole IIR filter and a FIR Hamming filter with decimation was used. An alternative data analysis method is proposed and presented in the second part of Chapter 6. The main differences between the current and the new data analysis methods include: (1) evaluation of the rolling noise characteristics, (2) designing individual digital filters for a particular set of RDD measurements using the LP th norm filter design method, and (3) filtering RDD data at the operating frequency without performing the amplitude demodulation procedure. This alternative data analysis method is then compiled into a software program, called the WinRDD, and the details of the functionality of the WinRDD are presented in Chapter 7.

8.2 CONCLUSIONS

The following conclusions result from the work performed as part of this project:

1. Prototypes of the second-generation rolling sensors were designed, built and tested in a number of field trials. Results from field trials indicate that the second-generation rolling sensors are ready for field deployment and use at testing speeds up to 3 mph (4.8 km/hr).

2. The second-generation rolling sensors allow the RDD to achieve a testing speed of 3 mph. An additional benefit of this new sensor is that the level of rolling noise is reduced when compared with the first-generation rolling sensors traveling at the same speed. This benefit is more significant on high-roughness pavement surfaces.
3. Comparable deflection profiles were collected in field trials using the first-generation and second-generation rolling sensors on both flexible and rigid pavements over a range of testing speeds between 1 to 3 mph (1.6 to 4.8 km/hr).
4. It is important to understand the characteristics of the rolling noise presented in the rolling sensor measurements. Three factors were identified which affect the rolling noise characteristics: (1) level of deflections, (2) pavement surface roughness, and (3) testing speed.
5. A simplified rolling noise envelope was proposed to model the rolling noise in the frequency domain. This information can be used in the design of new rolling sensors, and can also be used in designing more suitable digital filters.
6. An alternative analysis method was proposed in this work. The deflection profiles produced by this alternative analysis method are comparable to results produced by the existing analysis method.
7. A software program, called WinRDD, was written to incorporate some of the improvements presented in this study. This program is a tool that allows the user to inspect the RDD signal and perform calculations using the alternative analysis method presented herein.

8.3 RECOMMENDATIONS AND FURTHER DEVELOPMENT

1. The alternative data analysis method presented in this dissertation utilized the additional knowledge of the rolling noise characteristics to customize the digital filter used. Such digital filter optimizes the attenuation characteristic for a particular set of RDD data, and therefore improves the time resolution of the reported deflection profile. However, for RDD measurements which have low signal-to-noise ratio, only limited benefits can be obtained using this alternative data analysis method. Further work should be carried out in the following areas to continue improving the RDD analysis method:
    - **i.** Investigate the feasibility of using other advanced signal processing techniques for analyzing RDD data. For example, the Matrix-Pencil method should be investigated further.
    - **ii.** Further study on the rolling noise characteristics collected by rolling sensors, and finding alternative ways to cancel out the rolling noise. For example, adding rolling noise components at opposite polarity to the RDD sinusoidal signal, such that the rolling noise components are being cancelled out in the signal collected in the rolling sensor record.
2. Backcalculating modulus values for different pavement layers using RDD data and "rolling deflection basins".
3. Reduce the contact pressure applied by the loading rollers to a value that is more comparable to the wheel loads of typical highway and airport traffic.
4. Compare the RDD deflection profiles with displacement measurements made at close proximity to pavement features with rapidly changing deflection characteristics (e.g. pavement joints).

5. Include accelerometers on the future design of rolling sensors. Such measurements can be used to monitor the coupling / decoupling condition of the rolling sensors.
6. Incorporate real-time analysis to the RDD. The real time analysis should include both the quality control (QC) measures and the real-time reporting of RDD deflection profiles. An example of a QC parameter that can be used to indicate the quality of collected data is a signal-to-noise-ratio (SNR) during RDD testing.
7. Investigate the seasonal dynamic properties of different pavement systems, and study the changes in the measured deflection profiles using different RDD operating parameters. For examples: (1) operating frequency, (2) dynamic force levels, and (3) static (confining) force.

References

AASHTO, AASHTO Guide for the Design of Pavement Structures, 1996

AASHTO Standard Method of Test for Pavement Deflection Measurements. AASHTO Standard T 256-01, 2001.

ASTM Standard Guide for General Pavement Deflection Measurements, ASTM Standard D 4695 – 96, 1996.

Bay, J. A., "Development of a Rolling Dynamic Deflectometer", Ph.D Dissertation, University of Texas at Austin, 1997.

Bandara, N., Briggs, R., "Nondestructive Testing of Pavement Structures", Back to Basics Series, The American Society for Nondestructive Testing, July 2004 issue.

Bentson, R. A., Nazarian, S., Harrison, J. A., "Reliability Testing of Seven Nondestructive Pavement Testing Devices, ASTM Publication – STP 1026, Nondestructive Testing of Pavements and Backcalculation of Moduli, Bush/Baladi, editors, 1989, pp 41 – 58

Bracewell, R., The Fourier Transform and Its Applications, McGraw-Hill, 1965.

Bretonniere, S. Etude d'un Deflectometre â boulet. Bulletin de Liaison des Laboratoires Routiers, No. 2, 1963, pp. 53 – 55.

Carneiro, F.B.L. , "Benkelman Beam—Auxiliary Instrument of the Maintenance Engineer," Transportation Research Record 129, Transportation Research Board, Washington D.C., 1966, pp. 28-59.

Croney, D., Croney, P., Design and Performance of Road Pavements, McGraw-Hill Professional, third edition, 1997, p.327.

Duzan, H. C., Oehmann, J. C., Davis, J. M., "Use of Road Test Equipments in Pavement Cost Allocation, The AASHO Road Test – Proceedings, May 16 – 18, 1972, St. Louis, Mo. Session 3. Highway Research Board Special Report 73 – Publication 1012, National Academy of Sciences, 1962, pp 393 – 438.

ERES Consultants, "Rolling Wheel Deflectometer (RWD) Texas Demonstration and Comparison To Other Devices, Champaign, Illinois, Applied Research Associates (ARA), Inc., 2004.

Johnson, A. M., "Design of Flexible Pavement Overlays by Dynamic Deflections", Ph.D. Dissertation, University of South Carolina, 1992.

Forsyth, R. A., and Zube, E., Report on Pavement Deflection Research and Operations by the California Division of Highways Since 1938. California Division of Highways Materials and Research Department, Sacramento, California, April 1966.

Harvey, J., Popescu, L., Ali, A., Bush, D., "Performance of Dowel Bar Retrofitted Concrete Pavement Under Heavy Vehicle Simulator Loading", Transportation Research Record 1823, Washington D.C., 2003

Hass, R., Hudson, W., and Zaniewski, Journal of Modern Pavement Management. Krieger Publishing Company, Malabar, FL, 1994.

Hoffmann, O., Guzina, B., Drescher, A., "Stiffness Estimates Using Portable Deflectometers", Transportation Research Record 1869, Washington D.C., 2004, pp. 59 – 66.

Hossain, A. M., "Deflection Analysis of Flexible Pavements Using Nondestructive Test Data", Ph.D. Dissertation, Arizona State University, 1990.

Huang, Y. H., "Pavement Analysis and Design", Second Edition, Prentice Hall, 2003.

Hunter, R. (editor), Asphalts in Road Construction, Thomas Telford Ltd., 2000.

Hudson, W.R., Elkins, G.E. Uddin, W., and Reily, K. T., Evaluation of Pavement Deflection Measuring Equipment. Report FHWA-TS-87-208, FHWA, Washington, D.C., March 1987.

Ioannides et al., Interpretation of Falling Weight Deflectometer Test Results Using Principles of Dimensional, Proceedings, Fourth International Conference on Concrete Pavement Design and Rehabilitation, Purdue University, W. Lafayette, IN, April 23-25, 1989, pp. 231 – 247.

Irwin, L. H., Yang, W. S., Stubstad, R. N., "Deflection Reading Accuracy and Layer Thickness Accuracy in Backcalculation of Pavement Layer Moduli", ASTM Publication – STP 1026, Nondestructive Testing of Pavements and Backcalculation Moduli, Bush/Baladi, editors, 1989, pp 229 – 244.

Johnson, R. F., Rish, J. W., "Rolling Weight Deflectometer with Thermal and Vibrational Bending Compensation", Transportation Research Record 1540, Transportation Research Board, Washington D.C., 1996, pp. 77 – 82.

Kallas, B. (editor), Pavement Maintenance and Rehabilitation, ASTM Special Technical Publication STP 881, p.20, 1985, pp. 96.

Khazanovich, L., Tayabji, S., and Darter, M., Documentation of the Back-Calculation of Layer Parameters for LTPP Test Sections, Volume I: Slab on Elastic Solid and Slab on Dense-Liquid Foundation Analysis of Rigid Pavements, Report submitted

to FHWA, contract number DTFH61-96-C-00003, Final Report. January 2001. pp. 115.

Kim, W., Ground Penetrating Radar Application for Non-Destructive Testing: Bridge Deck Inspection and Dowel Bar Detection, Ph.D. Dissertation, University of Missouri – Rolla, 2003.

Lee, J., Stokoe, K. H., Chen, D., Garrison, M., Nam, B., "Monitoring Pavement Changes in a Rehabilitation Project with Continuous RDD Profiles", Transportation Research Record No. 1905, 2005, pp. 3 – 16.

Liddle, W. J., "Application of AASHO Road Test Results to the Design of Flexible Pavement Structures, International Conference on the Structural Design of Asphalt Pavements, Proceedings, University of Michigan, Ann Arbor, Michigan, August 20 – 24, 1962. pp. 42 – 51

McKendrick, W. B., History of [AASHO] Project, The AASHO Road Test – Proceedings, May 16 – 18, 1962, St. Louis, Mo., Highway Research Board Special Report 73 – Publication 1012, National Academy of Sciences, 1962, pp. 4 – 15.

Meshkani, A., Abdallah, I., Nazarian, S., "Feasibility of Backcalculation of Nonlinear Flexible Pavement Layer Parameters from Nondestructive Testing", Transportation Research Record 1860, Washington D.C., 2003, pp. 16 – 25.

Murphy, M., "A Mechanistic-Empirical Approach to Characterizing Subgrade Support and Pavement Structural Condition for Network-Level Applications", Ph.D Dissertation, University of Texas at Austin, Austin, Texas, 1998., pp. 499.

National Instruments, Labview – Digital Filter Design Toolkit User Manual, Austin, Texas, February 2005.

Nazarian, S., "Specification for Tools Used in Structural Field Testing of Flexible Layers", Research Project 0-1735 – Development of Structural Field Testing of Flexible Pavement Layers, Technical Memorandum 1735-1, Center for Highway Materials Research, University of Texas at El Paso, Marcy, 1997.

Romanoschi, S., Metcalf, J., "Simple Approach to Estimation of Pavement Structural Capacity", Transportation Research Record 1652, Washington D.C., 1999, pp198-205.

Smith, R. E., Lytton, R. L., "Operating Characteristics and User Satisfaction of Commercially Available NDT Equipment", Transportation Research Record 1007, TRB, National Research Council, Washington, D.C., 1985, pp. 1 – 10

Stolle, D., Hein, D., Parameter Estimates of Pavement Structure Layers and Uniqueness of the Solution, ASTM Publication – STP 1026, Nondestructive Testing of Pavements and Backcalculation of Moduli, Bush/Baladi, editors, 1989, pp 313 – 322.

Ullidtz, P., Coetzee, N. F., "Analytical Procedures in Nondestructive Testing Pavement Evaluation", Transportation Research Record (1482), 1995, pp. 61-66.

Wavemetric, "Igor Pro User Manual – Reference (Volume V)", Wavemetric, Inc, 2004.

Uzan, J., Briggs, R., Scullion, T., "Backcalculation of Design Parameters for Rigid Pavements", Transportation Research Record 1377, 1992, pp. 107-114.

Von Quintus, H. L. and Simpson A., Documentation of the Back-Calculation of Layer Parameters for LTPP Test Sections, Volume II: Layered Elastic Analysis for Flexible and Rigid Pavements, Report FHWA-RD-01-113 submitted to FHWA, October 2002.

Weaver, A., "Correlation of Non-Destructive Pavement Test Devices", Master Thesis, University of New Brunswick, 2000, Fredericton, Canada.

Yildirim, Y., Culfik, M., Lee, J., Smit, A., Stokoe, K. H., "Performance Assessment by Using Nondestructive Testing", Research Report 4185-3, Center for Transportation Research, The University of Texas at Austin, Austin, Texas, 2003.

Zaniewski, J. P., Hossain, M., "Effect of Thickness and Temperature Corrections on Prediction of Pavement Structural Capacity Using Falling Weight Deflectometer Data", Transportation Research Record 1377 – Nondestructive Deflection Testing and Backcalculation for Pavements, TRB, Washington, D.C., 1992, pp. 193 – 199.

Zhang, Z., Claros, G., Manuel, L., and Damnjanovic, I., "Development of Structural Condition Index to Support Pavement Maintenance and Rehabilitation Decisions at Network Level." Transportation Research Record 1827, Washington, D.C., 2003, pp. 10 – 17.

Vita

Jeffrey Lik Yeung Lee was born in Hong Kong on November 25, 1977, the son of Jim Ah Poon Lee and Amy Kit Shan Fung. After graduated from MacLeans College, Auckland, New Zealand, in 1995, he entered University of Auckland, New Zealand. He received the degree of Bachelor of Engineering with second class first division honor from University of Auckland in November 1995. In September 1999, he entered the Graduate School of The University of Texas at Austin. He received the degree of Master of Science from University of Texas at Austin in May 2001. After completing his master degree, he began his Ph.D study in June 2001.

Permanent address: 8 Trebor Road, Pennant Hills, Sydney, NSW 2120,
Australia.

This dissertation was typed by Jeffrey Lik Yeung Lee.